



**Modelling of unsteady pipe flow with “liquid column separation” (water hammer induced transient cavitation)**

**By**

**Mohamed Abdulsalam KASHADA**  
**B.Sc. (Mech. Eng.), M.Sc. (Pipeline Eng.)**

**Thesis submitted to the**  
**School of Mechanical and Systems Engineering**  
**for the degree of Doctor of Philosophy**

**Supervised by:**  
**Dr. Alexander Anderson**

**October 2017**

## ABSTRACT

Understanding of waterhammer pressure transients in liquid-filled pipelines and their computational (numerical) modelling as unsteady one-dimensional flow is well established in the literature and engineering practice. However, for the particular issue of the potential for low transient pressure to initiate a change of phase or release of dissolved gases, leading to the phenomenon of localised transient cavitation known as liquid column separation, there is not yet a consensus on the reliability of the various numerical models that have been proposed in the literature. To contribute to further progress on this, therefore, this present work builds primarily on two previous studies, by Bergant & Simpson (1999) at Adelaide University and Arfaie (1989) at Newcastle University.

The aim of this work is to repeat and extend the Bergant & Simpson (1999) comparison of the Discrete Vapour Cavity Method (DVCM) and Discrete Gas Cavity Method (DGCM) while also taking into account the contribution of Arfaie (1989) in respect of:

- his suggestion for an improved transient internal boundary condition at the moving liquid column separation interface;
- his recommendation that the greater damping associated with unsteady pipe friction models (as opposed to conventional quasi-steady friction) may improve overall model performance; and
- his observation that the mode of column separation behaviour (particularly when column separation causes a pressure spike that may exceed the widely regarded Joukowsky pressure maximum) may influence the choice of best model.

The basic DVCM and DGCM models tested (with the gas release physical parameters for the latter) are those established in the literature. In these the transient internal boundary condition at the moving column separation interface can be either the conventional Wylie & Streeter (1993) formulation as in Bergant & Simpson (1999) or the Arfaie (1989) improvement. There are many models available for unsteady friction, but previous work by Bughazem (1997) at Newcastle University had established that a Brunone-type Instantaneous Acceleration Based model is not only simple to implement but also works well on the specific experimental apparatus used

in this study. Bughazem & Anderson (1996) had outlined (but not implemented or tested) a possible alternative integration of this into a fully Method of Characteristics approach. This is developed and applied, but its additional implementation complexity for no obvious gain in performance led to its being set aside.

The very simple Arfaie (1989) experimental apparatus used is intended to eliminate any modelling issues (especially for external boundary conditions) not associated with column separation as well as to attempt to restrict column separation to a single location (to support its visualisation). Flow visualisation on this apparatus did not show the conventional full-bore vapour cavity suggested by the term “column separation”. Rather scattered vapour or released gas bubbles appeared along the pipe soffit during the transient column separation event. To support clarification of Arfaie’s views on the different modes of column separation behaviour, an extensive series of experimental runs were recorded to facilitate development of a map for the occurrence of these, with the intention of helping analysts and designers to determine if pressure higher than Joukowsky might occur. It was determined that these may occur for  $P_M = \sim 1.2 \sim 2$  where  $P_M$  is the Martin ratio:

$$P_M = \frac{\rho \cdot a \cdot V_o}{P_R - P_v}$$

Initially the comparison of computed against experimental results followed the conventional qualitative approach as in Arfaie (1989) and others. However, this proves problematic where a large number of experimental runs (with scatter due to uncertainties) have been taken, as well as when there are more than one factor for comparison. This process, though, did highlight an issue with predicting the data value for vapour pressure, where the actual value on the experimental traces is different from the Steam Tables value used for prediction and thus appearing on the computed traces. This introduced a further factor to the investigation.

Following Arfaie (1989) and others, initially qualitative comparison taken over a period including up to five pressure peaks were made (overall shape of peaks and ability to maintain phase of solution features). However, for consistent comparison across a number of experimental runs, two specific quantifiable criteria are defined:

- the time duration of the first column separation event; and

- the maximum pressure peak amplitude occurring as a result of that.

Graphs can be compiled to attempt to explore the behaviour of different model options, but with a large amount of data showing scatter due to uncertainty these do not lead to clear outcomes. Consequently, following previous work on CFD modelling at Newcastle University by Ahmeid (1997), a statistical approach using Design of Experiments (DOE) with Analysis of Variance (ANOVA) was adopted which demanded quantified criteria. ANOVA indicates whether significant differences can be detected from the data and the DOE approach (as compared with “one factor at a time” testing) can indicate if there are interactions present between the factors.

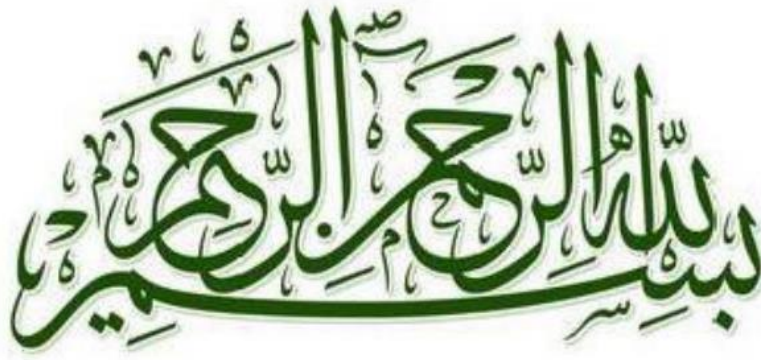
With this recourse to statistical methodology, Normal Probability plots indicated that the data for first cavity duration are better than data for maximum pressure peak amplitude, giving more significant ANOVA outcomes for the former than the latter. Though this first attempt at using these techniques has not produced clear or comprehensive outcomes, the methodology is promising for future studies. The present outcomes are that:

- For basic method, DGCM, as suggested by Bergant & Simpson (1999), performs best for cavity duration, but it is not yet possible to say this for maximum pressure amplitude.
- Similarly, with quasi-steady friction at least, the Arfaie (1989) internal boundary condition is a small improvement over the conventional Wylie & Streeter (1993), certainly for cavity duration.
- Unsteady friction does reduce error magnitude and scatter, but the greater damping may lead to non-conservative (under-estimation) prediction of maximum pressure amplitude.
- There is evidence that the mode of column separation behaviour does interact with the other factors, but it is not yet clear exactly what, if any, real effect it has.
- Finally, though the data value for vapour pressure is significant (certainly for cavity duration), in practice small variations in its value seem to make little difference to computed predictions.

There is sufficient evidence that with better quality data and further consideration of quantifiable criteria for comparison that the statistical methodology demonstrated can be an effective tool for computational model testing.



Unfortunately for this present study, it exposed the limitation of the apparatus used in producing repeatable results with controlled uncertainties, especially for peak pressure. A clear conclusion is that better experimental data from an improved experimental apparatus are required.



In the name of Allah  
The most gracious and the most merciful

To my family

## Acknowledgments

I thank Almighty God for giving me the courage and determination, as well as guidance, in conducting this research study. I extend my utmost gratitude to my supervisor, Dr. Alexander Anderson, for his valuable advice, suggestions and endless support and to the Technical Staff of the School of Mechanical and Systems Engineering for their work on the experimental rig and its instrumentation.

## Table of contents

Abstract .....	i
Acknowledgments .....	v
Tables of contents .....	vi
Nomenclature .....	ix
 Chapter 1.....	 1
1.1 Background .....	2
1.2 Study Aims and Objectives.....	4
1.3 Outline of Thesis.....	6
Chapter 2.....	7
2.1 Historical review of waterhammer and transient behaviours .....	8
2.2 Liquid pipelines and transient behaviours.....	9
2.2.1 Waterhammer behaviours .....	9
2.2.2 Cavitation and column separation .....	12
2.3 Experimental waterhammer induced column separation .....	14
2.3.1 Choice of boundary conditions and apparatus design.....	14
2.3.2 Visualization and results representation .....	16
2.4 Modelling 1-D waterhammer induced column separation.....	17
2.4.1 Waterhammer equations and MOC.....	17
2.4.2 Models of liquid column separation at a boundary .....	19
2.4.3 Discrete vapour cavity model (DVCM) .....	19
2.4.4 Discrete gas cavity method (DGCM) .....	20
2.4.5 Unsteady friction.....	22
2.5 Closing Remarks .....	24
Chapter 3.....	25
3.1 Standard waterhammer analysis with MOC .....	26
3.2 Unsteady friction.....	33
3.3 Implementation of Anderson and Bughazem (2000) unsteady friction model..	36
3.3.1 Analysis for internal nodes.....	37
3.3.2 Reservoir boundary condition.....	43
3.3.3 Valve boundary condition. ....	45
3.4 Models of column separation.....	48
3.4.1 Discrete vapour cavity model (DVCM) .....	49
3.4.2 Discrete gas cavity method (DGCM) .....	52
3.4.3 Arfaie interface model .....	57
Chapter 4.....	62
4.1 Choice of experimental apparatus layout .....	63

4.2	Details of experimental apparatus .....	64
4.3	The effect of valve closure time .....	72
4.4	Identification of apparatus characteristics.....	75
4.4.1	Evaluation of wave speed .....	76
4.4.2	Evaluation of pipe friction factor .....	84
4.4.3	Calibration of unsteady friction model .....	89
4.5	Visualisation of cavity formation .....	92
Chapter 5.....		103
5.1	Model comparison rationale.....	104
5.2	Observed pressure transient behaviour.....	105
5.3	Representation of experimental pressure transient .....	114
5.3.1	Single-phase waterhammer with no column separation.....	114
5.3.2	Limited column separation with pressure spikes higher than Joukowsky <b>PJ</b> .....	116
5.3.3	Typical severe column separation .....	119
5.4	Graphical explanation of pressure rises due to column separation. ....	120
Chapter 6.....		126
6.1	Assessment criteria .....	127
6.2	Visual comparison of computed vs experimental.....	131
6.2.1	Comparison of method (DVCM v DGCM).....	131
6.2.2	Comparison of unsteady friction models .....	137
6.2.3	Comparison of internal boundary condition models for DVCM .....	144
6.3	Quantitative assessment .....	148
6.4	Statistical design of experiments approach .....	158
Chapter 7.....		165
7.1	Limitation of experimental results and apparatus .....	166
7.2	Column separation-induced pressure spikes exceeding Joukowsky pressure 168	
7.3	Criteria for assessment of computational models .....	169
7.4	Other issues investigated .....	172
7.4.1	Properties of water (including vapour pressure) .....	172
7.4.2	IAB unsteady friction models .....	172
7.5	Suggestion for further study .....	173
References.....		177
Appendix A.....		191
A.1	WATERHAMMER WAVESPEED .....	192
A.1.1	Evaluation of theoretical value .....	192
A.1.2	Experimental value from Joukowsky pressure rise.....	194
A.1.3	Experimental value from wave period and frequency.....	195

A.2	DARCY FRICTION FACTOR .....	197
	Appendix B.....	198
	Appendix C.....	205
C.1	Experiments of Single-phase waterhammer, runs[1-6].....	206
C.2	Experiments of 1st transition zone, runs[7-10].....	209
C.3	Experiments of Limited column separation, runs[11-25].....	211
C.4	Experiments of 2nd transition zone, runs[26-36]. ....	218
C.5	Experiments of Typical column separation, runs[37-51]. ....	224
	Appendix D.....	232
	Appendix E.....	240
	Appendix F.....	243
F.1	Full data: comparison of Method, BC, $P_v$ using quasi-steady friction .....	244
F.2	Data selected for only limited and classic column separation models: comparison of Method, BC, $P_v$ but also Friction and behaviour Mode .....	253
F.3	Full data: comparison of Method, BC, $P_v$ using unsteady Friction.....	257
F.4	Data selected for only limited and classic separation modes: comparison of Method, BC, $P_v$ , Mode of behaviour.....	259
	Appendix G.....	266

## Nomenclature

A	pipe cross sectional area Eq.(3.5)	$m^2$
A	grid point node at initial time Fig.(3.5)	
a	wave propagation speed Eq.(2.4), Eq.(4.3)	$m/s$
$a_L$	variable wave propagation speed in the cavitation region Eq.(3.111)	
$a_m$	wave propagation speed in gas-liquid mixture Eq.(2.5)	$m/s$
$a_R$	variable wave propagation speed in the cavitation region Eq.(3.111)	
$a_S$	unconfined wave propagation speed. Eq.(A.1)	$m/s$
$a_Y$	Young wave propagation speed	$m/s$
B	pipeline characteristic impedance Eq.(3.9)	$kg/m^4s$
B	grid point node at initial time Fig.(3.5)	
BC	Boundary condition Appendix F	
BP, BM	names of compatibility coefficients Eq.(3.11)	$kg/m^4s$
$BP_f, BM_f$	names of compatibility coefficients Eq.(3.29) Eq.(3.31)	$kg/m^4s$
$BP_g, BM_g$	names of compatibility coefficients Eq.(3.44) Eq.(3.48)	$kg/m^4s$
C	grid point node at initial time Fig.(3.5)	
CP, CM	names of compatibility coefficients Eq.(3.11)	$Pa$
$CP_f, CM_f$	names of compatibility coefficients Eq.(3.28) Eq.(3.31)	$Pa$
$CP_g, CM_g$	names of compatibility coefficients Eq.(3.44) Eq.(3.48)	$Pa$
$C^- C^+$	name of characteristic equations Eq(3.8)	
$C^-$	characteristic curve transmitting information upstream Fig(3.2)	
$C^+$	characteristic curve transmitting information downstream	
D	pipe coil diameter	$m$
d	pipe internal diameter	$m$
$d_o$	pipe external diameter Table(4.2)	$m$
E	pipe modulus of elasticity Eq.(2.4), Table(4.2) App. A	$Pa$
E	grid point node at solution time Fig.(3.5)	
e	pipe wall thickness Table(4.2)	$m$
F	grid point node at previous time Fig.(3.5)	
f	Darcy friction factor Eq.(4.11)	—
$f_n$	natural frequency of single-phase waterhammer Eq.(4.5)	$H_z$
$f_q$	quasi-steady Darcy friction factor Section(3.2)	—

$f_u$	unsteady friction factor Section(3.2) Eq.(4.11)	—
$g$	gravitational acceleration Eq.(2.2)	$m/s^2$
$H$	water head Eq.(2.2)	$m$
$H_{NS}$	water head downstream valve (node NS) Eq.(4.10)	$m$
$H_o$	Initial (steady state) head at downstream end Fig.(2.2)	$m$
$H_R$	reservoir static head Fig.(3.3) Eq.(3.14)	$m$
$H_s$	reservoir static head	$m$
$H_v$	water head vapour pressure Eq.(2.5)	$m$
$J$	instantaneous local friction slope in unsteady flow Eq.(3.24)	
$K$	over all pipe line loss Appendix D	
$K$	fluid bulk modulus of elasticity Eq.(2.4), Table(4.1)	$Pa$
$K_e$	pipe entrance minor loss Eq.(3.14)	—
$k$	unsteady friction coefficient	—
$k_3$	(Bug hazem 1997) unsteady friction coefficient Section(3.3)	
$k_t$	(Bug hazem and Anderson, 2000) unsteady friction coefficient	—
$k_x$	non-dimensional unsteady friction coefficient	—
$L$	pipeline length Table(4.2)	$m$
$L$	liquid column Appendix D	$m$
LHS	left hand side Eq.(3.91)	
$M_g$	gas mass Eq.(3.82)	
$N$	number of pipe reaches of length $\Delta x$	
NS	node at downstream valve ( $NS = N + 1$ )	
$n$	number of single-phase waterhammer wave cycles	
$P$	local absolute pressure Eq.(3.1)	$Pa$
$P_2$	absolute pressure at node(2) Eq.(3.21)	$Pa$
$P_A$	absolute pressure at the point before solution point Eq.(3.8)	$Pa$
$P_a$	atmospheric pressure Appendix D	$Pa$
$P_B$	absolute pressure at the point after solution point Eq.(3.8)	$Pa$
$P_d, P_D$	driving pressure App C Eq.(D.1)	$Pa$
$P_E$	absolute pressure at solution point Eq.(3.12)	$Pa$
$P_G$	pressure at reservoir surface Fig(3.3) Eq.(3.14)	$Pa$
$P_g$	absolute gas partial pressure Eq.(3.82)	$Pa$
$P_i$	pressure at solution point Eq.(1.1)	$Pa$
$P_j$	Joukowsky pressure Eq.(1.1) Eq.(1.2) Fig(1.1)	$Pa$

$P_M$	Martin pressure ratio Eq.(5.1)	—
$P_{max}$	maximum liquid pressure at valve Eq.(1.3)	$Pa$
$P_{max2}$	post-cavity pressure amplitude Fig.(6.1)	$Pa$
$P_{min}$	minimum liquid local pressure Eq.(1.4)	$Pa$
$P_{NS}$	pressure at downstream valve	$Pa$
$P_o$	standard atmospheric pressure Eq.(3.82)	$Pa$
$P_R$	steady state reservoir pressure Fig (3.3) Eq.(3.15)	$Pa$
$P_U$	absolute pressure at non-grid point U Eq.(3.46)	$Pa$
$P_v$	vapour pressure Chapter 6 & Appendix F	$Pa$
$P_v$	vapour pressure	$Pa$
$P_Y$	absolute pressure at non-grid point Y Eq.(3.54)	$Pa$
$p$	$P$ -value or probability of chance Sec.(6.4)	
$Q$	local volume flowrate Eq.(3.5)	$m^3/s$
$Q_1$	volume flowrate at node(1) Fig.(3.3) Eq.(3.18)	$m^3/s$
$Q_2$	volume flowrate at node(2) Fig.(3.3) Eq.(3.19)	$m^3/s$
$Q_L$	flowrate at the left side of the node Eq.(3.79) Fig(3.10)	$m^3/s$
$Q_{L_i}$	flowrate into to solution node i, Eq.(3.108)	$m^3/s$
$Q_R$	flowrate at the right side of the node Eq.(3.79) Fig(3.10)	$m^3/s$
$Q_{R_i}$	flowrate out of solution node i, Eq.(3.108)	$m^3/s$
$Q_o$	initial volume flow rate	$m^3/s$
$Q_A$	flowrate at a point before solution point Eq.(3.8)	$m^3/s$
$Q_B$	flowrate at a point after solution point Eq.(3.8)	$m^3/s$
$Q_E$	flowrate at solution point Eq.(3.13)	$m^3/s$
$Q_U$	flowrate at non-grid point U Eq.(3.46)	$m^3/s$
$Q_Y$	flowrate at non-grid point Y Eq.(3.54)	$m^3/s$
$R$	pipeline resistance coefficient Eq.(3.9)	$kg/m^7$
$Re$	Reynolds number Eq.(4.9)	—
$R_g$	gas constant Eq.(3.82)	
$RHS$	right hand side Eq.(3.92)	
$S$	pipeline slop coefficient Eq.(3.9)	$Pa$
$T$	pipeline period of pressure wave reflection Fig.(1.1) Eq.(4.1)	$s$
$T$	absolute temperature Eq.(3.82)	$s$
$t$	time	$s$
$Tc1$	1 <sup>st</sup> cavity duration Fig.(6.1)	$s$



$T_{c2}$	2 <sup>nd</sup> cavity duration Fig.(6.1)	<i>s</i>
$T_{cr}$	Dimensionless 1 <sup>st</sup> cavity duration Eq.(5.2)	—
$T_{cav}$	theoretical 1 <sup>st</sup> cavity duration Table(5.2) Appendix D	<i>s</i>
$t_{max}$	theoretical maximum cavity duration time Appendix D	<i>s</i>
$U$	grid point node from space-line interpolation Fig.(3.6)	
$V$	flow velocity Fig.(3.2)	<i>m/s</i>
$V_1$	final flow velocity at cavity collapse Eq.(D.5)	<i>m/s</i>
$V_A$	flow velocity at node A Chapter 3	<i>m/s</i>
$V_B$	flow velocity at node B Chapter 3	<i>m/s</i>
$V_C$	flow velocity at node C Chapter 3	<i>m/s</i>
$V_E$	flow velocity at node E Chapter 3	<i>m/s</i>
$V_o$	initial water flow velocity Table(5.3), Eq.(D.5)	<i>m/s</i>
$V(x)$	local flow velocity Fig.(2.2)	<i>m/s</i>
$XL_i$	LHS liquid column length of the computational node Eq.(3.103)	
$XR_i$	RHS liquid column length of the computational node Eq.(3.103)	
$x$	distance between two nodes Eq.(3.7)	<i>m</i>
$x(t)$	cavity length Fig.(D.3)	<i>m</i>
$x_{max}$	Maximum cavity length Eq.(D.4)	<i>m</i>
$Y$	grid point node from space-line interpolation Fig.(3.5)	
$Z$	local elevation of the pipe Eq.(2.5)	<i>m</i>
$\alpha, \beta, \gamma$	shorthand convenience coefficients Eq.(3.19)	
$\alpha_o$	void ratio at atmospheric pressure Eq.(3.82)	—
$\alpha_g$	gas void fraction Eq.(3.82)	—
$\alpha_v$	vapour void fraction Eq.(2.1)	—
$\Delta a$	uncertainty in wave propagation speed	<i>m/s</i>
$\Delta d$	uncertainty in pipe internal diameter Eq.(A.7)	
$\Delta f$	uncertainty in Darcy friction factor Eq.(A.8)	
$\Delta H$	Transient head rise at downstream end Fig.(2.2)	<i>m</i>
$\Delta H_{NS}$	uncertainty in water head at downstream valve Eq.(A.8)	<i>m</i>
$\Delta K$	uncertainty in water bulk modulus of elasticity Eq.(A.2)	<i>Pa</i>
$\Delta K_e$	uncertainty in pipe entrance minor loss Eq.(A.8)	
$\Delta L$	uncertainty in pipe length Eq.(A.8)	<i>m</i>
$\Delta m$	mass of liquid column	<i>kg</i>
$\Delta P$	pressure rise Eq.(3.101)	<i>Pa</i>

$\Delta P_f$	pressure loss at downstream end of the pipe Eq.(4.6)	<i>Pa</i>
$\Delta P_j$	uncertainty in Joukowsky pressure rise Eq.(3.101)	<i>Pa</i>
$\Delta P_{NS}$	uncertainty in pressure at downstream valve Eq.(A.8)	<i>pa</i>
$\Delta P_R$	uncertainty in pressure at reservoir Eq.(A.8)	<i>pa</i>
$\Delta Re$	uncertainty in Reynolds number Eq.(A.7)	
$\Delta t$	finite-difference time grid step Fig.(3.1) – Fig(3.12)	<i>s</i>
$\Delta V$	change in flow velocity	<i>m/s</i>
$\Delta V_o$	uncertainty in flow velocity	<i>m/s</i>
$\Delta t$	time increment	<i>s</i>
$\Delta X$	finite-difference space step Fig.(3.11) Eq.(3.105)	<i>m</i>
$\Delta x$	finite-difference space step Fig.(3.1) – Fig(3.12)	<i>m</i>
$\Delta \mu$	uncertainty in viscosity Eq.(A.7)	<i>Pa. s</i>
$\Delta \rho$	uncertainty in density Eq.(A.2)	<i>kg/m<sup>3</sup></i>
$\theta$	pipe slop Eq.(2.2)	$^{\circ}$
$\lambda$	constant multiplier in MOC parameter Eq.(3.38)	—
$\mu$	water absolute viscosity Table(4.1)	<i>Pa. s</i>
$\nu$	water kinematic viscosity P89	<i>m<sup>2</sup>/s</i>
$\nu$	Poisson's ratio Table(4.2)	—
$\emptyset$	either flowrate Q or pressure P in Eq.(3.30)	
$\psi$	weighting factor Eq.(2.2) Section(6.2.1)	
$\rho$	water density Table(4.1)	<i>kg/m<sup>3</sup></i>
$\rho_g$	gas density	<i>kg/m<sup>3</sup></i>
$\tau$	effective valve closure time Eq.(4.1)	<i>s</i>
$\forall$	vapour cavity at solution node i Eq.(3.80)	<i>m<sup>3</sup></i>
$\forall$	volume of mixture Eq.(3.82)	<i>m<sup>3</sup></i>
$\forall_i$	volume of cavity at node i Eq.(3.105)	<i>m<sup>3</sup></i>
$\forall_g$	volume of gas Eq.(3.84)	<i>m<sup>3</sup></i>
$\forall_m$	total volume of mixture (liquid & vapour) Eq.(2.1)	<i>m<sup>3</sup></i>
$\forall_v$	vapour volume Eq.(2.1)	<i>m<sup>3</sup></i>

### Subscript

A, B, C, E	nodes labels for solution Eq.(3.6), Fig.(3.2)
i-1,i,i+1	nodes labels for solution Eq.(3.6), Fig.(3.2)
U, Y	non-grid points Chapter 3

## **Superscript**

new      solution time

old      know time

## **Chapter 1**

### **Introduction**

## 1.1 Background

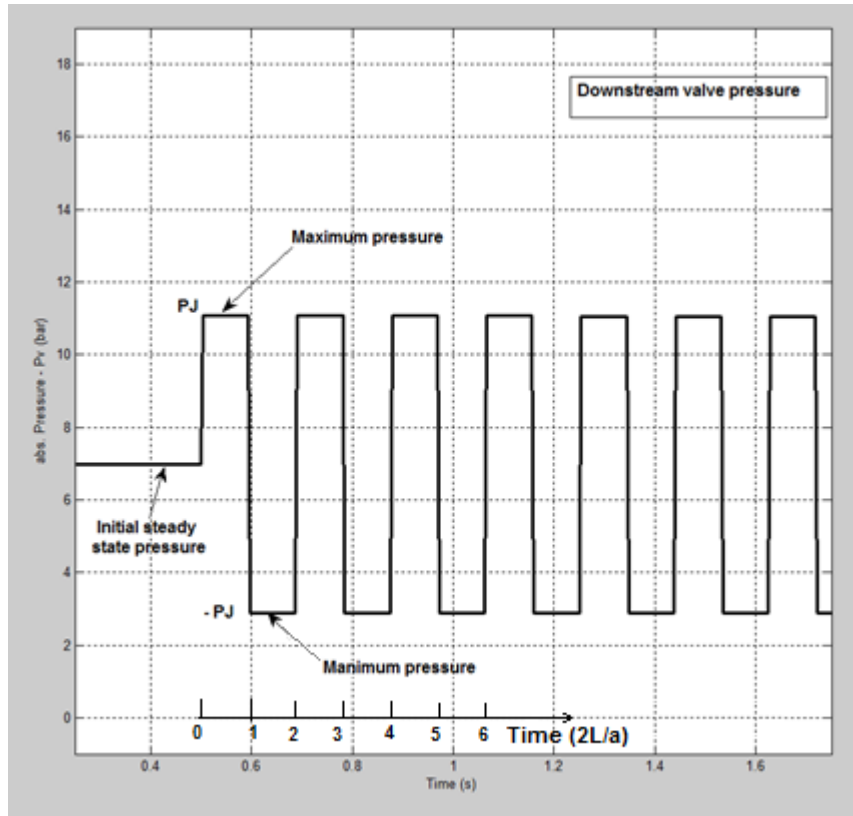
In fully filled liquid pipeline systems, hydraulic transients and waterhammer are often synonyms (Wylie and Streeter 1993). The phenomenon results from relatively rapid changes in flow conditions (Joukowsky pressure  $P_j$ ):

$$P_j = -\rho \cdot a \cdot \Delta V \quad (1.1)$$

where  $\rho$  is liquid density,  $a$  is pressure wave propagation speed and  $\Delta V$  is the velocity change between the final velocity and initial average flow velocity (Wylie and Streeter 1993). For the case of rapid valve closure which stops the flow almost instantaneously,  $\Delta V = -V_o$ , where  $V_o$  is the initial flow velocity as will be considered in the apparatus design for this study. Then Eq.(1.1) becomes:

$$P_j = \rho \cdot a \cdot V_o \quad (1.2)$$

Figure(1.1) shows these pressure changes in a theoretical waterhammer pressure history in time caused by instantaneous valve closure at the downstream valve of an idealised frictionless pipeline. The term waterhammer is a little misleading, because not only water but any liquid may be involved. This phenomenon is well known in terms of causes, Anderson (2008), fluid behaviour, likelihood of resultant damage and also the theories and techniques developed to predict hydraulic fluctuations within the pipe system, with commercial software packages available to be used for design purposes (for example Parmakian 1963; Chaudhry, 1987; Tullis, 1989; Simpson and Wylie 1989; Wylie and Streeter 1993; Swaffield and Boldy 1993; Anderson 2000; Thorley 2004; Ghidaoui et al 2005; Bergant et al 2006; Ellis 2008). It is well known that fluid transients could lead to severe hydraulic load (Wylie and Streeter 1993; Thorley 2004; Anderson 2008), that could damage the pipeline systems (e.g. seals, joints) or could cause leakage or rupture (Sharp and Sharp, 1996), leading to the potential for environmental contamination, reduced revenue and increased risks such as fire hazard if the liquid is flammable.



**Figure(1.1) Theoretical frictionless waterhammer pressure trace at downstream valve.**

The hydraulic transient in a fully filled liquid pipeline system, Figure(1.1), does not only involve high pressure, Eq.(1.3), but also low pressure, Eq.(1.4):

$$P_{\max} = P_R + P_J \quad (1.3)$$

$$P_{\min} = P_R - P_J \quad (1.4)$$

For the condition that Joukowski pressure rise is higher than the initial reservoir pressure  $P_R$ , then as a result of pressure fluctuation the local pressure could drop anywhere along the pipeline to the vapour pressure level to induce a transient cavitation phenomenon in the liquid (column separation). Localised and/or distributed vapour cavities could occur depending on factors like location, pipe profile and flow velocity.

At high points (Simpson and Wylie 1989, Wylie and Streeter 1993, Bergant and Simpson 1999, Bergant et al 2006), liquid columns are susceptible to rupture, i.e. splitting into two liquid columns with a vaporous cavity in between them (typical

column separation). At closed ends (the main focus of this study) the vaporous cavity could initiate between the liquid column itself and the closed valve that acts as the dead end of the pipe. The experimental apparatus used in this research was chosen to be a simple reservoir-pipe-valve system with fixed sloping pipe profile (at almost a half degree upward) and the variation of flow velocity by rapid end valve closure is the only parameter that plays a significant role to initiate a localised vapour cavity with relatively small initial flow rates (but higher than those producing only single-phase waterhammer).

In general, transient-induced cavitation causes two important phenomena. Firstly, any dissolved gases within the liquid are released (Wylie and Streeter 1993, Bergant et al 2006) and secondly, liquid starts to evaporate. The gas and vapour cavities grow locally within the liquid column. Their size and extent is dynamically driven by the inertia of the adjacent moving liquid columns. Usually the cavitation regions grow, shrink and collapse repeatedly (Adamkowski and Lewandowski 2012), until fluid friction damping brings the fluctuations to rest (i.e. final steady state which would be equal to the upstream pressure or head). In some situations, subsequent collapse of the first vapour cavities to appear could generate a rapid rise in pressure higher than the theoretical maximum Joukowsky pressure due to superposition of reflected pressure waves (Martin, 1983).

It can be seen from the literature that the study of waterhammer is a mature science but accidents still occur. Certain aspects continue to demand further investigation and reliable predictive modelling for design purposes of column separation is one of these (Anderson 2008).

### **1.2 Study Aims and Objectives**

In this investigation the objective is to evaluate approaches to relatively simple models that are easily incorporated into existing one-dimensional flow waterhammer software and which can be shown to give reliable predictions over the range of transient behaviours known to occur. The focus is on simple numerical modelling that provides reliable and accurate prediction of column separation for the different column separation behaviours that can be produced physically on a simple reservoir-pipe-valve apparatus. Real systems will be more complex, but this simple system

eliminates modelling error for other components and, also, any model that cannot represent such a simple system is unlikely to represent more complex ones.

The present work builds primarily on two previous studies, by Bergant and Simpson (1999) at Adelaide University and by Arfaie (1989) here at Newcastle University:

- Bergant and Simpson (1999) compared the two most widely used modelling approaches, the Discrete Vapour Cavity Method (DVCM) and Discrete Gas Cavity Method (DGCM), with their experimental results. The present aim is to repeat their study but using a different experimental rig and a wider range of column separation behaviours (as introduced by Arfaie, 1989).
- However, Arfaie (1989) and Anderson and Arfaie (1991) had suggested three further modelling issues not really addressed by Bergant and Simpson (1999). The previous work at Newcastle University suggested that some models of column separation perform well, but only for a limited range of types of column separation behaviour (Arfaie 1989). In addition, Arfaie (1989) suggested an improved internal boundary condition for the column separation interface, as well as suggesting that incorporating greater damping (unsteady friction) could improve models. The present aim is to explore these three issues further.

To support this objective, experimental hydraulic transient induced column separation will be conducted on an apparatus (reservoir-pipe-valve system) in order to investigate cavitation at the downstream valve. Physically the hydraulic transient is generated on the upstream side of the valve by a rapid valve closure (operated manually in this experiment). With valve closed completely before the reflected wave returns to the valve, the valve closure time  $\tau$  was measured to be about 16ms, Figure(4.6). This value is less than the theoretical fast valve closure time of approximately 100ms (Parmakian 1963):

The reservoir-pipe-valve system was deliberately chosen to provide simply modelled upstream and downstream pipe boundary conditions, so that modelling deficiencies must be associated with modelling of column separation.

The experimental work will be mainly to provide data with which to compare various column separation models, but it will also support preliminary investigations of under what circumstances pressure wave reflection can lead to a maximum pressure higher



than Joukowsky (Martin 1983). To facilitate interpretation of what physically occurs, the behaviour of column separation will be captured through a transparent polycarbonate section of the pipe at the downstream valve using a synchronised high speed camera.

### 1.3 Outline of Thesis

Chapter 2 presents a literature review that covers the topics and latest published work relating to the study of waterhammer-induced column separation and which informs the modelling aspects chosen to be investigated in this study.

Chapter 3 describes the theoretical background for modelling waterhammer induced column separation with a focus on the widely used Method of Characteristics (MOC) solution technique. MATLAB codes were developed to solve the governing equations for validation with experimental results of both waterhammer and column separation runs.

Chapter 4 covers the experimental part of this research. It describes the experimental apparatus, with experimental results for single-phase waterhammer and two-phase column separation modes. In addition, this chapter shows the visualisation of column separation modes synchronised with their pressure history to capture the development stages of the cavities through the transparent polycarbonate section using a high-speed camera.

Chapter 5 provides a rationale for the classification of experimental column separation behaviours (operational map), supported by graphical representation for the wave reflections (facilitated by the simple apparatus layout).

Chapter 6 addresses the issues of comparison of combinations of column separation models and unsteady friction models against experimental results which cover all the column separations behaviours observed on the apparatus.

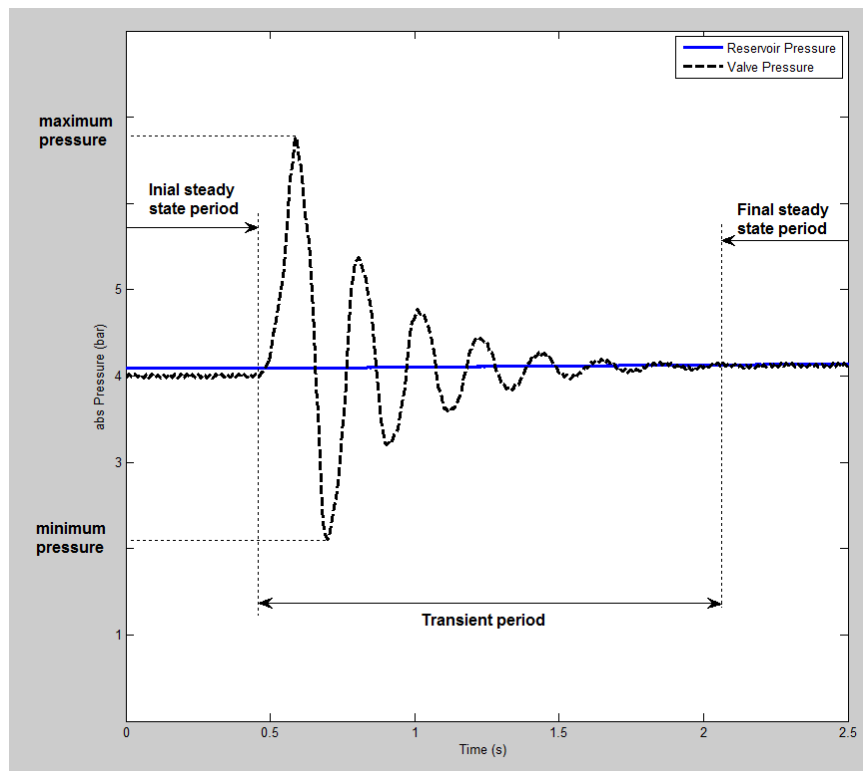
Chapter 7 identifies the limited conclusions that can be drawn from the study and suggests how further progress might be made to overcome these limitations.

## **Chapter 2**

### **Review of Modelling Waterhammer Induced Column Separation**

Pressure transients in fully filled liquid pipeline systems do not only involve high pressure, but also low pressure Figure(2.1). Severe hydraulic transients in pressurised pipe could put the systems at a high risk of damage (e.g. pipe leak, pipe collapse, pump or valve break) (Anderson 2008), that might be a consequence of at least one of hydraulic-transient associated phenomena (e.g. vapour cavitation, column separation or release of dissolved gas).

If the absolute local pressure drops to vapour pressure level anywhere along the pipeline (depends on the location, pipe profile, and flow conditions), this could induce cavitation. These phenomena are still an area of interest in both fields, experimental and mathematical modelling, with need for better understanding and attempts to improve existing models (Bergant et al 2006, Anderson 2008).



**Figure(2.1) Illustrative diagram of hydraulic transient measured at downstream valve of reservoir-pipe-valve system.**

### 2.1 Historical review of waterhammer and transient behaviours

There is a rich literature and interesting resources (e.g. Ghidaoui et al 2005, Bergant et al 2006, Anderson 1976, Anderson 2000, Tijsseling and Anderson 2004, 2007, 2008) providing historical development of waterhammer and column separation in pipeline systems. Fundamentals and basics of waterhammer analysis and column

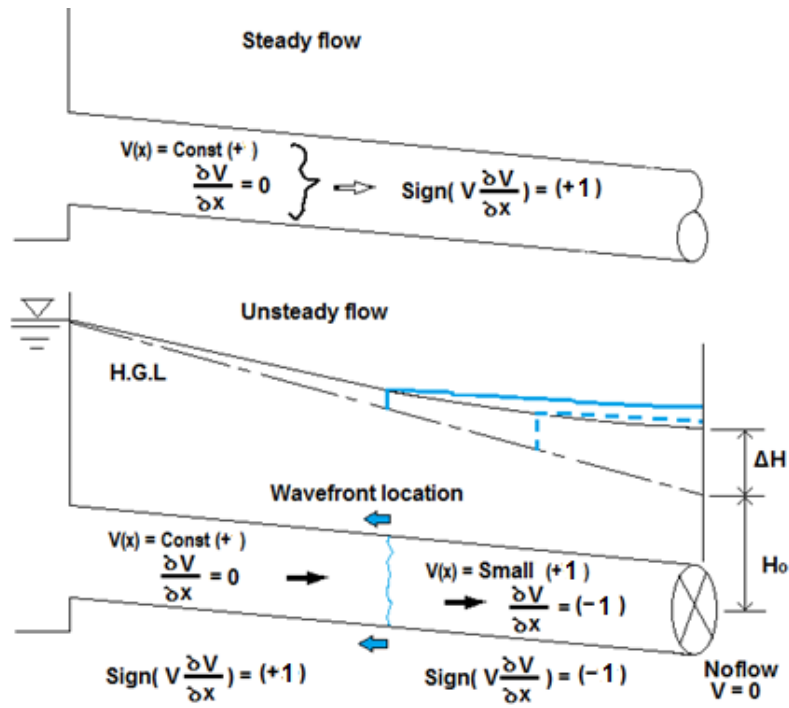
separation can be found in textbooks (e.g. Parmakian 1963, Tullis 1989, Wylie and Streeter 1993, Swaffield and Boldy 1993, Thorley 2004, Chaudhry 1987). According to Bergant et al (2006), by the use of computers since the 1960s comprehensive investigations have been conducted on column separation models. This started in Belgium at Lie`ge by Thibessard (1961) then in USA by Streeter and Wylie (1967), Baltzer (1967a,b) and Weyler (1969), and Vreugdenhil (1964) and Siemons (1967) in the Netherlands (Bergant et al 2006). The International Working Group of the IAHR conducted a major research on column separation in industrial systems during the period 1971–1991. One of the main aims of the Group was the development of computer codes with validation against well documented experimental results.

## **2.2 Liquid pipelines and transient behaviours**

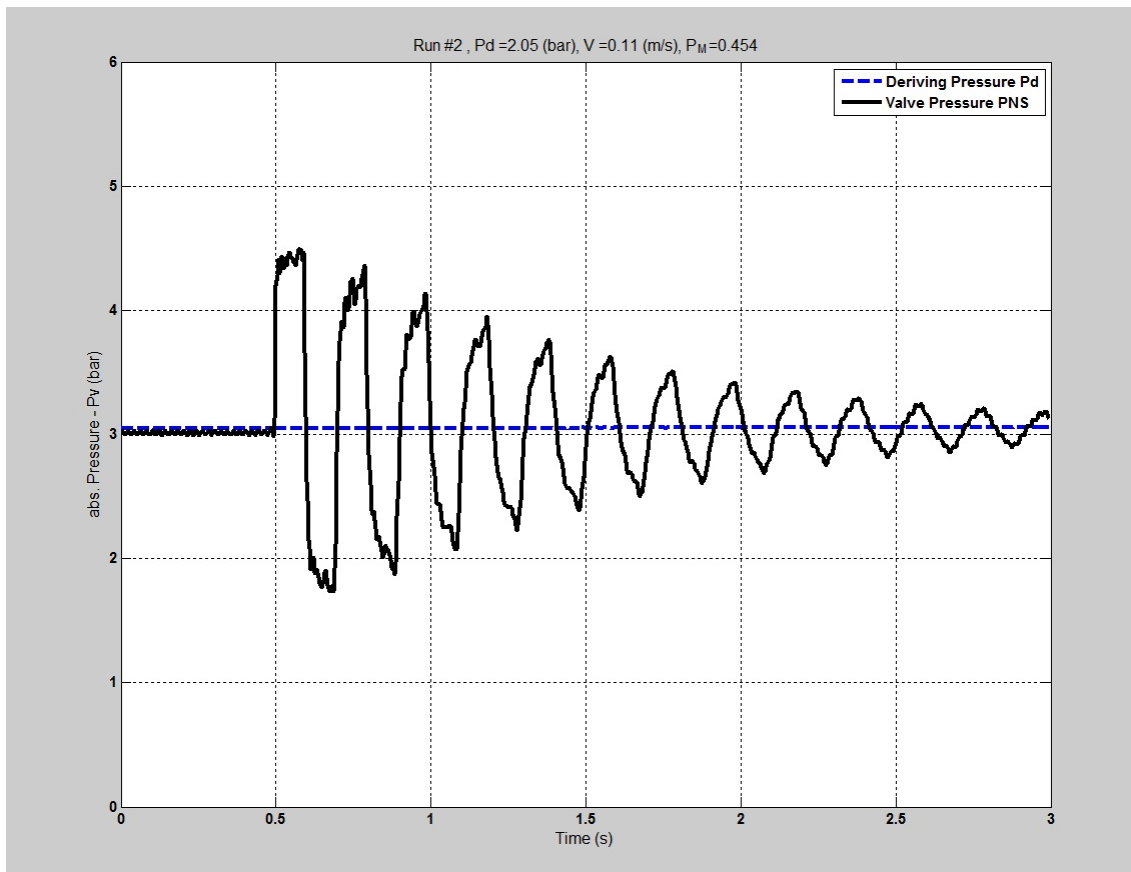
Generally, water pipeline systems from the economical point of view are operated to their maximum allowable pressure. Humans' everyday activities as well as the typical life style, influence changes in flow demand that cause pressure fluctuations which in most cases are manageable by design, for example Figure(2.1). However, in case of emergency and unplanned events related to changes in flow velocity (hydraulic transients) that are caused by any operational accident (e.g. pump failure, power cut, pipe rupture or rapid valve actuation), the consequence could lead to big and rapid changes in local pressure and flow direction (waterhammer pressure waves), Figure(2.2), in short times as small as few seconds. These scenarios of big changes (e.g. instantaneous flow stoppage) caused by valve closure provide pressure waves (Joukowsky pressure, Eq.(1.1) traveling in the pipeline, i.e. propagating forward and backward along the pipeline (Wylie and Streeter 1993) at the speed of sound in the working fluid. This happens on both sides of the transient source (Swaffield and Boldy 1993, Thorley 2004).

### **2.2.1 Waterhammer behaviours**

Hydraulic transients in liquid pipeline systems could cause one of two different types of transient flow regimes. The first mode is referred to as the waterhammer regime (single-phase waterhammer), Figure(2.3), in which for the period between the initial and the final steady state, the minimum of fluctuated pressure remains above the vapour pressure of the liquid (Parmakian 1963).



Figure(2.2) Unsteady flow in reservoir-pipe-valve system.



Figure(2.3) Experimental waterhammer pressure wave at downstream valve.

However the pressure difference between Joukowsky pressure and the upstream reservoir pressure plays the major role in how severe the transient will be. If the reservoir pressure is higher than the Joukowsky pressure, single-phase would be

dominant; on the other hand if the reservoir pressure is less than Joukowsky pressure the cavitation flow regime would be dominant. So, the second mode of hydraulic transient is the cavitation regime (Simpson and Wylie 1989) at some locations (e.g. high points or knees profiles), where the minimum of the fluctuated pressure drops as low as the liquid vapour pressure (waterhammer induced cavitation). Then cavitation could occur, after a period of time ( $t = 2L/a$ ) from the instant of valve completely closed (Simpson and Wylie 1989), depending on the initial flow velocity. Then the rarefaction wave starts at the valve pulling the liquid column back towards the reservoir, until this reverse motion stops because of the pressure difference between the reservoir and the vapour cavity (Tullis 1989). If this happened in sufficient time (while the rarefaction wave has not reflected back yet towards the valve as a pressure wave), this could bring the local minimum pressure to the level of vapour pressure (at close to ambient temperature). Then air may be released from the liquid in the form of microbubbles and water is evaporated to fill-in air bubbles that were already initiated and vapour cavities expand in size. One of three situations might happen; localised cavitation at the downstream end, distributed cavitation or a combination of both along the pipe (Simpson and Wylie 1989, Bergant et al 2006).

Theoretically, the cavity is assumed to fill in the entire cross section of the pipe, consisting almost only of vapour at the vapour pressure of the working liquid. This cavity is assumed to separate the water column into two single-phase liquid water columns, or to separate the water column from the dead end (downstream valve) (Pejovic et al 1987, Tullis 1989, Wylie and Streeter 1993, Chaudhry 2014).

While the pressure wave reflects back ( $t > 2L/a$ ), the water column starts to reverse its direction towards the downstream valve causing collapse of cavities (Tullis 1989). This collapse could lead to increase of local pressure significantly to the theoretical maximum pressure (Joukowsky pressure) (Simpson and Wylie 1991), and as a consequence, it may cause damage to the pipeline system. Nowadays, risk and hydraulic transient analyses are carried out during the design stages of pipe systems in order to guarantee safety in the operational activity (Anderson 2008). Scenarios of major hydraulic transient induced column separation in water pipeline systems was and still is an active area of interest for researchers worldwide in both experimental and mathematical modelling (Ghidaoui et al 2005, Bergant et al 2006).

Not all pressure transients are dangerous. Experimentally classification is needed to distinguish the high risk cases. In their experimental work, Bergant and Simpson (1999) proposed a classification of column separation (active or passive), based on whether overpressure rise exceeds the theoretical maximum pressure (Joukowsky pressure) in the pipe for rapid valve closure.

In this study, behaviour of waterhammer pressure waves induced cavitation is investigated experimentally on a reservoir-pipe-valve system, Figure(4.1), where rapid valve closure is the source of the pressure transient, in order to investigate experimentally the range of flow behaviour and also to test fitness of numerical models of transient cavitation and unsteady friction. The models were chosen from the literature for both distributed and localized cavitation at the upstream side of the rapid closing valve.

Martin (1983), considered the upstream face of the fast closure valve in a reservoir-pipe-valve system, Figure(4.7). If the flow was stopped almost instantaneously at the downstream valve, as it will be in this apparatus, Figure(4.2), both upstream reservoir and the downstream valve work systematically as boundary conditions to reflect back the pressure waves, where the downstream valve works as a dead-end (Parmakian 1963). In all systems, pressure waves attenuate because of energy dissipations toward the final reservoir static head eventually.

### **2.2.2 Cavitation and column separation**

The effect of severe hydraulic transients in pressurised water pipeline systems does not only come from high pressure but also from low pressure leading to cavitation anywhere along the pipeline. Fundamentally, three requirements are essential for transient cavitation to occur in liquid pipelines; nuclei in the liquid or on the pipe wall, local pressure drops to vapour pressure, and the ambient pressure around the cavity is high enough leading to cavitation collapse (Tullis 1989).

As has been mentioned before, dissolved gases are released in cavities as a resultant of the negative pressure wave (rarefaction wave) that could drop the local pressure to sub-atmospheric (Chaudhry 2014). If there were considerable free air content in the liquid, or the cavitation process was slow enough, allowing more gas release, then the rate of growth and collapse of those cavities are slower because of free air content and consequently the process is not as damaging.

Two types of vapour cavities can be distinguished (Simpson and Wylie 1989, Wylie and Streeter 1993, Bergant et al 2006): local and distributed vapour cavities. The differentiation parameter between these two types was the vapour void fraction ( $\alpha_v$ ), that is defined as the ratio of the volume of the vapour ( $V_v$ ), to the total volume of the mixture (liquid & vapour) ( $V_m$ ):

$$\alpha_v = \frac{V_v}{V_m} \quad (2.1)$$

For local vapour cavities, the vapour void fraction is almost equal to unity ( $\alpha_v \approx 1$ ), while it is very small in the case of the distributed vapour cavity ( $\alpha_v \approx 0$ ). The pressure wave propagation speed in rigid (e.g. steel) water pipelines is usually, for simplicity, assumed to be constant in engineering analysis ( $\approx 1200 \pm 200$  m/s). Pressure wave speed is function of both characteristics of the pipe and the working fluid (e.g. cross section, density, bulk modulus and elasticity) (Wylie and Streeter 1993, Thorley 2004), but depending on dissolved-gas content, with excess of its content reducing the propagation speed.

As a result of the rarefaction wave in horizontal pipelines or pipes having small slopes, a thin cavity (localised) may be formed near the top of the pipe just adjacent to the pipe end, or it could appear at high points along the pipeline (Wylie and Streeter 1993). Moreover, series of these cavities could be formed, and extended over a long distance of the pipeline (distributed cavities). The cavity in liquid pipelines may become as large as to fill the entire cross section of the pipe and thus divide the liquid into two columns (Wylie and Streeter 1993, Bergant et al 2006, Chaudhry 2014). This is usually connected with changes in pipe profiles, for example steep slopes or knees or at dead ends (Malekpour and Karney 2014). In papers by Arfaie (1989) and Anderson et al (1991), three categories of cavitation have been suggested to represent water column separation related to the cavity duration: limited, intermediate and severe water column separation. Interestingly among these, the intermediate is that characterised with pressure rise higher than the Joukowsky pressure which will be investigated graphically and experimentally.



## **2.3 Experimental waterhammer induced column separation**

Bergant et al (2006) and Ghidaoui et al (2005) reviewed practical and experimental work of researchers worldwide on liquid pipelines for the phenomenon of hydraulic transient induced cavitation (column separation) in various liquid pipeline systems, seeking better understanding of the phenomenon and also to enable the possibility of improvement to the available techniques (Anderson and Arfaie 1991, Simpson and Bergant 1994a). This field of waterhammer in laboratory still attracts researchers worldwide inducing column separation on either sides of a fast acting valve, Figure(2.4), Bergant et al (2006).

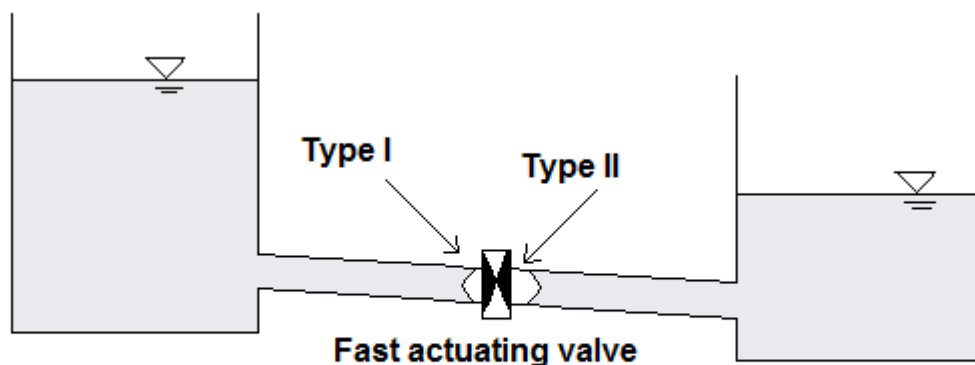
### **2.3.1 Choice of boundary conditions and apparatus design**

Martin's (1983) simple water pipeline system consisted of an upstream reservoir, pipeline and downstream fast acting valve, Figure(4.1), running at steady state operation before the hydraulic transient event took place at the far end valve. Typically (Parmakian 1963, Simpson and Wylie 1989, Wylie and Streeter 1993), it would cause pressure fluctuation between the maximum pressure (theoretical Joukowsky pressure) and the minimum pressure, which could drop to reach the level of vapour pressure at the liquid temperature. Martin (1983) investigated the case of limited column separation along the pipeline with four pressure transducers installed at equal distances along the pipe (i.e.  $\frac{1}{4}$ ,  $\frac{1}{2}$ ,  $\frac{3}{4}$  and 1 of the pipe length). Martin (1983) argued the pressure spikes are due to superposition of collapse of at least two vapour cavities and one cavitation adjacent to the downstream valve.

According to the literature, there are two typical systems of apparatus. The first is a simple fixed design reservoir-pipe-valve system (e.g. Martin 1983, Simpson and Wylie 1989, Anderson et al 1991), where the transient is initiated by rapidly closing the downstream valve. The hydraulic transient develops in the pipeline, pressure waves of the values of Joukowsky pressure propagate upstream from the valve and reflect back at the reservoir boundary, i.e. between the two boundary conditions: the constant pressure (upstream reservoir) and the constant no-flow (downstream closed valve) that progresses to a constant vapour pressure. After  $2L/a$  from the instant of closure the pressure-wave reflected at the upstream reservoir as a rarefaction wave may bring the local minimum pressure at the valve to the level of vapour pressure for the case of cavitation. When this occurs, it changes the boundary condition at the closed valve from constant velocity (no flow) to constant pressure (vapour pressure).

The other experimental setup is described by Simpson and Bergant (1994b) as a flexible system that consists of two reservoirs connected with a pipeline in between with a fast closing valve that could be flexibly allocated at either end of the pipeline or at the middle of the pipeline, Figure(2.4), in order to simulate hydraulic transient and subsequent column separation of various systems (e.g. pumping system, gravitational system). Cavitation might occur on either side of the valve with the option of flow reversal (Swaffield and Boldy 1993); also the column separation could be reached at low operating pressures.

Swaffield and Boldy (1993) mentioned some practical work on simulation by the introduction of the method of characteristics of column separation following hydraulic transients caused by pump failure and valve actuation by Richards (1956), Brown (1968) and Duc (1959), who provided photographs of cavitation cycles following pump failure. Then the general interest was shifted to study column separation on both sides (upstream/downstream) of the fast acting valve (Swaffield and Boldy, 1993). Swaffield (1970), Weyler et al (1971), Safwat and De Kluyver (1972), Safwat and Van Den Polder (1973) and Martin (1983) studied the case of upstream valve closure; their results showed reasonable agreement with the experimental data for the first cycle of the cavity. In the last five years, some researchers studied column separation downstream of the valve (e.g. Adamkowski and Lewandowski 2012, Autrique et al 2012, Himr 2015); they utilized high speed camera to provide a series of photographs of the cavitation cycles.



**Type I : Column separation occurs at the downstream valve.**

**Type II : Column separation occurs at the upstream valve.**

Figure(2.4) Illustrative diagram of localized column separation occurring upstream and downstream of the fast actuating valve in pipe system (Swaffield and Boldy, 1993, p174).

### **2.3.2 Visualization and results representation**

Following work done by Arfaie (1989) photographing the column separation phenomenon on the same apparatus (reservoir-pipe-valve system), Figure(4.1), this is taken further. A high-speed camera was synchronised with the pressure transducers data recording to capture the cavitation process alongside the pressure history at the valve, through the polycarbonate section of the pipe, Figure(4.2). Different transient behaviours were recorded successfully and will be presented in Section(4.5). Arfaie (1989) presented photographs of intermediate cavities and bubbles (Arfaie 1989) which are much longer compared to the ones that were captured in this study, Figure(4.19) and Figure(4.21). However, the overall appearance of the photograph by Arfaie (1989) is rather similar to the typical column separation observed Figure(4.19). The images from the high-speed camera show no evidence of big vaporous bubbles occupying the pipe cross section (within the expected column separation region close to the valve).

Several researchers have attempted to provide their interpretations of column separation behaviours. Based on experimental results dimensionless parameters have been used to characterise their experimental results for better understanding of water column separation. Recently, Autrique et al (2012), defined a ratio between the Joukowsky head pressure and the initial absolute head. This is the same parameter Anderson et al (1991), in attribution to Martin (1983), expressed as Martin pressure  $P_M$ . Also, Autrique et al (2012) also utilised the ratio between the maximum overpressure and the Joukowsky pressure, and finally, the relative duration of vapour cavity existence to the pipeline period, which is agreed by all researchers as one of the significant parameters used to describe column separation.

In this study, a new representation of the experimental results will be introduced in the form of an operational map on which all modes of transient behaviour are plotted and classified and segregated into clear zones, Figure(5.1), Figure(5.5) and Table(5.3). As Martin (1983) pointed out, this region is particularly important because the Joukowsky pressure ceases to be a conservative criterion of peak pressure. Arfaie (1989) overestimated the extent of this transient mode with his “low and medium cavity” identified in the wider range of 1 – 3 of Martin pressure based on a smaller sample of only 18 experimental runs.

Arfaie (1989) and Anderson et al (1991) explained graphically a sample of their experimental results on the reservoir-pipe-valve system. On the distance time plane, the mechanism of a limited column separation could be established utilizing the characteristic lines. The initial valve closure causes a series of propagation and reflection of waterhammer waves, which are then superimposed by the propagation and reflection of a second series induced by the pressure wave resultant from the collapse of the first cavity. The combination successfully predicted the first pressure spike. Bergant et al (2006) explained the duration of the pressure spike using the water hammer model for the frictionless case. Recently, Autrique et al (2012), applied the same graphical explanation, proposed by Anderson et al (1991), for their experimental results of the case of closure of an upstream valve of a two-reservoir-valve-pipe system. Although the group graphically managed to match the first pressure spike, enforcing matching the duration of the second cavity and the following pressure spikes has been achieved only at the expense of a variable pipeline period.

## **2.4 Modelling 1-D waterhammer induced column separation**

### **2.4.1 *Waterhammer equations and MOC***

The importance of modelling waterhammer and column separation is the ability of the model to accurately predict the peak pressure and more credit is paid to the model if the overall features (i.e. the pressure peaks, attenuation of pressure traces and cavity duration) agree with measurement. Of course, limitations and assumptions are needed for the analysis, e.g. the flow is limited to one-dimensional analysis, the pipe is considered a straight uniform element without lateral inflow or outflow, its length fully filled with water all the time, water is effectively incompressible and homogeneous (Parmakian 1963). Any changes in temperature and density are negligible. The water column may not match the pipe length in some cases (Thorley 2004), where cavities occupy parts of the pipe causing column separation. Also the pipe walls are considered to be effectively rigid (Parmakian 1963), giving the assumption that keeps the cross sectional area constant regardless of the pressure increase. Both the cross sectional distribution of velocity as well as the pressure is considered to be uniform with changes felt immediately across the pipe section.

Notwithstanding these approximations, along the pipe pressure and velocity changes propagate at the finite speed of sound in water.

Waterhammer equations which include both continuity and x-momentum (Chaudhry 1987, Wylie and Streeter 1993, Bergant et al 2006) can satisfactorily describe the hydraulic transient behaviour of a pressurized liquid in a closed conduit. The waterhammer equations are commonly presented in the form of head and flow velocity dependent variables (Wylie and Streeter 1993).

$$\frac{\partial H}{\partial t} + V \frac{\partial H}{\partial x} - V \sin \theta + \frac{a^2}{g} \frac{\partial V}{\partial x} = 0 \quad (2.2)$$

$$g \frac{\partial H}{\partial x} + \frac{\partial V}{\partial t} + V \frac{\partial V}{\partial x} + \frac{fV|V|}{2} = 0 \quad (2.3)$$

Any disturbance induced in the flow is propagated at the speed of sound which strongly influences the dynamic response in the pipeline (Chaudhry 1987, Wylie and Streeter 1993). The elastic wave speed corresponds to the transient storage capacity of the fluid compressibility and pipe hoop and axial deformation:

$$a = \sqrt{\frac{K/\rho}{1 + \left(\frac{K}{E}\right)\left(\frac{d}{e}\right)}} \quad (2.4)$$

E is Young's modulus of elasticity of the pipe wall material; K is fluid bulk modulus of elasticity;  $\rho$  is fluid density; d is pipe internal diameter and e is pipe wall thickness.

Generally, waterhammer equations are classified as hyperbolic and rarely to be solved analytically (Ghidaoui et al 2005). Therefore different numerical techniques are used to provide approximate solutions for head and velocity, including finite difference (FD) schema, finite volume (FV) method, the finite element (FM) method and the method of characteristics (MOC). The most desirable has been seen as the Method of Characteristics (MOC) (Wylie and Streeter 1993, Ghidaoui et al 2005), not only because of its simplicity and computational efficiency but also because it reflects the underlying wave propagation nature of the waterhammer phenomenon. Therefore

MOC is adopted in this study for predicting pressure fluctuation with features of cavitation and column separation.

To adopt MOC in the analysis (Wylie and Streeter 1993), there is a necessity to transform the waterhammer partial differential equations to ordinary differential equations that can be integrated easily along the two compatibility equations valid along the characteristic lines, Figure(3.1), and used to obtain the unknown head and velocity at each computational node. Boundary condition equations are derived in the same manner (full derivations are presented in Chapter 3).

### ***2.4.2 Models of liquid column separation at a boundary***

The development of a successful model that can represent waterhammer induced cavitation has been an area of interest worldwide for the last century, and the challenges still exist for better understanding and possible improvements (Ghidaoui et al 2005, Bergant et al 2006). According to Bergant et al (2006), Angus in 1935 and 1937 introduced a mathematical model of single vapour cavity at a boundary using the graphical method for a pump failure model on the discharge side of a check valve near to the pump. After the cavity formed and expanded, the liquid column returned back to the closed valve and the resultant pressure record was found almost four times the normal pressure. According to Arfaie (1989) and Bergant et al (2006), an example of the formation of a cavity at a valve was presented by Bergeron in 1939 and 1950 on a reservoir-pipe-valve system with friction losses included in the graphical analysis. Bergeron assumed the vapour pressure in the cavity at the liquid temperature was dominant instead of the barometric vacuum and he gave a description of cavity growth and collapse using the continuity equation; the pressure wave speed was assumed constant.

### ***2.4.3 Discrete vapour cavity model (DVCM)***

From the literature, the most popular technique for modelling waterhammer induced column separation is the Discrete Cavity Model (Bergant et al 2006) that includes both discrete vapour cavity (DVCM) and discrete gas cavity (DGCM). Bergant et al (2006) mentioned that DVCM is the most commonly used model for simulating column separation and distributed cavitation in conduits. The principle mechanism of DVCM states that, when the local pressure reaches the vapour pressure, the fluid

column breaks itself to form a cavity. These cavities are concentrated at the computational nodes and the model assumes that the cavity occupies the cross sectional area of the pipe, which is filled with liquid vapour. The pressure stays at vapour pressure  $P_v$  until the cavities collapse, then the computation returns to normal waterhammer analysis as a single-phase liquid is assumed and constant pressure wave speed is maintained between computational nodes.

This model has been adopted in this study as the basic model; these conditions were employed in a MatLAB code, which is capable to predict any behaviour of transient mode (waterhammer, limited and severe column separation). Wylie and Streeter (1984), Tullis (1989) and Wylie and Streeter (1993) have described DVCM in detail. Moreover Wylie and Streeter (1984, 1993) provided FORTRAN codes for modelling column separation in a simple pipeline system.

Anderson and Arfaie (1991) suggested an improvement to the DVCM at the cavity and liquid interface for better prediction of the cavitation behaviour. For the computational reach ( $\Delta x$ ) in which the moving interface occurs, rigid column theory (including inertia and friction) is combined with the MOC, resulting in an apparently variable wave speed at the internal boundary. Based on the conventional assumption the cavity occupies the full cross-section of the pipe, the variable wave speed is estimated from the computed length of the vapour cavities in each segment. Arfaie (1989) tested this with the DVCM model and showed it could improve it, but did not extend it to the DGCM model.

### **2.4.4 Discrete gas cavity method (DGCM)**

The other principle technique of discrete cavity method assumes a small amount of free gas in the liquid for modelling column separation in liquid pipelines. Simpson and Bergant (1994a) mentioned that the discrete gas cavity model was introduced by Provoost and Wylie (1981). The model generally states that water is a liquid which almost always contains dissolved gases in a state of solution, although the fraction volume of the gases is tiny compared to the liquid (Wylie 1984, Wylie and Streeter 1993). At constant temperature the concentration of dissolved gas is directly proportional to the partial pressure of the gas as stated by Henry's law. During the hydraulic transient in liquid pipelines, pressure fluctuates between maximum and minimum. If the local pressure is lowered for enough time to sub-atmospheric (i.e.

saturation pressure), gas bubbles initiate, grow and randomly distribute in pipe segments during the rarefaction wave period. But when the pressure starts to rise, the rate of absorbing the gas bubbles back into solution is not enough, allowing bubbles of free gas to remain as a result of the slower reverse process.

Existence of small amounts of free gas in liquid (gas–liquid mixture) has a big effect on the wave propagation speed (Bergant et al 2008a). The wave speed in a gas–liquid mixture  $a_m$  Eq.(2.5) is a replacement of the wave speed  $a$  in single-phase liquid Eq.(2.4).  $a_m$  is pressure dependent and generally significantly lower than for the case of single-phase liquid:

$$a_m = \sqrt{\frac{a^2}{1 + \frac{\alpha_g a^2}{g(H - Z - H_v)}}} \quad (2.5)$$

For modelling hydraulic transients with existence of free gas, Wylie and Streeter (1993) suggested a simplified discrete gas cavity model for the free gas bubbles which are assumed to be distributed homogenously in the liquid as a mixture, Figure(3.10). During waterhammer pressure fluctuations, when the local pressure is reduced to the vapour pressure, large gas volumes may exist at computing sections (Wylie and Streeter 1993), as long as the gas volume is smaller in size than the reach volume (Wylie and Streeter 1993). The free gas is lumped together at the computational nodes. As a result of pressure fluctuation, each isolated gas cavity expands and contracts isothermally according to the perfect gas law, and between gas cavities there are pure liquid columns without gas. The model gave good agreement with the experimental results (Wylie and Streeter 1993). Waterhammer equations for unsteady liquid flow are valid when the pressure is above the liquid vapour pressure and the effect of lumped free gas on pressure wave speed is matching that of a distributed gas-liquid mixture. Dalton's law states that total absolute pressure is equal to the summation of gas component partial pressures (Wylie and Streeter 1993).

DGCM is similar to DVCM in the way of using waterhammer compatibility equations, but with the addition of the gas volume continuity equation plus the ideal gas law (isothermal process). Wylie (1984) and Wylie and Streeter (1993) provide details of



derivation for the two reservoirs-pipe-valve system, in addition to a FORTRAN code for this case, with limited amount of free gas and void fraction as small as  $\alpha_g \leq 10^{-7}$  (Wylie 1984, Wylie and Streeter 1993). This model has been adopted in this study as an alternative model for comparison with DVCM. Full derivations of the governing equations are presented in Chapter 3.

#### **2.4.5 Unsteady friction**

The friction term in the momentum equation may be divided into steady and unsteady parts. Modelling pressure fluctuation during hydraulic transient using quasi-steady state friction resistance evaluated by Darcy-Weisbach can give acceptable prediction of the first pressure peak (Chaudhry 2014) as well as the following down-pressure of the waterhammer cycles but however can lose the pattern of predicting energy dissipation. Without taking into consideration the part of unsteady friction, the mathematical modelling can show slow energy dissipation over the period of transient compared with the experimental results, Figure(4.15), and therefore accurate modelling of complex cases, for example, waterhammer induced gas release and column separation, could not be achieved. From the literature, several techniques have been proposed and developed for evaluating unsteady friction within the waterhammer equations, attempting to correctly predict pressure oscillations (Chaudhry 2014). These techniques could be classified in three categories: (a) the quasi-2D method, (b) the convolution integral method and (c) instantaneous acceleration based methods (IAB).

##### **(a) Quasi Two Dimensional method**

The quasi-two-dimensional method was adopted in some literature (e.g. Vardy and Hwang 1991; Brunone et al 1995; Silva-Araya and Chaudhry 1997; Pezzinga 1999; Zhao and Ghidaoui 2004), where the cross sectional velocity profile is taken into account. In this technique, that increases the computation time, the limitation for practical usage is just for simple transient applications.

##### **(b) Convolution Integral method**

The convolution integral method (Chaudhry 2014) was introduced in 1968 by Zielke. Primarily, it was a development for the exact solution of the laminar unsteady friction of one-dimensional flow, using past local accelerations and weighting functions. The solution is time consuming (Chaudhry 2014) and requires large computer memory.

Improvement of Zielke's method with economical use of memory at the cost of accuracy have been proposed by Trikha (1975), Kagawa et al (1983), Suzuki et al (1991), and Schohl (1993). Vardy and Brown (1995, 2003 & 2004) extended the analyses to cover turbulent flow for smooth and for rough pipes. Because of the approximation of the convolution integral by a limited number of weighted coefficients (Vitkovsky et al 2006b), these solutions provide acceptable results at the expense of numerical accuracy.

### **(c) Instantaneous Acceleration Based methods (IAB)**

The instantaneous acceleration based methods are founded on the assumption that the damping of pressure waves is attributed to the unsteady friction influenced by both instantaneous local and convective accelerations. The accelerations are computed based on the average cross sectional values without taking into consideration the velocity distribution at a cross section. This method has been recognized as more rapid in computational time (Storli and Nielsen 2011). It was introduced in 1959 by Carstens and Roller (Chaudhry 2014). Since then several different formulations have been proposed (Brunone and Golia 1990, Brunone et al 1991ab, Vardy and Brown 1995, Bughazem and Anderson 2000, Bergant et al 2001, Vardy and Brown 2003, Ramos et al 2004, Vitkovsky et al 2000, 2006a). Reddy et al (2012) presented a Genetic Algorithm to estimate decay coefficients (both the one and two coefficient models) for IAB models that appears to give satisfactory results. Their analysis was based on investigation of experimental results for pressure transient histories following instantaneous valve closure at the upstream and downstream side of the valve, conducted on simple pipe systems in 14 laboratories worldwide. Their pipe materials include steel, copper and PVC, with pipe lengths varied between 14 – 160m and internal diameter ranges between 12 – 400mm.

In this study, for simplicity and easy implementation the one coefficient IAB technique has been adopted to provide the necessary unsteady friction for modelling waterhammer induced column separation as was suggested by Arfaie (1989). Bughazem and Anderson (1996) and Bughazem (1997) investigated unsteady friction on the apparatus used in this study and the group have demonstrated that (Bughazem and Anderson 2000), with an appropriate choice of unsteady friction coefficient ( $k$ ), variants of the Brunone (1991b) unsteady friction model could give very good representation of waterhammer behaviour including pressure wave

attenuation for this particular apparatus. However, the “best” unsteady friction coefficient (i.e. that giving the best comparison between experiment and calculation) was strongly dependent on the actual finite difference implementation of Brunone’s model. Consequently, it was decided to exploit this previous work at Newcastle and to use both the implementation tested by Bughazem (1997), which was known to give good correlation, as well as a variant he suggested (Bug hazem and Anderson 2000) but did not actually test, presented in Section(3.3.1).

### 2.5 Closing Remarks

In conclusion, a number of guidelines to be used in this study have been drawn from this literature review and these can be summarized as follows:

- Experimental results are compared with the prediction of numerical models.
- 1D waterhammer equation is solved with MOC.
- Implementation separately of both DVCM and DGCM techniques.
- Implementation of Anderson and Arfaie (1991) cavity interface internal boundary condition as an alternative to the conventional Wylie and Streeter (1993) implementation in both classical models (DVCM and DGCM).
- Implementation separately of both techniques of original Bughazem  $k_3$  and the implementation of Bughazem and Anderson (2000)  $k_t$  as single- coefficient transient friction models in MOC.

## **Chapter 3**

### **Mathematical and Computational Work**

### 3.1 Standard waterhammer analysis with MOC

Generally, waterhammer equations applied for calculation of the unsteady pipe flow (Bergant and Tijsseling 2001) are based on some assumptions, including:

- The flow is one-dimensional with average cross section velocity (which in itself implies that the flow is mostly turbulent).
- The pipe remains full of single-phase liquid during the transient events so the pressure inside the pipe remains above the pipe fluid vapour pressure or the pressure at which dissolved gases are released.
- For one-dimensional transient flow the friction dissipation can be represented by the “quasi-steady” Darcy Weisbach expression for pipe flow.
- Though the pressure disturbance wave propagates at a finite velocity with the fluid (liquid) and pipe wall both assumed to behave elastically, for single-phase liquids in relatively rigid pipes the resulting changes in fluid density and pipe cross-sectional area are negligible and are not computed.
- With small free or dissolved gas content in the liquid, the wave speed remains constant at any particular location.

With these assumptions the waterhammer equations are (written in terms of absolute static pressure  $P$  rather than head  $H$  to avoid confusion over the definition of the latter, (i.e. static or piezometric):

x-momentum equation:

$$\frac{1}{\rho} \frac{\partial P}{\partial x} + V \frac{\partial V}{\partial x} + \frac{\partial V}{\partial t} + \frac{f}{2 \cdot d} V |V| + g \cdot \sin \theta = 0 \quad (3.1)$$

continuity equation:

$$V \frac{\partial P}{\partial x} + \frac{\partial P}{\partial t} + \rho \cdot a^2 \frac{\partial V}{\partial x} = 0 \quad (3.2)$$

In the momentum Eq.(3.1):

- The 4<sup>th</sup> and 5<sup>th</sup> terms are the frictional and pipe slope terms.
- The 2<sup>nd</sup> term is a convective acceleration term, corresponding to the spatial (x) change in kinetic energy or velocity head:

$$V \frac{\partial V}{\partial x} = \frac{\partial}{\partial x} \left[ \frac{1}{2} V^2 \right] \quad (3.3)$$

The other convective term is the 1<sup>st</sup> term in the continuity Eq.(3.2).

Because these hyperbolic equations contain non-linear terms (notably for the dissipation term in Eq.(3.1) and the convective term Eq.(3.3) solutions cannot be achieved analytically and therefore numerical techniques are necessary to give approximate solutions for both pressure and the flow velocity. Several numerical techniques have been used to solve the waterhammer equations (Wylie and Streeter 1993), including finite difference (FD) (e.g. Arfaie 1989), finite volume (FV), finite element (FM) and the method of characteristics (MOC). In this study MOC is adopted because it is the most widely used approach in liquid flow transients.

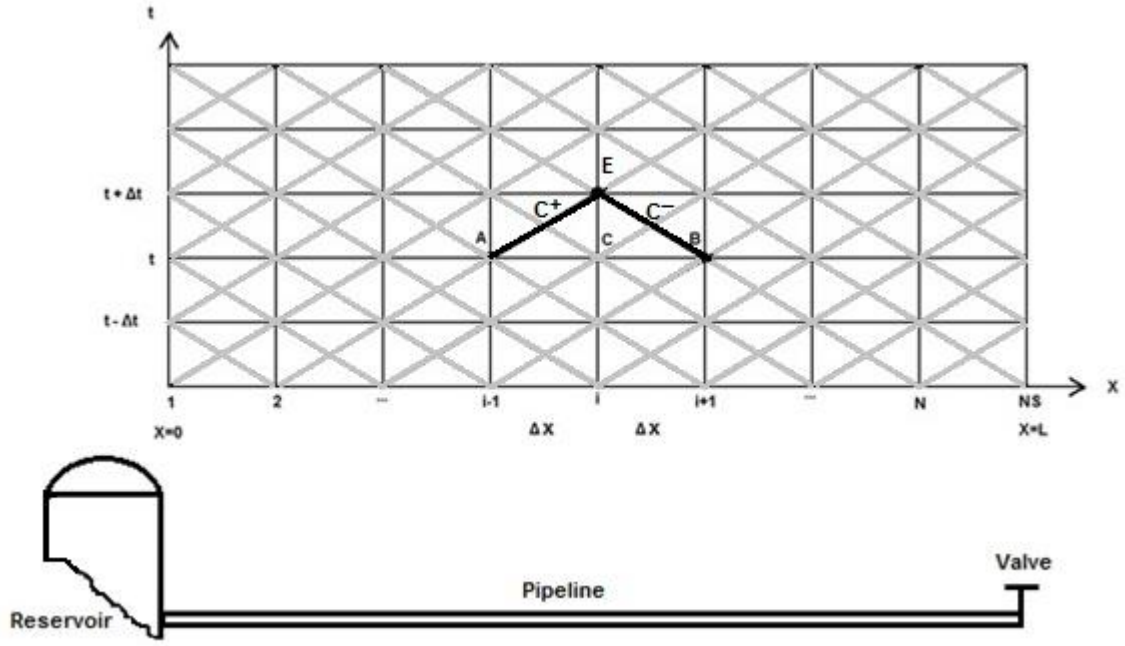
The MOC is used to transfer the partial differential equations to ordinary differential equations which are then solved by FD (Wylie and Streeter 1993). Neglecting the convective terms  $\left( V \frac{\partial V}{\partial x}, V \frac{\partial P}{\partial x} \right)$  in Eq.(3.1) and Eq.(3.2) (Anderson 1988, Sections 7-8):

Along the characteristics lines, Figure(3.1):

$$\frac{dx}{dt} = \pm a \quad (3.4)$$

then (with volume flow rate  $Q = A \cdot V$ ):

$$\pm \left( \frac{dP}{dt} \right) + \frac{\rho \cdot a}{A} \left( \frac{dQ}{dt} \right) + \rho \cdot a \cdot g \cdot \sin \theta + \frac{\rho \cdot a \cdot f}{2 \cdot d \cdot A^2} Q|Q| = 0 \quad (3.5)$$



Figure(3.1) MOC lines in space-time plane for reservoir-pipe-valve system, (Wylie and Streeter 1993).

The MOC formulation highlights the role of the disturbance wave propagation velocity  $a$  and for waterhammer i.e. single-phase liquid in relatively rigid elastic pipes leading to high values of  $a \gg V$ , the convective terms  $\left(\frac{V \partial V}{\partial x}, \frac{V \partial P}{\partial x}\right)$  in Eq.(3.1) and Eq.(3.2) can be neglected. In Chapter 4 it will be shown that, for the experimental apparatus used in this study, the experimental uncertainty  $\pm \Delta a$  in wavespeed  $a$  exceeds the initial fluid flow velocity  $V_0$ , justifying the application of this conventional assumption.

For integration Eq.(3.5) can be written for each  $C^\pm$  characteristic in Eq.(3.6), Figure(3.2) :

$$C^+: \quad + \int_{P_A}^{P_E} dP + \frac{\rho a}{A} \int_{Q_A}^{Q_E} dQ + \rho \cdot g \cdot \sin \theta \int_{X_A}^{X_E} dx + \frac{\rho f}{2 \cdot d \cdot A^2} \int_{Q_A}^{Q_E} Q|Q| \cdot dx = 0 \quad (3.6)$$

$$C^-: \quad - \int_{P_B}^{P_E} dP + \frac{\rho a}{A} \int_{Q_B}^{Q_E} dQ + \rho \cdot g \cdot \sin \theta \int_{X_B}^{X_E} dx + \frac{\rho f}{2 \cdot d \cdot A^2} \int_{Q_B}^{Q_E} Q|Q| \cdot dx = 0$$

The first three terms are represented by finite differences and can be integrated exactly, but the fourth (i.e. friction) term cannot. There are a number of

approximations for its integration. Suwan (1989) and Arfaie (1989) showed that for all but very long pipelines the best of these is (Wylie and Streeter 1993):

$$\int_{x_A}^{x_E} Q^2 dx \cong Q_E |Q_A| (x_E - x_A) \quad (3.7)$$

giving:

$$C^+: \quad (P_E - P_A) + \frac{\rho \cdot a}{A} (Q_E - Q_A) + \rho \cdot g \cdot \Delta x \cdot \sin \theta + \frac{\rho \cdot f \cdot \Delta x}{2 \cdot d \cdot A^2} Q_E |Q_A| = 0 \quad (3.8)$$

$$C^-: \quad -(P_E - P_B) + \frac{\rho \cdot a}{A} (Q_E - Q_B) + \rho \cdot g \cdot \Delta x \cdot \sin \theta + \frac{\rho \cdot f \cdot \Delta x}{2 \cdot d \cdot A^2} Q_E |Q_B| = 0$$

Following Wylie and Streeter (1993) by setting the following abbreviations for computational efficiency:

$$\begin{aligned} B &= \frac{\rho \cdot a}{A} \\ S &= \rho \cdot g \cdot \Delta x \cdot \sin \theta \\ R &= \frac{\rho \cdot f \cdot \Delta x}{2 \cdot d \cdot A^2} \end{aligned} \quad (3.9)$$

then:

$$C^+: \quad P_E = CP - BP \cdot Q_E \quad (3.10)$$

$$C^-: \quad P_E = CM + BM \cdot Q_E$$

where:

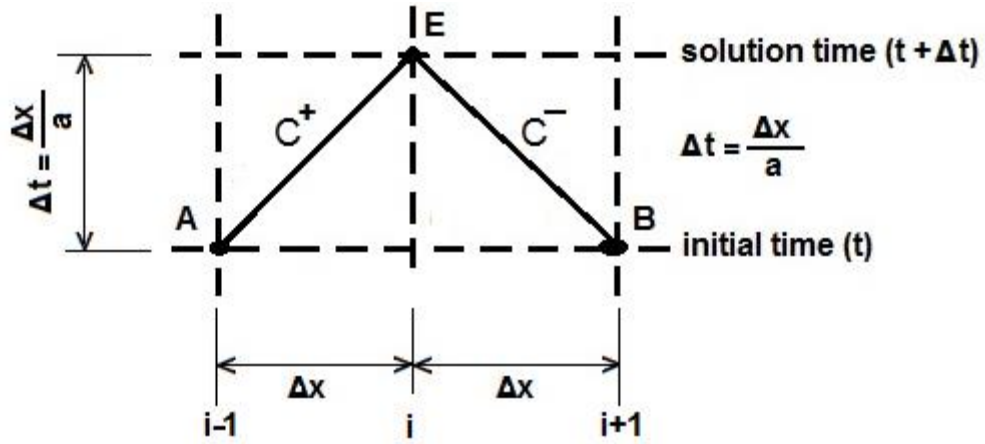
$$\begin{aligned} C^+: \quad CP &= P_A + B \cdot Q_A - S & \& \quad BP &= B + R \cdot |Q_A| \\ C^-: \quad CM &= P_B - B \cdot Q_B + S & \& \quad BM &= B + R \cdot |Q_B| \end{aligned} \quad (3.11)$$

For internal nodes, Figure(3.2), i.e. nodes between (2 – N) along the pipeline, where node(1) is at the reservoir pipe entrance and node NS = (N + 1) is at the valve, by combining both equations in Eq.(3.10):

$$P_E = \frac{CP \cdot BM + CM \cdot BP}{BP + BM} \quad (3.12)$$

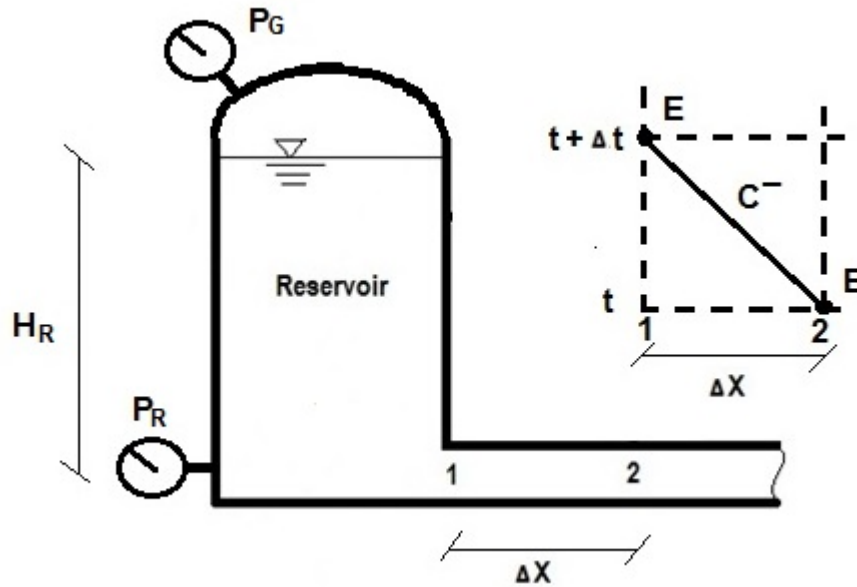


$$Q_E = \frac{CP - CM}{BP + BM} \quad (3.13)$$



Figure(3.2) Fixed grid MOC for internal nodes.

For the reservoir boundary condition, Figure(3.3), i.e. node(1), located at the pipeline entrance, then neglecting the inertia and compressibility of the flow in the reservoir and pipe entrance, Bernoulli gives:



Figure(3.3) Reservoir boundary condition

$$P_G + \rho \cdot g \cdot H_R + \frac{\rho \cdot V_0^2}{2} = P_1 + \rho \cdot g \cdot Z_1 + \frac{\rho}{2} \cdot V_1^2 + \frac{\rho \cdot K_e}{2} V_1 |V_1| \quad (3.14)$$

defining:

$$V = \frac{Q}{A} , \quad P_R = P_G + \rho \cdot g \cdot H_R \quad (3.15)$$

and assuming the reservoir is large enough and any change in water surface level can be neglected giving  $V_0^2 \cong 0$  and with elevation datum taken at the pipe entrance ( $Z_1 \cong 0$ ), then at node(1):

$$P_1 = P_R - \frac{\rho}{2A^2} [1 + K_e \cdot \text{sign}(Q_1)] Q_1^2 \quad (3.16)$$

With definitions equivalent to Eq.(3.11), then combining the negative characteristic compatibility criterion Eq.(3.8) and Eq.(3.16), gives the quadratic equation in discharge  $Q_1$  at node(1):

$$\frac{\rho}{2A^2} [1 + K_e \cdot \text{sign}(Q_1)] Q_1^2 + B.M. \cdot Q_1 + C.M. - P_R = 0 \quad (3.17)$$

which can be rearranged as:

$$\frac{\rho}{2A^2} [1 + K_e \cdot \text{sign}(Q_1)] + B.M. \cdot \left(\frac{1}{Q_1}\right) - [P_R - C.M.] \cdot \left(\frac{1}{Q_1^2}\right) = 0 \quad (3.18)$$

The three coefficients of this quadratic in  $Q_1^{-1}$  can be written as in Eq.(3.11):

- $\alpha = P_R - C.M.$       where       $C.M. = (P_2 - B \cdot Q_2 + S)$
- $\beta = B.M.$       where       $B.M. = B + R \cdot Q_2$       (3.19)
- $\gamma = \frac{\rho}{2 \cdot A^2} [1 + K_e \cdot \text{sign}(Q_1)]$       where       $\text{sign}(Q_1) = \text{sign}(\alpha)$

Thus the solution for discharge at the pipe entrance, node(1), can be evaluated in the form:

$$Q_1 = \frac{2\alpha}{\beta + \sqrt{\beta^2 + 4 \cdot \alpha \cdot \gamma}} \quad (3.20)$$

The choice between the two possible solutions of the quadratic (i.e. of the  $\pm$  sign before the determinant) is made to satisfy the limiting case of the loss-free (i.e.  $f = K_e = 0$ ) and horizontal ( $S = 0$ ) pipe which, along with the physical requirement for a real (not imaginary) solution, identifies the result shown in Eq.(3.20) above. By substituting for all the parameters in Eq.(3.20), the flow solution becomes:

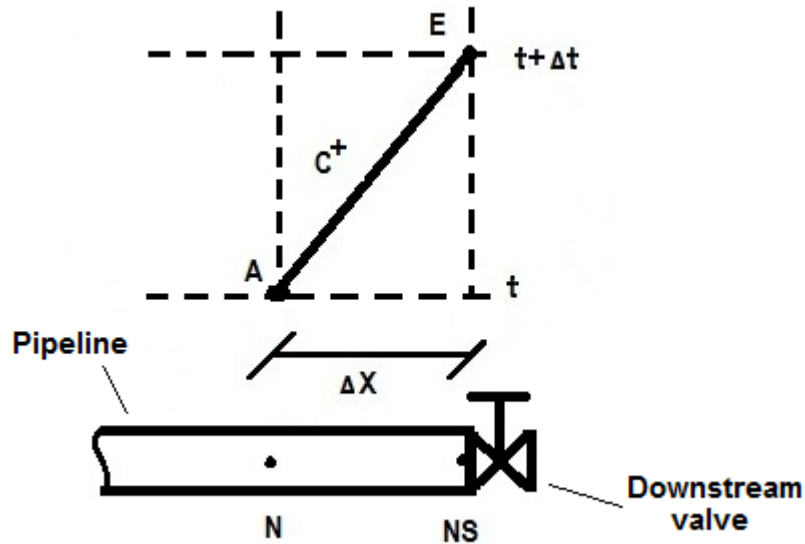
$$Q_1 = \frac{2[P_R - (P_2 - B \cdot Q_2 + S)]}{BM + \sqrt{BM^2 + 4(P_R - CM) \frac{\rho}{2A^2} [1 + K_e \cdot \text{sign}(P_R - CM)]}} \quad (3.21)$$

For the valve boundary condition, after shutting the valve almost instantaneously (transient initiation), the flow at the valve stops with value  $Q_{NS} = 0$  for the unsteady period. Utilising the positive characteristic Eq.(3.10) at the downstream valve between both nodes (N, NS) as shown in Figure(3.4), with this boundary condition the pressure at the valve is:

$$C^+: \quad P_{NS} = CP \quad (3.22)$$

where:

$$CP = P_N + B \cdot Q_N - S$$



Figure(3.4) Schematic diagram of valve boundary condition

**3.2 Unsteady friction.**

Employing quasi-steady Darcy friction  $f_q$  in hydraulic transient analysis does give an acceptable prediction of the first pressure peak as well as the following minimum pressure of the waterhammer cycles (Chaudhry 2014). However, it shows slow energy dissipation over the period of transient compared to the experimental results. Modelling complex cases, for example waterhammer-induced gas release and column separation, could not match measured results without taking into consideration the role of unsteady friction  $f_u$  (Chaudhry 2014). From the literature, several techniques have been proposed and developed for evaluating unsteady friction within waterhammer, attempting to correctly predict pressure oscillations (Chaudhry 2014).

Full investigation on unsteady friction is not intended for this study, but nevertheless it is known in advance that the present small scale apparatus needs additional dissipation in unsteady flow numerical models to match experimental results (e.g. Arfaie 1989, Bughazem 1997). Building on previous work at Newcastle done by Bughazem and Anderson (1996, 2000) makes an instantaneous acceleration based method preferable. Bughazem and Anderson (1996) and Bughazem (1997) previously showed that the Brunone et al (1991b) model could work well for a very similar apparatus to the one used in this present study. Instantaneous acceleration based models assume that the damping of pressure waves is attributed to the unsteady friction influenced by both instantaneous local ( $\partial V/\partial t$ ) and convective ( $\partial V/\partial x$ ) accelerations. The accelerations are computed based on the average cross sectional values without taking into consideration the velocity distribution at the cross section of the computational node.

Two variants for unsteady friction will be used in this study:

- Firstly, the most successful of the implementations of the Brunone et al (1991b) model tested by Bughazem (1997) (Bughazem and Anderson 1996). The equations for this are summarised below.
- Secondly, Bughazem and Anderson (2000) suggested a full MOC implementation of this model but did not test this themselves. The equations for this are derived in Section(3.3).

The waterhammer x-momentum Eq.(3.1) without convective acceleration can be written with the general dissipation term  $J$  as:

$$\frac{\partial V}{\partial t} + \frac{1}{\rho} \frac{\partial P}{\partial x} + g \sin \theta + g \cdot J = 0 \quad (3.23)$$

The dissipative term  $J$  may be divided into quasi-steady (i.e. Darcy Weisbach) and unsteady (i.e. Brunone et al 1991b, Bughazem and Anderson 1996) parts, collectively producing the total head loss per unit length (where  $k_3$  is a single unsteady friction coefficient) and in contrast to Eq.(3.23) this does include the convective acceleration:

$$J = \frac{f \cdot V|V|}{2 \cdot g \cdot d} + \frac{k_3}{g} \left[ \frac{\partial V}{\partial t} - a \frac{\partial V}{\partial x} \right] \quad (3.24)$$

The full derivation can be found in Bughazem (1997) and is only summarised here.

Eq.(3.23) and Eq.(3.24) can be combined as:

$$(1 + k_3) \frac{\partial V}{\partial t} + \frac{1}{\rho} \frac{\partial P}{\partial x} + g \sin \theta + \frac{fV|V|}{2d} - a \cdot k_3 \frac{\partial V}{\partial x} = 0 \quad (3.25)$$

Combined with continuity this can be given in characteristic form:

along  $C^+$ :

$$\frac{dx}{dt} = \frac{+a}{(1 + k_3)}$$

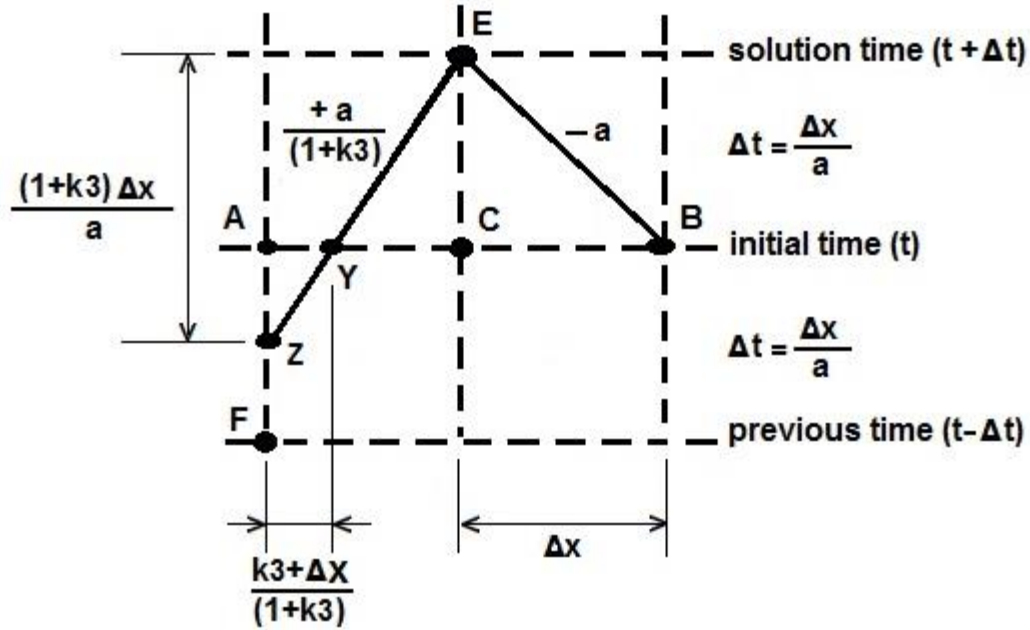
$$\frac{dP}{dt} + \frac{(\rho \cdot a)}{A} \frac{dQ}{dt} + \frac{(\rho \cdot a)}{(1 + k_3)} \cdot \left[ g \sin \theta + \frac{f}{2dA^2} Q|Q| \right] = 0 \quad (3.26)$$

along  $C^-$ :

$$\frac{dx}{dt} = -a$$

$$\frac{dP}{dt} - (1 + k_3) \frac{(\rho \cdot a)}{A} \frac{dQ}{dt} - (\rho \cdot a) \left[ g \sin \theta + \frac{f}{2dA^2} Q|Q| \right] = 0 \quad (3.27)$$

With a single unsteady coefficient  $k_3$  Figure(3.5) shows the schematic diagram for the internal nodes on the  $x - t$  plane presented in Figure(3.1).



Figure(3.5) Schematic diagram for internal nodes ( $0 \leq k_3 \leq 1$ )

Evaluating the derivatives by finite differences:

- $\frac{dV}{dt} \cong \frac{V_E - V_C}{\Delta t}$
- $\frac{dV}{dx} \cong \frac{V_C - V_A}{\Delta x}$
- $\frac{dV}{dx} \cong \frac{V_B - V_C}{\Delta x}$

Integration along the positive characteristic line (Y – E) gives:

$$P_E = CP_f - BP_f \cdot Q_E \quad (3.28)$$

Where (with B, S and R as in Eq.(3.9)):

$$\begin{aligned} \blacksquare \quad & \text{CPf} = P_Y + B \cdot Q_Y - \frac{S}{1 + k3} \\ \blacksquare \quad & \text{BPf} = B + \frac{R}{1 + k3} |Q_Y| \end{aligned} \quad (3.29)$$

Interpolation is required for the  $C^+$  lines to identify values at node(Y) on Figure(3.5). (Bughazem 1997), adopted space line interpolation (where  $\phi = P$  or  $Q$ ):

$$\phi_Y = \phi_A + \frac{k3}{(1 + k3)} [\phi_C - \phi_A] \quad (3.30)$$

Integration of Eq.(3.27) along the negative characteristic line (E-B) gives:

$$P_E = CM_f + BM_f \cdot Q_E \quad (3.31)$$

where:

$$\begin{aligned} \blacksquare \quad & CM_f = P_B - B \cdot (1 + k3) \cdot Q_B + S \\ \blacksquare \quad & BM_f = B \cdot (1 + k3) + R \cdot |Q_B| \end{aligned} \quad (3.32)$$

### 3.3 Implementation of Anderson and Bughazem (2000) unsteady friction model

Though incidental to the main study aims, this Section(3.3) describes an attempt to implement the alternative unsteady friction model that was suggested by Bughazem and Anderson (2000), as they did not actually implement it in full. In brief, it is based on the model of unsteady friction by Brunone and Vitkovsky which has two coefficients  $k_t$  and  $k_x$ . Eq.(3.33) replaces the previous Eq.(3.24) and incorporates the  $\text{sign}(V)$  term identified by Vitkovsky for flows that can reverse:

$$g \cdot J = \frac{f \cdot V |V|}{2d} + \left\{ k_t \frac{\partial V}{\partial t} + [k_x \cdot \text{sign}(V)] \cdot a \left| \frac{\partial V}{\partial x} \right| \right\} \quad (3.33)$$

In contrast to the previous implementation of Section(3.2) above, Eq.(3.33) will be fully incorporated into the MOC. The method is implemented on a fixed uniform rectangular grid, Figure(3.1), which is the most commonly used grid, with 12 uniform space (i.e.  $NS = 13$ , nodes  $1 \leq i \leq NS$ ) and time increments satisfying the CFL

criterion,  $\Delta x = L/(N)$  and  $\Delta t \leq \Delta x/a$ , where  $a$  is the wave propagation speed. However, it is problematic even on the deliberately simple apparatus to calibrate for two unsteady coefficients  $k_t$  and  $k_x$  simultaneously. So, based on Bughazem's success with a single coefficient  $k_x = k_t$  as in the original Brunone model, only a single coefficient  $k_t$  will be determined from comparison with the experimental runs by simplifying Eq.(3.33) to:

$$\begin{aligned} g.J &= \frac{f.V|V|}{2d} + k_t. \left\{ \frac{\partial V}{\partial t} + \text{sign}(V). a. \left| \frac{\partial V}{\partial x} \right| \right\} \\ &= \frac{f.V|V|}{2d} + k_t. \left\{ \frac{\partial V}{\partial t} + a. \frac{\partial V}{\partial x} \text{sign} \left( V \frac{\partial V}{\partial x} \right) \right\} \end{aligned} \quad (3.34)$$

The assumption that  $k_x = k_t$  made for Eq.(3.34) is essentially arbitrary and based only on the apparent success of the single coefficient mode of Section(3.2). Other possibilities (e.g.  $k_x \propto k_t$ ) have not been considered. For this study distances ( $x$ ) are measured from the reservoir and flow velocities ( $V$ ) are positive in the direction of the initial steady flow from reservoir to valve.

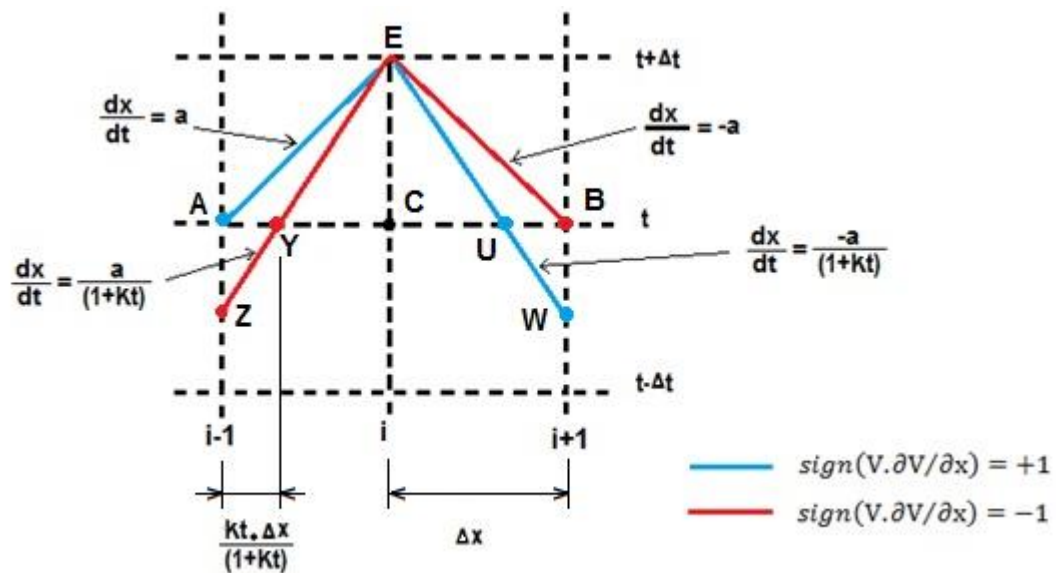
### **3.3.1 Analysis for internal nodes**

Figure(3.6) shows the schematic grid of Bughazem and Anderson (2000) for the implementation of the unsteady friction model on the internal nodes.

Two schemes can be distinguished from Figure(3.6) depending on the value of  $\text{sign}(V.\partial V/\partial x)$ . Each computational node along the pipe is checked for  $\text{sign} = \pm 1$ , based on the known flow direction at the central and both adjacent nodes:

$$\text{sign} \left( V \frac{\partial V}{\partial x} \right) = \frac{U}{|U|} \quad \text{where} \quad U \cong V_i^t (V_{i+1}^t - V_{i-1}^t) \quad (3.35)$$





**Figure(3.6) Implementation of Bughazem and Anderson (2000) unsteady friction model.**

The characteristics equations and their corresponding compatibility criteria are as given by Bughazem and Anderson (2000), but they do not give details of an implementation which are set out below. In addition to the  $kx = kt$  assumption, for consistency with the rest of this study it is also assumed that all terms in  $\{V/a\}$  can be neglected, which considerably simplifies the algebra:

$$\frac{dx}{dt} \cong \frac{a}{\lambda} \quad \text{where} \quad \lambda \cong \pm 1 + \frac{1}{2}kt \left[ \pm 1 - \text{sign}\left(V \cdot \partial V / \partial x\right) \right] \quad (3.36)$$

$$\frac{(1 + kt)}{A} \frac{dQ}{dt} + \frac{\lambda}{(\rho \cdot a)} \frac{dP}{dt} + g \sin \theta + \frac{f}{2dA^2} Q|Q| = 0 \quad (3.37)$$

$$(1) \quad \textit{sign}(\mathbf{V} \partial \mathbf{V} / \partial \mathbf{x}) = +1$$

In this case from Eq.(3.36):

$$\lambda = \begin{cases} +1 & \text{for } C^+ \\ -(1 + kt) & \text{for } C^- \end{cases} \quad (3.38)$$

**Along the positive characteristic lines:**

From Eq.(3.38):

$$C^+: \quad \lambda = +1 \quad (3.39)$$

With re-arrangement of Eq.(3.37) in preparation for integration:

$$\frac{\rho \cdot a}{A} \cdot (1 + kt) \cdot dQ + dP + \rho \cdot g \cdot a \cdot dt \cdot \sin \theta + \frac{\rho \cdot a \cdot f}{2d \cdot A^2} Q|Q| \cdot dt = 0 \quad (3.40)$$

Integrating Eq.(3.40) between the points E and A, as illustrated in Figure(3.6)

$$\frac{\rho \cdot a}{A} \cdot (1 + kt) \cdot \int_{Q_A}^{Q_E} dQ + \int_{P_A}^{P_E} dP + \rho \cdot g \cdot dx \cdot \sin \theta + \frac{\rho \cdot f}{2dA^2} \int_{Q_A}^{Q_E} Q|Q| dx = 0 \quad (3.41)$$

gives (with friction as in Eq.(3.7)):

$$\frac{\rho \cdot a}{A} \cdot (1 + kt) \cdot [Q_E - Q_A] + [P_E - P_A] + \rho \cdot g \cdot \Delta x \cdot \sin \theta + \frac{\rho \cdot f \cdot \Delta x}{2dA^2} Q_E|Q_A| = 0 \quad (3.42)$$

With B, S and R as in Eq.(3.9) rearrange Eq.(3.42) for solution of unknown pressure:

$$P_E = P_A - B(1 + kt) \cdot [Q_E - Q_A] \pm S \pm R \cdot Q_E|Q_A| \quad (3.43)$$

To simplify the computation Eq.(3.43) can be rearranged as:

$$P_E = CP_g - BP_g \cdot Q_E \quad (3.44)$$

where:

$$CP_g = P_A + B \cdot (1 + kt) \cdot Q_A - S$$

$$BP_g = B \cdot (1 + kt) + R \cdot |Q_A|$$

**Along the negative characteristic lines:**

From Eq.(3.38):

$$C^-: \quad \lambda = -(1 + kt)$$

With re-arrangement of Eq.(3.37) in preparation for integration:

$$\frac{\rho \cdot a}{A} \cdot (1 + kt) \cdot dQ - (1 + kt) \cdot dP + \rho \cdot g \cdot a \cdot \Delta t \cdot \sin \theta + \frac{\rho \cdot a \cdot f}{2dA^2} Q|Q| \cdot dt = 0 \quad (3.45)$$

Dividing Eq.(3.45) by  $(1 + kt)$  and integrating between points E and U on Figure(3.6):

$$P_E = P_U + B \cdot [Q_E - Q_U] + \frac{S}{(1 + kt)} + \frac{R}{(1 + kt)} \cdot Q_E |Q_U| \quad (3.46)$$

To simplify the computation Eq.(3.46) can be rearranged as:

$$P_E = CM_g + BM_g \cdot Q_E \quad (3.47)$$

where:

$$CM_g = P_U - B \cdot Q_U + \frac{S}{(1 + kt)} \quad (3.48)$$

$$BM_g = B + \frac{R}{(1 + kt)} \cdot |Q_U|$$

However, while point U lies on the known time line, it does not coincide with a fixed rectangular grid point (unlike A, C, B or E). Non-grid points in the MOC are normally associated with either including the convective terms or variable wavespeed (a) or varying grid size ( $\Delta x$ ,  $\Delta t$ ), none of which apply in this case. In Figure(3.6) the non-grid points U arise from the unsteady friction model, Eq.(3.38). Nevertheless, just as with the other instances variable values at these points can be estimated by “reach out” interpolation in either the space-line (point U) or time-line (points Z, W). The simplest implementation is linear interpolation along the known space-line, which allows a gradient discontinuity to propagate past this location (Wylie and Streeter 1993).

Where  $\phi$  stands for either of dependent variables, i.e.  $\phi \equiv Q$  or  $P$ , then from Figure(3.6):

$$\phi_U = \phi_C + \frac{kt}{(1 + kt)} [\phi_C - \phi_B] = \frac{1}{(1 + kt)} [\phi_B + kt. \phi_C] \quad (3.49)$$

Note that  $\phi_U \rightarrow \phi_B$  for  $kt \rightarrow 0$ , i.e. for quasi-steady friction ( $kt = 0$ ) the characteristics pass through the fixed rectangular grid points.

**(2)  $sign(V \partial V / \partial x) = -1$**

In this case, from Eq.(3.36) previously (Figure(3.6)):

$$\lambda = \begin{cases} (1 + kt) & \text{for } C^+ \\ -1 & \text{for } C^- \end{cases} \quad (3.50)$$

**Along the positive characteristic lines:**

From Eq.(3.50):

$$C^+: \quad \lambda = (1 + kt)$$

With re-arrangement of Eq.(3.37) in preparation for integration:

$$\frac{\rho. a}{A} dQ + dP + \frac{1}{(1 + kt)} \left[ \rho. g. a. dt. \sin \theta + \frac{\rho. a. f}{2dA^2} Q|Q|. dt \right] = 0 \quad (3.51)$$

Integrating Eq.(3.51) between the points E and Y, as illustrated in Figure(3.6) **Figure(3.6) :**

$$\frac{\rho. a}{A} \int_{Q_Y}^{Q_E} dQ + \int_{P_Y}^{P_E} dP + \frac{1}{(1 + kt)} \left[ \rho. g. \Delta x. \sin \theta + \frac{\rho. f}{2dA^2} \int_{Q_Y}^{Q_E} Q|Q| dx \right] = 0 \quad (3.52)$$

Gives (with friction as in Eq.(3.7)):

$$\frac{\rho \cdot a}{A} [Q_E - Q_Y] + [P_E - P_Y] + \frac{1}{(1 + kt)} \left[ \rho \cdot g \cdot \Delta x \cdot \sin \theta + \frac{\rho \cdot f \cdot \Delta x}{2dA^2} Q_E |Q_Y| \right] = 0 \quad (3.53)$$

With B, S and R as in Eq.(3.9) rearrange Eq.(3.53) for solution of unknown pressure:

$$P_E = P_Y - B \cdot [Q_E - Q_Y] + \frac{1}{(1 + kt)} [S + R \cdot Q_E |Q_Y|] \quad (3.54)$$

To simplify the computation Eq.(3.54) can be rearranged as:

$$P_E = CP_f - BP_f \cdot Q_E \quad (3.55)$$

where:

$$CP_f = P_Y + B \cdot Q_Y + \frac{1}{(1 + kt)} S \quad (3.56)$$

$$BP_f = B + \frac{R}{(1 + kt)} |Q_Y|$$

As before point Y on the known time (t) line does not coincide with a fixed rectangular grid point so “reach out” space-line interpolation is necessary for the two dependent variables,  $\phi \equiv Q$  or  $P$ , Figure(3.6):

$$\phi_Y = \phi_A + \frac{kt}{(1 + kt)} [\phi_C - \phi_A] = \frac{1}{(1 + kt)} [\phi_A + kt \cdot \phi_C] \quad (3.57)$$

Note that  $\phi_Y \rightarrow \phi_A$  for  $kt \rightarrow 0$ , similarly to Eq.(3.49) above.

#### **Along the negative characteristic lines:**

From Eq.(3.50):

$$C^-: \quad \lambda = -1$$

With re-arrangement of Eq.(3.37) in preparation for integration:

$$\frac{\rho \cdot a}{A} \cdot (1 + kt) \cdot dQ - dP + \rho \cdot g \cdot a \cdot dt \cdot \sin \theta + \frac{\rho \cdot a \cdot f}{2dA^2} Q|Q| \cdot dt = 0 \quad (3.58)$$

Integrating Eq.(3.58) between the points E and B with Eq.(3.7) as illustrated on Figure(3.6):

$$P_E = P_B + B \cdot (1 + kt) \cdot [Q_E - Q_B] + S + R \cdot Q_E |Q_B| \quad (3.59)$$

To simplify the computation Eq.(3.59) can be rearranged as:

$$P_E = CM_f + BM_f \cdot Q_E \quad (3.60)$$

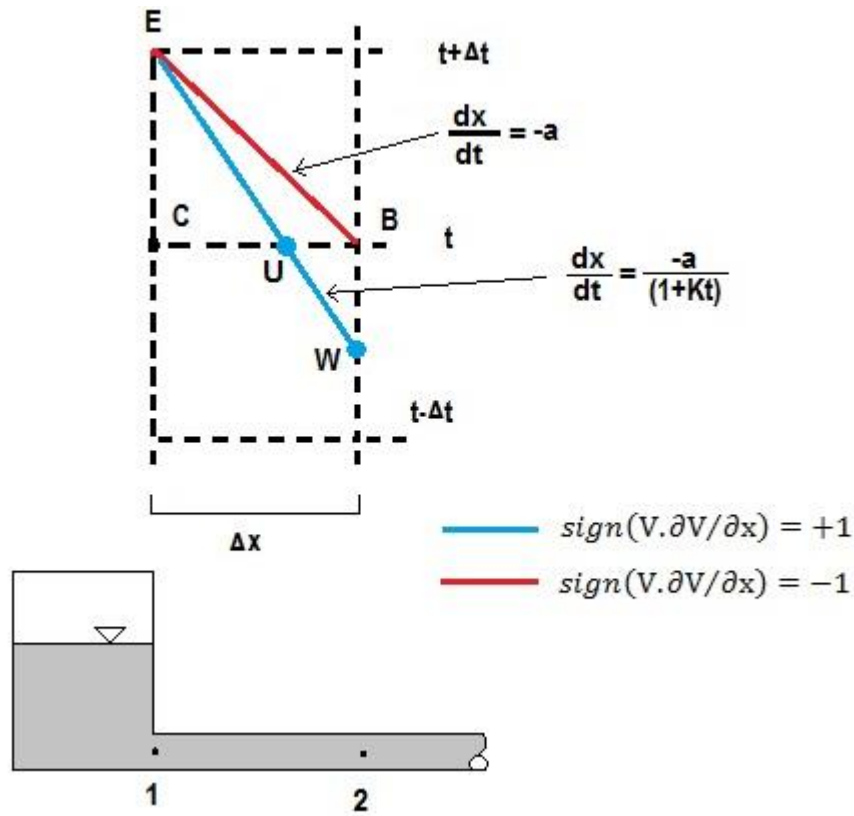
where:

$$CM_f = P_B - B \cdot (1 + kt) \cdot Q_B + S$$

$$BM_f = B \cdot (1 + kt) + R \cdot |Q_B|$$

### 3.3.2 Reservoir boundary condition

At the reservoir constant head is assumed during the whole transient duration. The appropriate negative compatibility equation is solved at constant reservoir pressure (i.e.  $P_R = \text{constant}$ ) where the choice depends on the local flow behaviour, as determined by Eq.(3.35). Figure(3.7) shows the schematic diagram of the reservoir boundary condition with consideration of unsteady friction.



### A $sign(V \partial V / \partial x) = +1$

Applying the negative characteristic of Eq.(3.38):

$$C^-: \quad \lambda = -(1 + kt)$$

With re-arrangement of Eq.(3.37) for integration:

$$\frac{\rho \cdot a}{A} \cdot (1 + kt) \cdot dQ - (1 + kt) \cdot dP + \rho \cdot g \cdot a \cdot dt \cdot \sin \theta + \frac{\rho \cdot f}{2dA^2} Q|Q| \cdot a \cdot dt = 0 \quad (3.61)$$

Dividing Eq.(3.61) by  $(1 + kt)$  and integrating between points E and U as illustrated in Figure(3.7):

$$P_E = P_U + B \cdot [Q_E - Q_U] + \frac{S}{(1 + kt)} + \frac{R}{(1 + kt)} \cdot Q_E |Q_U| \quad (3.62)$$

The solution for the unknown  $Q_E$  is:

$$Q_E = [(1 + kt)(P_E - P_U + B \cdot Q_U) - S] / [B(1 + kt) + R|Q_U|] \quad (3.63)$$

As previously, the values at the non-grid point U ( $Q_U$ ,  $P_U$ ) are obtained by linear reach-out space-line interpolation Eq.(3.49).

### **B** $sign(V \partial V / \partial x) = -1$

In this case, in place of Eq.(3.38) the negative characteristics is from Eq.(3.50):

$$C^-: \quad \lambda = -1$$

with re-arrangement of Eq.(3.33) in preparation for integration:

$$\frac{\rho \cdot a}{A} (1 + kt) \cdot dQ - dP + \rho \cdot g \cdot a \cdot dt \cdot \sin \theta + \frac{\rho \cdot a \cdot f}{2dA^2} Q|Q| \cdot dt = 0 \quad (3.64)$$

Integrating between points E and B on Figure(3.7) with rearrangement:

$$P_E = P_B + B \cdot (1 + kt) \cdot [Q_E - Q_A] + S + R \cdot Q_E |Q_B| \quad (3.65)$$

The solution for the unknown  $Q_E$  is:

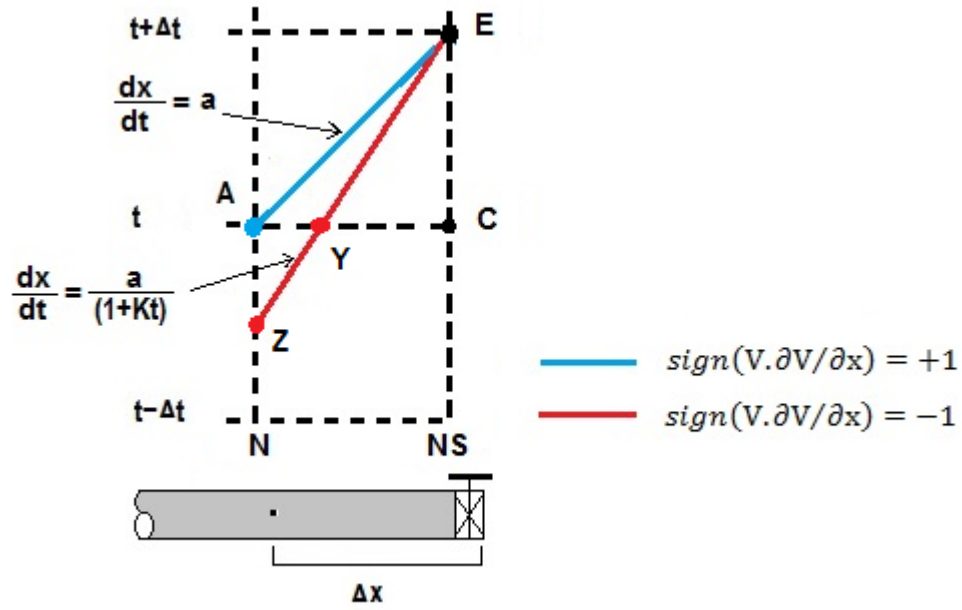
$$Q_E = [(P_E - P_B) + (1 + kt) \cdot B \cdot |Q_A| - S] / [B \cdot (1 + kt) + R \cdot |Q_A|] \quad (3.66)$$

In this case all values are at fixed rectangular grid points and no interpolation is required.

### **3.3.3 Valve boundary condition.**

At the downstream valve zero flow is considered during the whole transient duration. The appropriate positive compatibility equation is solved at constant flow rate (i.e.  $Q_{NS} = 0$ ) where the choice depends on the flow behaviour, as determined by Eq.(3.35). Figure(3.8) shows the schematic diagram of the valve boundary condition with consideration of unsteady friction.





Figure(3.8) Schematic diagram of the downstream valve

**A**  $sign(V \partial V / \partial x) = +1$

Applying the positive characteristic of Eq.(3.38):

$$C^+: \quad \lambda = +1.$$

with re-arrangement of Eq.(3.37) in preparation for integration:

$$\frac{\rho \cdot a}{A} \cdot (1 + kt) \cdot dQ + dP + \rho \cdot g \cdot dx \cdot \sin \theta + \frac{\rho \cdot a \cdot f}{2dA^2} Q|Q| \cdot dt = 0 \quad (3.67)$$

Integrating Eq.(3.67) between the points E and A, as illustrated in Figure(3.8)

$$\frac{\rho \cdot a}{A} (1 + kt) \cdot [Q_E - Q_A] + [P_E - P_A] + \rho \cdot g \cdot \Delta x \cdot \sin \theta + \frac{\rho \cdot f \cdot \Delta x}{2dA^2} Q_E |Q_A| = 0 \quad (3.68)$$

Rearranging, Eq.(3.68) for the unknown boundary pressure:

$$P_E = P_A - (1 + kt) \cdot [Q_E - Q_A] - S - R \cdot Q_E |Q_A| \quad (3.69)$$

Eq.(3.69) can be rearranged as:

$$P_E = CP_g - BP_g \cdot Q_E \quad (3.70)$$

where:

$$CP_g = P_A + B \cdot (1 + kt) \cdot Q_A - S$$

$$BP_g = B \cdot (1 + kt) + R \cdot |Q_A|$$

$$\mathbf{B} \quad \text{sign}(\mathbf{V} \partial \mathbf{V} / \partial \mathbf{x}) = -1$$

Applying the positive characteristic of Eq.(3.50)

$$C^+: \quad \lambda = (1 + kt)$$

With re-arrangement of Eq.(3.37) in preparation for integration:

$$\frac{\rho \cdot a}{A} \cdot dQ + dP + \frac{1}{(1 + kt)} \left[ \rho \cdot g \cdot a \cdot dt \cdot \sin \theta + \frac{\rho \cdot a \cdot f}{2dA^2} Q|Q| \cdot dt \right] = 0 \quad (3.71)$$

Integrating Eq.(3.71) between the points E and Y, as illustrated in Figure(3.8)

**Figure(3.8)**

$$\frac{\rho \cdot a}{A} \cdot [Q_E - Q_Y] + [P_E - P_Y] + \frac{1}{(1 + kt)} \left[ \rho \cdot g \cdot \Delta x \cdot \sin \theta + \frac{\rho \cdot a \cdot f}{2dA^2} Q_E |Q_Y| \cdot dt \right] = 0 \quad (3.72)$$

Rearranging Eq.(3.72) for the unknown boundary pressure.

$$P_E = P_Y - B \cdot [Q_E - Q_Y] + \frac{S}{(1 + kt)} + \frac{R}{(1 + kt)} \cdot Q_E |Q_Y| \quad (3.73)$$

As previously, the values at the non-grid point Y ( $Q_Y$ ,  $P_Y$ ) are obtained by linear reach-out space-line interpolation Eq.(3.57).

**3.4 Models of column separation**

Focusing on the classical one-dimensional pipe flow approach to waterhammer, there have been many variant implementations of column separation (or transient cavitation) models. Simpson and Bergant (1994a) characterised these as following two main schools of thought which they characterised as DVCM (Discrete Vapour Cavity Model) and DGCM (Discrete Gas Cavity Model). At Newcastle, Arfaie(1989) had focused only on the DVCM approach and introduced an improvement to modelling the single-phase/two-phase interface at the moving internal column separation boundaries.

This study will follow both Simpson and Bergant (1994a,b) and Bergant and Simpson (1999) in adapting the Wylie and Streeter (1993) DVCM and DGCM as “industry standard” reference points, making comparisons for differing column separation responses, in particular for the situation where cavity collapse produces a pressure spike higher than Joukowsky (Martin 1983). In addition, the Arfaie(1989) interface model improvement will be applied not only to DVCM but also to DGCM. With these codes column separation may occur at any node except the reservoir boundary (node 1).

In contrast to Bergant and Simpson (1999), the experimental results used for comparison will be restricted to those where column separation has occurred only at a single region immediately adjacent to the valve where complete rapid closure initiated the transient. For real situations, cavitation may occur at multiple locations along the pipe (e.g. Tullis 1989, Wylie and Streeter 1993, Bergant and Simpson 1999, Chaudhry 2014), but the apparatus design in this study is intended to ensure that there will be cavitation at the closed downstream valve (node NS).

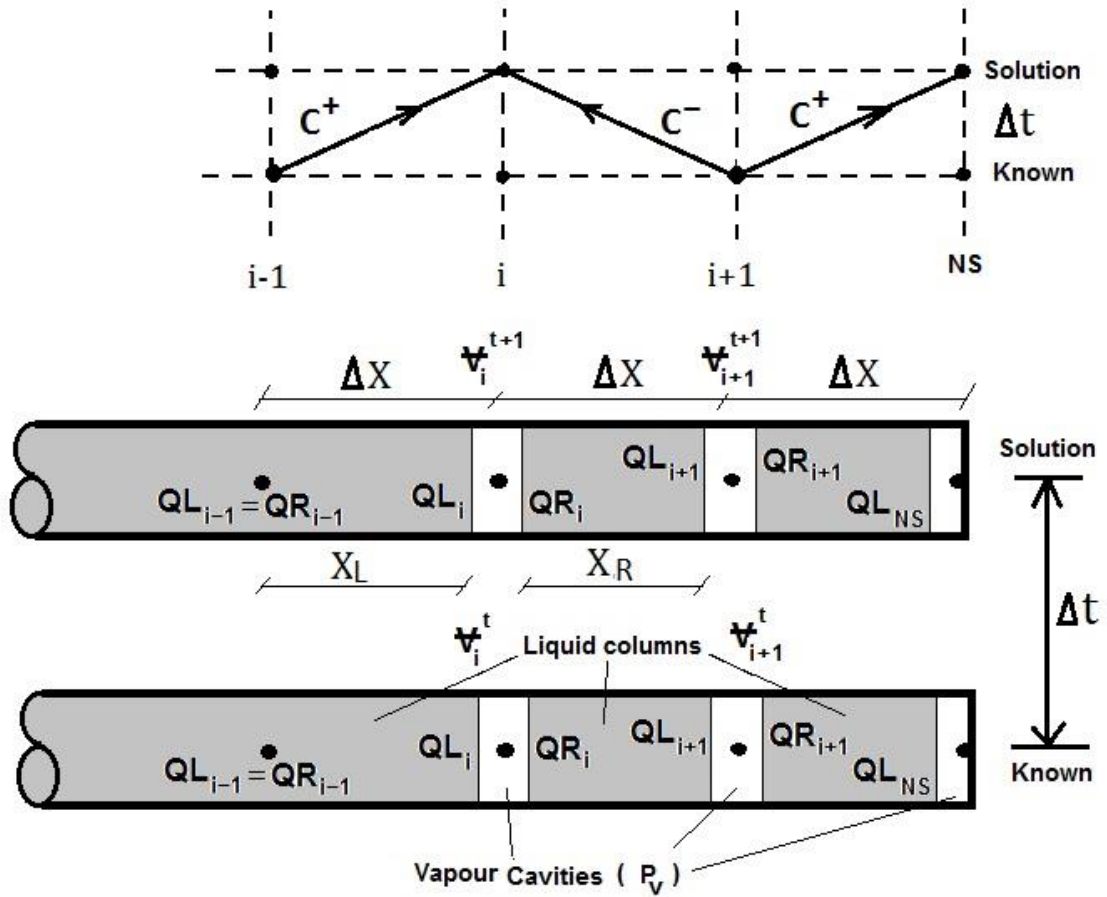
The key feature of the Discrete Cavity Model (both vapour and gas) is that the cavities are assumed to be lumped at the discrete computational nodes e.g. Figure(3.9) and Figure(3.10), even though the DGCM is based on an awareness that bubbles are distributed throughout the low pressure regions, Figure(3.10). Furthermore, for both DVCM and DGCM it is assumed that the cavity volume is equally shared on either side of an internal node. Within the one-dimensional flow approximation, these assumptions lead to the idea that the vapour cavity occupies

the full pipe cross-section, irrespective of whether this is what actually happens in reality (as discussed in Chapter 5).

### **3.4.1 Discrete vapour cavity model (DVCM)**

The Wylie and Streeter (1993) DVCM model assumes that along the pipeline system, in some location during the waterhammer cycles, wherever the local pressure is lowered to the level of vapour pressure, the liquid column breaks to form a stationary vapour cavity in between two liquid columns. Cavitation is assumed to occupy the whole cross section area of the pipe at a particular node with pressure constant at the level of vapour pressure for the liquid working temperature until the cavity collapses eventually. When that condition is not satisfied any more then the model will switch the computation to a normal (single-phase liquid) waterhammer analysis. The model permits cavitation to form at any discrete node along the pipe, except at pipe entrance where the reservoir pressure is dominant.

Figure(3.9) shows a schematic diagram of DVCM for internal and valve boundary conditions. This approach starts by first considering single-phase waterhammer without column separation. The MOC compatibility criteria of Eq.(3.5) and Eq.(3.6) are applied, but at each node  $i = (2 \leq i \leq N)$  giving two variables instead of one for fluid velocity or flow rate, Figure(3.9), i.e. QL to the left of the node for the positive ( $C^+$ ) characteristic and QR to the right of the node for the negative ( $C^-$ ) characteristic (noting that, in contrast to Eq.(3.5) and Eq.(3.6), an explicit approximation is used for pipe friction):



Figure(3.9) DVCM for internal and valve boundary conditions

along  $C^+$ :

$$P_i = P_{(i-1)} - \frac{\rho \cdot a}{A} [QL_i - QR_{(i-1)}] - g \cdot \Delta t \cdot A \cdot \sin \theta - \frac{f \cdot A \cdot \Delta t}{2 \cdot d \cdot A^2} QL_i |QR_{(i-1)}| \quad (3.74)$$

along  $C^-$ :

$$P_i = P_{(i+1)} + \frac{\rho \cdot a}{A} [QR_i - QL_{(i+1)}] + g \cdot \Delta t \cdot A \cdot \sin \theta + \frac{f \cdot A \cdot \Delta t}{2 \cdot d \cdot A^2} QR_i |QL_{(i+1)}| \quad (3.75)$$

Wylie and Streeter (1993) presented the solutions of these for flow in abbreviated from as:

$$\text{along } C^+: \quad QL_i = \frac{CP - P_i}{BP} \quad (3.76)$$

$$\text{along } C^-: \quad QR_i = \frac{P_i - CM}{BM}$$

Where B, S and R are defined in Eq.(3.9) and:

$$\begin{aligned}
 CP &= P_{(i-1)} - S + B \cdot QR_{(i-1)} \\
 CM &= P_{(i+1)} + S - B \cdot QL_{(i+1)} \\
 BP &= B + R \cdot |QR_{(i-1)}| \\
 BM &= B + R \cdot |QL_{(i+1)}|
 \end{aligned} \tag{3.77}$$

For single-phase waterhammer without column separation ( $P_i > P_v$ ) then  $QL_i = QR_i$  and from Eq.(3.76) and Eq.(3.77), the local pressure can be predicted as:

$$P_i = \frac{CP \cdot BM + CM \cdot BP}{BP + BM} \tag{3.78}$$

Eq.(3.74) or Eq.(3.75) or both with  $Q = \frac{1}{2}(QL + QR)$  can then be used for the other dependent variable. However, if the solution pressure  $P_i \leq P_v$  then column separation has occurred (with separate liquid/cavity interfaces to the left and right of the node, Figure(3.9)), so  $P_i$  becomes a constant ( $P_i = P_v$ ) and acts as a transient internal boundary condition causing waterhammer wave reflections. Eq.(3.76) and Eq.(3.77) are then solved for the two unknowns QL and QR. To complete this solution it is necessary to calculate the cavity volume  $\forall$  by continuity, neglecting the cavity vapour mass (assume negligible density compared with liquid state):

$$\frac{d\forall}{dt} = (QR - QL) \tag{3.79}$$

This can be implemented in various ways, e.g. using the average flow over the time step  $\Delta t$  from time  $t$  to time  $(t + \Delta t)$ :

$$\forall^{new} = \forall^{old} + \frac{\Delta t}{2} [(QR_{(i)}^{t+\Delta t} - QL_{(i)}^{t+\Delta t}) + (QR_{(i)}^t - QL_{(i)}^t)] \tag{3.80}$$

When the new cavity volume  $\forall$  reaches zero, then at that node the cavity is assumed vanished and solution will revert to the usual waterhammer calculation with equal discharge values at the computational node:

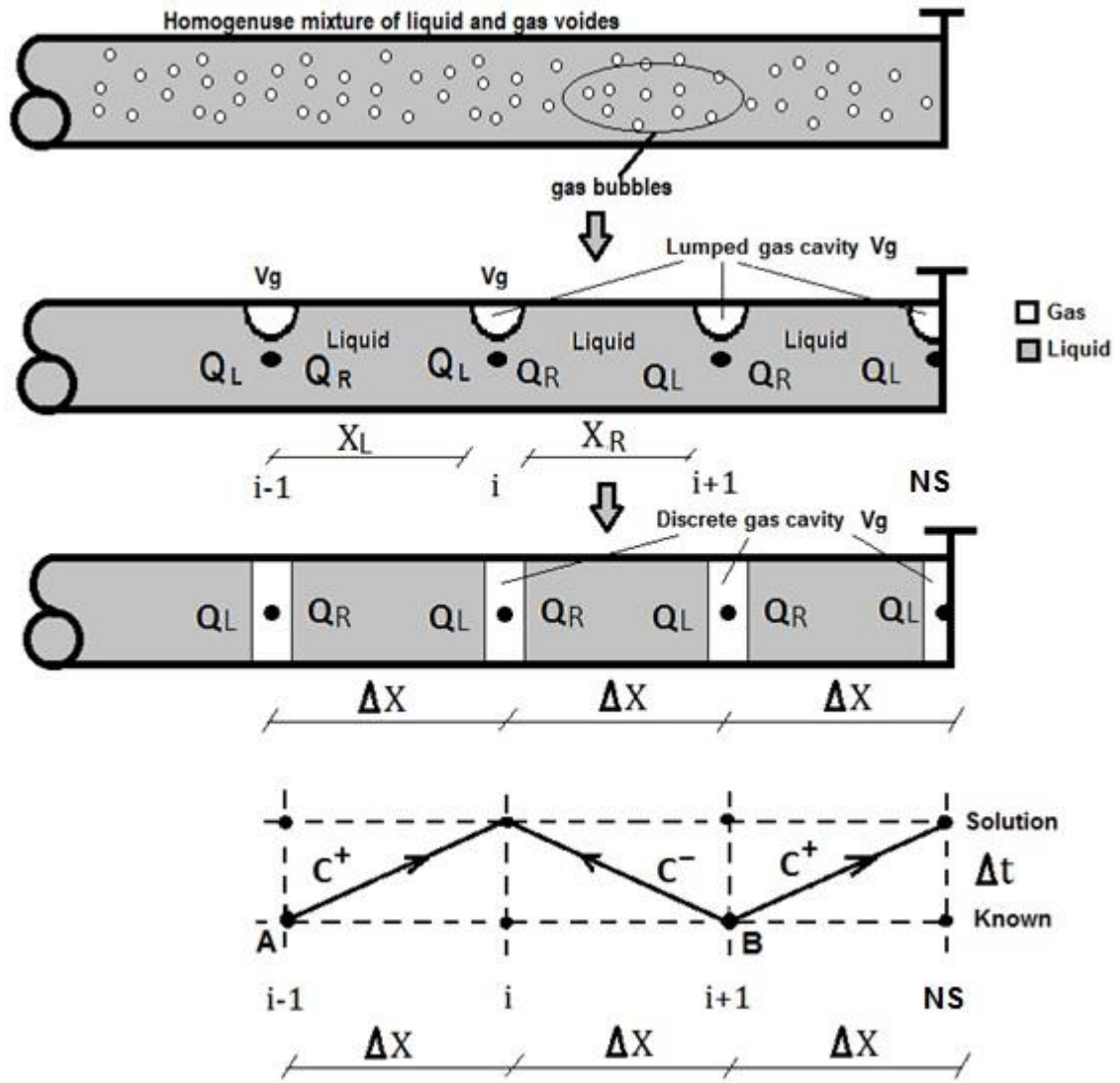
$$QR^t = QL^t \tag{3.81}$$

**3.4.2 Discrete gas cavity method (DGCM)**

An alternative way of modelling column separation in liquid pipelines is the discrete gas cavity model DGCM, which was introduced by Provoost and Wylie (1981). It assumes limited amounts of free gas with void fractions as small as  $\alpha_g \leq 10^{-7}$  (Simpson and Bergant 1994b). In reality, almost all liquids contain dissolved gases in solution, although the volume fraction of these gases is very small, and at constant temperature the concentration of dissolved gas is directly proportional to the partial pressure of the gas by Henry's law (Wylie and Streeter 1993).

During a hydraulic transient in liquid pipelines, pressure fluctuates and if the local pressure is lowered towards sub-atmospheric saturation pressure, gas bubbles initiate and grow during the rarefaction wave period. But when the pressure starts to rise, generally the duration is not sufficient to absorb the gas back. As a consequence this allows bubbles of free gas to appear as a result of this slower reverse process. The existence of a small amount of free gas in a liquid has a big effect on the pressure wave propagation speed.

Wylie and Streeter (1993) outline a simplified discrete gas cavity model for the free gas bubbles which are assumed to be distributed homogenously in the liquid as a mixture, as illustrated in Figure(3.10), so that the free gas can be lumped at each computational node, and between lumped gas cavities there are pure liquid columns free from gas. As a result of pressure variation, each isolated gas cavity expands and contracts isothermally according to the perfect gas law. The effect on the pressure wave speed of lumping the free gas matches results in the case of a distributed gas-liquid mixture (Wylie and Streeter 1993, Liou 2000). During the transient pressure fluctuation, when the local pressure is reduced, large gas volumes may exist at computing nodes, but as long as the gas volumes are smaller in size than the reach volumes, the model should give good agreement with the experimental results (Wylie and Streeter 1993).



Figure(3.10) Schematic diagram for discrete gas cavity model

The basic method of solution for DGCM progresses similarly to that described for DVCM above (Section 3.4.1), as comparing Figure(3.10) (DGCM) with Figure(3.9) (DVCM) suggests. However there are two important differences. Firstly, the lumped gas volumes are subject to the ideal gas law (assuming an isothermal process) for the gas partial pressure  $P_g$ , which is related to the total absolute pressure  $P$  by Dalton's law of partial pressure:

$$\text{Ideal gas:} \quad M_g \cdot R_g \cdot T = P_g \cdot \alpha_g \cdot V = P_o \cdot \alpha_o \cdot V = P_g \cdot V_g \quad (3.82)$$

$$\text{Dalton:} \quad P_o = P_g + P_v \quad (3.83)$$



where:

$M_g \equiv$  gas mass.

$P_g \equiv$  absolute gas partial pressure.

$P_o \equiv$  standard atmospheric pressure = 101325 Pa.

$P_v \equiv$  absolute vapour partial pressure by the ideal gas law.

$R_g \equiv$  gas constant.

$T \equiv$  absolute temperature.

$\alpha \equiv$  void ratio.

$\alpha_o \equiv$  void ratio at atmospheric pressure.

$V \equiv$  volume of mixture.

$V_g \equiv$  volume of gas.

These may be used to determine the volume of the gas at each node:

$$V_g = \frac{C_1}{P_g} \quad (3.84)$$

in which:

$$C_1 = P_o \cdot \alpha_o \cdot V \quad (3.85)$$

Secondly, the existence of a small amount of free gas in the gas–liquid mixture has an effect on the wave propagation speed (Bergant et al 2008a). The wavespeed in a gas–liquid mixture  $a_m$  is pressure dependent and generally significantly lower than the wave speed  $a$  in single-phase liquid Eq.(2.4)

$$a_m = \sqrt{\frac{a^2}{1 + \frac{\alpha_o \cdot \rho \cdot a^2}{P}}} \quad (3.86)$$

and  $a_m$  replaces  $a$  in Eq.(3.9):

$$B = \frac{\rho \cdot a_m}{A} \quad (3.87)$$

In Eq.(3.86), as the pressure  $P$  increases (especially for low values of  $\alpha_o$ ) the wavespeed tends towards the classical waterhammer wavespeed ( $a_m \rightarrow a$ ).

However, in contrast to DVCM, in principle waterhammer waves can still progress through the distributed cavity region.

As with DVCM, continuity for the cavity at each computational node is the rate change of gas volume equal to the difference in flow between the inlet and outlet sides of the cavity, Eq.(3.79). However, the DVCM simple finite difference Eq.(3.84) is replaced in DGCM by substituting from the compatibility criteria for each characteristic to give (where  $\psi$  is weighting factor):

$$\begin{aligned} \frac{V_g^{new}}{\Delta t} \cdot \left\{ \frac{BM \cdot BP}{\psi(BP + BM)} \right\} = \frac{V_g^{old}}{\Delta t} \cdot \left\{ \frac{BM \cdot BP}{\psi(BP + BM)} \right\} - \left[ \frac{CM \cdot BP + CP \cdot BM}{BP + BM} \right] \\ + \left[ \left( \frac{1 - \psi}{\psi} \right) \cdot [Q_R - Q_L] \cdot \left\{ \frac{BM \cdot BP}{\psi(BP + BM)} \right\} \right] + H \end{aligned} \quad (3.88)$$

To simplify the solution of Eq.(3.88), some parameters need to be identified as:

$$V_g^{new} = \frac{C_3}{H - Z - H_v} \quad \& \quad B_2 = \frac{1}{(BP + BM)} \quad (3.89)$$

$$C_4 = \frac{C_3 \cdot B_2 \cdot BM \cdot BP}{\Delta t \cdot \psi} \quad \& \quad B_v = \frac{V_g}{\Delta t \cdot \psi} + \left( \frac{1 - \psi}{\psi} \right) \cdot [Q_{out} - Q_{in}] \quad (3.90)$$

The left hand side (LHS) and right hand side (RHS) of Eq.(3.88) become:

$$LHS = \frac{C_4}{(H - Z - H_v)} \quad (3.91)$$

$$RHS = \frac{B_v \cdot (BM \cdot BP)}{(BM + BP)} - \left[ \frac{CM \cdot BP + CP \cdot BM}{BM + BP} \right] + P \quad (3.92)$$

Let:

$$B_1 = \frac{B_v \cdot B_2 \cdot BM \cdot BP}{2} - B_2 \cdot \left[ \frac{CM \cdot BP + CP \cdot BM}{2} \right] + \left( \frac{P_v}{2} \right) \quad (3.93)$$

Then by assembling both sides of the governing equation with rearrangement into the form of a quadratic equation:

$$C_4 = 2 * B_1 * (P - P_v) + (P - P_v)^2 \quad (3.94)$$

the solution for this governing quadratic equation Eq.(3.94) would be (Wylie and Streeter 1993):

$$\text{Solution} = \frac{-2B_1 \pm \sqrt{4B_1^2 - 4C_4}}{2} \quad (3.95)$$

$$(P - P_v) = -B_1 + \sqrt{4B_1^2 - 4C_4} \quad \text{if} \quad B_1 < 0 \quad (3.96)$$

$$(P - P_v) = \sqrt{C_4} \quad \text{if} \quad B_1 = 0 \quad (3.97)$$

$$(P - P_v) = -B_1 - \sqrt{4B_1^2 - 4C_4} \quad \text{if} \quad B_1 > 0 \quad (3.98)$$

Wylie and Streeter (1993), found that at both critical conditions of high pressure linked with very low gas cavity volume and also low pressure linked with high gas cavity volume, the solution of Eq.(3.96) and Eq.(3.98) produced unrealistic results due to inaccurate numerical evaluation. The group  $|C_4/B_1^2| \ll 1$  is responsible at those conditions for these errors in results and they suggested that the solution can be reached by linearization of Eq.(3.96) and Eq.(3.98):

$$(P - P_v) = -2B_1 - \frac{C_4}{2B_1} \quad \text{if} \quad B_1 < 0 \quad (3.99)$$

$$(P - P_v) = \frac{C_4}{2B_1} \quad \text{if} \quad B_1 > 0 \quad (3.100)$$

**3.4.3 Arfaie interface model**

Arfaie (1989) developed a transient internal boundary condition at a transient cavity interface for the DVCM model of Figure(3.9) and suitable for a fixed rectangular grid MOC with or without interpolations. He defined the lengths XL (to the left of the solution node i ) lengths XR (to the right of the solution node i ) of the lumped liquid column (as distinct from the lumped (vapour cavity) as in Figure(3.11). Arfaie (1989) then used the general equation of motion applied to a uniform cross section pipe filled with a rigid liquid column of mass  $\Delta m$  between any two adjacent nodes distance  $\Delta X$  apart to include inertia, friction and pipe slop terms (RHS):

$$\Delta P = \frac{\Delta m}{A} \frac{dV}{dt} + \frac{\rho \cdot f \cdot \Delta X}{2 \cdot d} V|V| + \rho \cdot g \cdot \Delta X \cdot \sin\theta \quad (3.101)$$

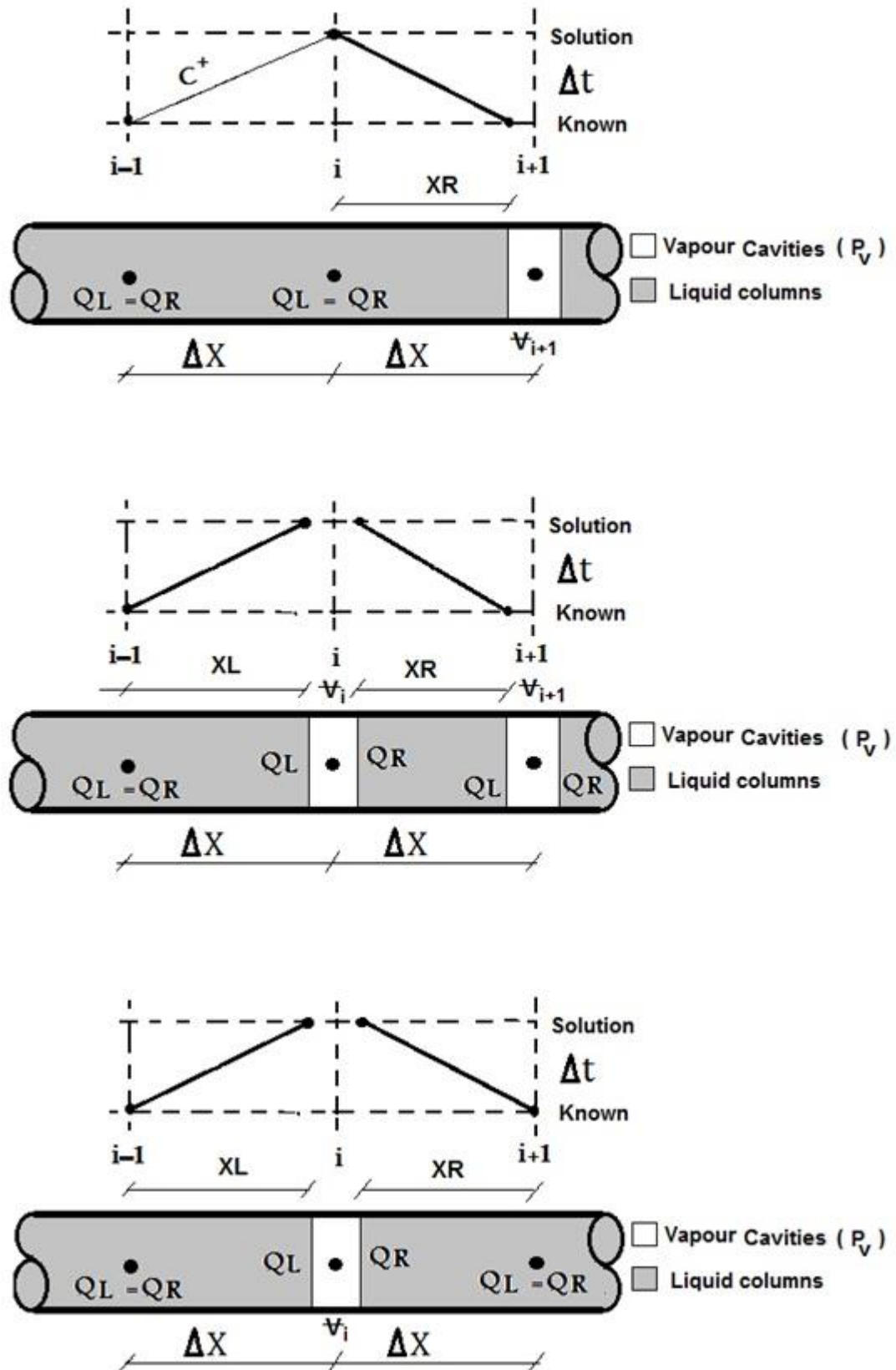
with some assumptions:

- The mass of vapour in the cavity is neglected.
- No mass transfer is considered.
- No thermodynamic interactions are considered.
- The vapour pressure  $P_v$  inside the cavity is considered to be constant during the cavitation period.

For single-phase liquid column regions the classical waterhammer MOC equations are solved as before to predict the unknowns P and Q. But for regions with cavitation, Figure(3.11), the rigid column Eq.(3.101) equation of motion is used to obtain the unknown velocity at the interface of the solution node, with the assumption that the node remains in the centre of the cavitation as the cavity is assumed to expand and contract symmetrically.

Reforming Eq.(3.101) in pressure P and discharge Q to be applied in the analysis, for the rigid column to the left of the cavity:

$$\Delta P = \left( \frac{\rho \cdot XL}{A} \right) \cdot \frac{dQ}{dt} + \left[ \frac{\rho \cdot f \cdot XL}{2 \cdot d \cdot A^2} \right] \cdot Q|Q| + \rho \cdot g \cdot XL \cdot \sin\theta \quad (3.102)$$



Figure(3.11) Variable wave speed for internal nodes with cavitation (Arfaie 1989).

Applying Eq.(3.102) for internal boundaries at the current time as illustrated in Figure(3.11) with the approximation  $QR_{i-1}|QR_{i-1}|$ :

$$P_i - P_{i-1} = \frac{\rho \cdot XL_i}{A \cdot \Delta t} (QL_i - QR_{i-1}) + \left[ \frac{\rho \cdot f \cdot XL_i}{2 \cdot d \cdot A^2} \right] \cdot QR_{i-1} |QR_{i-1}| + \rho \cdot g \cdot XL_i \cdot \sin\theta \quad (3.103)$$

Substituting with  $P_i = P_v$  (vapour pressure) where the cavity exists and solving Eq.(3.103) for the discharge  $QL_i$ :

$$QL_i = QR_{i-1} + \frac{A \cdot \Delta t}{\rho \cdot XL_i} (P_v - P_{i-1}) - \left[ \frac{f \cdot \Delta t}{2 \cdot d \cdot A} \right] \cdot QR_{i-1} |QR_{i-1}| - A \cdot g \cdot \Delta t \cdot \sin\theta \quad (3.104)$$

The variable length of the left side liquid rigid column at the current time can be estimated by:

$$XL_i = \Delta X - \left( \frac{V_i + V_{i-1}}{2 \cdot A} \right) \quad (3.105)$$

Corresponding equations can be developed for the lumped liquid rigid column to the right of the solution node:

$$P_i - P_{i+1} = \frac{\rho \cdot XR_i}{A \cdot \Delta t} (QR_i - QL_{i+1}) - \left[ \frac{\rho \cdot f \cdot XR_i}{2 \cdot d \cdot A^2} \right] \cdot QL_{i+1} |QL_{i+1}| - \rho \cdot g \cdot XR_i \cdot \sin\theta \quad (3.106)$$

$$QR_i = QL_{i+1} - \frac{A \cdot \Delta t}{\rho \cdot XR_i} (P_v - P_{i-1}) - \left[ \frac{f \cdot \Delta t}{2 \cdot d \cdot A} \right] \cdot QL_{i+1} |QL_{i+1}| - A \cdot g \cdot \Delta t \cdot \sin\theta \quad (3.107)$$

$$XR_i = \Delta X - \left( \frac{V_i + V_{i+1}}{2 \cdot A} \right) \quad (3.108)$$

To complete the analysis, it is necessary to calculate the rate of volume change of the vapour cavity by subtracting the two averages (in-flow from out-flow) of the cavity in a similar way to Eq.(3.80) for the DVCM. Arfaie (1989) suggested an improvement to Eq.(3.80) for DVCM in order to achieve more accuracy. The average volume of the cavity over the reach could be taken into consideration using an iterative procedure for the column length:

$$\text{XR}_i = \Delta X - \left( \frac{\mathbb{V}_i^{t+\Delta t} + \mathbb{V}_{i+1}^t}{2 \cdot A} \right) \quad (3.109)$$

$$XL_i = \Delta X - \left( \frac{V_i^{t+\Delta t} + V_{i-1}^t}{2A} \right) \quad (3.110)$$

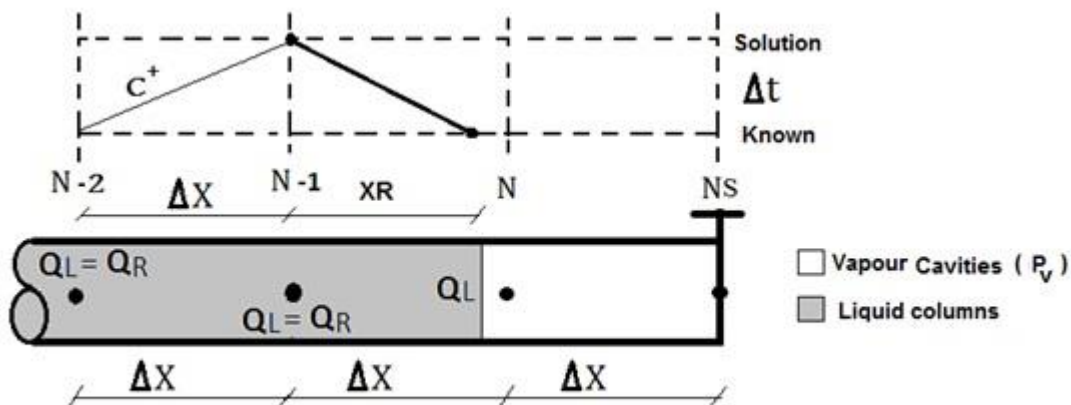
Anderson and Arfaie (1991) observed that comparing Eq.(3.104) and Eq.(3.107) from this approach with the DVCM single-phase waterhammer solution Eq.(3.74) and Eq.(3.75) it gives two apparent variable wave propagation speeds in the cavitation region:

$$a_L = \frac{XL_i}{\Delta t} \quad \text{and} \quad a_R = \frac{XR_i}{\Delta t} \quad (3.111)$$

For the physical limits  $0 \leq X_L \leq \Delta x$  and  $0 \leq X_R \leq \Delta x$  then:

$$\begin{array}{lll} a_L \rightarrow a & as & XL \rightarrow \Delta x \\ a_R \rightarrow a & as & XR \rightarrow \Delta x \end{array} \quad (3.112)$$

In this case of  $X_L$  or  $X_R < 0$  Arfaie (1989) considered the case of a cavity extending over more than one solution node, e.g. Figure(3.12) for the valve boundary. Note that Eq.(3.112) removes the restriction that the lumped vapour cavity has to be equally distributed on either side of the solution node.



**Figure(3.12) Single vapour cavity at valve extending over two solution nodes**

This approach contrasts with the DGCM which assumes the distributed gas cavities lumped at the solution nodes have a small volume compared with the total reach volume. The essential feature of the DVCM is that the “cavity” is simply a region at constant solution pressure ( $P_v$ ) in which gas release and cavitation are occurring, but it does not imply that all of the liquid has yet completely evaporated, as illustrated by the visualisation in Chapter 5. Therefore with fine numerical discretisation ( i.e. small  $\Delta x$ ) especially, there is no reason why a “cavity” may not extend over more than one node.



## **Chapter 4**

### **Experiments on Waterhammer and Column Separation**

#### 4.1 Choice of experimental apparatus layout

Bergant et al (2006) mentioned that, for over a century, many laboratory and field investigations on hydraulic transients in pipeline systems have been done for better understanding of hydraulic transient behaviour and to develop mathematical models for design purposes. Water column separation in transient pipe flow is an aspect of hydraulic transients which has been an area of interest for numerous researchers and scientific centres worldwide (Bergant and Simpson 1992, Bergant and Simpson 1999, Bergant et al 2006). Ghidaoui et al (2005) and Bergant et al (2006) have illustrated two typical systems to replicate the phenomena experimentally; reservoir-valve-pipe-reservoir or reservoir-pipe-valve. In these systems, water column separation was initiated by closing rapidly fast acting valves, causing high and low pressure waves to propagate and reflect along the pipe system. Because of the hydraulic fluctuations, local pressure might drop as low as vapour pressure in some locations and cavitation could occur on either side of the acting valve, depending on apparatus design.

From the literature, pipe layout has varied between straight, U-bend or coiled to save laboratory space with small slope, usually with uniform upslope, with pipes varied in dimensions (pipe diameter 10–100mm, pipe length 10–100m) (Bergant et al 1999). A good understanding has already been developed of the relationship between pipe slope, hydraulic grade-line slope and vaporous cavitation (Simpson and Wylie 1989). Their apparatus (reservoir-pipe-valve system) is similar to that used by Streeter and Lai (1962), Carstens and Hagler (1964) and Martin (1983), who had a coiled tube of 102m length and 13mm diameter. In this research, the apparatus, Figure(4.1), of 62.75m pipe length and 12.7mm diameter, Table(4.2), has been utilized by previous Newcastle researchers, including Arfaie (1989) and Bughazem (1997). Because the apparatus has been relocated with minor changes, calibration has been necessary for the whole setup. The experimental work covers not only measurement of the pressure history, but also visualization of cavity zones arising at the downstream valve in the laboratory test rig.

A simple reservoir-pipe-valve system was chosen to experimentally investigate water column separation on the upstream side of a fully-closed downstream valve. The choice is so that both end boundary conditions can be modelled easily, i.e. constant pressure (upstream reservoir) and zero velocity (closed downstream quick closure

valve). This ensures that the modelling of these elements does not become an issue influencing any assessment of the column separation models.

Any wave noise interference would affect the validity of the experimental results, as well as making the comparison against the numerical models difficult to judge. To avoid any wave reflections that could be caused by pipe fittings, only two pressure transducers were fitted to the apparatus, one to measure the upstream pressure (at the reservoir) and one fitted just before the quick closure valve in order to measure the pressure fluctuation close to the valve during the pressure transient events inducing the column separation region. To facilitate visualisation of the column separation, a transparent polycarbonate pipe section was included as close to the quick closure valve as possible, meaning that the pressure transducer is actually 300mm away from the valve itself.

The pipeline sloped uniformly upwards in the flow direction to ensure column separation occurs at the quick closing valve (the highest point in the pipe system).

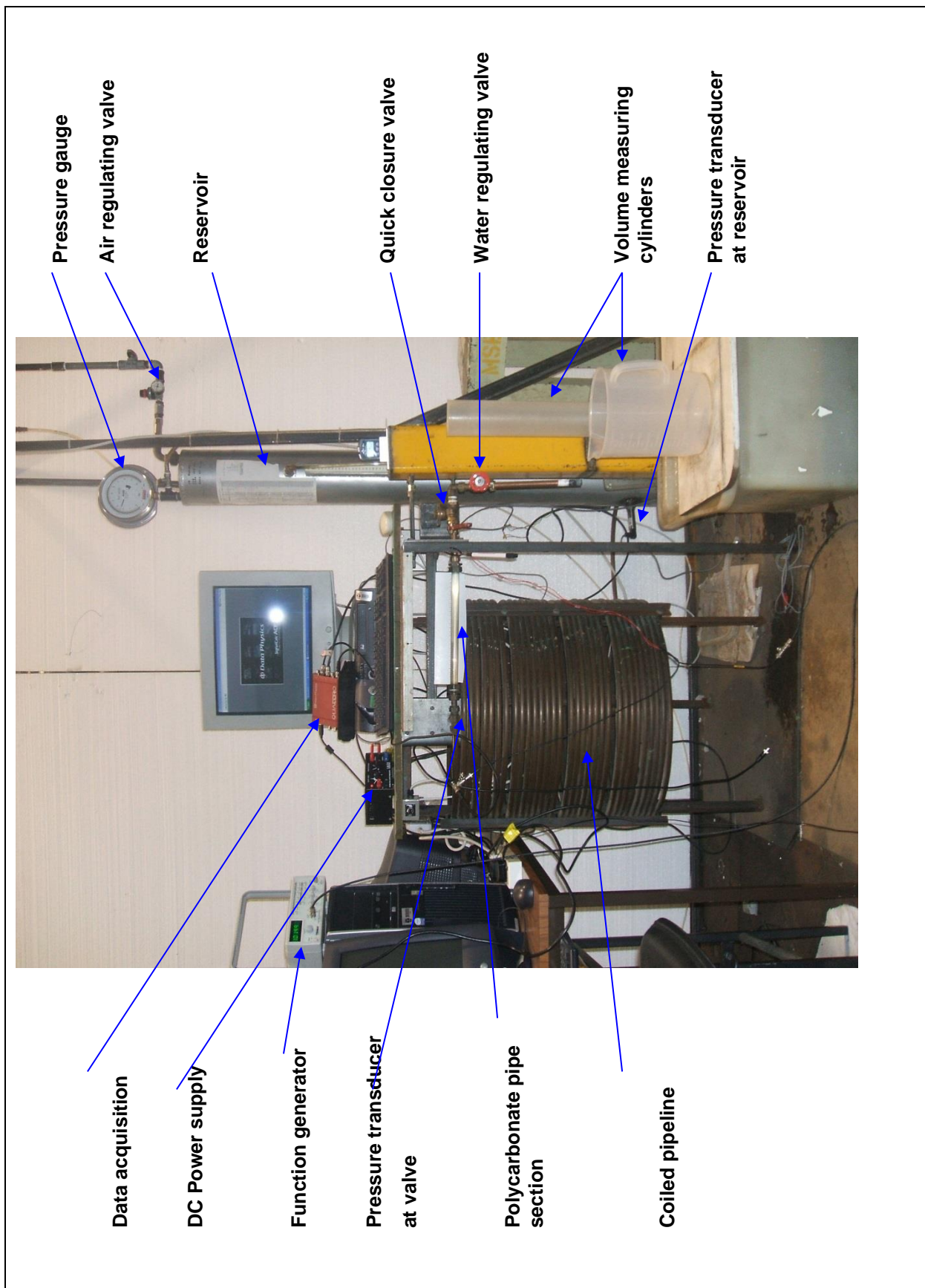
## 4.2 Details of experimental apparatus

The apparatus, Figure(4.1), consists of three main parts: firstly the pipeline system; secondly a pressure control system and thirdly a system of data acquisition as well as the flow visualisation system. A schematic diagram is presented in Figure(4.2) to show the high speed camera as well as the location of the visualisation section.

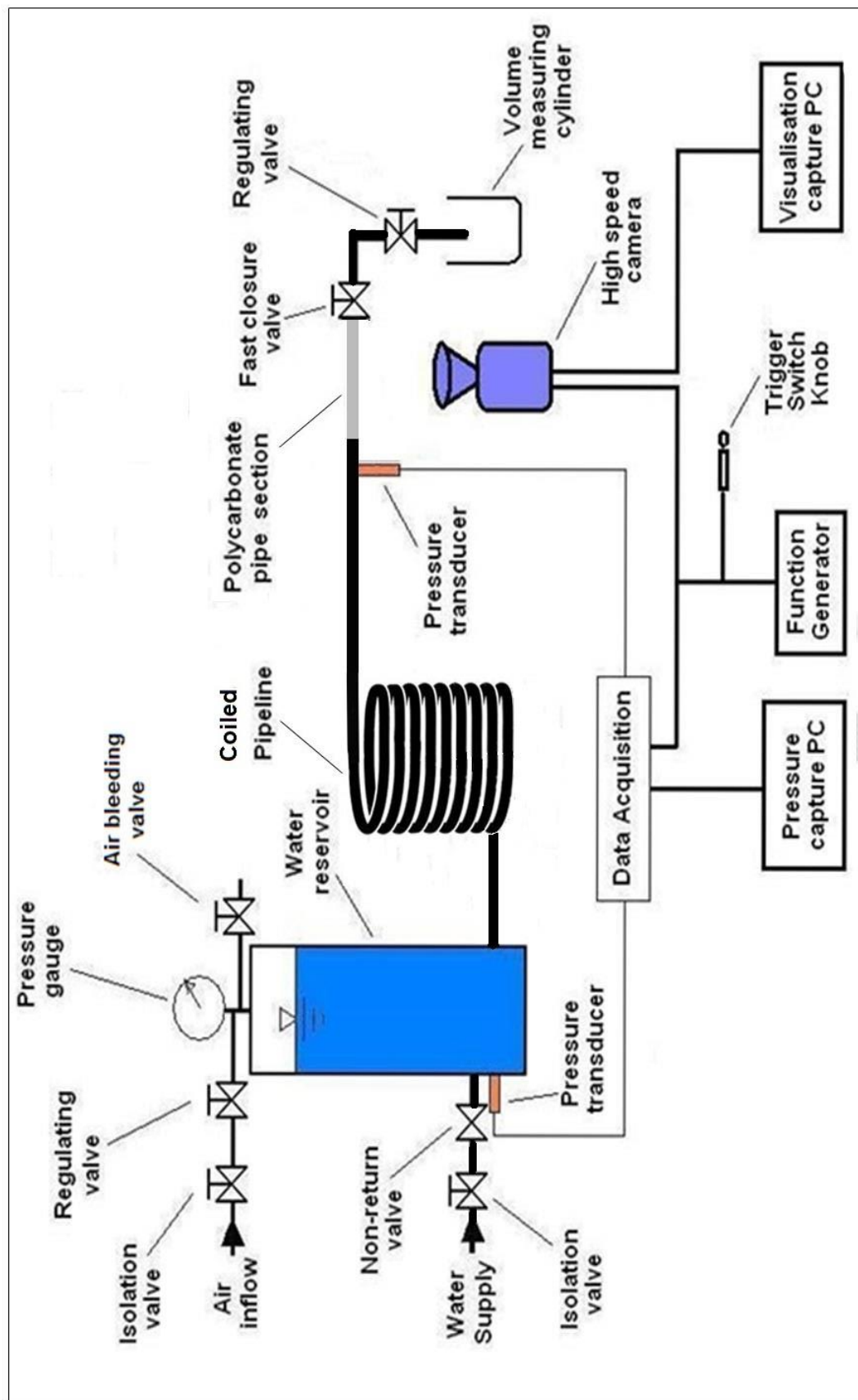
The system consists of a water reservoir and a pipeline anchored to the foundation frame in an attempt to avoid any structural vibration during the transient events:

- (a) The reservoir is a pressurised tank located upstream of the pipeline. It is a 150mm nominal internal diameter steel pipe closed from both ends with capacity of 29.5 litre (Arfaie 1989) supplied with water from the mains through a non-return valve at its bottom and with pressurised air through a regulated valve from the top in order to deliver water at constant pressure during the transient experiments. It was designed to minimize the static water head fluctuation during the experimental runs, to isolate the system from external disturbance and noise in the water mains and to provide variable reservoir pressure.

(b) The pipeline is a coiled copper tube, to save space (Anderson and Johnson, 1990). The pipe is mostly uniformly sloping upward at 0.54 degrees, and essentially the pipe is rigidly fixed to the foundation frame to eliminate structural vibration during pressure transient events. The average coil diameter ( $D$ ) is  $625 \pm 5\text{mm}$ , and the ratio coil / pipe diameters is almost 52, which should be sufficient to consider the coiled tube would therefore act in a similar manner to straight tube (Anderson and Johnson, 1990) with no disturbance along the tube that could affect the propagation of the pressure waves (Martin 1983). The pipe is  $62.75 \pm 0.25\text{m}$  in length including a  $300 \pm 2\text{mm}$  polycarbonate tube (about  $\frac{1}{2}$  % of the overall pipe length) with the same internal diameter ( $d$ ) as the copper pipe ( $\frac{1}{2}$  inch, BS 1386:1957) of  $12.7 \pm 0.3\text{mm}$ . The polycarbonate pipe does not have a standard specification with specified tolerances like the coiled copper tube, but from external diameter measurements its wall thickness is on average about  $1.5\text{mm}$  (i.e. slightly greater than the copper tube, Table 4.2). The polycarbonate section was connected directly to the downstream quick closure valve fitting, to observe the aspect of cavitation and column separation at the downstream valve using the visualisation facilities. However, the combination of the non-standard fitting of polycarbonate tube to brass valve, along with visual blockage from the valve support structure, restrict camera visibility for about  $4\text{cm}$  from the plane of the valve closure disc. Previously Arfaie(1989) had the pressure transducer connected directly to the valve, so that the transparent tube was about  $7.5\text{cm}$  from the closure disc, but moving the transducer to the upstream end of the transparent tube reduced the extent of this visual blockage.



Figure(4.1) Photograph of the pressure transient apparatus.



Figure(4.2) Schematic diagram of the hydraulic transient apparatus.

Properties of both the working liquid (water) and pipe material are listed in Table(4.1) and Table(4.2), which are needed for theoretical evaluation of pressure wave speed and all the numerical simulations.

**Table(4.1) Water properties for experimental pressure transient analysis**

Property	Value	Units	Source
Water temperature	$17 \pm 1$	$^{\circ}\text{C}$	Measured
Water density $\rho$	$999 \pm 2$	$\text{kg}/\text{m}^3$	(Tullis 1989)
Water bulk modulus K	$2.18 \pm 0.02$	$\text{GPa}$	(Bahadori and Vuthaluru 2009)
Water absolute viscosity $\mu$	$(1.082 \pm 0.028)10^{-3}$	$\text{Pa.s}$	(Bahadori and Vuthaluru 2009)

**Table(4.2) Pipeline dimensions and properties of material (copper).**

Property	Value	Units	Source
Modulus of elasticity E	$120 \pm 6$	$\text{GPa}$	(Arfaie 1989)
Pipeline length L	$62.75 \pm .25$	$\text{m}$	Measured
Pipe external diameter $d_o$	15.14	$\text{mm}$	BS1386:1957
Pipe thickness e	$1.22 \pm 0.15$	$\text{mm}$	BS1386:1957
Poisson's ratio $\nu$ at $20^{\circ}\text{C}$	0.34		(Kaye & Laby 2015)

The phenomenon of waterhammer depends on the compressibility of water, but it is conventional (e.g. Wylie and Streeter 1993, Tullis 1989, et al) to assume a constant value for its density  $\rho$ , though it actually varies slightly with both pressure and temperature. With waterhammer in liquids, temperature variations due to waterhammer are very small, but by contrast pressure variation can be very large, this being the main feature that makes waterhammer a potential problem in pipe systems. Tables of water properties (ASME 2006) show that its density varies more with temperature than with pressure, e.g.:

- at 1bar (absolute) it varies by  $+1.5/-2.5\%$  over  $\pm 10^{\circ}\text{C}$  (an order of magnitude greater temperature change than waterhammer is likely to cause); and

- at 20°C it varies by only 1% over the pressure range 0.05 – 23 bar (typical of experiments recorded).

The bulk modulus of water  $K$  similarly varies more with temperature than with pressure, but is also more susceptible to the presence of dissolved gases than density is. For the range of experimental pressure expected (up to 10 bar gauge) and for low dissolved gas content (below saturated) in the water supply, the data in Bahadori and Vuthaluru (2009) suggest  $K = 2.18 \pm 0.2 \text{ GPa}$ , spanning the range of values typically given in textbooks, e.g. Tullis (1989), et al

Waterhammer also depends on the elasticity of the pipe wall giving rise to variation in the pipe cross-sectional area, but following similar arguments these variations are assumed negligible and the pipe cross-section taken as constant.

Copper is not a perfectly linear elastic material so there is quite a large uncertainty in its modulus of elasticity.

The pressure control system consists of two valves that enable different reservoir pressures to be set:

1. Water flow regulating valve, connected downstream of the quick closure valve and discharging to the atmosphere (for initial steady volume flow rate measurements). Reducing the opening of this increases the initial pressure at entry to the quick closing valve.
2. An air regulating valve, connected at the top of the reservoir to control the pressure at the reservoir water surface. The pressurized air is monitored with a pressure gauge (160mm Dial Test Gauge, range 0-10bar with accuracy  $\pm 0.25\%$  F S D).

The data recording system consists of data acquisition and two pressure transducers. The first pressure transducer is connected to the reservoir at the same level as the pipe entrance, in order to measure the pressure head at the pipe inlet (Model PXM 4100-010 MMG 150 V10B3MCT3A5, with pressure range between zero and 10 bar gauge compatible with the maximum reservoir pressure) and the second pressure transducer (type BHL-425-00), to measure the pressure fluctuation at the



valve boundary condition (compatible with the maximum pressure measured at the valve), is connected close to the pipeline downstream end at  $500 \pm 0.5mm$  distance upstream from the quick closing valve (to accommodate the transparent polycarbonate visualisation section).

The data acquisition (dp Data Physics Quattro) was employed to acquire pressure history for both pressure transducers during the 4 seconds time frame of the experimental hydraulic transient at a frequency of  $256Hz$  (about 50 times the expected waterhammer frequency), which gives an acquire interval of  $3.91ms$ . This time-step allows detailed investigation of the pressure traces, for example measuring the duration of the effective valve closure time, cavitation period, pressure steps and high pressure spikes. This setting is also appropriate for synchronisation with the high speed camera to capture cavitation images alongside the pressure trace.

A high speed camera (Motion Pro X5™) was used to capture the possible modes of water column separation through the transparent polycarbonate section of the pipe. The high speed camera and the data acquisition were both set to wait for a trigger in order that visualisation could be exactly correlated with the measured pressure trace to acquire images for each run of the experiment. The camera and data acquisition both worked at a frequency of  $256Hz$  for a period of  $4s$  time frame, which gives a snapshot frame every  $3.91ms$ , accordingly the pipeline numerically was divided to a uniform reaches of ( $N = 12$ ) to satisfy the criteria  $\Delta t \leq \Delta x/a$  in the numerical modelling (Wylie and Streeter 1993, Anderson et al 1991, Arfaie and Anderson 1991). A function generator (TENMA 72-7710) was used as a source of external excitation in order to synchronise the data acquisition and the camera. TTL (transistor-transistor logic) was chosen for this synchronisation process because of compatibility with the camera and simplicity in setting up the instrumentation.

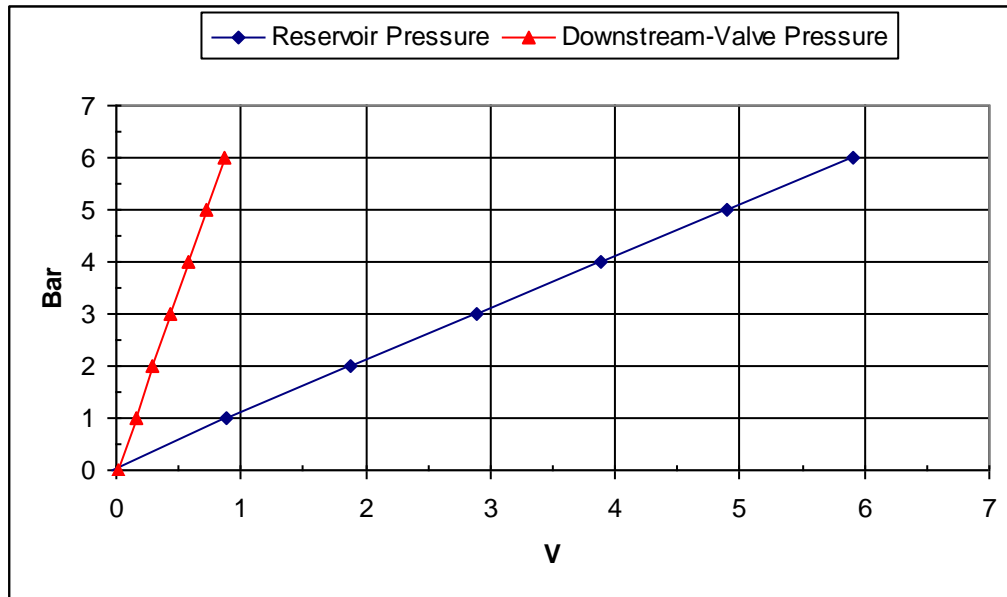
The only transient measurements taken were from the two pressure transducers that measure pressure at both ends of the pipe (reservoir pressure and downstream valve pressure) so these are calibrated individually. The combination of pressure transducers, the data acquisition and its software as a whole system, is connected for calibration to a hydraulic dead-weight calibration unit (type Budenberg gauge), Figure(4.3). The output voltage was acquired at various pressure settings in a range

of 1 – 6bar (the limit of the dead weight manometer). Figure(4.4) shows a good linear relationship between gauge pressure and voltage for both transducers.



**Figure(4.3) Deadweight tester unit with pressure transducer fitted for calibration.**

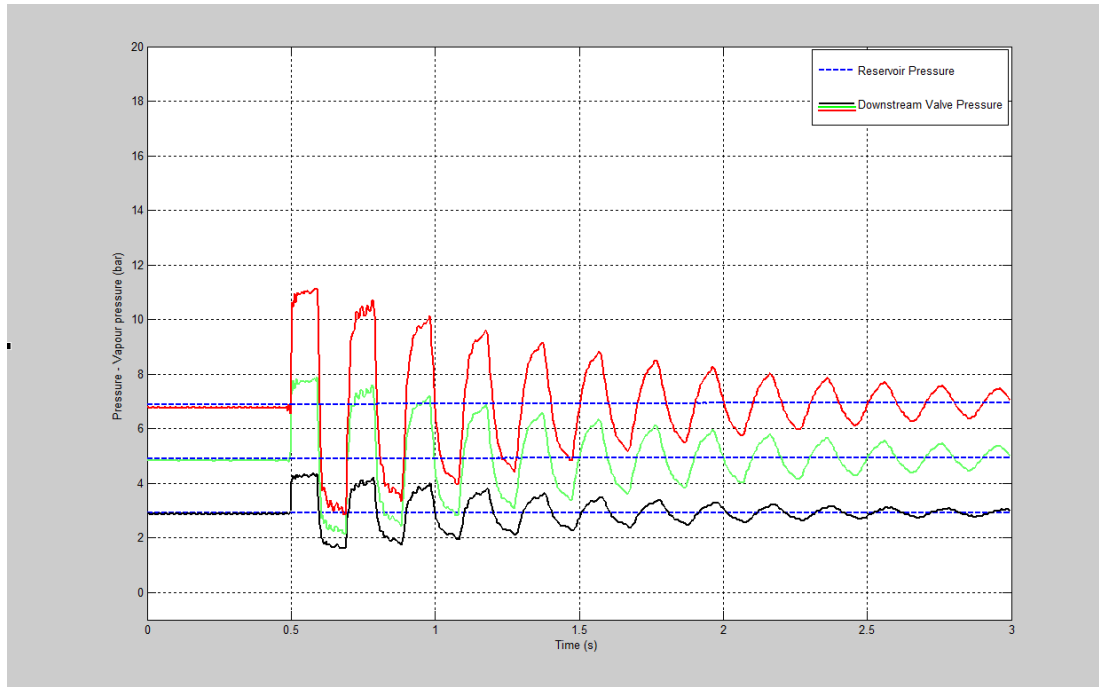
Figure(4.4) illustrates that the voltage produced by reservoir pressure transducer is  $1.0 \pm 0.005$  (bar/V) while for the downstream valve pressure transducer the gradient was  $7.14 \pm 0.003$  (bar/mV) with an intercept of  $(-0.12 \text{ bar})$  which will influence the value of vapour pressure recorded during column separation. This systematic error can simply be adjusted for.



Figure(4.4) Calibration of pressure transducers.

### 4.3 The effect of valve closure time

Three experimental runs of single-phase waterhammer at various reservoir pressures are presented in Figure(4.5). They show that the shape of the first two cycles of waterhammer could be considered as steep front waves while the later cycles become rather sinusoidal in appearance as time progresses and the transient tends to the final steady-state reservoir pressure. This change of behaviour could be related to the effect of a small amount of dissolved air released within the liquid during low-pressure fluctuations, though the similar pattern at higher reservoir pressure makes this questionable. Alternatively, it could be related to wave energy dissipation because of unsteady pipe friction (Wylie and Streeter 1993) coupled with the fact that the “instantaneous” closure in fact occurs over a finite (though short) time.

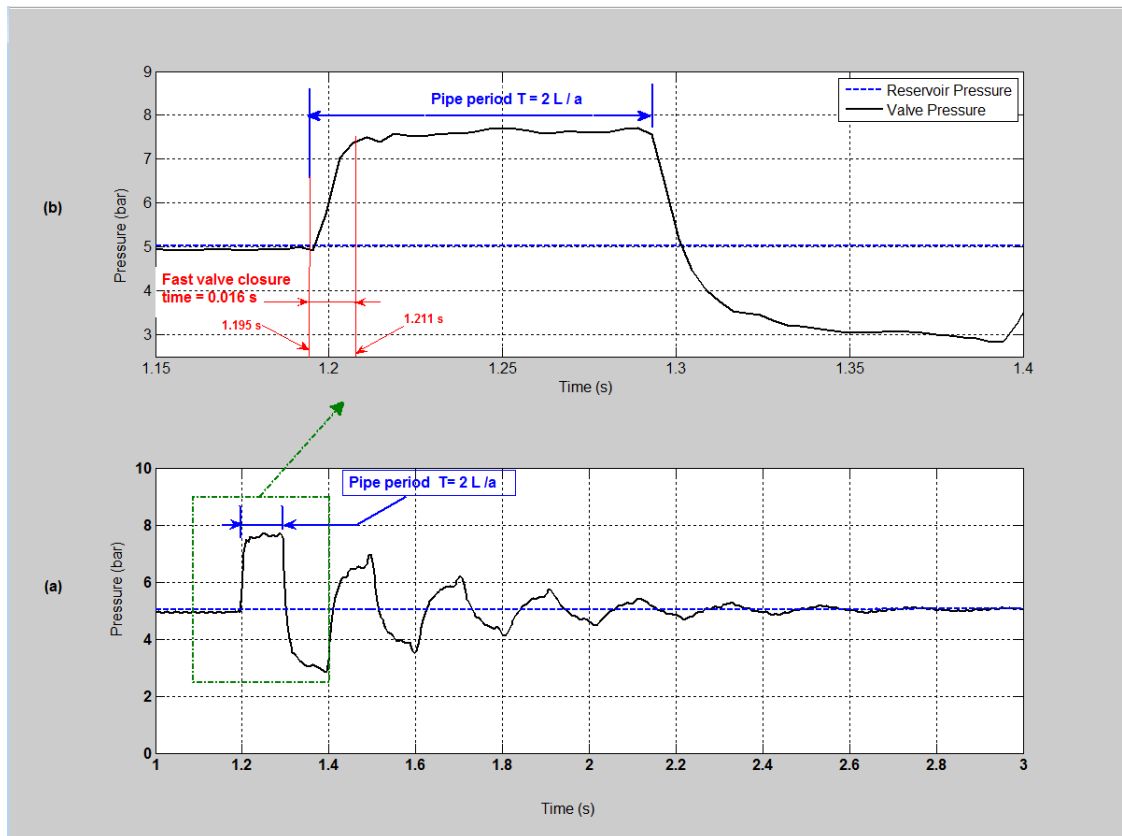


**Figure(4.5) Collection of three experimental runs for waterhammer with no column separation.**

The transient events in this experimental work are generated by rapidly closing the fast closure valve, Figure(4.2), in order to generate a front edge square pressure wave suitable for simple modelling of the valve boundary condition (i.e. in the transient event the flow velocity is rapidly brought to zero). Actual closing time ( $\tau$ ) is a key factor for shaping the pressure wave. The effective valve closing time can be measured from the actual hydraulic transient tests. Conventionally, whether the valve is closed rapidly or slowly is judged from the comparison with the theoretical limit to a fast valve closure time (Parmakian, 1963):

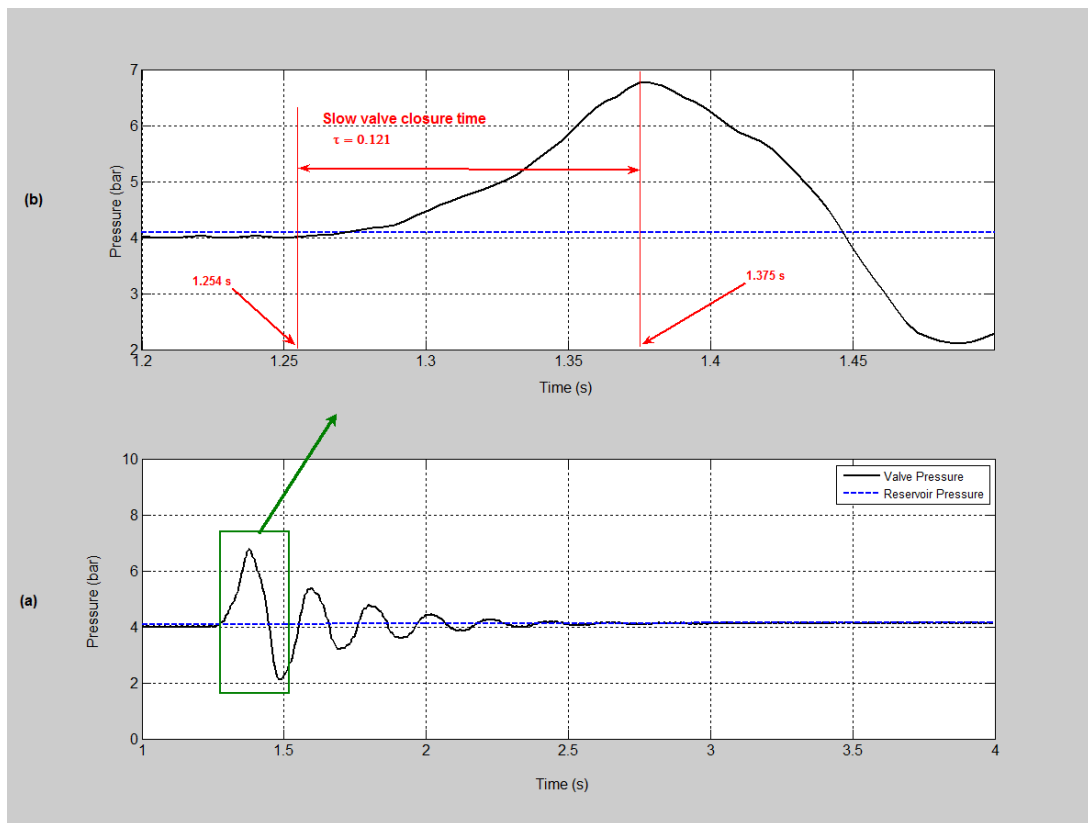
$$\tau \leq \frac{2L}{a} = T \quad \text{where} \quad T = 98.4 \pm 3.9 \text{ ms} \quad (4.1)$$

In Eq.(4.1) the valve is considered to be shut sufficiently rapidly so as to be effectively instantaneous if the reflected pressure wave reaches back to the valve after it has reached its fully closed position. Figure(4.6) shows the effective valve closure time on a pressure trace of a single-phase waterhammer run in such a situation. Experimentally, the effective valve closure time was measured to be in the range of 11 – 16 ms. This value is less than 16% of the pipeline period  $T$  (pressure wave reflected time) in Eq.(4.1).



Figure(4.6) Effective valve closure time

If the closing time takes more time than the pipeline period in Eq.(4.1), then it should be considered as a slow closure (Parmakian 1963), where the resulting transient pressure wave is shaped by the valve closure time. Figure(4.7) shows an example of a slow valve closure where the closing time took  $121\text{ms}$ , and as a result the wave shape gives a peak pressure less than the Joukowsky pressure, Eq.(1.1). However, it is noticeable that the reacting “sinusoidal” second and subsequent waves have a different shape to these in Figure(4.6) with a rapid closure.



**Figure(4.7) Pressure transient for a slow closing valve**

From Figure(4.6) and Figure(4.7) it can be seen that the finite valve closure time results, as would be expected, in a finite wave double reflection time of time  $2L/a$  (repeating each damped cycle thereafter). Though the valve closure is rapid, nevertheless Figure(4.6)(b) shows that its reflection at time  $2L/a$  reproduces the effect of the finite closure time. This introduces wave dispersion which, coupled with unsteady friction effects in this small scale laboratory apparatus, leads to the progressive smoothing behaviour in the time domain pressure trace.

#### 4.4 Identification of apparatus characteristics

The procedure for each experimental run starts at the reservoir side, Figure(4.2). The two regulating valves control both the flow velocity and the overall hydraulic pressure drop along the pipe for each experimental run. With flow control valve initially open, the reservoir is filled with water through the water supply inlet to reach a reservoir level of about  $1m$  height above datum. Keeping the fast closure valve in fully opened position, the reservoir is pressurised with air to a pre-set gauge pressure which is measured with the overhead pressure gauge.

The downstream regulating valve is adjusted to discharge the desired water flow rate for enough time ( $1 - 2min$ ) to stabilize the steady-state condition. Then water is

collected in a measuring cylinder of 2000ml against time, in less than 100s, to evaluate volume flow rate (and hence flow velocity), with care taken to maintain the test initial conditions throughout the period of measurement.

Then the data acquisition system is initiated about two seconds earlier than the hydraulic transient initiation (by shutting the quick closure valve as quickly as possible) to record the pressure history of the initial steady-state flow condition and the subsequent transient condition. The transient period is needed to validate the numerical modelling but also for experimental determination of both the true waterhammer wave speed ( $a$ ) and the unsteady friction coefficient (see Section 4.4.2). As neither of these are under investigation, the actual apparatus values are used to remove any impact they may have when investigating column separation. The initial period confirms the steady state and provides data for later calibration and analysis, for example evaluation of pressure drop between the reservoir pressure transducer  $P_R$  and the downstream valve pressure transducer  $P_{NS}$  and also for evaluation of Reynolds number and steady-state friction factor.

#### **4.4.1 Evaluation of wave speed**

Evaluation of the pressure wave speed is essential for hydraulic transient analysis. In the course of equipment design, analytical predictions were obtained for waterhammer wave speed, frequency and pressure rise. Pressure wave speed for thin-walled pipes of circular cross section can be evaluated (Wylie and Streeter 1993) using Eq.(4.2) which is usually judged to be applicable for pipes of diameter/thickness ratio  $(d/e) > 10$  (Thorley, 2004), where, for this apparatus  $(d/e) = 10.41$ :

$$a = \sqrt{\frac{K/\rho}{1 + \left[\frac{K}{E} \cdot (d/e)\right]}} \quad (4.2)$$

$K$  is the water bulk modulus of elasticity,  $\rho$  is the water density,  $E$  is Young's modulus of elasticity of the pipe wall material which is assumed to respond in linear elastic manner,  $d$  is the pipe internal diameter and  $e$  is the pipe wall thickness (Wylie and Streeter 1993).

The calculated value of this theoretical wave speed is shown in Appendix (A.1.1) to be:

$$a = 1355 \pm 27 \text{ m/s}$$

This value, though, is not the actual wave speed in the apparatus as pipe cross sectional shape becomes more oval than perfectly circular as a result of coiling the pipe (Anderson and Johnson, 1990). Because the apparatus has been relocated and modified since the measurements by Anderson and Johnson (1990), these measurements have all been repeated, showing slight differences for the circular cross sectional copper pipeline filled with only water at 17°C.

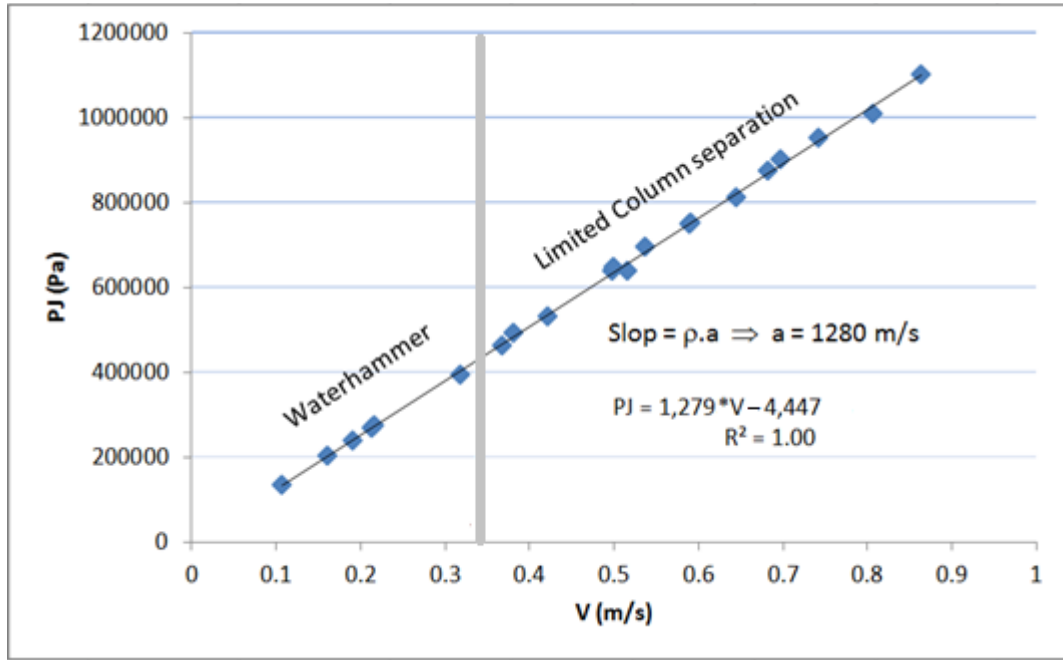
The pressure wave propagation speed  $a$  was measured for single-phase waterhammer pressure traces in two ways (Anderson and Johnson, 1990). Firstly, using Joukowsky theory, Eq.(1.1), in which water density  $998 \text{ kg/m}^3$  is known at the 17°C working temperature (White 1986), the immediate Joukowsky pressure rise  $P_j$  can be measured from the transient pressure trace Figure(4.5) for the initial flow velocity  $V_o$  as the flow was brought to rest almost instantaneously (to final flow velocity  $V = 0$ ). Applying these values in Eq.(4.3) (Anderson and Johnson 1990):

$$a = \frac{P_j}{\rho \cdot V_o} \quad (4.3)$$

gives an initial estimation of the pressure wave speed. This process is not precise because of the small effect of fluid-structure interaction (Williams 1977) as a result of the impact of the valve closure and the resultant pipe vibration during and after valve closure as evident in Figure(4.9), but it provides an estimate of wave speed value compared to the theoretical wave speed. Figure(4.8) summarises runs over a range of initial velocities. As it is the initial pressure rise immediately after valve closure, any subsequent column-separation will not affect the results, so a wide range of initial flow velocities can be covered. Figure(4.8) shows the expected linear response, but with some increasing scatter in the points as initial velocity increases, as might be expected (Appendix A.1.2). Consequently there are other lines that could have been plotted on Figure(4.8) than the overall but average gradient line shown. Looking at the range of possible lines that could go through the majority of the points gives the



likely value of  $a$  in the range  $a = 1280 \pm 40 \text{ m/s}$ , with a narrower range of values than obtained previously by Anderson and Johnson (1990).

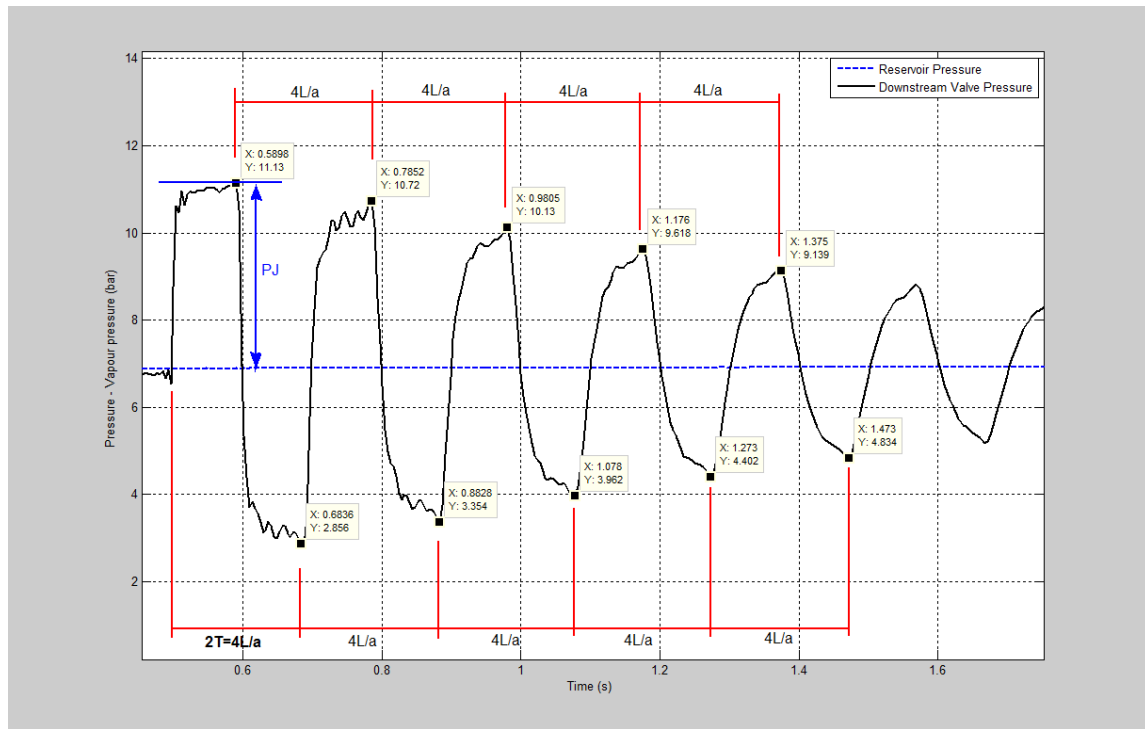


**Figure(4.8) Direct evaluation of wave propagation speed from initial rapid pressure rise.**

Secondly, the pressure wave speed can be estimated experimentally, by considering the same pressure history for the case of single-phase waterhammer recorded at downstream valve, Figure(4.9), (Wylie and Streeter 1993) and using Eq.(4.4):

$$a = \frac{4 \cdot L}{2 \cdot T} = \frac{2 \cdot L}{T} \quad (4.4)$$

The value of the wave speed could be estimated by taking the average periods of waterhammer cycles from traces of single-phase waterhammer without column separation, at different reservoir pressure settings as illustrated in Figure(4.9). Though in principle, this could be done over a single waterhammer wave cycle, in practice time measurement uncertainties are reduced by taking more than one cycle. Unlike the previous method of Figure(4.8), the range of initial flow velocities excludes those leading to any column-separation. With the uncertainty calculated as in Appendix (A.1.3), the wave-speed measured this way is  $1275 \pm 25 \text{ m/s}$ .



**Figure(4.9) Evaluating pressure wave speed on a waterhammer pressure trace.**

An alternative approach to time-based wave speed determination could be more reliable than the previous by identifying the fundamental frequency of waterhammer ( $f_n = 1/2T$ ) (Martin 1983, Arfaie 1989, Anderson and Johnson 1990). Using Figure(4.10), the value of the wave speed can be estimated from natural frequency by recasting Eq.(4.4) as:

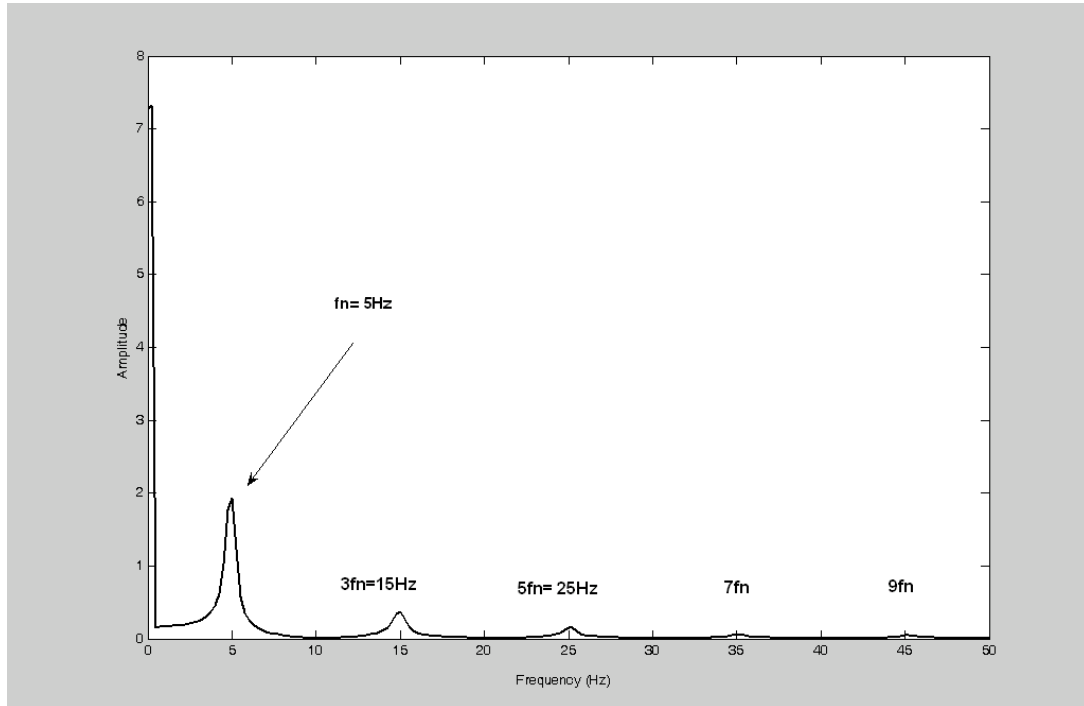
$$a = \frac{4.L}{2T} = 4.L.f_n \quad (4.5)$$

Figure(4.10) gives the frequency response for one of the waterhammer runs without column separation. The fundamental frequency  $f_n = 5.08 \pm 0.05\text{Hz}$  Figure(4.10), and applying this value in Eq.(4.5) gives an estimation of pressure wave propagation speed of value  $1275 \pm 13\text{m/s}$ .

**Table(4.3) Summary of calculated wave speeds  $a$**

Method of calculation	$a \pm \Delta a$
Theoretical	$1345 \pm 30 \text{ m/s}$
Amplitude	$1275 \pm 25 \text{ m/s}$
Period	$1280 \pm 40 \text{ m/s}$
Frequency	$1275 \pm 13 \text{ m/s}$

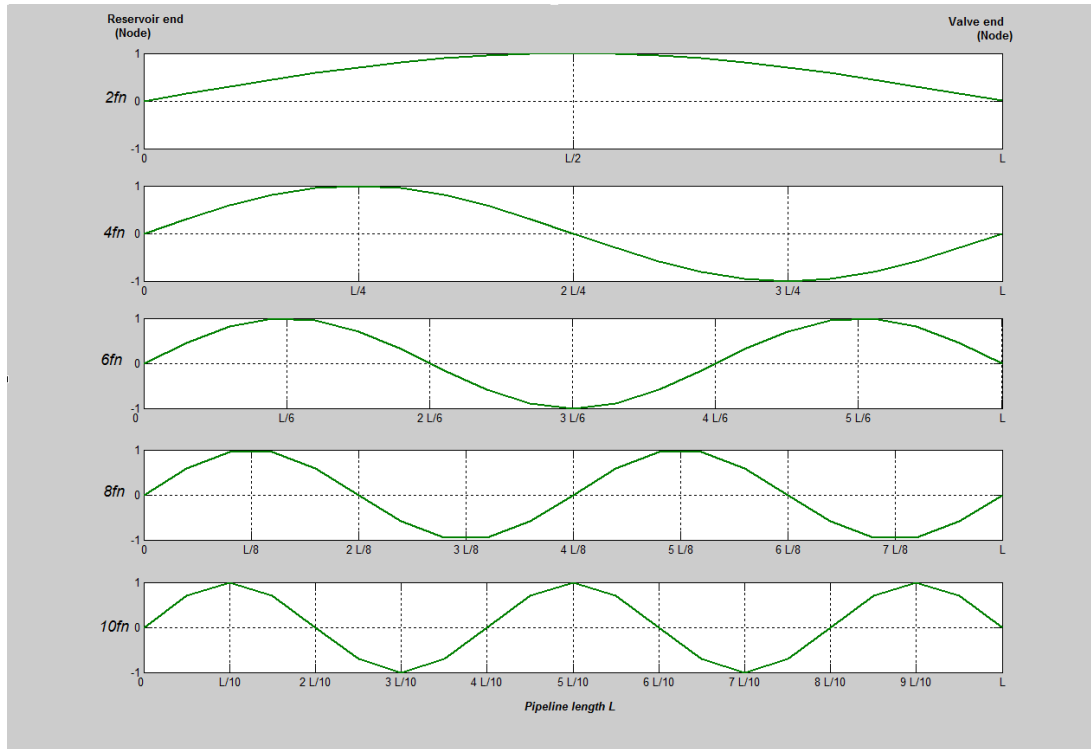
In summary, Table(4.3) provides the calculated wave speeds  $a$ . The theoretical wave-speed is 6% higher than the experimental, supporting the contention by Anderson and Johnson (1990) that it is inappropriate (no overlap of uncertainties). The experimental value of  $a = 1275 \text{ m/s}$  should be used in computation to eliminate this difference.



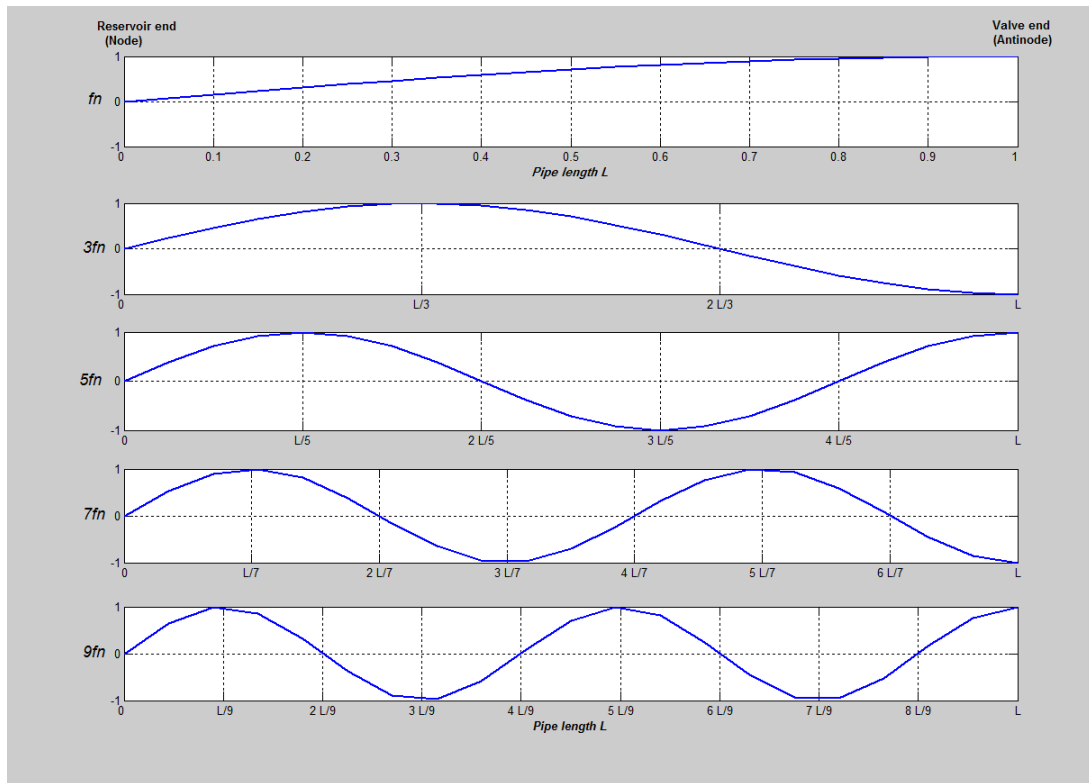
**Figure(4.10) Pressure wave natural frequency and the harmonic frequencies for single phase waterhammer pressure trace at valve.**

Figure(4.10) shows the higher harmonic frequencies of the wave propagation at 15,25,35 and 45Hz. These are not single sharp value spikes, indicating significant wave dispersion, as illustrated in Figure(4.9) where the wave shape evolves at every successive repetition. As these results came from the single-phase waterhammer alone, they indicate apparatus behaviour in terms of transient damping which might influence comparisons between observed and modelled behaviour, even though this is not specifically part of the column separation phenomena under investigation in this Thesis. The results indicate, though, that it may be appropriate to adopt some model of transient damping from the literature in order to eliminate this issue from any comparing of model and experiment.

Comparison with theoretical frictionless standing wave solutions in Figure(4.11) and Figure(4.12) clearly demonstrates that there were no signs of any frequencies of  $2f_n, 4f_n, 6f_n, \dots$  that would indicate valve opening or leakage during the pressure transient event, with all measured frequencies in Figure(4.10) matching closely the peaks in Figure(4.12) and no evidence of any minor peaks, especially at the frequencies of Figure(4.11).



**Figure(4.11) Demonstration of pipeline natural frequency diagrams with downstream valve opened. (Thorley 2004).**



**Figure(4.12) Demonstration of pipeline natural frequency diagrams with downstream valve closed. (Thorley 2004).**

These conventional experimental methods used for measuring the real waterhammer wave speed in the laboratory apparatus are based on the time-domain transient pressure recordings from a single fixed point along the pipe (the pressure transducer close to the rapid-closure valve) and consequently raise the issue (rarely discussed for waterhammer) whether it is the group velocity or phase velocity which is being identified by the methodology (Feather 1961, Coulson and Jeffrey 1977, Lighthill 1978):

- Group Velocity: the speed with which the overall envelope of wave amplitudes propagates through space.
- Phase Velocity: the speed of travel of any one phase of the frequency components contributing to the overall wave “packet”.

The concept of group velocity arises wherever a waveform is Fourier analysed (as in the frequency-domain approach above) into a set of harmonic wave components where each does not necessarily have the same phase velocity. Only a single harmonic wave train can be transmitted without change of shape, so any wave profile that can be analysed into two or more wave trains will change the overall wave profile shape as it is propagated. This is frequency dispersion, causing the group velocity to

be different to the separate component wave phase velocities. Group velocity and phase velocity coincide only in non-dispersive systems (Feather 1961, Coulson and Jeffrey 1977, Lighthill 1978).

Classically, acoustic waves, of which one-dimensional pipe waterhammer waves are an isotropic (i.e. all wave propagation directions are the same) variant, have been treated as non-dispersive (Feather 1961, Coulson and Jeffrey 1977, Lighthill 1978). However, the time-domain pressure wave traces used above, e.g. Figure(4.9), show clear evidence of not only attenuation (i.e. reduction of amplitude over time due to viscous pipe friction and other dissipative effects), but also dispersion (i.e. change of overall amplitude wave shape over time, with progressive “rounding” of the repeating waveforms and “smearing” of spikes or sharp change gradients).

Evidence of dispersion is also provided by the frequency-domain plot Figure(4.10) where the amplitude peaks, though clearly defined with obvious amplitude maxima, are not sharp spikes at isolated frequencies but show narrow bands of frequencies around each peak. This is evidently, from the actual experimental traces, an issue for even this very simple single pipe system with clearly defined reflective boundary conditions (constant velocity at valve, constant pressure at reservoir or vapour cavity).

Even the classical textbook description of idealised single-phase waterhammer in a frictionless uniform horizontal pipe subject to instantaneous valve closure (e.g. Parmakian 1963, Wylie and Streeter 1993, et al) can indicate that dispersion is inevitable with waterhammer. The classic derivation of the frequency ( $f_n$ ) or period of oscillation ( $2T$ ) of the idealised “square” wave (apparently, therefore, non-dispersive as well as being attenuation-free) as  $f_n = (a/4L)$  or  $2T = (4L/a) \equiv f_n^{-1}$  (Eq. 4.5) neglects the effect of the wave propagating into the initial steady flow velocity ( $V_o$ ), ie initially at velocity  $(a - V_o)$  as indicated by the fundamental characteristic equation, Eq.(3.6). Even in this idealised case, therefore, taking into account the four traverses of the pipe length ( $L$ ) by the wave, the group velocity (measured from the overall “square” waveform) differs from the wave phase velocity by a fraction that can be shown to be  $(2V/a)$ . In real systems with pipe friction, this fraction will be reduced slightly by attenuation but increased slightly by the phenomenon of “line packing”.

In addition, real rapid valve closures are not “instantaneous” but occur over a finite (if short) time  $\tau < T/2$ . These can be modelled (as in any numerical method based on discretisation) as a series of discrete small instantaneous steps over the actual closure time  $\tau$  (as in any discretised numerical simulation), but each individual small wave pulse will be initiated from a different fluid velocity  $V(t)$  (where  $V \geq V(t) \geq 0$  over  $0 \leq t \leq \tau$ ) and hence the rapid valve closure disturbance propagation wave will be dispersive.

However, unless the pipe is highly distensible, the low compressibility of liquid water (Chaplin, 2015) results in high disturbance velocities ( $a$ ) of the order of 1 km/s, while in conventional engineering practice pipe water flow velocities rarely exceed 5m/s so the difference between group and phase velocities will be of the order of  $5/1000 \equiv 0.5\%$ . Therefore, just as it is conventional to simplify waterhammer calculations by neglecting the convective terms because  $V \ll a$  (e.g. Wylie and Streeter 1993, et al), so it can be argued for these experiments that the difference between wave group and phase velocities is smaller than the measurement uncertainties given above and so cannot be resolved.

#### 4.4.2 Evaluation of pipe friction factor

In this research, initial steady flow velocity was measured for each run of pressure transient to evaluate friction factor. Both steady state friction factor and initial flow velocity are needed for the purpose of mathematical modelling of waterhammer and column separation.

For each run, the basic steady state friction factor (Darcy friction coefficient  $f$ ) is evaluated using the Darcy Weisbach formula (White 1986), Eq.(4.6):

$$\Delta P_f = \frac{f \cdot L \cdot \rho \cdot V^2}{d \cdot 2} \quad (4.6)$$

In this the Moody chart (Lomax and Saul 1979, White 1986) would be used to predict Darcy friction factor; e.g. for hydraulically smooth pipe it can be evaluated for both laminar and turbulent flows respectively (Lomax and Saul 1979, White 1986) using the two formulas Eq.(4.7) and the empirical Eq.(4.8).

$$\text{Theoretical} \quad f = \frac{64}{\text{Re}} \quad \text{for } \text{Re} < 2000 \quad (4.7)$$

$$\text{Empirical} \quad f = \frac{0.316}{\text{Re}^{0.25}} \quad \text{for } 4000 \leq \text{Re} < 10^5 \quad (\text{Blasius Equation}) \quad (4.8)$$

where the flow Reynolds number (White 1986) is:

$$\text{Re} = \frac{\rho \cdot V \cdot d}{\mu} \quad (4.9)$$

However, in this study, it is a simple process to measure the true Darcy friction factor for greater accuracy than is possible with estimates from the Moody diagram. Steady state friction factor was evaluated from the acquired data of each experimental run during the initial steady state period. To avoid any additional pressure measurements the Bernoulli equation (Lomax and Saul 1979) was applied between the reservoir pressure transducer  $P_R$  and the downstream valve pressure transducer  $P_{NS}$  as illustrated in Figure(4.13). The pipe entrance minor loss  $K_e$  value 0.5 for a sharp edge (White 1986) was taken into account and also the assumption of negligible water velocity in the reservoir with the datum at the level of the upstream pressure transducer  $P_R$ :

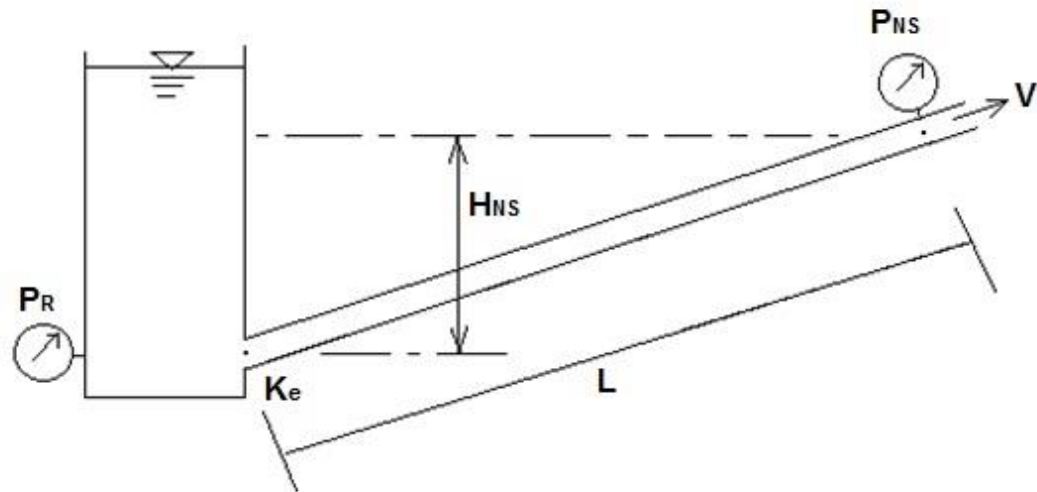
$$P_R = P_{NS} + \frac{\rho \cdot V^2}{2} + \rho \cdot g \cdot H_{NS} + K_e \frac{\rho \cdot V^2}{2} + \frac{f \cdot L}{d} \frac{\rho \cdot V^2}{2} \quad (4.10)$$

in which  $V$  is the steady pipe flow velocity,  $H_{NS}$  is the downstream pressure transducer depth elevation and  $L$  is the pipe length. Rearranging Eq.(4.10) for Darcy friction factor gives:

$$f = \frac{\left[ P_R - P_{NS} - \rho \cdot g \cdot H_{NS} - (1 + K_e) \cdot \frac{\rho \cdot V^2}{2} \right]}{\frac{L}{d} \cdot \frac{\rho \cdot V^2}{2}} \quad (4.11)$$

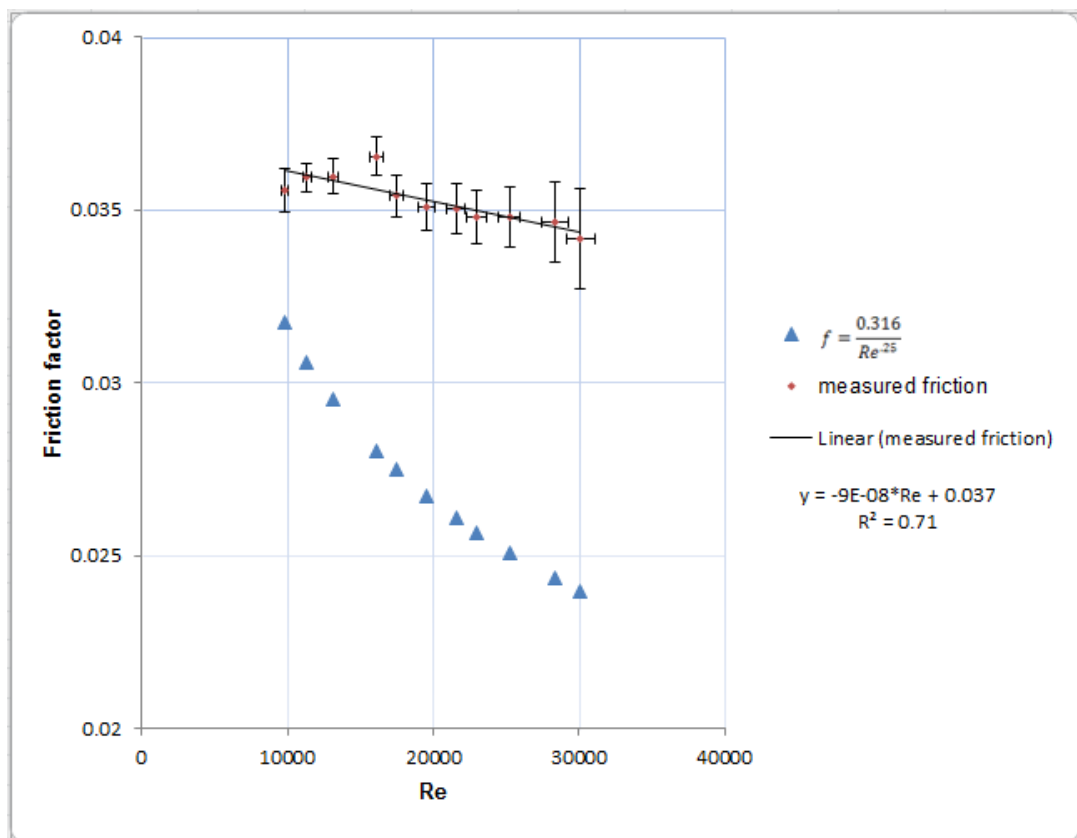
The average temperature of collected water was measured using a thermometer and found to be  $17 \pm 1^\circ C$  with the corresponding kinematic viscosity  $\nu = (1.08 \pm 0.03) \times 10^{-6} m/s^2$





Figure(4.13) Illustrative diagram for steady-state flow in a pipe, Eq.(4.10).

The associated uncertainty analysis for experimental data are presented in Appendix (A.2). Experimental values are presented in Table(4.4) and also Table(5.3).



Figure(4.14) Measured and estimated frictional factor.

Some of the experimental steady state friction factors against Reynolds number are plotted in Figure(4.14) with the uncertainty base being calculated as in Appendix (A.2). It can be seen that, apart from an occasional outlier, it is possible (over this limited Reynolds number  $Re$  range) to draw a straight line through the points (within their uncertainty). This shows the actual values of friction factor are closer to constant within the uncertainty suggesting fully turbulent flow rather than hydraulically smooth pipe flow as estimated by Eq.(4.8). As the range of gradient is very small, it is a reasonable approximation during any transient (in which the range of Reynolds number will be smaller) that friction factor is effectively constant, with a mean value  $f = 0.035 \pm 0.002$  .

Table(4.4) Steady flow conditions to determine Darcy friction factor  $f$ 

#	$P_R$ (Pa)	$P_{Ns}$ (Pa)	Initial velocity $V_o$ (m/s)	Friction factor ( $4f$ )
1	602883	597668	0.16	0.034
2	205385	202100	0.11	0.051
3	603004	596743	0.32	0.041
4	404471	397718	0.22	0.045
5	606666	597176	0.47	0.036
6	302325	295788	0.21	0.045
7	605993	572554	0.58	0.034
8	402940	392280	0.43	0.042
9	503128	476216	0.54	0.029
10	601614	561922	0.64	0.033
11	605654	560777	0.682	0.034
12	403267	378664	0.499	0.030
13	404097	378784	0.516	0.029
14	304818	287006	0.421	0.027
15	606482	545227	0.806	0.034
16	404024	370782	0.589	0.032
17	403065	369547	0.591	0.032
18	602439	532225	0.863	0.035
19	503978	451736	0.742	0.034
20	303274	278992	0.498	0.030
21	204021	188842	0.382	0.026
22	402122	362619	0.644	0.033
23	203848	186226	0.419	0.027
24	402933	356846	0.698	0.033
25	502599	434787	0.860	0.034
26	303045	268442	0.602	0.032
27	204465	182216	0.475	0.029
28	403786	342671	0.806	0.035
29	605721	486642	1.150	0.035
30	404224	336555	0.857	0.034
31	403057	347001	0.855	0.028
32	502934	407403	1.034	0.034
33	402797	331115	0.880	0.035
34	604830	466070	1.247	0.035
35	304220	253581	0.731	0.034
36	201929	173271	0.548	0.031
37	404990	321163	0.960	0.034
38	606345	415741	1.484	0.034
39	303591	234017	0.859	0.035
40	203193	163893	0.648	0.032
41	303056	226675	0.905	0.035
42	303357	163664	1.172	0.040
43	303593	163664	1.249	0.035
44	202163	111627	0.993	0.034
45	104453	54104	0.732	0.033
46	604472	29003	2.684	0.032
47	505031	25334	2.415	0.033
48	405222	20371	2.130	0.034
49	302306	47884	1.724	0.034
50	302774	27945	1.785	0.034
51	203275	27981	1.412	0.034

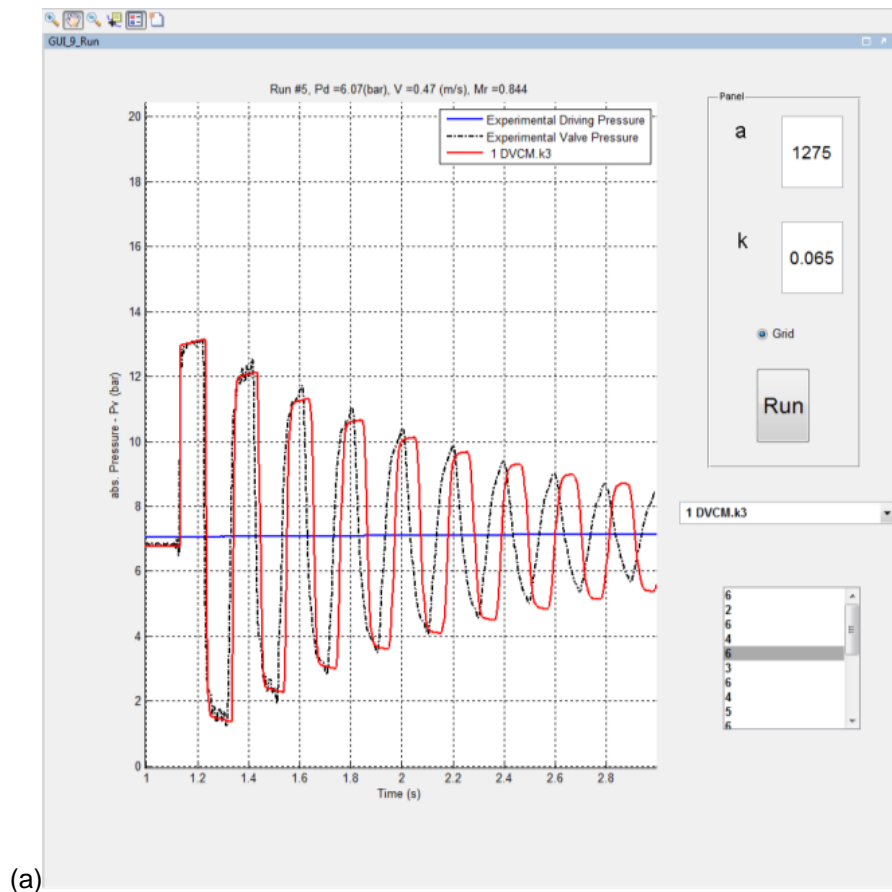
#### **4.4.3 Calibration of unsteady friction model**

Arfaie (1989) suggested that with this small scale experimental apparatus agreement between experimental and column separation models could be improved by taking into account unsteady friction. While it is not a part of this present study to investigate unsteady friction, it is appropriate to use an appropriate unsteady friction model from the literature to investigate its effect on modelling column separation. Previously Bughazem (1997) had investigated unsteady friction on the experimental apparatus used in this study and had demonstrated that (Bug hazem and Anderson, 2000):

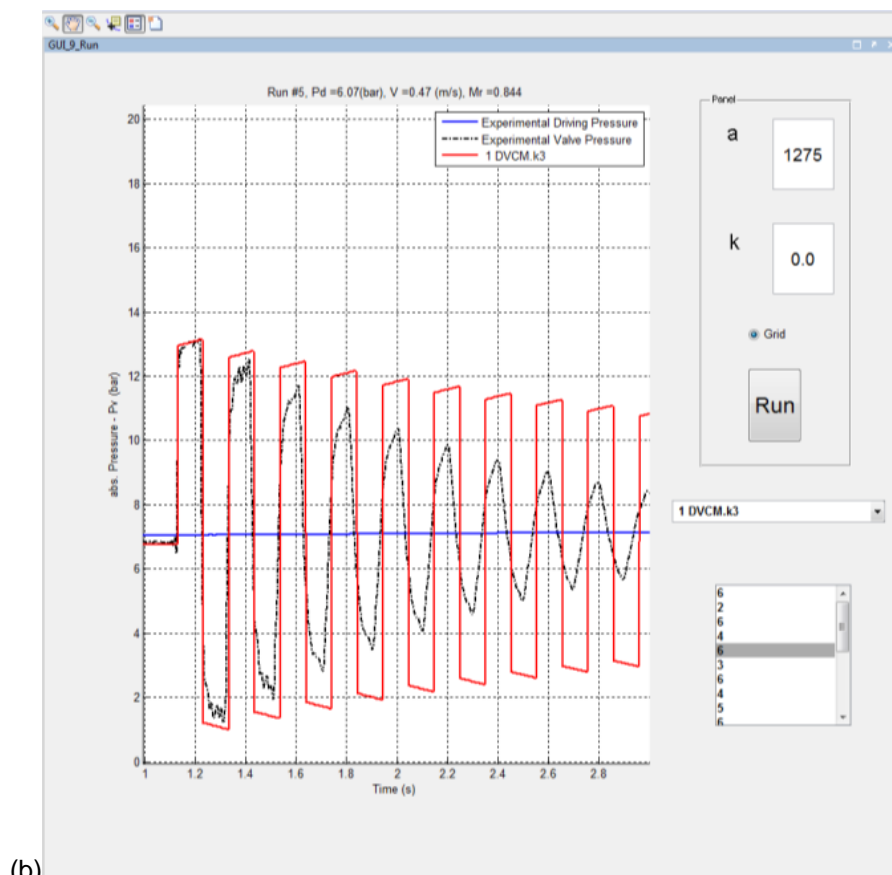
- (a) With an appropriate choice of unsteady friction coefficient ( $k$ ), variants of the Brunone et al (1991b) unsteady friction model could give very good representation of waterhammer behaviour including pressure wave attenuation for this particular apparatus.
- (b) However, the “best” unsteady friction coefficient (i.e. that giving the best comparison between experiment and calculation) was strongly dependent on the actual finite difference implementation of the Brunone model.

Consequently, it was decided to exploit this previous work at Newcastle and to use both the implementation tested by Bug hazem and Anderson(1996) and Bug hazem (1997), which was known to give good correlation, as well as a variant he suggested (Bug hazem and Anderson, 2000) but did not actually test.

Bearing in mind point (b) above concerning the sensitivity of the best unsteady “friction” coefficient ( $k$ ) to the actual code implementation, it was not only necessary to obtain the best value of  $k$  for the new model but also sensible to repeat the exercise for the existing model. In addition, though the column separation model should not in itself influence this aspect of the waterhammer behaviour, the codes for the two classic column separation models from the literature ( DVCM and DGCM, Section 3.4) were both used in this exercise as a basic check. The MatLAB user interface was used for this exercise, as shown in Figure(4.15) where quasi-steady friction (effectively unsteady friction  $k = 0$ ) is compared with unsteady friction ( $k > 0$ ) (Bergant and Tijsseling 2001).

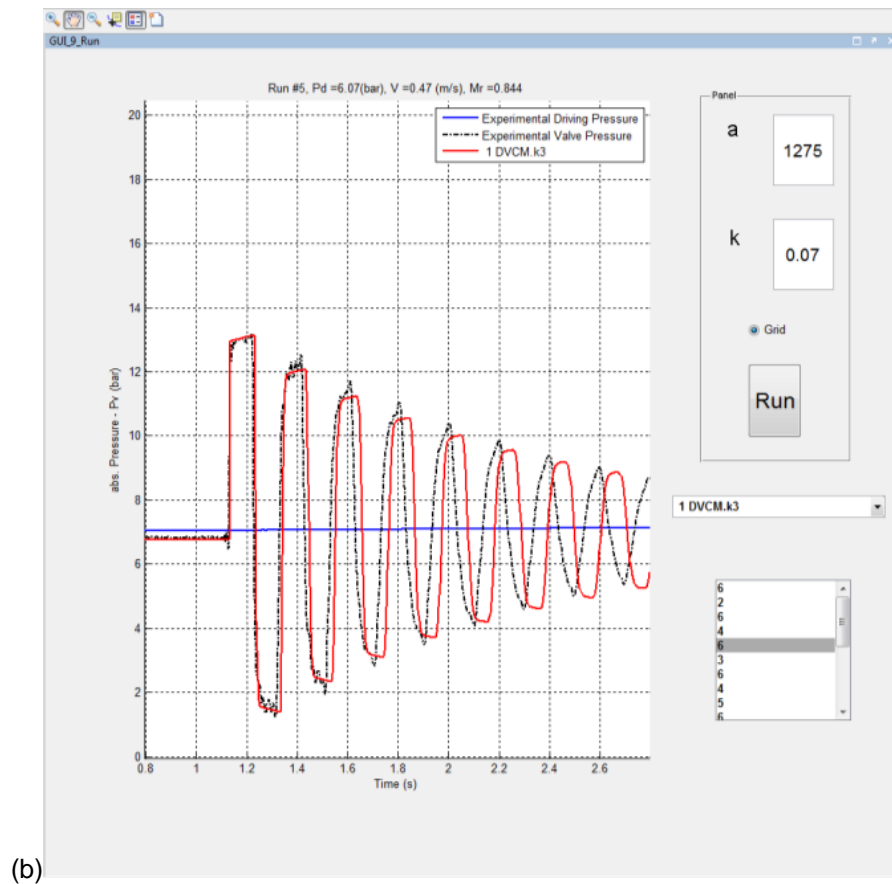
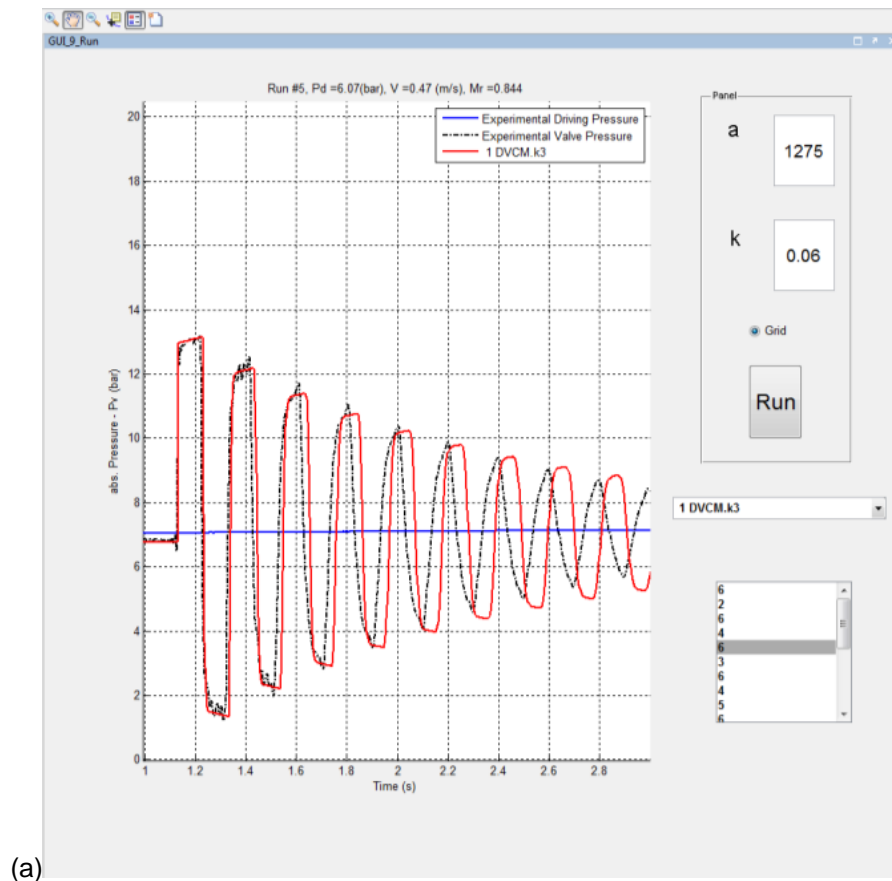


(a)



(b)

Figure(4.15) Effect of unsteady friction model  $k_t = 0.065$  (a) over the quasi-steady friction (b).



Figure(4.16) Sensitivity measure of unsteady friction model  $k3 = 0.065 \pm 0.005$

As a result of this exercise, it was found that:

- (i) The new model proposed by Bughazem and Anderson (2000) (Section 3.3) with  $k_t = 0.035$  has given as good a comparison with the single-phase waterhammer experiments as the original Bughazem and Anderson(1996) implementation.
- (ii) The best values of the unsteady friction coefficients were found from repeated calculation comparisons to be:  $k_3 = 0.065$  for both the new implementation and the Original Bughazem implementation (Section 3.3).
- (iii) With the original Bughazem implementation, the best value is not particularly sensitive. Figure(4.16) shows effect of varying the value by  $\pm 0.005$ .

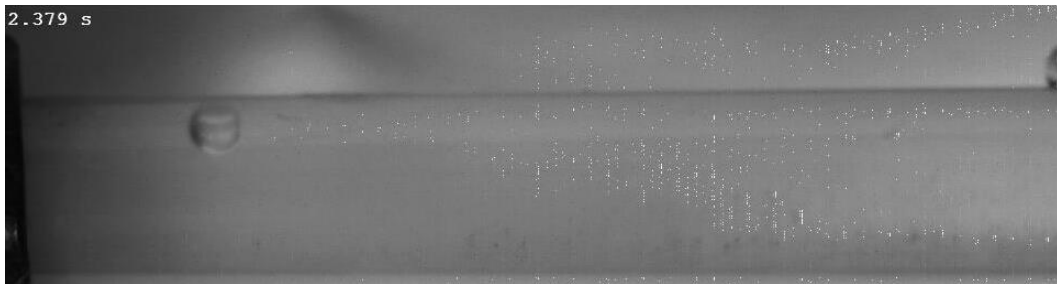
### 4.5 Visualisation of cavity formation

Bergant et al (2006) reported that early visualisation of column separation by pioneers (e.g. Bunt in 1953; Kamel in 1954; Blind in 1956), who conducted laboratory column separation experiments, reported large vapour cavities following the valve closure (hence the expression “column separation”). By contrast, recently Adamkowski and Lewandowski (2012) reported no sign of bubbles in the discharge line of a pump for the previous experimental work done by Adamkowski (in 1996 and 2004). This group conducted experimental column separation work on a reservoir-pipe-valve-reservoir apparatus. To capture the cavitation behaviour they fitted two visualisation sections to the pipe, one close to the valve and the other close to the upstream reservoir ( $3L/4$  away from the valve). They found cavitation at both locations and confirmed earlier observations of other researchers (Wiggert and Sundquist 1979; Martin 1983) that cavitation could form and develop anywhere along the pipe.

Arfaie (1989) conducted limited visualisations on an earlier installation of the current test rig which were not synchronised to the pressure traces. He did not observe large vapour cavities but rather an indeterminate region of distributed small bubbles that occasionally coalesced. There was some unverified suggestion that these bubbles might move in the opposite direction to that which would be expected.

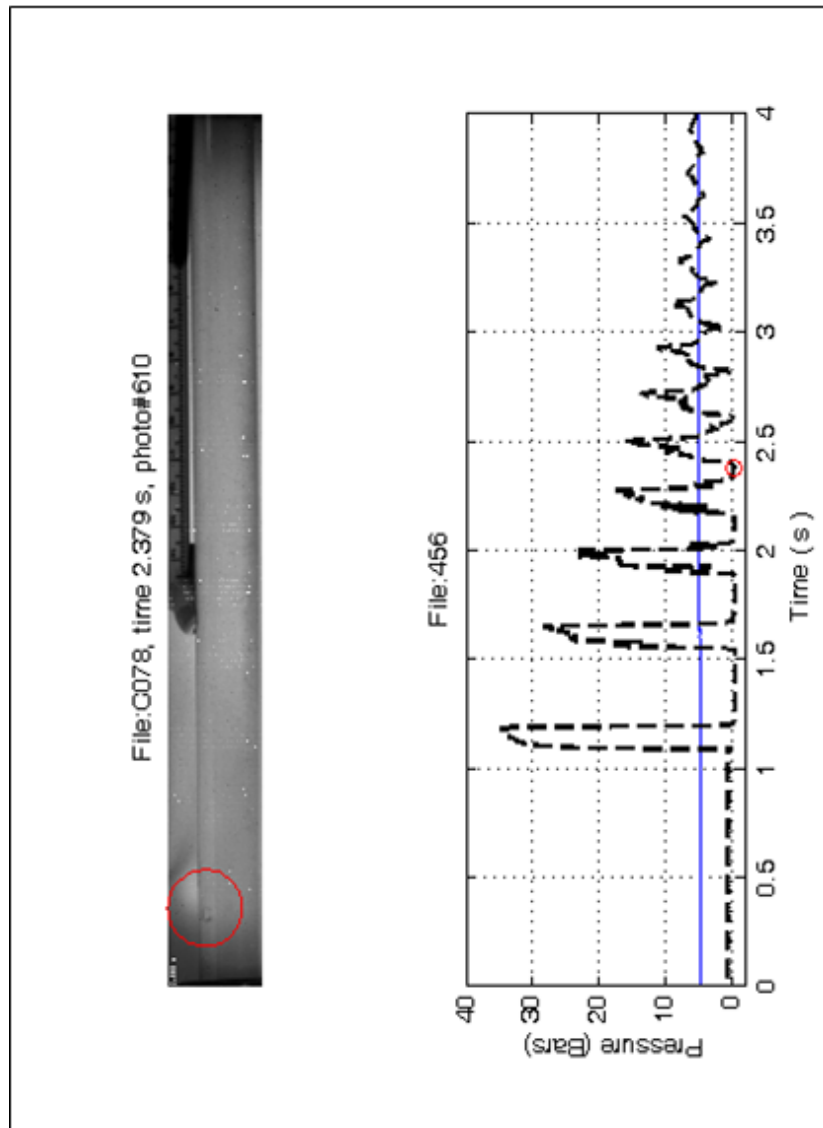
To clarify this situation, visualisation of the column separation region was undertaken, to investigate whether or not there was some observed difference in the cavity formation behaviour that might be a factor in the different modes of behaviour. The phenomenon was investigated visually using a high-speed camera (Motion Pro X5 <sup>TM</sup>), synchronised with the data recorder system to provide a series of frames

(short film) linked to the pressure traces for the two different types of water column separation at the upstream side of the fast closure valve (the highest point in the reservoir-pipe-valve system, at which the cavitation forms) through the polycarbonate pipe section located close to the valve, Figure(4.1). Figure(4.18) shows a typical column separation but the image is for the last (fourth in this case) cavity occurrence. It shows few vapour bubbles, as would be expected from the much shorter cavity duration over which they could evolve due to both gas release and vaporisation (Tullis, 1989). Figure(4.17) is a zoom of Figure(4.18), showing an example of the observed maximum size of the last clear vapour cavity in the time sequence of Four transient cavitation events. The time of 2.379s is recorded on both the photo frame and the cursor information on the pressure trace of the same experimental run. Initial flow direction is from left to right with the closed valve just to the right of the image on Figure(4.18).



**Figure(4.17) Zoom in a synchronised photo frame of Figure(4.18) of the 4<sup>th</sup> cavitation at 2.379s.**

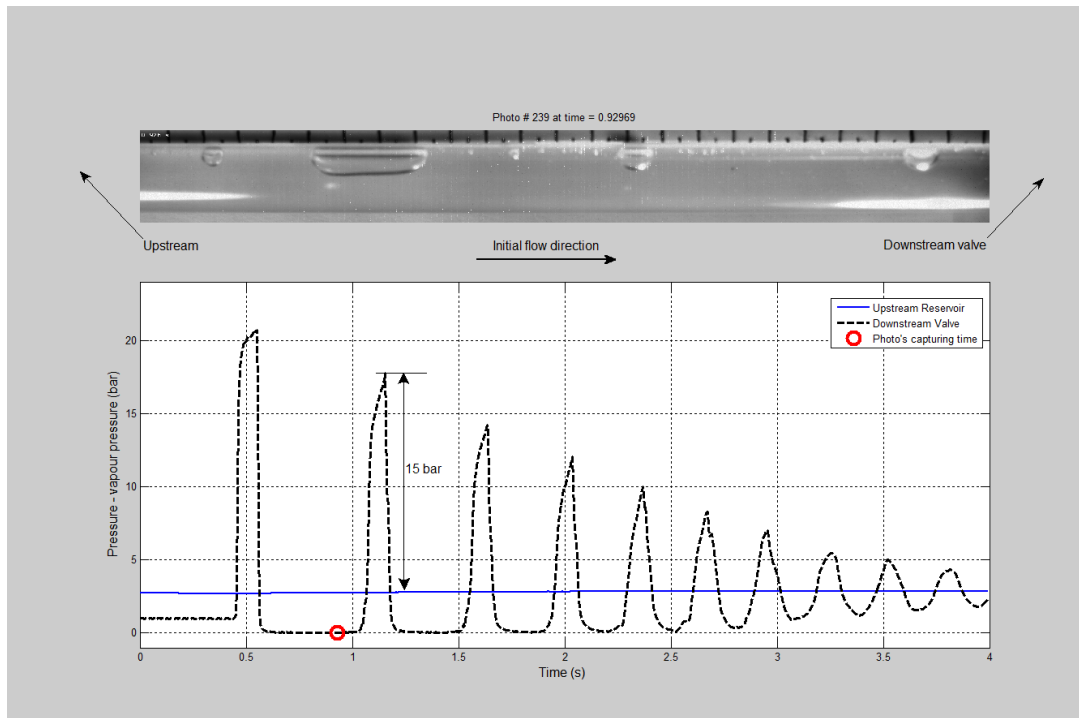




**Figure(4.18) Synchronised pressure trace with high speed camera of the 4<sup>th</sup> cavitation at 2.379s.**

A typical first water column separation event is shown in Figure(4.19), for initial steady-state condition 1.84barg reservoir pressure and initial flow velocity 1.35m/s. Some features can be drawn from the photograph, Figure(4.19):

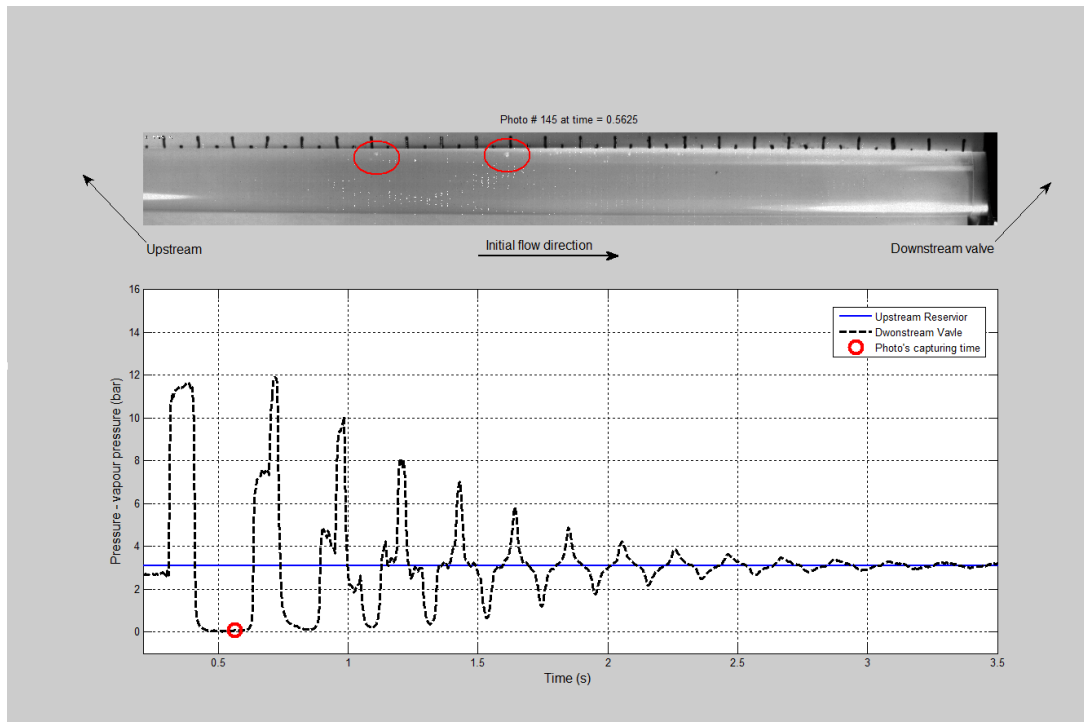
- (i) There is not a complete full-section vapour cavity with a visible end limit. Cavitation is partial, with column separation being a two-phase flow region incorporating both larger and smaller vapour bubbles, with those located along the top of the pipe about a maximum of 8mm in depth.
- (ii) In this case the maximum bubble size within the cavitation region reached almost 33mm length within a clearly longer cavitation region.



**Figure(4.19) Photograph of vapour cavities for a typical column separation synchronised with pressure trace at reservoir pressure 1.84barg.**

This maximum cavity size was captured at time 0.929s, i.e. 0.485s after closing the valve, giving a duration of bubble growth from initiation and subsequent collapse 0.363s and 0.169s, respectively, which led to a subsequent high pressure rise up to 15bar above reservoir pressure. This typical column separation high-pressure rise is less than the Joukowsky pressure with a decline in the amplitude of successive peaks. The visualization image is similar in character to that previously obtained by Arfaie (1989), but now these images can be directly correlated with the transient pressure trace.

Another column separation with a pressure spike just equal to the Joukowsky pressure rise has been recorded in Figure(4.20) for initial conditions of 2.2barg reservoir pressure and 0.83m/s flow velocity. This photograph shows groups of very tiny distributed bubbles. The maximum bubble size reached  $\sim 1\text{mm}$  diameter at time 0.188s from the valve closure, where it initiated and grew in 0.144s. Furthermore, the cavity subsequently shrunk and collapsed in 0.085s, which led to second pressure rise up to 8.8bar above reservoir pressure for a duration of 0.037s, almost as high as the Joukowsky pressure rise (first pressure peak).

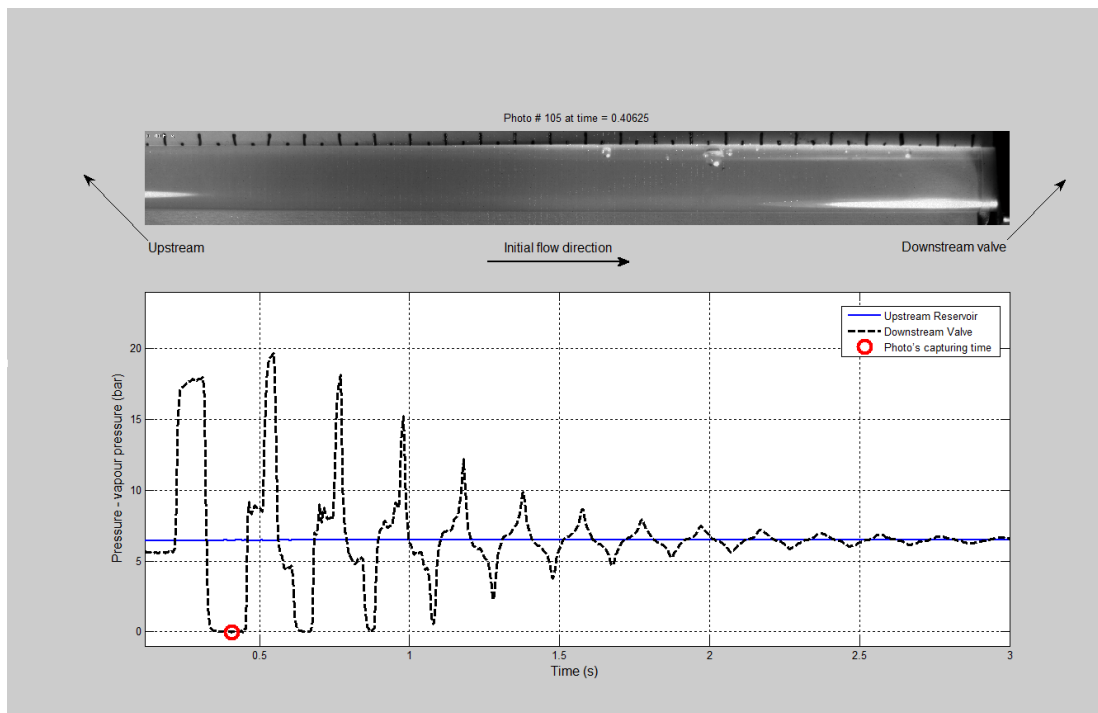


**Figure(4.20) Synchronised photograph of column separation with spikes lower than or equal to Joukowsky pressure rise at reservoir pressure 2.2 barg and initial flow velocity 0.83 m/s.**

In comparison with the case of typical column separation shown in Figure(4.19), in Figure(4.20) the total cavity duration is quite small ( i.e. less than half of the cavity duration in the case of typical column separation) and consequently the vapour cavities appear as tiny bubbles distributed along the section whereas in the case of typical column separation the cavities had more time to grow to localized groups of bubbles, indicating that the non-equilibrium phenomenon of boiling takes a finite time to occur.

To confirm this observation, limited column separation with a pressure spike higher than the Joukowsky pressure rise is shown in Figure(4.21). The initial operational conditions were 5.6 barg reservoir pressure and 1.15 m/s flow velocity. The graph shows the vapour cavity that initiated and reached its maximum bubble size of almost 5 mm diameter in 0.074 s. It was captured at 0.188 s from shutting the valve and its subsequent collapse duration was 0.121 s, which led to high pressure rise up to 12.43 times reservoir pressure. This high-pressure rise exceeds the Joukowsky pressure rise by about 2.5 bar. In this case, though the total cavity duration is smaller than in Figure(4.20), there were fewer but larger bubbles produced (almost five times the size). As it is almost impossible to entirely eliminate dissolved air, and a programme of repeated tests is likely to be influenced by any dissolved gases acting as bubble

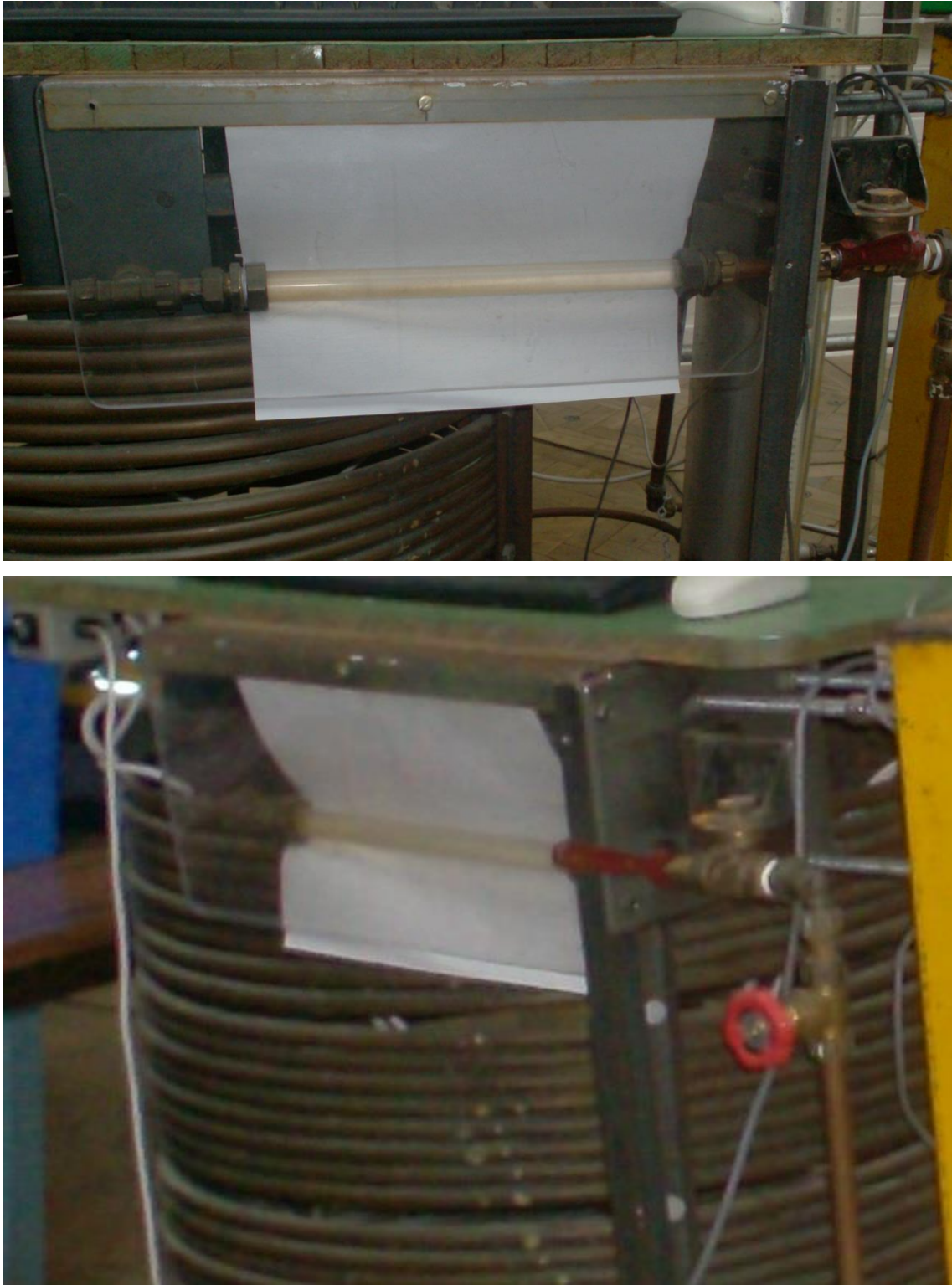
nuclei, this observation suggests that the macro-behaviour evinced in the pressure traces is not significantly influenced by the micro-behaviour within the overall cavitation region. It suggests that it is the existence of an effectively constant pressure (at or close to saturation pressure), rather than the distribution of saturated liquid and saturated vapour within that region, that drives the form of the pressure transient.



**Figure(4.21) Photograph of vapour cavities for a column separation with spike higher than Joukowsky pressure, synchronised with pressure trace at reservoir pressure 5.6 barg at 0.406s.**

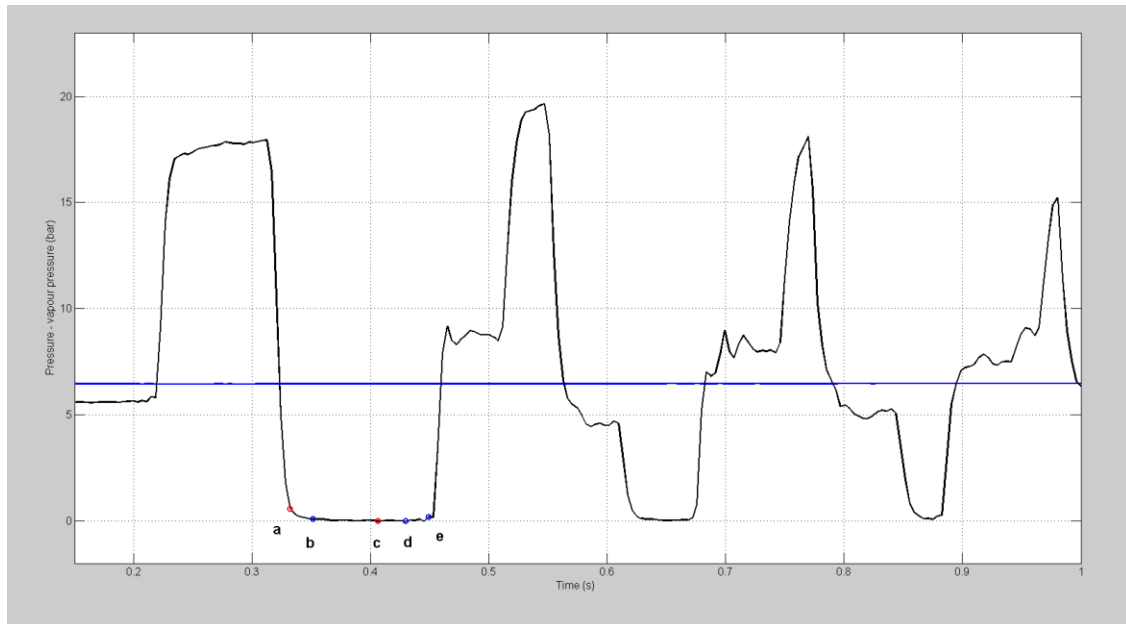
Figure(4.22) shows two images of the visualisation section and shows how it was connected to the end closure valve. Table(4.5) connects the experimental pressure trace of Figure(4.23) to the time series of images in Figure(4.24).

Bubbles have already appeared in image (a), even though the pressure has not reached its minimum value. These grow in images (b) and (c) before coalescing and collapsing in image (d), with none visible in image (e) just before the sharp post-cavity pressure rise. With limited cavitation, there is little time for bubbles to evolve. Table(4.6) connects the experimental pressure trace of Figure(4.25) to the time series of images in Figure(4.26).

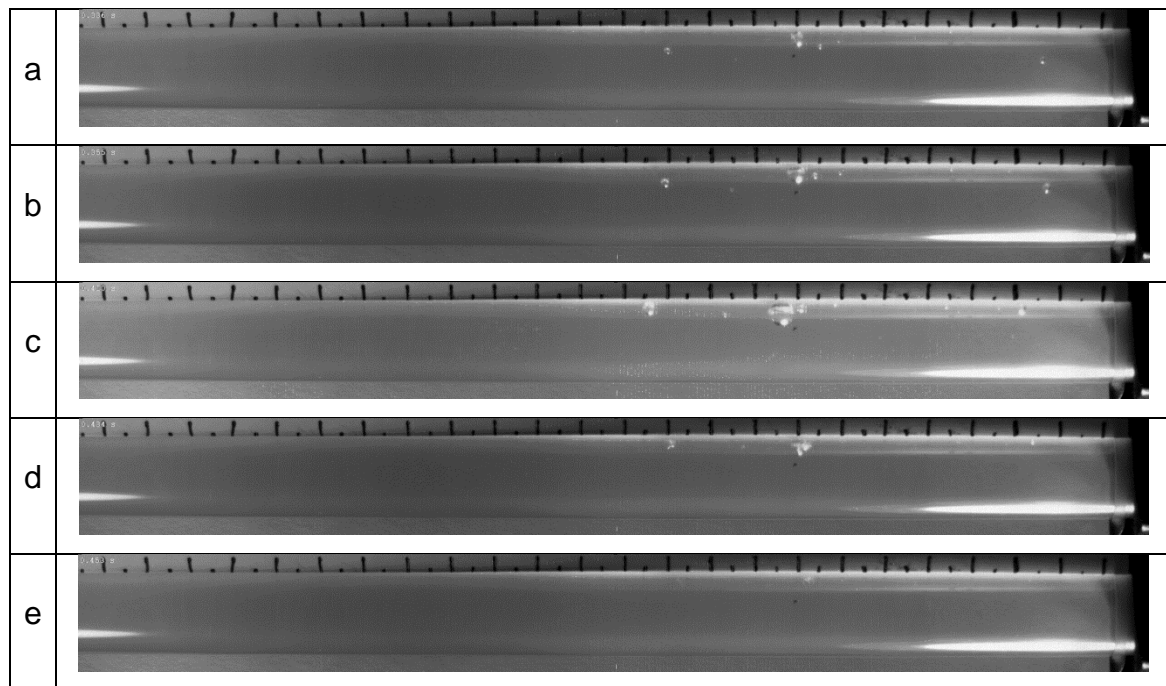


Figure(4.22) Photograph of right end of the polycarbonate section and the fast closure valve.





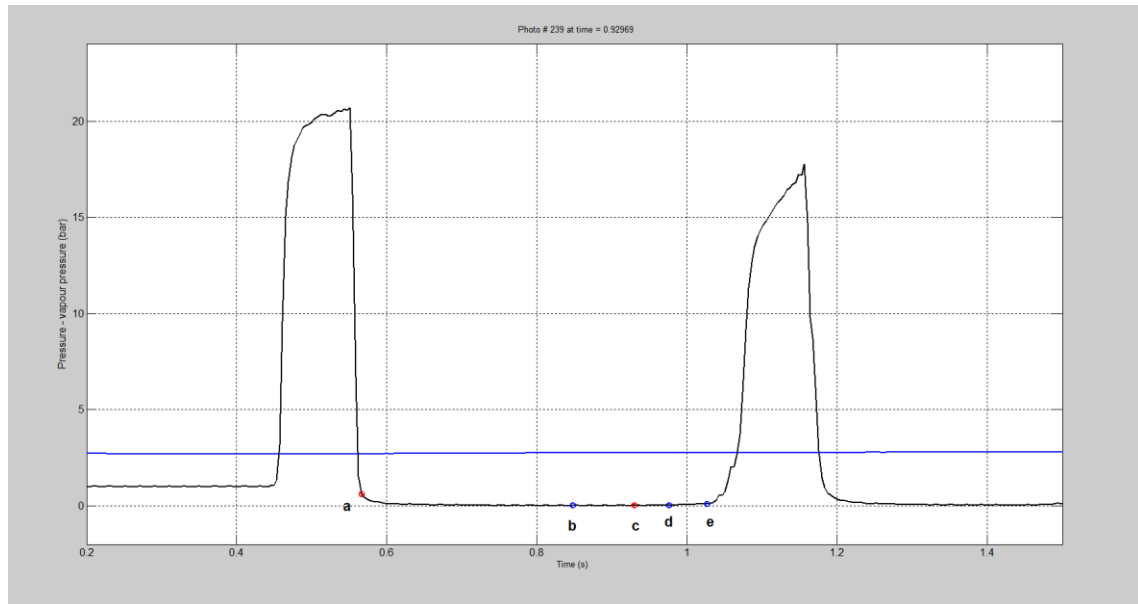
Figure(4.23) Pressure trace for series (a) – (e) of visualisation in Figure(4.24), Table(4.5)



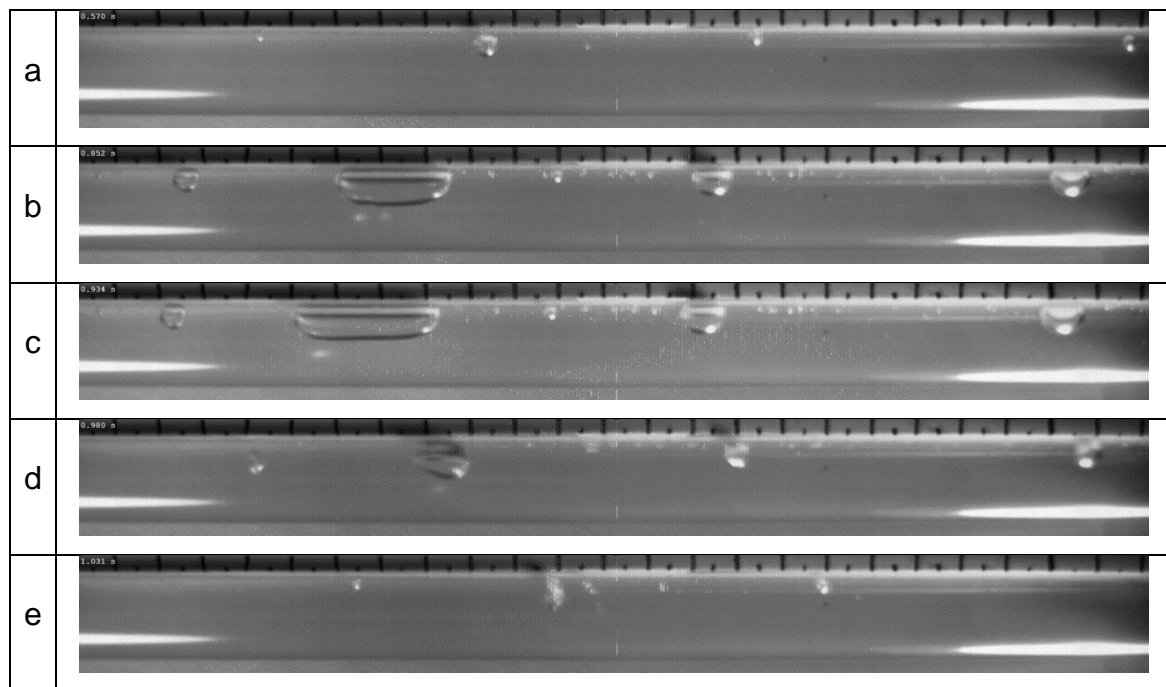
Figure(4.24) Photo-Record of synchronised visualisation for limited cavitation

Table(4.5) Data-Record of synchronised visualisation for limited cavitation

	Time	Stage	Pressure (bar)	Photo #
a	0.332	Initiation	0.5610	86
b	0.3516	Growing	0.08522	91
c	0.4063	Maximum size	-0.009649	105
d	0.4297	Contraction	-0.02293	111
e	0.4492	Collapse	0.1833	116



Figure(4.25) Pressure trace for series (a) – (e) of visualisation in Figure(4.26), Table(4.6)



Figure(4.26) Photo-Record of synchronised visualisation for classic severe cavitation

Table(4.6) Data-Record of synchronised visualisation for classic severe cavitation

	Time	Stage	Pressure (bar)	Photo #
a	0.5664	Initiation	0.6233	146
b	0.8477	Growing	0.0249	218
c	0.9297	Maximum size	0.0359	239
d	0.9766	Contraction	0.0437	251
e	1.0270	Collapse	0.1028	264

The lack of evidence of vaporous bubbles occupying the pipe cross section (within the expected column separation region close to the valve) from the high speed camera images requires discussion. The chemistry of water (Chaplin 2015) provides an explanation for the behaviour observed in these experiments. Water ( $H_2O$ ) is a liquid very commonly associated with pipeline transients, including the experiments reported in this study, but the results (e.g. visualisations) of measurements with water may well not be applicable to other fluids also associated with fluid transients because “water is an atypical liquid” with a number of “anomalous” or “unusual” properties associated with its hydrogen bonding (Chaplin 2015). The explanations provided by Chaplin (2015) are beyond the original scope of this study, but a summary of a selection of them helps to explain features of the current visualisations of column separation:

- Water has an unusually high *boiling point* (its hydrogen bonding reduces *vapour pressure*). Consequently, the change in volume as liquid changes to vapour is relatively very large (about double typical values). Because of its excellent solvent properties it is very difficult to get really pure water, but on the other hand solutes have a low impact on boiling point elevation.
- Water has a high *latent heat of evaporation/cooling* (highest of any molecular liquid), i.e. a great deal of energy (as work or heat) is required to convert liquid to vapour, especially at the temperatures associated with typical waterhammer events. Correspondingly, it also has a high *entropy of evaporation*, which, coupled with the high amount of evaporative cooling also required, may suggest an expectation of additional (i.e. non-frictional) dissipation from transient cavitation.
- Compared with most other liquids, water has unusually *high surface tension*, with its hydrogen bonding stronger at interfaces than in the bulk liquid. Consequently, liquid water is easily superheated, i.e. liquid temperature may rise above the saturation temperature corresponding to the pressure, an observation that has a long history but remains widely overlooked (Chang 2007). This is facilitated by any dissolved gas but conversely inhibited by the presence of gas bubbles or cavities that act as vaporisation initiation sites, so bubble growth would be expected to be restricted.
- Liquid water has a high *specific heat capacity* (highest of all liquids except ammonia), with the liquid phase having over double the specific heat capacity of the ice or vapour phases, i.e. it can absorb a significant amount of energy as heat



without large temperature changes, especially as it also has high *thermal conductivity* (highest for liquids other than liquid metals).

Chaplin (2015) also highlights other “anomalous” properties of water which do not bear directly on the column separation observations but which do influence waterhammer modelling and experimentation:

- Water has an unusually low *liquid compressibility* (with both isothermal and adiabatic compressibility dropping slightly as temperature increases up to 45°C), as assumed in the basic waterhammer model which allows compressive acoustic wave propagation but neglects changes in density.
- Water has an unusually high *liquid viscosity*, which coupled with laboratory scale apparatus makes it difficult to get physical experiment results at the Reynolds Numbers typical of engineering pipe flows.

## **Chapter 5**

### **Experimental Results for Model Comparison**

### 5.1 Model comparison rationale

To focus effectively on the modelling of the column separation, the experiments described in the previous Chapter 4 were designed to eliminate aspects of the modelling of the transient which might confuse the effects of modelling the column separation region itself, i.e.:

- The basic rig geometry and method of transient initiation (by rapid valve closure) were chosen to eliminate complex boundary conditions (Section 4.2).
- The basic rig geometry (i.e. uniform pipe upslope with rapid closure valve at high point) was chosen to promote column separation at a single location where flow visualisation could be enabled (i.e. adjacent to rapid closure valve) (Section 4.5).
- Flow and waterhammer properties such as Darcy friction factor ( $f$ ) and waterhammer wavespeed ( $a$ ) were not predicted but measured directly from the behaviour of the apparatus (Section 4.4).
- As Arfaie (1989) had indicated that additional unsteady friction damping was necessary for this particular apparatus, an unsteady friction model that has been demonstrated to give good results for waterhammer on this apparatus (Bughezem and Anderson 2000) was adopted and the necessary additional unsteady friction coefficient determined from the experiments rather than taken from the literature (Section 4.3.3).

In his earlier comparison of column separation models, Arfaie (1989) had suggested that the relative performance of these might be influenced by the form of column separation transient response, i.e. whether it was of the classical “severe” type, as in Figure(4.18) and Figure(4.19), or whether it exhibited the post separation pressure spike behaviour identified by Martin (1983), as in Figure(4.20) and Figure(4.21). While Martin (1983) explained this occurrence by multiple cavitation locations, Arfaie (1989) was able to explain that it could also occur with only a single cavitation location at the rapid closure valve (Anderson et al 1991), as intended (above) for the experimental apparatus in this study.

The model comparison rationale for this study is to use only transient experimental results where that single cavitation location dominates the modelling of the specific column separation behaviour. To that end, it will be useful to extend the previous work by Arfaie (1989) to explain the physical basis of the Martin (1983) pressure

spike phenomenon in these circumstances, as well as to see whether there are simple parameters which could identify the possibility of its occurrence. Informed by the previous experiments by Arfaie (1989), the large number of transient experiment traces (Appendix C) provide a selection of different modes of column separation behaviour for comparison with models.

## **5.2 Observed pressure transient behaviour**

Martin (1983) investigated limited cavitation on a reservoir-pipe-valve system with four pressure-transducers at equal distances along the pipe, and argued that the pressure spikes are due to superposition of multiple pressure waves from collapse of at least two cavities. Martin (1983) also noticed an audible cracking sound accompanying cavity collapse and he concluded that both negative and positive pressure spikes are due to at least two negative and positive pressure waves. Anderson et al (1991) attributed to Martin (1983) the dimensionless parameter Martin ratio  $P_M$  (Joukowski pressure relative to initial static head over water vapour pressure):

$$P_M = \frac{\rho \cdot a \cdot V_o}{P_R - P_v} \quad (5.1)$$

The dimensionless first cavity duration  $T_{cr}$  (1<sup>st</sup> cavity duration relative to pipe wave reflection period  $T$  where  $T = 2 \cdot L/a$ ):

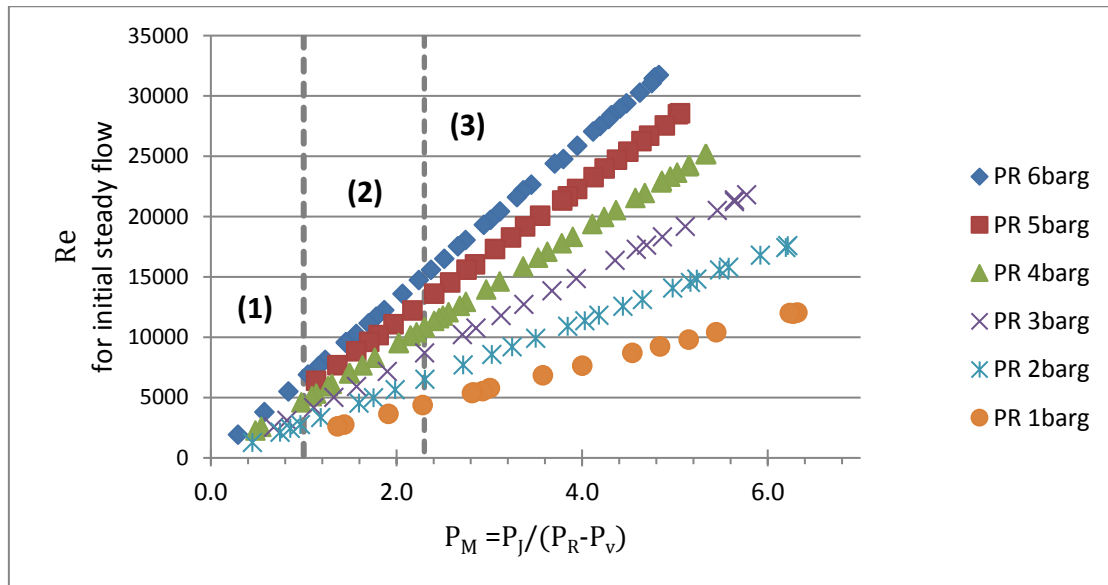
$$T_{cr} = \frac{T_{c1}}{T} \quad (5.2)$$

and the pipe line-packing and wave-attenuation properties (Arfaie 1989) were used to present experimental results of water column separation following an upstream valve closure in a reservoir pipe valve system. Autrique et al (2012) presented their experimental results of water column separation following an upstream valve closure in a horizontal pipe (two reservoir-pipe-valve system) with three parameters: the magnitude of the transient,  $M$  (ratio between the Joukowski head pressure and the initial absolute head),  $\Delta H_r$  (ratio between the maximum overpressure and the Joukowski pressure) and  $T_{cr}$  as in Eq.(5.2). Based on this literature (Martin 1983,

Anderson et al 1991, Autrique et al 2012), operational maps of experimental water column separation modes are presented in Figure(5.1), Figure(5.2) and Figure(5.3).

Figure(5.1), particularly at reservoir pressures between 1–2 *bar*<sub>g</sub>, shows that the Joukowsky pressure could be increased by column separation up to 10 to 13 times the initial reservoir pressure, indicating the significance of column separation in low pressure pipe system design. Over the range of reservoir pressure used in this research ( $P_R = 1$  to 6 *bar*), Figure(5.1) shows the expected linear relation between Martin number  $P_M$  and pipe Reynolds number  $Re$  (initial steady flow), with an increase in the gradient as the reservoir pressure  $P_R$  increases (increase in flow velocities), because the ratio of these two numbers is inversely proportional to  $(P_R - P_v)$  if  $\mu$ ,  $d$ ,  $V_o$  and wave speed  $a$  are constant. Indeed, it suggests that over the range of tests the experimental wave speed  $a$  is effectively constant from test to test. Also it strongly suggests that the three clear zones of pressure transient behaviour, respectively single phase waterhammer (1), limited column separation (2) and typical column separation (3), are distinguished by Martin ratio  $P_M$  rather than Reynolds number. Furthermore, the fact that transition from single-phase waterhammer (1) to limited column separation (2) occurs as expected at Martin ratio  $P_M = 1$  confirms that the apparatus effective vapour pressure  $P_v$  was at (or very close to) its normal water saturation pressure value. Obviously, at very low Reynolds number (i.e. initial flow rate) with  $P_M$  less than unity (zone 1), the single phase waterhammer, e.g. Figure(4.5) and Figure(4.9) does not create a down surge of sufficient magnitude to reach the level of vapour pressure whatever the value of reservoir pressure  $P_R$ .

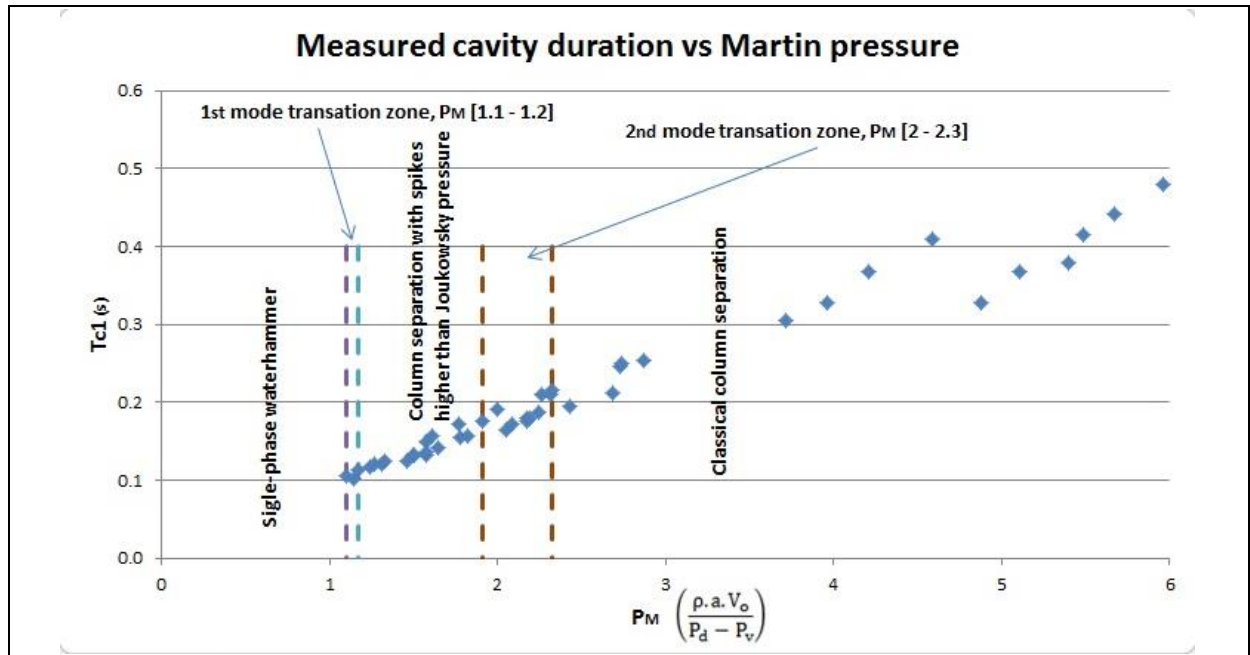
For greater flow velocity, on the same operational map, Figure(5.1), when the value of Martin number  $P_M$  is bigger than 2.3, the region of typical column separation with instantaneous pressure rise after cavity collapse is as shown in both Figure(4.18) and Figure(4.19). This behaviour happens at high initial flow rates and is characterised with long cavity duration and decrease in successive pressure peaks, where cavities open and close with decrease in duration (Swaffield and Boldy 1993) until sufficient energy has been dissipated for the minimum pressure to remain above vapour pressure.



**Figure(5.1) Operational map of waterhammer and column separation.**  
**(1) No column separation, (2) Limited column separation (Martin, 1983),**  
**(3) Typical (severe) column separation.**

In between these two zones, the region for limited column separation within the range of Martin number  $P_M = 1$  to 2.3, any pressure traces of column separation are characterised with a pressure spike at the second pressure peak which may be higher than the Joukowsky pressure, Figure(4.20) and Figure(4.21), which is a potential serious design issue as the pressure upper bound is no longer given by the Joukowsky pressure as had traditionally been thought (Martin 1983).

The experimental results, Table(5.3), have been plotted, Figure(5.2), in terms of cavity duration  $T_{c1}$  versus Martin pressure ratio  $P_M$ , to outline a summary of pressure transient behaviours Table(5.3). Both illustrate clearly the three modes of pressure transient (single-phase waterhammer, limited column separation and the classical column separation). The cavity duration  $T_{c1}$  is proportional to Martin pressure ratio  $P_M$  because increasing initial velocity  $V_0$  increases  $P_M$  but would also be expected to increase cavity duration (in line with the approximate analytical model of Appendix D). The pressure transient behaviour develops from single-phase waterhammer to limited column separation and then to classical column separation. Between these two clear regions there are two transition zones, the 1<sup>st</sup> transition (from waterhammer to column separation) in an observed range of  $P_M \approx [1.1 - 1.2]$  and the 2<sup>nd</sup> transition (from limited to severe cavitation) in a range of  $P_M \approx [1.9 - 2.3]$ .

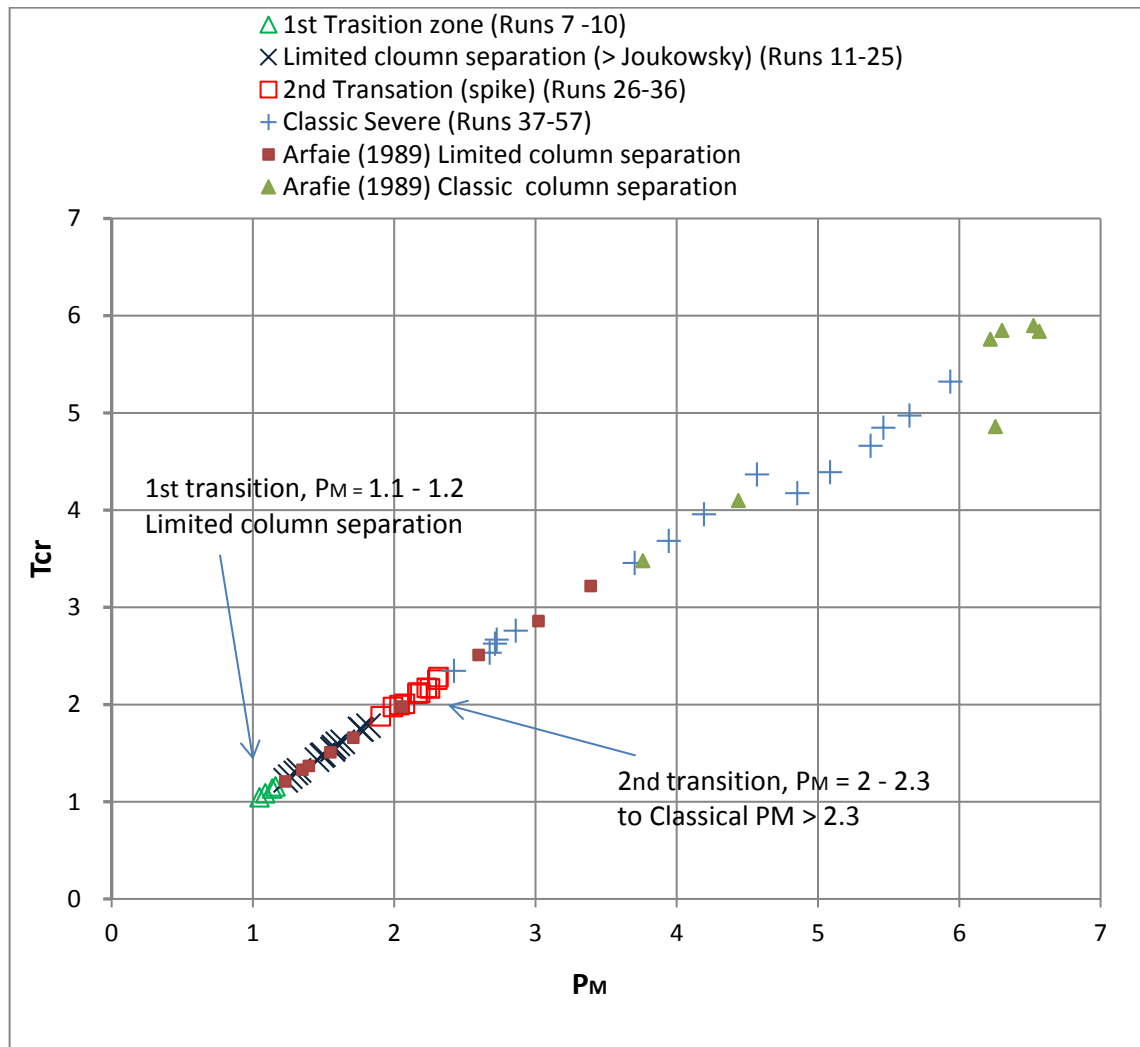


Figure(5.2) Map for pressure transient behaviours.

Table(5.1) Summary of pressure transient behaviours

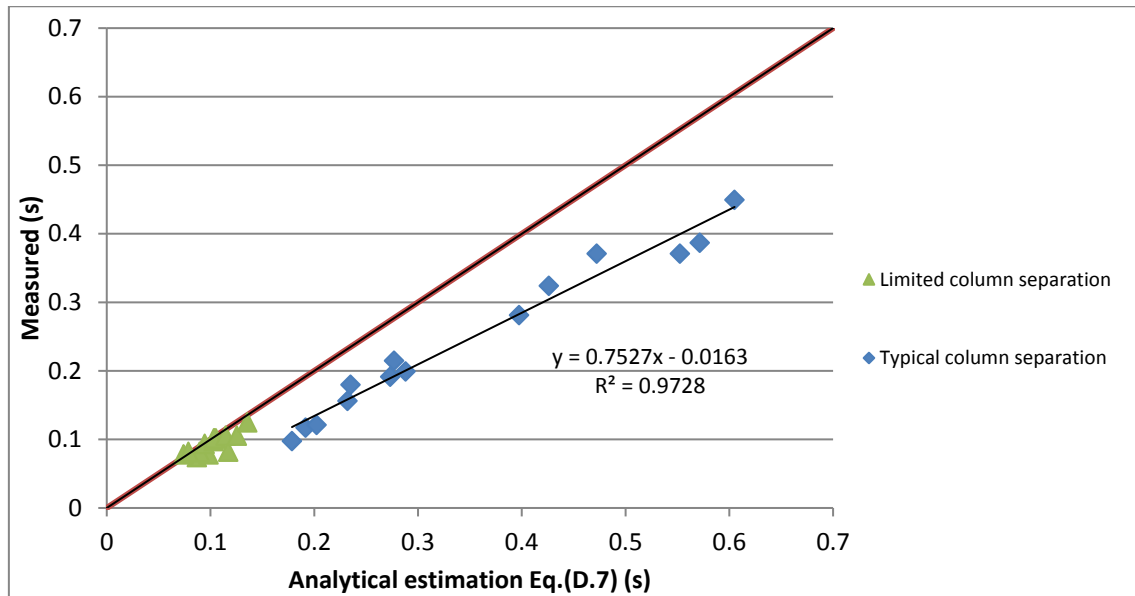
Transient mode	Martin pressure ratio $P_M$ Eq.(5.1)	Cavity duration $T_{cr}$ Eq.(5.2)
Single-phase waterhammer	$< 1$	
1 <sup>st</sup> transition mode	$\sim 1 \sim 1.2$	$\simeq 1$
Limited column separation with pressure rise higher than Joukowski pressure	$\sim 1.2 \sim 1.9$	$\sim 1.2 \sim 1.9$
2 <sup>nd</sup> transition mode	$\sim 1.9 \sim 2.3$	$\sim 1.9 \sim 2$
Classical column separation	$> \sim 2.4$	$> 2$

Figure(5.3) shows the dimensionless first cavity duration  $T_{cr}$  plotted against Martin number  $P_M$ . This also shows a clear trend, but with scatter due to the additional measurement of first cavity duration to obtain  $T_{cr}$ , Table(5.3). The point symbols are used to distinguish the observed modes of column separation behaviour. This suggests that the transition from occurrence of a spike on the post-cavity peak to classic column separation is associated with a first cavity duration of around  $\sim 2 \sim 2.5$  reflection periods ( $2L/a$ ). Unlike the Martin ratio  $P_M$ , though,  $T_{cr}$  cannot be known in advance.

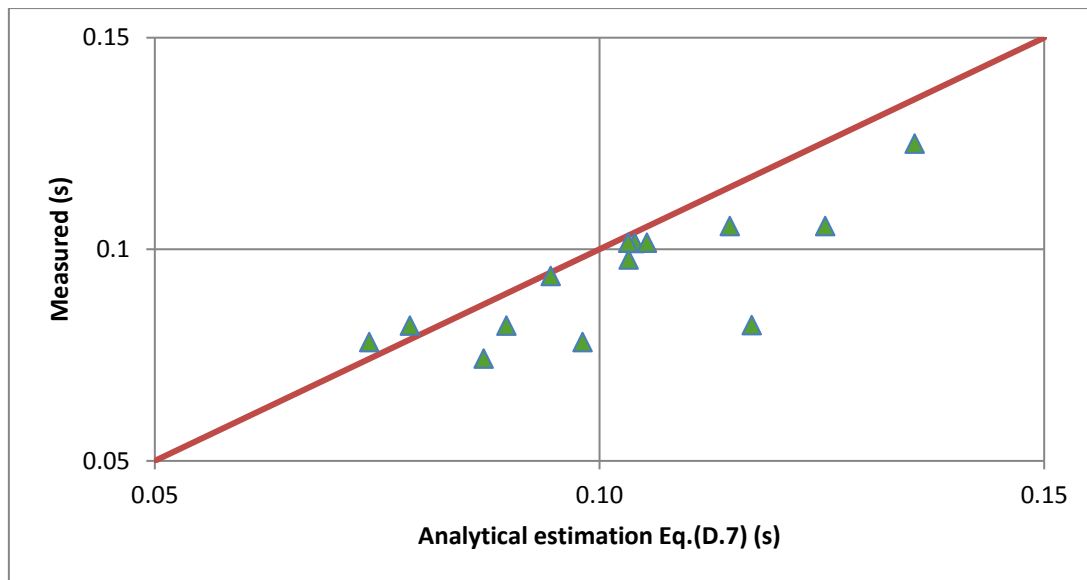


Figure(5.3) Nondimensional first cavity duration plotted against Martin ratio  $P_M$ .





Figure(5.4) Measurements against estimation of cavity durations, (the range 0.05 to 0.15s is shown in detail in Figure(5.5))



Figure(5.5) Measurements against estimation of cavity durations for limited column separation.

Using the Arfaie (1989) experimental work, Table(5.2) gives an initial outline of possible prediction values and these have been extended in Table(5.3) to the new experimental results from this investigation. The maximum (first) cavity duration  $T_{cav}$  can be estimated using Eq.(D.7) from an approximate analytical solution (Appendix D). The measured maximum cavity duration is plotted against the mathematical estimation in Figure(5.4) and Figure(5.5). Given the assumptions implicit in the theory, the experimental results show a fairly consistent trend. The analytical predictions are close at low initial velocities  $V_0$  but become increasingly too long as

initial velocity  $V_0$  increases. The theory is derived for column separation downstream of a valve that is closed (as in a pumping system), whereas in these experiments the column separation occurs after an initial waterhammer wave which is subject to greater damping as the initial velocity  $V_0$  is increased, thus explaining the discrepancy. However, the results do indicate that this simple theory does work best for the region (2) of limited column separation.

Table(5.2) Arfaie (1989) representative experimental results for single-phase waterhammer and different modes of column separation

Arfaie (1989, Table 7.4) results*					Additional values calculated from Arfaie (1989) experiments						
Experiments (Arfaie 1989, Fig 7.8-7.16)					Rigid column model (Appendix D)						
Run No	Behaviour mode	Initial velocity Vo (m/s)	Friction factor (4f)	1st cavity duration Tcav (s)	Drive pressure Pd (bar) (Eq D.1)	PM = $\frac{\rho a V_o}{P_d - P_v}$	(V1/Vo) (Eq. D.5)	Calculated Tcav (s) (Eq D.7)	Calculated Tcav /(2L/a)	Ratio of calc/expt Tcav	Evidence from pressure traces?
10	single-phase liquid	0.33	0.04	-	6.634	0.614	-	-	-	-	Other cavity ?
11		0.49	0.036	-	6.547	0.923	-	-	-	-	
12		0.35	0.039	-	6.320	1.001	-	-	-	-	
13	spike < PJ	0.65	0.034	0.102	6.525	1.229	0.974	0.123	1.21	1.21	
14		0.71	0.033	0.109	6.444	1.350	0.970	0.135	1.33	1.24	
15		0.73	0.033	0.115	6.453	1.396	0.968	0.140	1.37	1.22	
16		0.80	0.032	0.122	6.372	1.549	0.963	0.154	1.51	1.26	
17	spike > PJ	0.90	0.031	0.134	6.494	1.710	0.956	0.170	1.66	1.27	
18		1.04	0.03	0.171	6.250	2.053	0.942	0.202	1.98	1.18	
19		0.85	0.032	0.200	4.044	2.598	0.936	0.256	2.51	1.28	
20		1.46	0.028	0.200	5.965	3.021	0.896	0.292	2.86	1.46	
21	spike < PJ	1.05	0.03	0.256	3.830	3.390	0.908	0.328	3.22	1.28	Other cavity ?
22	"classical" severe column separation	1.76	0.026	0.257	5.777	3.760	0.863	0.355	3.48	1.38	Other cavity ?
23		1.32	0.028	0.331	3.683	4.436	0.868	0.419	4.10	1.27	
24		1.66	0.027	0.461	3.284	6.256	0.801	0.496	4.86	1.08	
25		1.58	0.027	0.482	2.980	6.566	0.801	0.595	5.84	1.23	
26		1.20	0.029	0.516	2.282	6.525	0.822	0.602	5.90	1.17	
27		0.85	0.031	0.533	1.707	6.219	0.869	0.588	5.76	1.10	
28		0.79	0.032	0.551	1.562	6.302	0.871	0.596	5.85	1.08	

\* Arfaie(1989) data: L=62.5m, a=1230 m/s, Pv = 0.02bar, (2L/a) =0.102, (L/d) = 4921

\* Arfaie(1989) data:  $L=62.5m$ ,  $a=1230 m/s$ ,  $P_v = 0.02bar$ ,  $(2L/a) = 0.102$ ,  $(L/d) = 4921$

Table(5.3) Representative experimental results for single-phase waterhammer and different modes of column separation

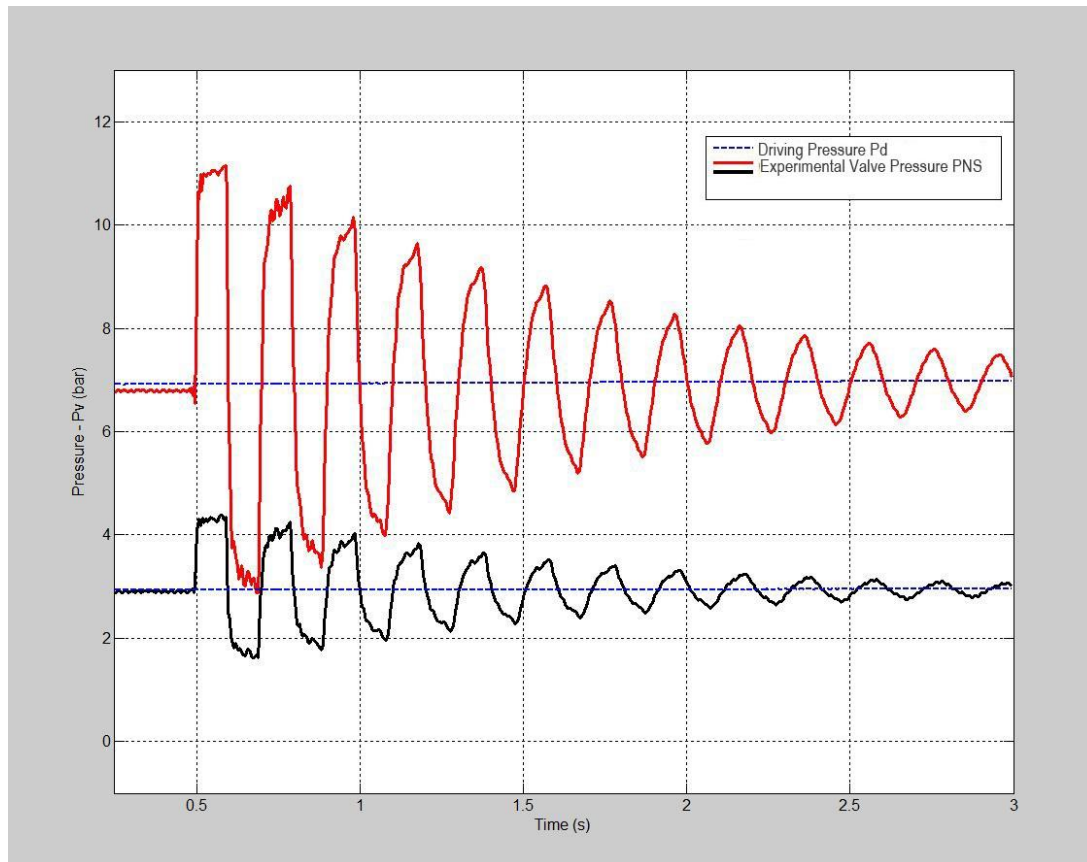
Representative experimental results					Additional values calculated from experiments						
					Rigid column model (Appendix D)						
#	Observed behaviour	Initial velocity $V_0$ (m/s)	Friction factor (4f)	Measured cavity duration $T_{cav}$ (s)	$P_d - P_v$ Drive pressure (bar) (Eq D.1)	$P_M =$ $\left( \frac{\rho \cdot a \cdot V_0}{P_d - P_v} \right)$	$(V1/V_0)$ (Eq. D.5)	Calculated $T_{cav}$ (s) (Eq D.7)	Calculated $T_{cav} / (2L/a)$	Ratio of calcu/expt $T_{cav}$	PJ = ( $\rho a V_0$ ) (bar)
1	Liquid Single-phase waterhammer	0.16	0.034	-	7.022	0.292	-	-	-	-	2.052
2		0.11	0.051	-	3.047	0.452	-	-	-	-	1.378
3		0.32	0.041	-	7.023	0.577	-	-	-	-	4.053
4		0.22	0.045	-	4.045	0.679	-	-	-	-	2.748
5		0.47	0.036	-	7.060	0.840	-	-	-	-	5.931
6		0.21	0.045	-	3.023	0.902	-	-	-	-	2.726
7	waterhammer transition zone	0.58	0.034	0.102	7.053	1.052	0.98	0.103	1.05	1.01	7.419
8		0.43	0.042	0.105	5.04	1.093	0.98	0.107	1.09	1.01	5.505
9		0.54	0.029	0.102	6.025	1.141	0.98	0.111	1.14	1.10	6.877
10		0.64	0.033	0.113	7.009	1.168	0.98	0.114	1.16	1.00	8.185
11	Limited column separation	0.682	0.034	0.117	7.050	1.232	0.974	0.120	1.22	1.02	8.684
12		0.499	0.030	0.121	5.026	1.264	0.982	0.123	1.26	1.02	6.354
13		0.516	0.029	0.121	5.034	1.303	0.981	0.127	1.30	1.05	6.562
14		0.421	0.027	0.125	4.041	1.327	0.986	0.130	1.32	1.04	5.362
15		0.806	0.034	0.125	7.058	1.453	0.963	0.140	1.43	1.12	10.257
16		0.589	0.032	0.133	5.033	1.489	0.974	0.145	1.48	1.09	7.496
17		0.591	0.032	0.133	5.024	1.498	0.974	0.146	1.49	1.10	7.526
18		0.863	0.035	0.133	7.018	1.566	0.957	0.151	1.54	1.14	10.986
19		0.742	0.034	0.137	6.033	1.566	0.964	0.151	1.54	1.11	9.447
20		0.498	0.030	0.148	4.026	1.573	0.978	0.153	1.56	1.03	6.333
21		0.382	0.026	0.156	3.033	1.601	0.985	0.156	1.60	1.00	4.856
22		0.644	0.033	0.141	5.014	1.635	0.968	0.158	1.62	1.13	8.201
23		0.419	0.027	0.172	3.032	1.758	0.981	0.171	1.75	1.00	5.329
24		0.698	0.033	0.156	5.023	1.768	0.963	0.171	1.74	1.10	8.880
25		0.860	0.034	0.156	6.019	1.818	0.952	0.175	1.78	1.12	10.944
26	Column separation transition zone	0.602	0.032	0.176	4.024	1.904	0.966	0.184	1.88	1.05	7.660
27		0.475	0.029	0.191	3.038	1.991	0.974	0.193	1.97	1.01	6.050
28		0.806	0.035	0.164	5.031	2.038	0.949	0.195	1.99	1.19	10.253
29		1.150	0.035	0.172	7.050	2.076	0.928	0.197	2.01	1.15	14.635
30		0.857	0.034	0.180	5.035	2.165	0.944	0.207	2.11	1.15	10.903
31		0.855	0.028	0.176	5.024	2.166	0.953	0.208	2.12	1.18	10.880
32		1.034	0.034	0.180	6.023	2.184	0.933	0.208	2.12	1.16	13.154
33		0.880	0.035	0.188	5.021	2.231	0.940	0.213	2.17	1.14	11.200
34		1.247	0.035	0.211	7.042	2.253	0.917	0.212	2.17	1.01	15.865
35		0.731	0.034	0.211	4.035	2.305	0.949	0.221	2.26	1.05	9.304
36		0.548	0.031	0.215	3.013	2.314	0.965	0.224	2.28	1.04	6.970
37	"Classical" Severe column separation	0.960	0.034	0.195	5.043	2.423	0.931	0.230	2.35	1.18	12.219
38		1.484	0.034	0.211	7.057	2.676	0.890	0.248	2.53	1.18	18.880
39		0.859	0.035	0.246	4.029	2.713	0.930	0.257	2.63	1.05	10.932
40		0.648	0.032	0.250	3.025	2.726	0.949	0.261	2.67	1.05	8.246
41		0.905	0.035	0.254	4.024	2.861	0.923	0.270	2.76	1.06	11.511
42		1.172	0.040	0.305	4.027	3.702	0.866	0.339	3.46	1.11	14.909
43		1.249	0.035	0.328	4.029	3.943	0.867	0.361	3.68	1.10	15.887
44		0.993	0.034	0.367	3.015	4.192	0.885	0.388	3.96	1.06	12.639
45		0.732	0.033	0.410	2.038	4.568	0.907	0.428	4.37	1.04	9.308
46		2.684	0.032	0.328	7.038	4.853	0.743	0.409	4.17	1.25	34.152
47		2.415	0.033	0.367	6.044	5.085	0.748	0.430	4.39	1.17	30.731
48		2.130	0.034	0.379	5.045	5.372	0.755	0.457	4.66	1.21	27.103
49		1.724	0.034	0.414	4.016	5.462	0.787	0.475	4.85	1.15	21.938
50		1.785	0.034	0.441	4.021	5.648	0.776	0.487	4.97	1.10	22.709
51		1.412	0.034	0.480	3.026	5.937	0.802	0.521	5.32	1.09	17.965

### 5.3 Representation of experimental pressure transient

The experimental transient runs in Figure(5.1) and Table(5.3) have been grouped into five segregated categories with the three main ones being those suggested previously by Arfaie (1989). Examples of each of these will be examined in the following sections.

#### 5.3.1 Single-phase waterhammer with no column separation

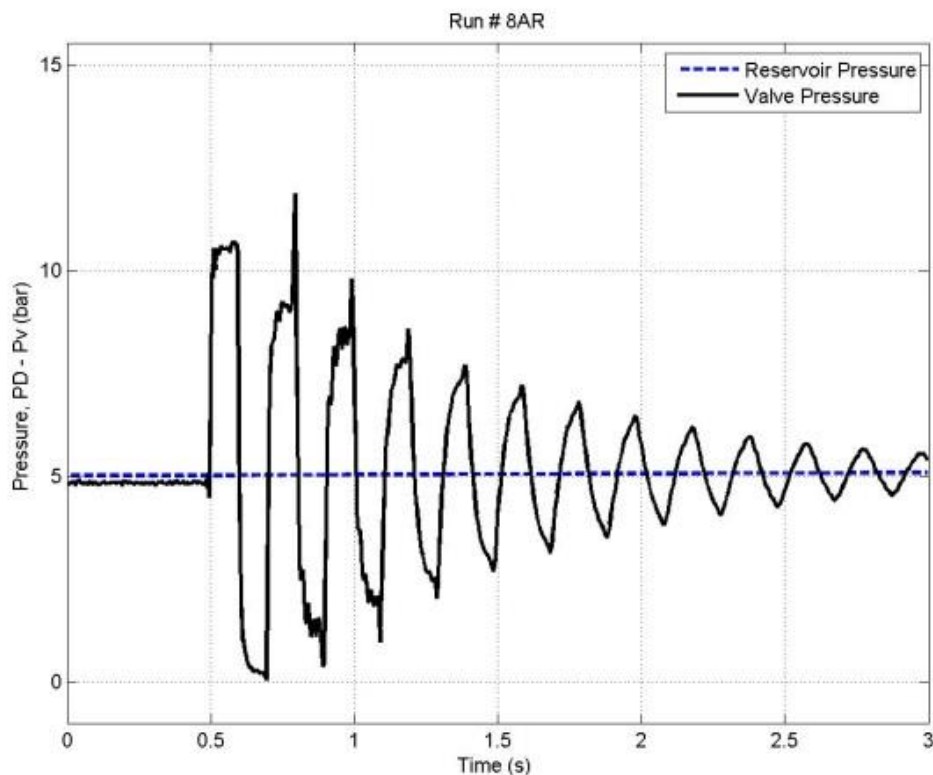
Though the objective is to model column separation, it is essential to measure single-phase waterhammer without column separation for two reasons. Firstly, to test the ability of the proposed mathematical models to represent all non-column separation aspects for the experimental data accurately. Secondly, to calibrate this model to give damping additional to that provided by the quasi-steady friction model to be able to calculate simple unsteady flow dissipation. Examples of single phase waterhammer are presented in Figure(5.6). These demonstrate two regions; the initial steady state condition (time before 0.5s) and the unsteady flow condition (time after 0.5s).



Figure(5.6) Set of two waterhammer pressure waves with no column separation at different driving pressures.

Both illustrate the case that the Joukowsky pressure rise was significantly less than the driving pressure so that the fluctuating transient pressure was not enough to reach the level of vapour pressure.

As the controlled flow rate through the regulating valve was increased gradually it would be expected that column separation would occur at Martin ratio  $P_M = 1$ . However, within experimental uncertainty, there is a narrow transitional region before evidence of a vapour cavity is observed with the occurrence of a pressure spike on the second peak, as in Figure(5.7). This may be the result of frictional “line packing” or evidence of column separation at a location other than at the closure valve. Simpson and Wylie (1989) reported that the occurrence of this phenomenon was first recognised by Lupton in 1953 and further work done in the following years by O’Neill in 1959 and Sharp in 1960.

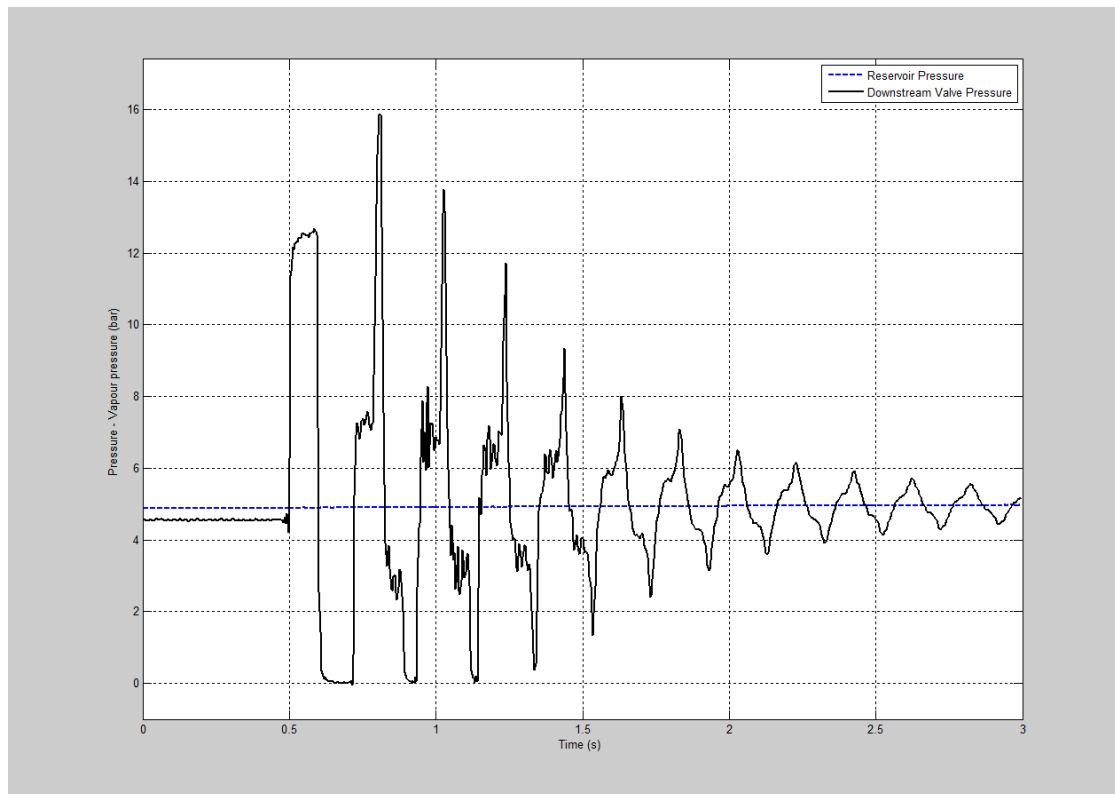


Figure(5.7) Transitional situation with spike on 2<sup>nd</sup> peak but no obvious cavity.

### 5.3.2 Limited column separation with pressure spikes higher than Joukowsky

$$P_J$$

With an increase in the initial flow velocity over that producing single-phase waterhammer, the Joukowsky pressure becomes bigger than the reservoir pressure, allowing the reflected down pressure to reach the level of vapour pressure. This not only causes a localised cavitation at the valve but the collapse of this cavity could create a pressure spike on the second peak higher than the Joukowsky pressure rise (Arfaie 1989, Anderson and Arfaie 1991), e.g. Figure(5.8) and Figure(5.9). The existence of water column separation with spike higher than Joukowsky pressure rise (limited column separation) is a potential risk, because the theoretical prediction of Joukowsky pressure is not conservative for design purposes, even though the overpressure spikes may not last very long (23 – 35)ms.

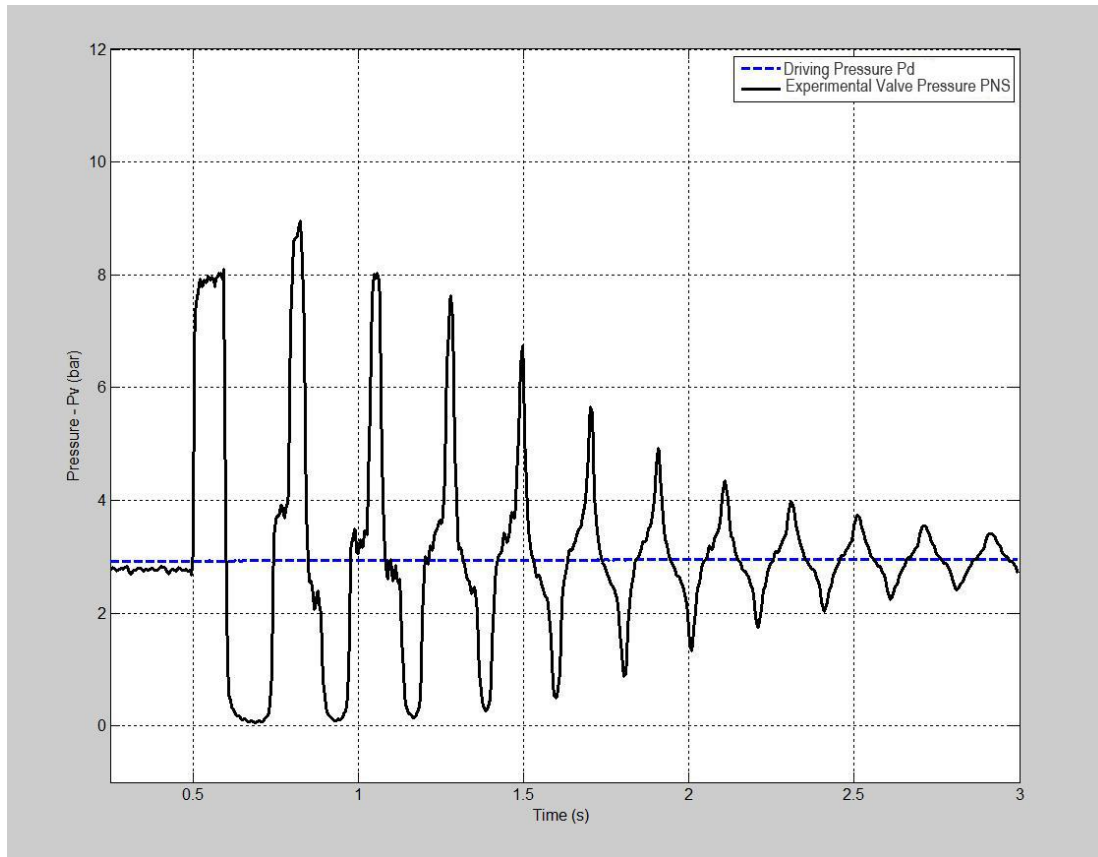


**Figure(5.8) Experimental water column separation with a spike higher than Joukowsky pressure at high operating reservoir pressure.**

Comparing the shape of the second pressure peak from Figure(5.8) and Figure(5.9), the shorter duration pressure spike of Figure(5.8) rises higher above Joukowsky than the longer duration pressure spike of Figure(5.9), with both preceded by a relatively short first cavity duration (not much longer than the reflection time of  $2L/a$ ) and



followed by an initial pressure step up. In both cases the pressure spike drops down to a level above vapour pressure, before a subsequent further drop (in both cases illustrated) to the second cavity formation.



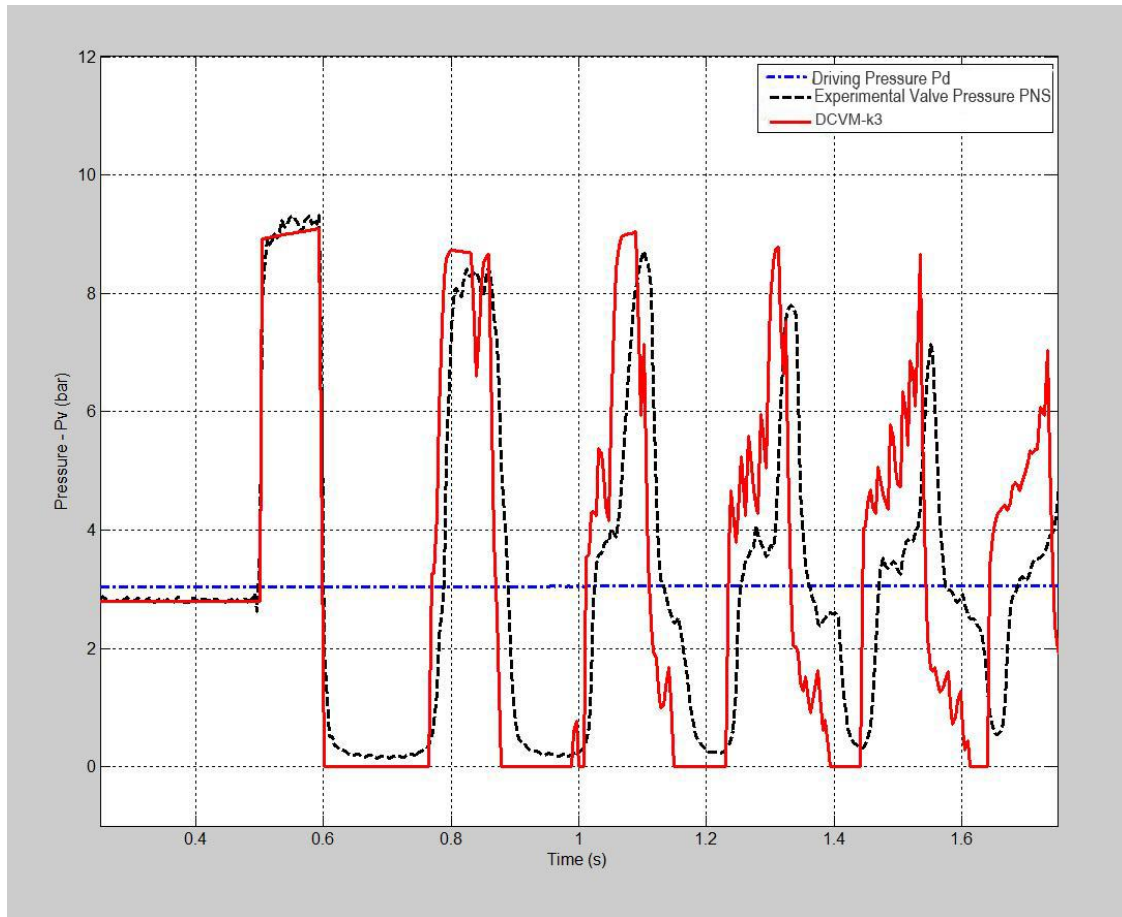
**Figure(5.9) Experimental water column separation with spike higher than Joukowsky pressure at low operating reservoir pressure.**

The Arfaie (1989) results in Table(5.2) indicate that at the transition from pure single-phase waterhammer (Section 5.3.1) to this limited cavitation behaviour, the pressure spike on the first cavity may initially be lower than the initial Joukowsky pressure rise. His results also showed that as the trend from Figure(5.8) to Figure(5.9) progresses further, the magnitude of the pressure spike diminishes until it is again equal to or lower than Joukowsky, e.g. Figure(5.10). This forms a second behaviour transition zone, as shown in Table(5.2) and Table(5.3) as well as in Figure(5.1) to Figure(5.3).

However, Arfaie (1989) did not detect further classes of behaviour within this, which do not appear to correspond to his explanation of the cause of the pressure spike by a single cavity at the valve. Figure(5.10) shows the pressure spike phenomenon described above after the second (not first) cavity, with the behaviour after the first cavity being apparently of the classical severe cavitation type (to be discussed in

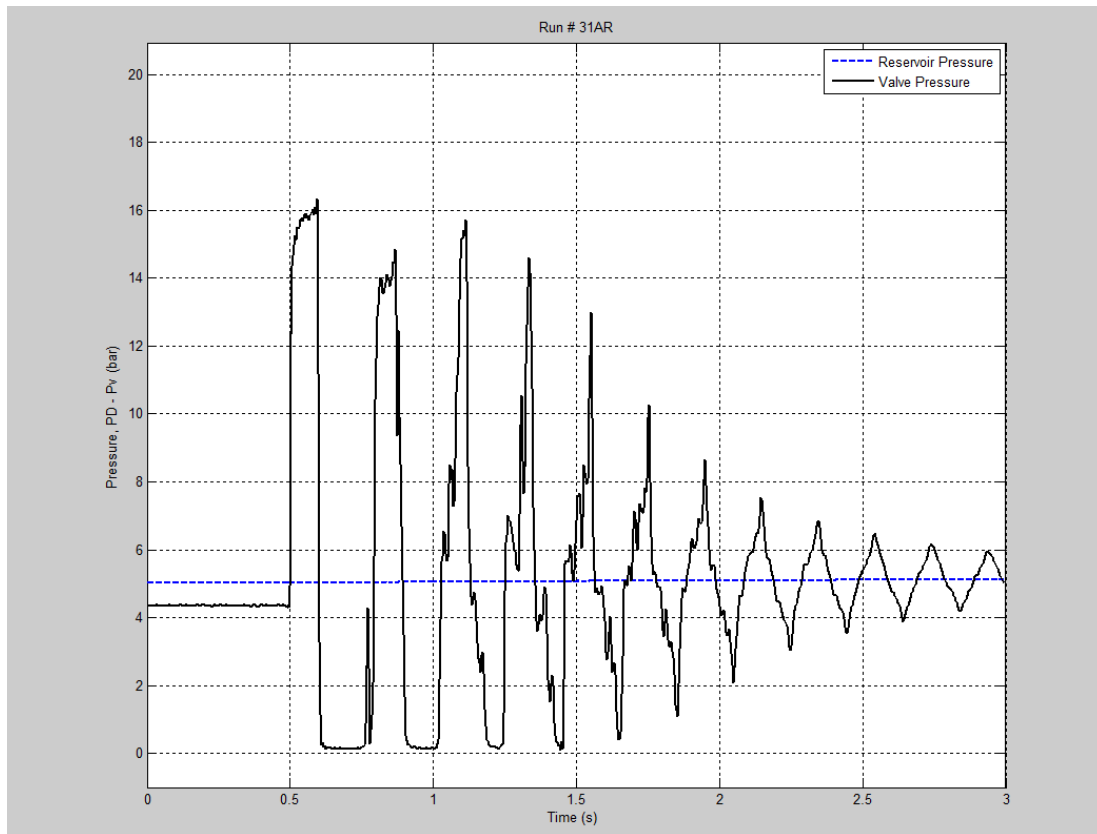


Section 5.3.3 to follow). Figure(5.11) shows something similar, but with the addition of a very brief “precursor” pressure spike at the end of the first cavity, which cannot be explained by pressure waves from a single cavity at the valve as shown subsequently in Section(5.4).



**Figure(5.10) Experimental water column separation with spike lower than Joukowski pressure at low operating reservoir pressure.**

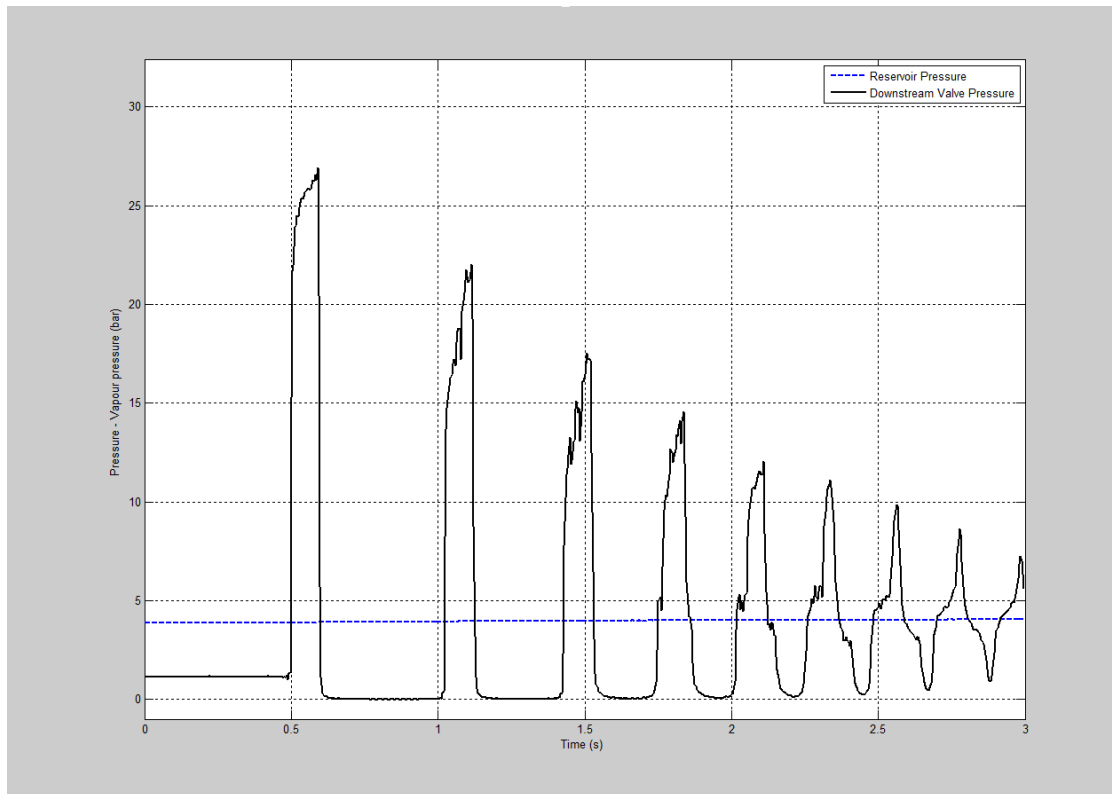
These traces indicate transient events not anticipated with this apparatus. They involve possibly the impact of fluid-structure interaction (as it was not possible to fully restrain the pipe) or of multiple cavity locations, e.g. Simpson and Wylie (1989) illustrated the relationship between the steeper hydraulic grade line and the formation of a distributed vaporous cavitation region (typical column separation). Figure(5.10) shows that a calculation can reproduce the presence of a spike on the third peak, suggesting that this is not due to FSI as that is not modelled.



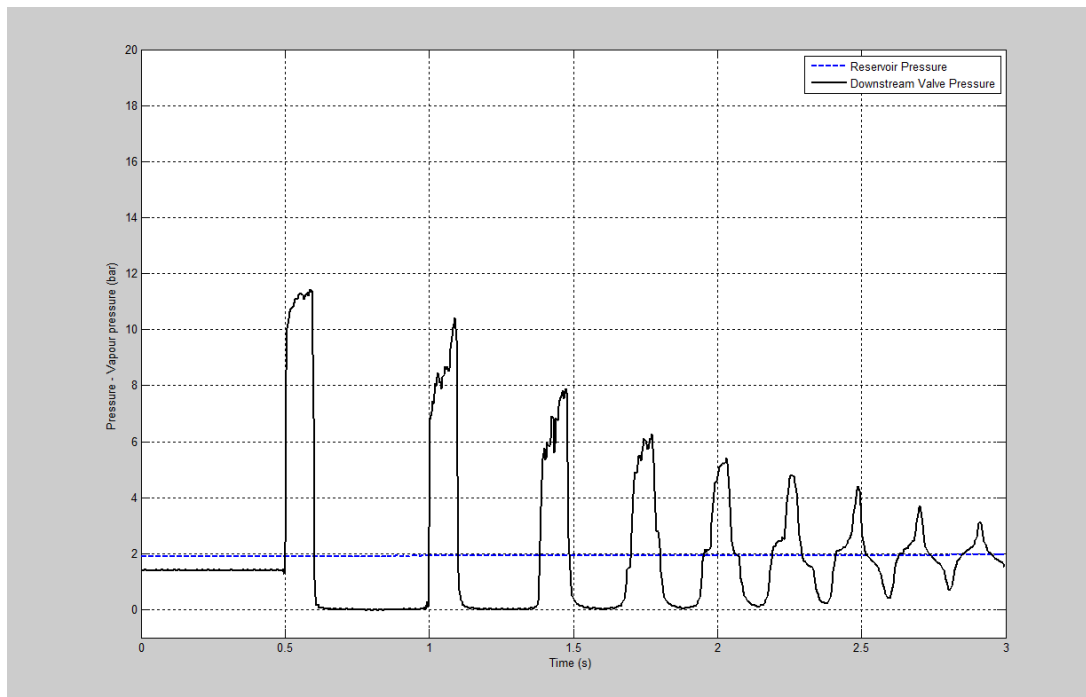
Figure(5.11) Column separation with spike at the third pressure peak.

### 5.3.3 Typical severe column separation

“Typical” water column separation behaviour was observed at large initial flow velocities over a range of reservoir pressures, as in Figure(5.12) and Figure(5.13). This pattern of behaviour is characterised by long cavity durations ( $\gg 2L/a$ ) and repeated cavity formations. However, close inspection of the traces in Figure(5.12) and Figure(5.13) indicates that the pressure peaks after the cavities (even the first cavity) have a tendency of a two-step pressure rise with a small amplitude pressure rise after a large initial post-cavity collapse pressure rise. To reinforce this, the second and third peaks have a greater upward slope than that caused by line-packing on the first peak, so there must be a phenomenon additional to line-packing to produce this effect. This suggests a continuity of behaviour from limited to severe cavitation, rather than a jump in mode of behaviour, to be shown in Figure(5.16) below. In that case, it can also be observed that as the pressure oscillations progress and diminish in amplitude, they begin to take on the shape characteristic of limited cavitation in Section(5.3.2), i.e. with a step up, then a spike, followed by a step down before dropping to a minimum.



**Figure(5.12) Experimental typical water column separation at 4 barg reservoir pressure.**



**Figure(5.13) Experimental typical water column separation at 2 barg reservoir pressure.**

#### 5.4 Graphical explanation of pressure rises due to column separation.

By tracing the pressure wave paths and reflections, Arfaie (1989) was able to demonstrate that the phenomenon of the pressure spike greater than the initial

pressure rise identified by Martin (1983) could also be explained with only single cavity occurring at the valve where the transient was initiated by rapid closure (Anderson et al 1991, Simpson and Wylie 1991). Arfaie (1989) identified that:

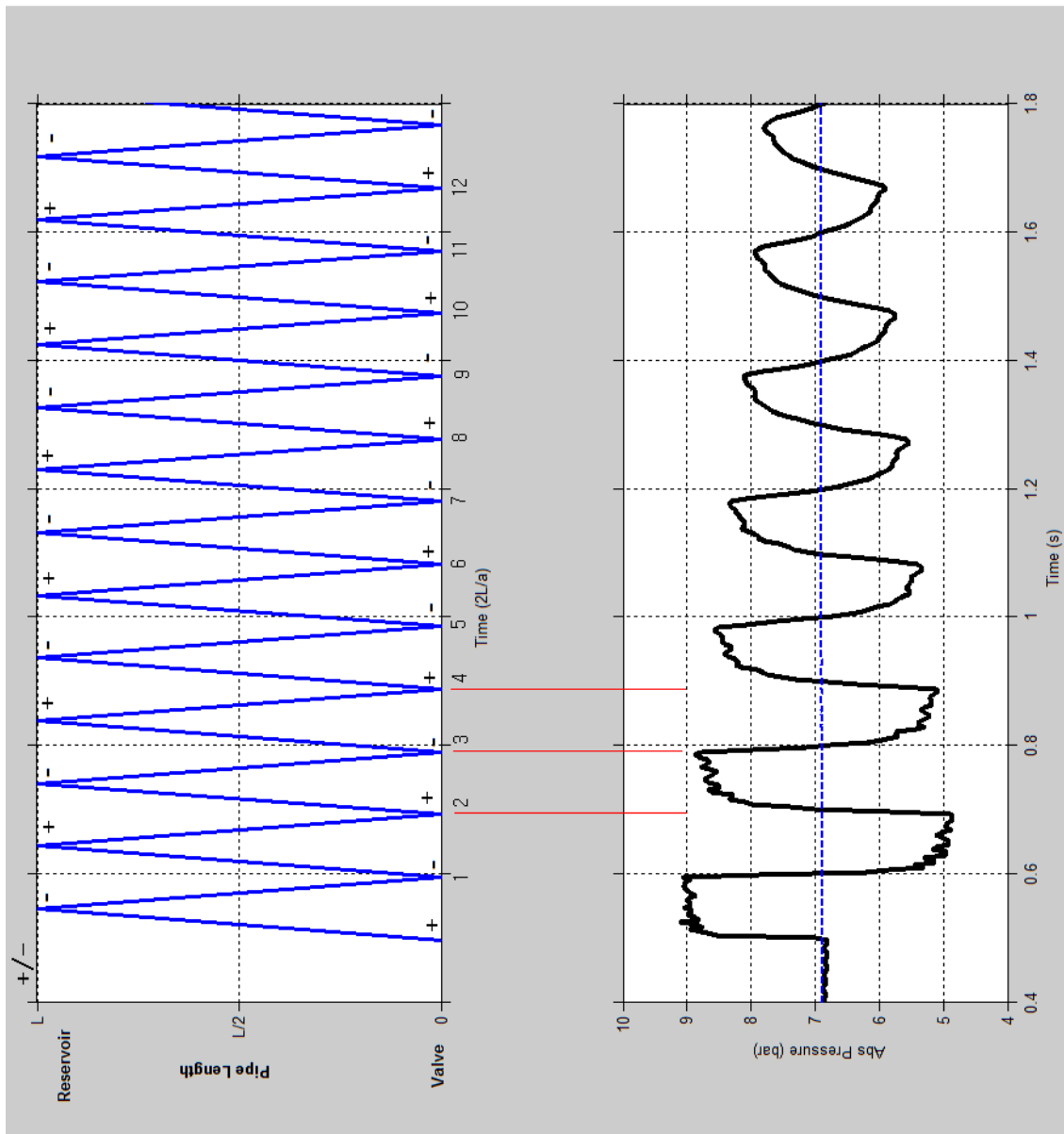
- There are multiple sets of waterhammer pressure disturbance waves: the first one initiated by the initial rapid valve closure, followed by others from each successive cavity collapse.
- The presence of a column separation region adjacent to the valve changes the nature of the wave reflection at that boundary for as long as the cavity lasts (from constant velocity to constant pressure, at vapour pressure).

The experimental apparatus has been designed (Chapter 4) to have only two simple waterhammer boundary conditions:

- At the reservoir:  $P = \text{constant pressure}$ , giving a reversal of the incident pressure wave; and
- At the rapidly closed valve:  $V = \text{constant velocity}$  (in this case  $V = 0$  giving a doubling of the incident pressure wave).

However, when column separation occurs at the valve, then for the duration of the “cavity” existence the pressure becomes constant at the vapour pressure  $P_v$ , transforming this boundary from constant velocity ( $V$ ) to constant pressure ( $P$ ) and thus changing the nature of the pressure wave reflection.

Autrique et al (2012) graphically explained a sample of their results of high-pressure spikes associated with limited column separation and credited Anderson et al (1991) for their representation. To provide a reference basis for this explanation, Figure(5.14) shows a diagram for pure single-phase waterhammer with no column separation. The lower part shows actual experimental pressure transient (pressure amplitude against time) recorded at valve end. The upper part has the same horizontal time axis and shows the zigzag path up and down the length of the pipe of the waterhammer pressure wave initiated by the valve closure. Each time the wave returns to the valve (every  $2L/a$  period) it can be seen how the pressure at the valve changes. The boundary at the reservoir is always constant pressure ( $P$ ) and wave reversing and, for pure waterhammer, the boundary at valve is always constant velocity ( $V$ ) and doubling. The direction of pressure change at each reflection is indicated (+ for pressure increase, – for decrease) and it can be seen how the pressure trace at the valve is caused by these.



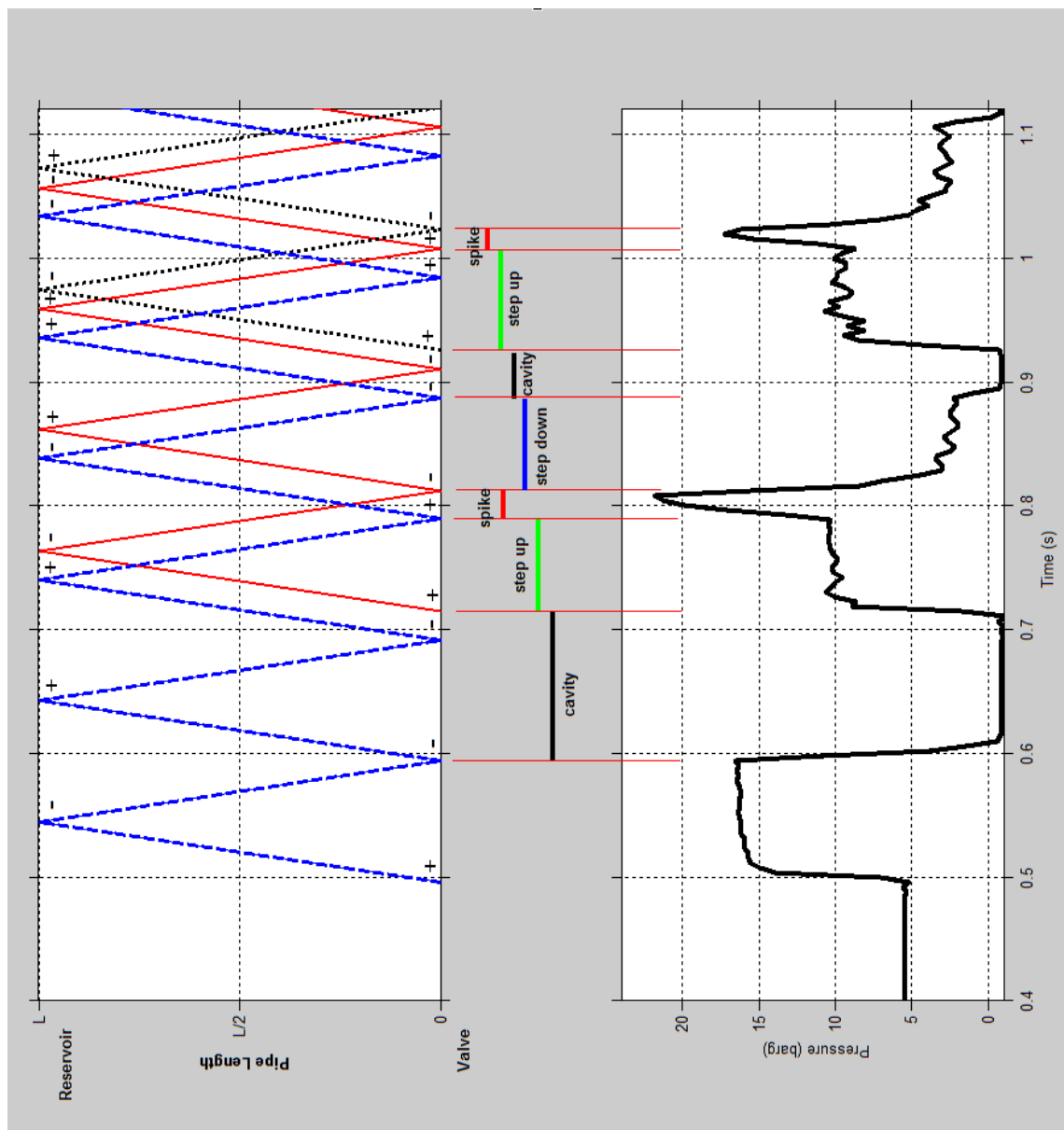
Figure(5.14) Graphical representation of experimental waterhammer propagation.

The same principle can be used to represent the behaviour with water column separation. Figure(5.15) shows a similar case to that analysed by Arfaie (1989) for limited column separation (but using a trace from this present study). The vapour cavity formed at the valve causes:

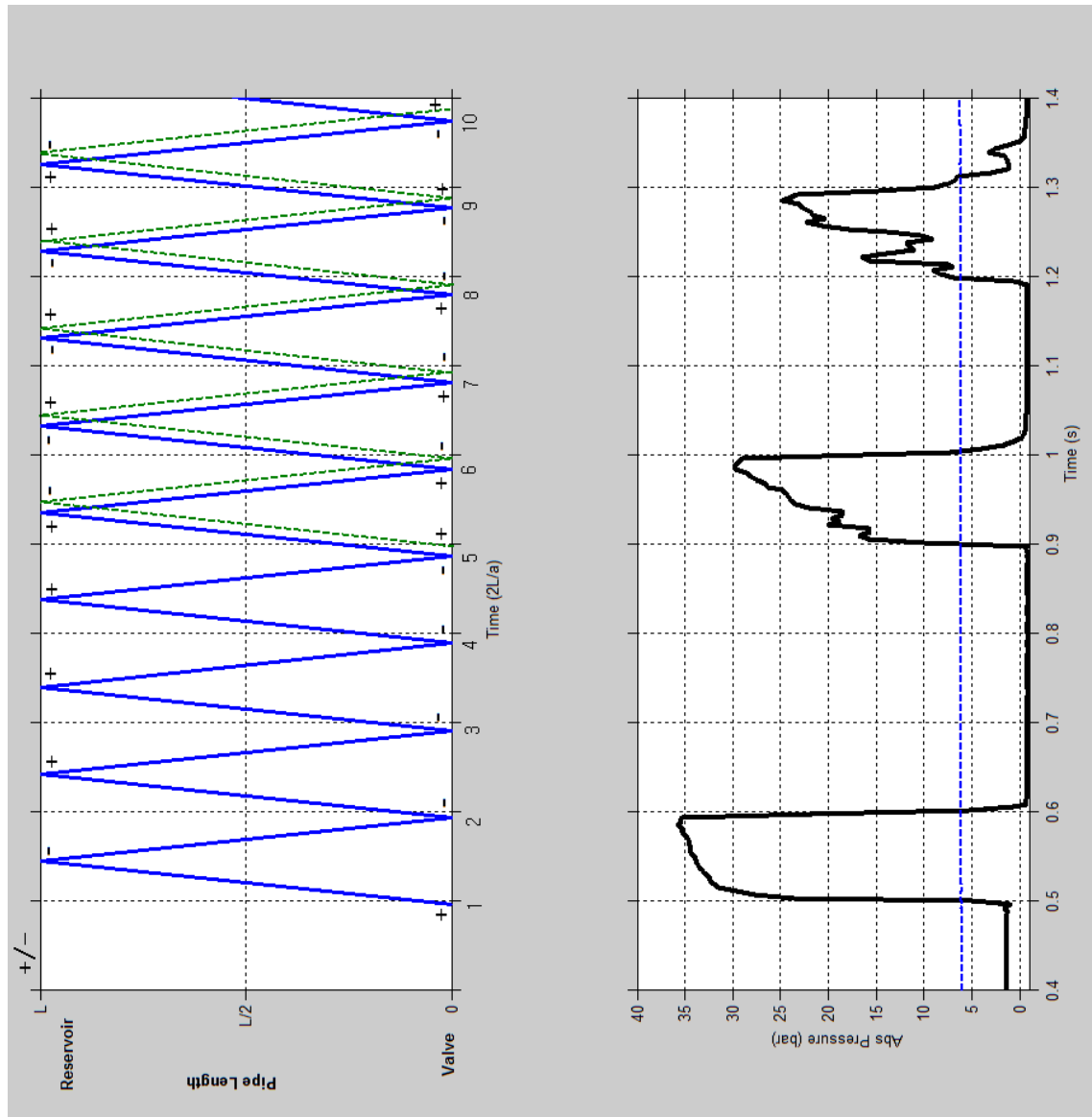
- A temporary change in the nature of the reflection at this boundary (from constant velocity  $V$  to constant pressure  $P$ ); and
- Collapse of the cavity initiates a second set of pressure waves which are superimposed on the original (rapid valve closure) set.

It can be seen that the combination of these two sets of pressure waves results in an initial pressure step up (caused by the collapse of the cavity) followed by a further

pressure spike superimposed on this (from the original disturbance). Figure(5.15) goes further than Arfaie (1989) did by starting to illustrate the effect of the second cavity, the collapse of which creates a third set of pressure waves. Bergant et al (2006), argued that if the collapse of the vapour cavity would have taken place exactly at the arrival of a pressure wave front, or at times that are multiples of pipeline period, then the high pressure peak might not have occurred. In Figure(5.15) it can be seen that the duration of the first cavity is just a little longer than  $(2L/a)$ , with the duration of the second cavity very much less than this. Figure(5.16) shows a similar analysis for a severe cavitation case (not done by Arfaie 1989) where the first cavity duration is more than twice as long (greater than  $4L/a$ ).



Figure(5.15) Graphical explanation of limited column separation with effect of collapsing the 2<sup>nd</sup> vapour cavity.



**Figure(5.16) Graphical representation of experimental typical water column separation.**

Viewed in isolation, this pressure trace may not appear to show the two-step pressure rise with spike evident for limited cavitation as in Figure(5.15). However it can be seen with this type of behaviour that the continuing pressure rise across the top of the second and subsequent peaks is considerably steeper than the line-packing pressure rise of the first (purely waterhammer) pressure peak. From the upper pressure wave tracing in Figure(5.16) it is obvious that the same sort of phenomenon as shown in Figure(5.15) must still be occurring, but the two-step nature of this is obscured by:

- the initial cavity closure pressure rise being both much greater with the more severe (large cavity region) column separation, but at the same time also less steep due to the large cavity collapse required; with

- the superimposed spike from the original closure being both much smaller in amplitude (though longer in duration) and also more attenuated and dispersed, due to the repeated wave reflections up and down the pipe over the long cavity duration.

The analytical analysis of Appendix (D) examines only the effect of the pressure wave generated by the cavity collapse and does not apply in the present situation where these are superimposed on an existing set of pressure waves caused by the rapid valve closure. That theory will obviously work best for severe cavitation where these original waves have been significantly attenuated, but it will not be appropriate for limited cavitation because it does not include the waves causing the high-pressure spike.



## **Chapter 6**

### **Comparison of Column Separation Models**

This chapter compares the various user-selected aspects of the numerical models of column separation described in Chapter 3, assessed against the full spectrum of experimental runs covering different modes of pressure transient summarised in Table(5.2).

## **6.1 Assessment criteria**

From the literature, almost all researchers have based their validation on visual assessment, i.e. qualitative assessment, e.g. Simpson and Wylie (1989), Bergant and Simpson (1999), Shu (2003), Bergant et al (2008ab), Adamkowski and Lewandowski (2009), Autrique et al (2012). Arfaie (1989) followed this accepted procedure. Previously Arfaie (1989) attempted to assess the performance of his model over an extended time (typically  $\sim 4 - 6$  waterhammer periods  $4L/a$ ), which was a key factor in his proposal that, for the experimental rig used in his study and this (Chapter 4), an unsteady friction model was appropriate. However, this approach demands considerable subjective judgment so to avoid this a different assessment procedure is introduced here, restricted to judging the fitness of the numerical models on the quantified error for just two parameters, both as recorded by the transient pressure at the closed valve:

- a) First cavity duration  $T_{c1}$ , and
- b) Immediate post-cavity pressure peak amplitude  $P_{max2}$ .

These two parameters have been selected because they are the most dominant observations on the pressure transient traces for these experiments after the initial Joukowsky pressure. Due to water hammer being a wave propagation phenomenon, it can be reasonably argued that a model that cannot reproduce these key features of the first column separation event is unlikely to satisfactorily reproduce subsequent events.

It can be seen from the pressure traces of column separation, Figure(6.1), that the first cavity period  $T_{c1}$  is defined as a period of time at which the local pressure at the downstream closed valve drops to and stays at the minimum pressure (theoretically the vapour pressure) thus causing column separation. It can be seen from Figure(6.1) that the pressure trace does not drop instantaneously (sharply) to vapour pressure. It typically takes  $(2 - 3)\Delta t$  to reach the level of vapour pressure, as in Figure(6.1), and the reasons for that might be related to:

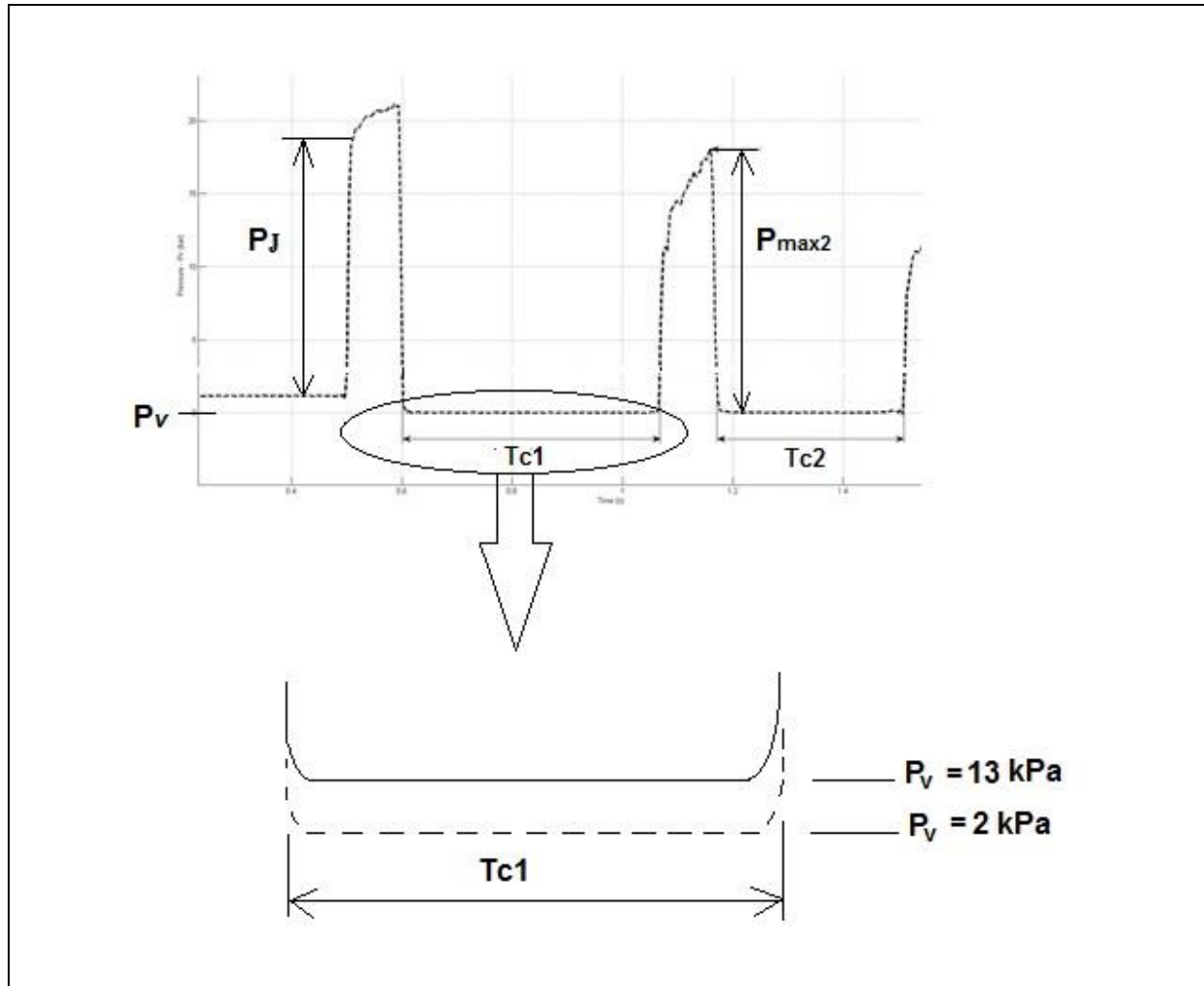
- Release of dissolved gases (air), initiated when the transient pressure becomes sub-atmospheric but possibly not as low as water vapour pressure.
- The fact that boiling (cavitation) and condensation processes are not instantaneous but take some finite time to reach the new status.

Consequently, as shown in Figure(6.1) the cavity duration is not defined as the duration over which the pressure is actually at a constant minimum value (the vapour pressure). Rather, the two periods at the cavity beginning and end over which the transition from the rapid (more or less linear) “Joukowsky” pressure drop or rise to or from constant vapour pressure are included in the overall cavity time, as these more accurately represent the waterhammer wave reflection occurrences initiating and terminating the transient cavitation. This is justified at cavity collapse because the filmed observations show the vapour/gas cavities distributed over the cavitation region rather than forming the classic full cross-section “column separation” (Section 4.5). In practice (for this apparatus with the transient initiated by rapid valve closure, leading to clearly defined rapid pressure changes due to wave reflections), inspection of the actual discrete recorded pressure data showed that the uncertainty involved in taking the cavity durations to be simply the period over which recorded pressure is sub-atmospheric is no greater than that from inspecting the actual cavity start and end times Figure(6.1). However, this makes automatic and therefore completely consistent measurement possible (Appendix E).

The second criterion is the maximum post-cavity amplitude  $P_{max2}$ , which is a single value at which a maximum pressure amplitude can be observed between the first two cavities on a pressure trace for both the experiments and the predictions of numerical models, as identified on Figure(6.1). This second peak on the trace may be less than the initial Joukowsky waterhammer peak, as in the classic column separation shown on Figure(6.1), or it may be larger, as in limited cavitation (Section 5.3.2). (Martin 1983).

A consistent procedure for quantifying both  $T_{c1}$  and  $P_{max2}$  from both observed and calculated discrete results using a MATLAB code (listed in Appendix E), was applied to the full spectrum of column separation modes. The algorithm reads in the experimental pressure trace data. It identifies the periods of both first and second cavities  $T_{c1}$  and  $T_{c2}$  with the post-cavity pressure amplitude evaluated by calling in a

standard MATLAB function (maximum.m) for the predetermined period between the first and the second cavities. The algorithm applies the same procedure to the predictions (calculated) of all the assigned models. Single values of error are calculated for each of the period  $T_{c1}$  and the post-cavity amplitude  $P_{max2}$ .



Figure(6.1) Taking measurements of  $T_{c1}$  and  $P_{max2}$  on pressure trace

Error is defined in Eq.(6.1) as the difference between calculated and observed values for each experimental run with the relative error (%), in Eq.(6.2). These will be applied to both the first cavity period  $T_{c1}$  and the post-cavity pressure peak  $P_{max2}$ :

$$\text{Error} = \text{calculated} - \text{observed} \quad (6.1)$$

$$\text{Relative Error \%} = \frac{\text{calculated} - \text{observed}}{\text{observed}} * 100 \quad (6.2)$$

This model error is itself subject to uncertainty. The experimental uncertainties have been discussed in Appendix A.2, along with the uncertainty in the data supplied to the model, where the values for wavespeed ( $a$ ) and Darcy friction factor ( $f$ ) were taken from experimental measurements to reduce their impact on the modelling errors. In addition, though, both the model calculation and observed experimental results exist only as a series of discrete points at a time interval ( $\Delta t = 0.0039$  s at 256Hz) for both the model numerical method and also the transient recorder discrete recording frequency interval. Consequently, there is a minimum time uncertainty of  $\pm \frac{1}{2} \Delta t$  for both:

- Post-initiation waterhammer wave event occurrence, in particular for the start and end of column separation cavity events.
- Timing of maximum pressure peaks, where the true experimental peak may lie between two recorded values. For the step-by-step numerical model, however, the maximum calculated value will be at a defined time. The mode of column separation behaviour (limited cavitation) giving sharp pressure spikes will increase this error compared with the more gradual line-packing pressure rise associated with classic column separation.

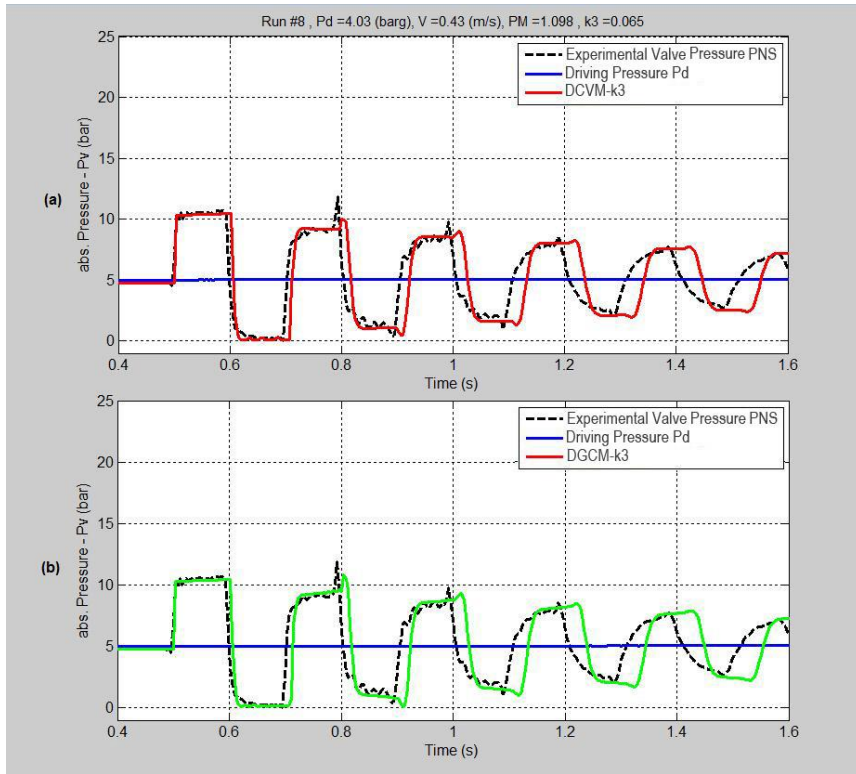
In addition, it must be noted that the model pressure values are calculated at the assumed upstream plane of the closed valve but, as noted in Section(4.2), it was physically not possible to locate the experimental pressure transducer at this location (particularly because of the inclusion of the transparent polycarbonate tube for cavity visualisation), so this is  $\Delta l = 500$  mm upstream of the valve. Consequently there is a time difference ( $\pm$  depending on direction of waterhammer wave travel) of  $(\Delta l/a) = 0.00039$ s  $\ll \Delta t$  between observed and calculated values. It is assumed that this has a negligible effect compared with the other uncertainties.

## 6.2 Visual comparison of computed vs experimental

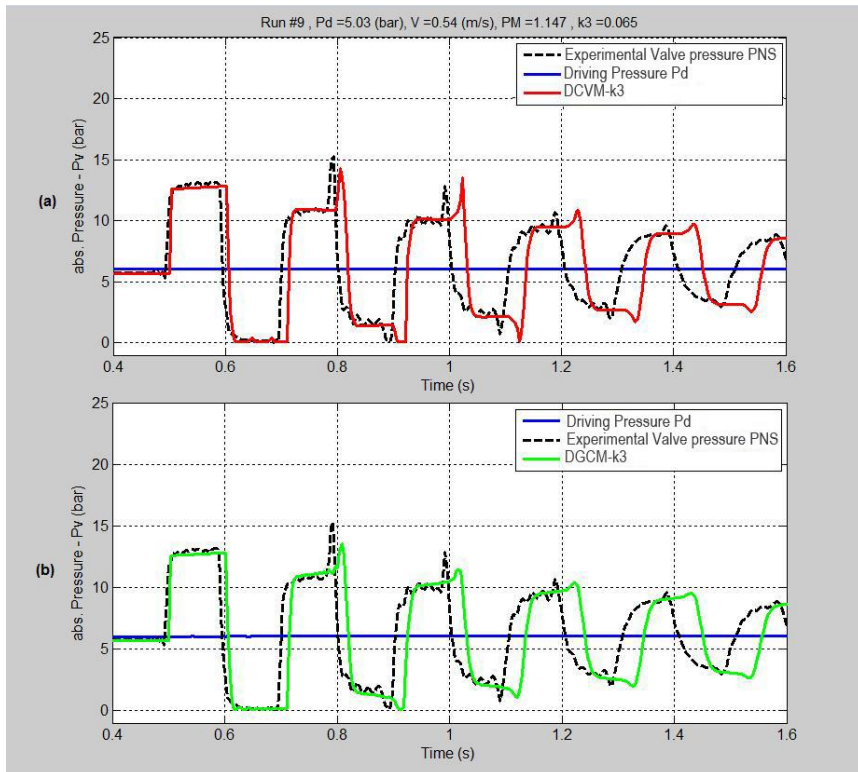
Initial work followed Arfaie (1989) in attempting to use conventional qualitative assessment over a range of different modes of column separation (see Appendix B). To illustrate the problems with this approach. This section will show comparisons with examples from the full spectrum of the behaviour modes described in Sections(5.2) and (5.3). Essentially this becomes a “one factor at a time” process, with Sections(6.2.1) to (6.2.3) comparing first method (DVCM v DGCM), then unsteady friction models and finally the internal cavity interface boundary condition models.

### 6.2.1 Comparison of method (DVCM v DGCM)

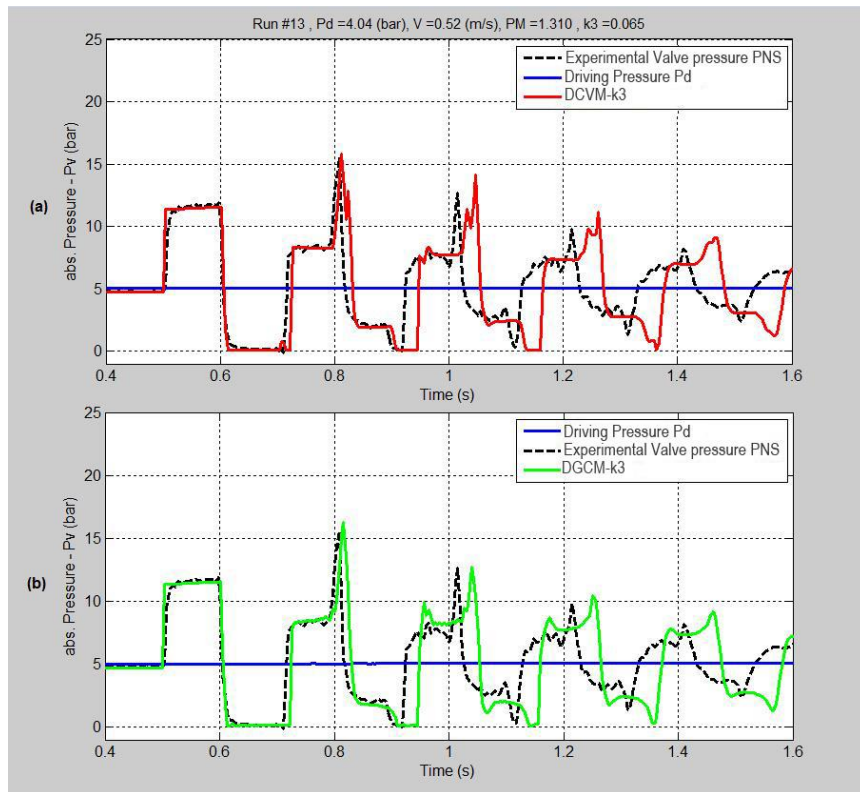
Figure(6.2) to Figure(6.9) compare DVCM and DGCM models, as compared by Bergant and Simpson (1999), but with unsteady friction (as suggested by Arfaie 1989). A weighting factor of  $\Psi = 0.85$  and value of free gas void fraction of  $\alpha_g = 10^{-7}$  has been used in DGCM for all computational analyses. For unsteady friction the published model tested by Bughazem (1997) (Bughazem and Anderson 2000) was used with the value for  $k_3 = 0.065$  (determined on the apparatus). The boundary condition at the column separation is the conventional Wylie and Streeter (1993) implementation and the data value for vapour pressure is that from ASME (2006) for the laboratory water temperature ( $P_v = 2 \text{ kPa}$ ).



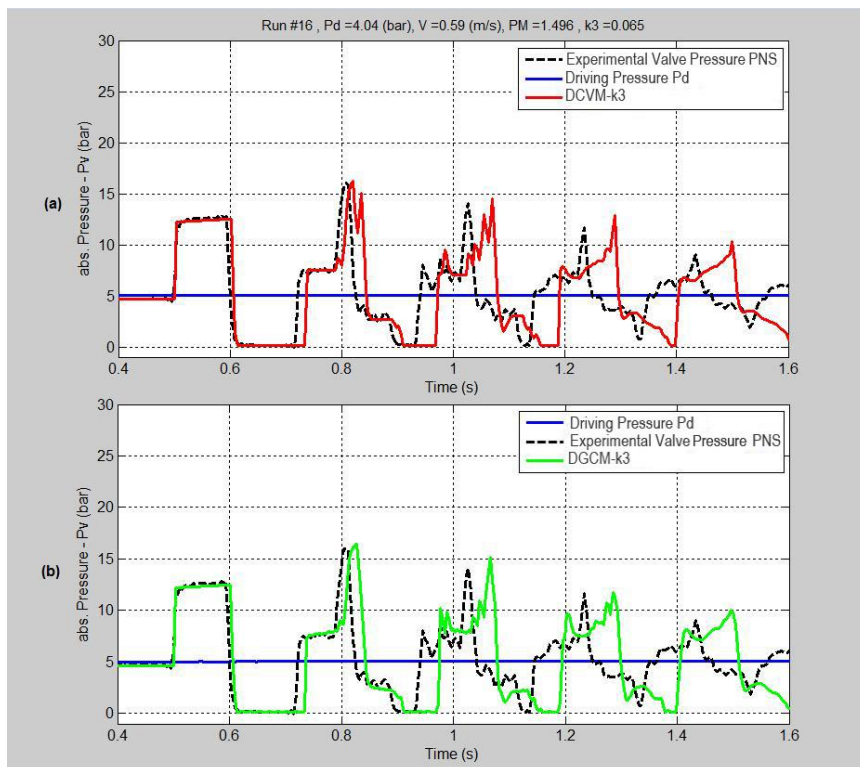
Figure(6.2) Transient behaviour of 1<sup>st</sup> transition zone, (run 8) versus prediction of both (a) DVCM-k3 , (b) DGCM-k3.



Figure(6.3) Transient behaviour of 1<sup>st</sup> transition zone (run 9) versus prediction of both (a) DVCM-k3 , (b) DGCM-k3.

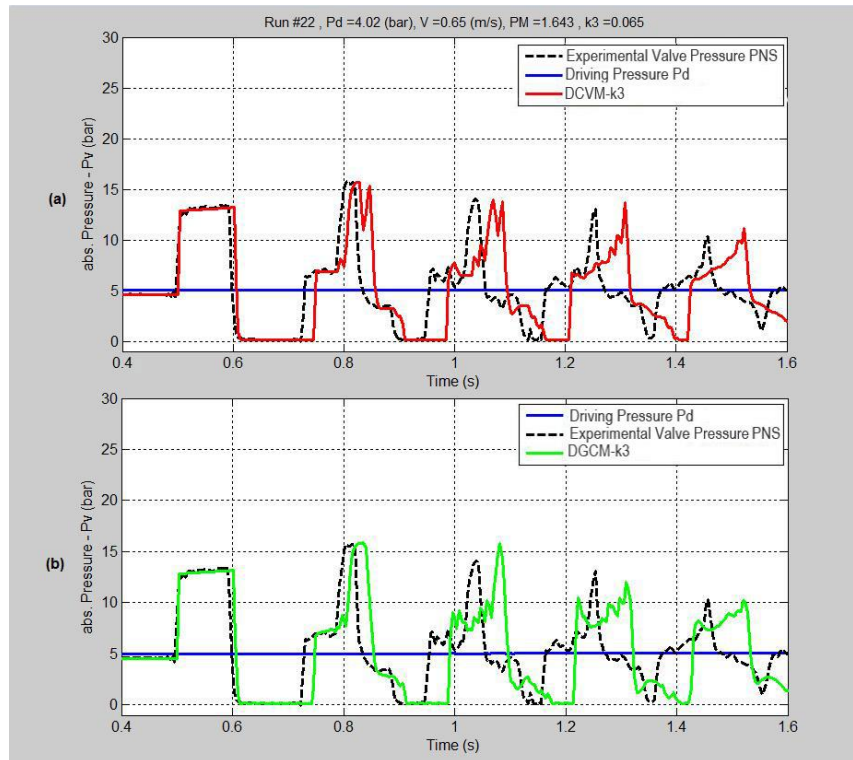


Figure(6.4) Comparison of Limited column separation (run 13) versus prediction of both models, (a) DVCM-k3, (b) DGCM-k3.

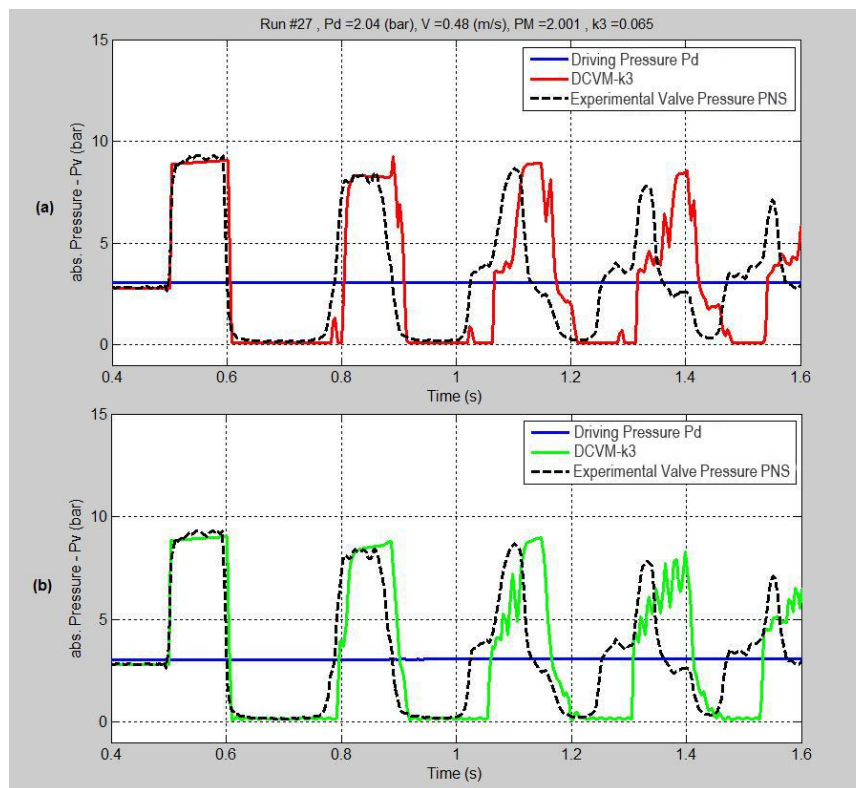


Figure(6.5) Comparison of Limited column separation (run 16) versus prediction of both models, (a) DVCM-k3, (b) DGCM-k3.

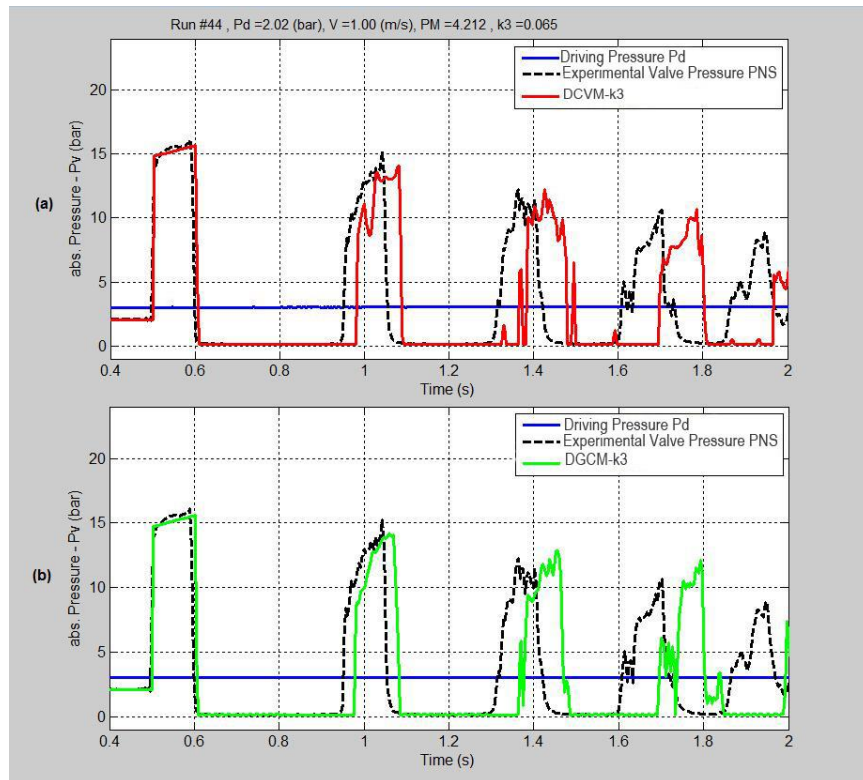




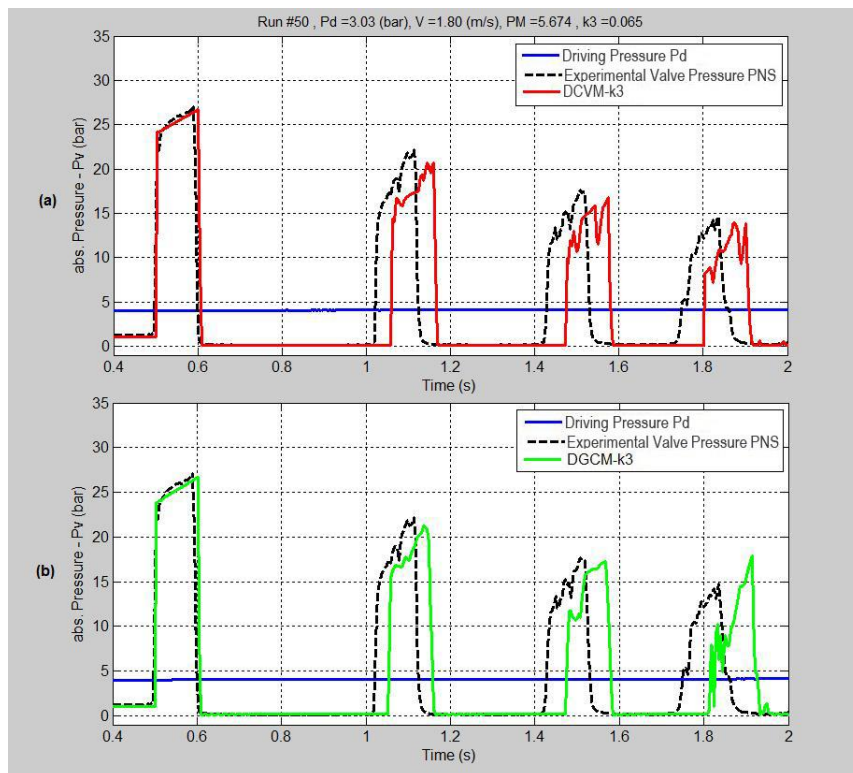
Figure(6.6) Comparison of Limited column separation (run 22) versus prediction of both models, (a) DVCM-k3 , (b) DGCM-k3.



Figure(6.7) Transient behaviour of 2nd transition zone (run 27) versus prediction of both models, (a) DVCM-k3 , (b) DGCM-k3.



Figure(6.8) Comparison of Typical column separation (run 44) versus prediction of both models, (a) DVCM-k3 , (b) DGCM-k3.



Figure(6.9) Comparison of Typical column separation (run 50) versus prediction of both models, (a) DVCM-k3 , (b) DGCM-k3.

There is little point to detailed discussion of each of Figure(6.2) to Figure(6.9) along the lines of Appendix B. Together they indicate that over a range of modes of column separation behaviour meaningful qualitative comparison becomes hard to carry out, even with just one factor (i.e. method) at two levels (DVCM vs DGCM). With the limited set of model options illustrated, some broad generalisation can be made as in Appendix B:

- Both these models represent the first post-cavity pressure wave (2<sup>nd</sup> peak) quite well, but with error in magnitude.
- They tend to overestimate the first cavity duration, with increasing phase shift after the 2<sup>nd</sup> pressure peak, though the continuing general shape of the pressure wave is reasonable.
- The calculated peak after the 1<sup>st</sup> cavity could be underestimated, Figures (6.2), (6.3), (6.8), (6.9) or overestimated Figures (6.6), (6.7).

It is difficult to establish which method is better. With Figure(6.2) and Figure(6.3) both methods give similar results, which replicate the waveforms quite well, though with increasing phase error. From Figure(6.4) and Figure(6.5), the methods start to give slightly different responses, both differing in details from experiment. This is illustrated in Figure(6.6) to Figure(6.8) where the two methods show different patterns of pressure spikes to each other and to experiment. However, with the more classic column separation on Figure(6.9), both methods become closer again to the extended experimental waveform (with contrast to Appendix B).

In addition, this process then has to identify the effect of the other factors (e.g. friction and internal cavity boundary condition) on prediction. Finally, all of these results raised a new and unexpected issue. All the calculations used the “correct” value for vapour pressure taken from Steam Tables, ASME (2006) ( $P_v = 2\text{kPa}$ ). However, even at the scales plotted in Figure(6.2) to Figure(6.9), it is possible to observe that the experimental results show an apparently higher value of vapour pressure at about  $P_v \cong 13\text{kPa}$ , Figure(6.1). In retrospect this can be explained. Steam Table values are for pure  $\text{H}_2\text{O}$  (demineralised, deionised, with all non-condensable gases removed, especially air) as used typically in thermal power station applications. The town mains water used in this apparatus does not match these conditions and, in particular (Section 6.1), evidence of the presence of dissolved gas has already been presented, which also explains the higher effective vapour pressure.

### 6.2.2 Comparison of unsteady friction models

This section compares two implementations of the Brunone et al (1991b) type instantaneous acceleration based unsteady friction and model:

- The version tested by Bughazem (1997) and Bughazem and Anderson (2000) with best coefficient for this apparatus  $k_3 = 0.065$ .
- The alternative MOC implementation of this derived in Section(3.3) with the best coefficient for this apparatus  $k_t = 0.035$ .

The models are compared first for DVCM, Figure(6.10) to Figure(6.14) and then for DGCM (with  $\psi = 0.85$  and  $\alpha_g = 10^{-7}$ ), Figure(6.15) to Figure(6.19). The cavity interface internal boundary condition is the conventional Wylie and Streeter (with vapour pressure 2kPa).

Qualitative assessment criteria are hard to define and then apply consistently. These graphs can be compared, for example, in terms of:

- amplitude of second (post-cavity) peak, as in Eq.(6.1);
- general shape of modelled as compared with experimental pressure-time response, as in Arfaie(1989); and
- ability to maintain the phase of the oscillation overall (as opposed to a specific feature, e.g. first cavity duration by Eq.(6.2).

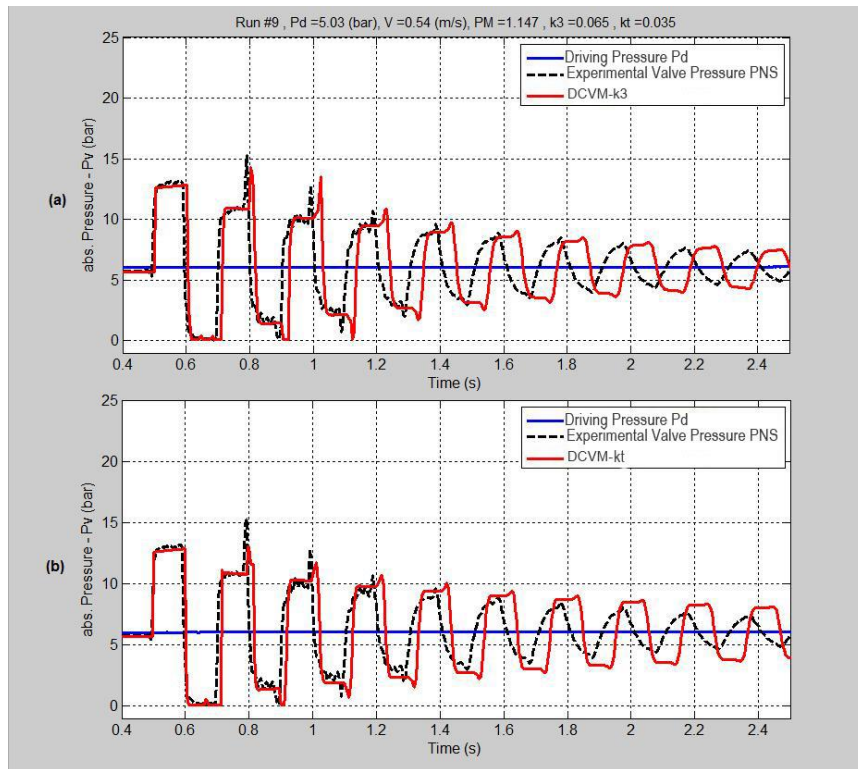
Table(6.1) gives a summary of the qualitative assessments that could be made. It can be seen that in all cases there is little to chose between the methods for the first (waterhammer) peak over the initial  $(2L/a)$ , but there is significant variation in all three aspects above after transient cavitation is initiated. A number of issues are revealed by Table(6.1):

- (a) It tends to confirm that the opinion of Arfaie (1989) that the choice of best method is dependent on the column separation mode of behaviour, but even the three limited cavitation cases do not show completely consistent evaluations.
- (b) Each of the three criteria can lead to different evaluations. For phase the  $k_t$  method is more widely better, whereas for overall shape of response the  $k_3$  method is widely better and for the actual peak amplitude there is little to

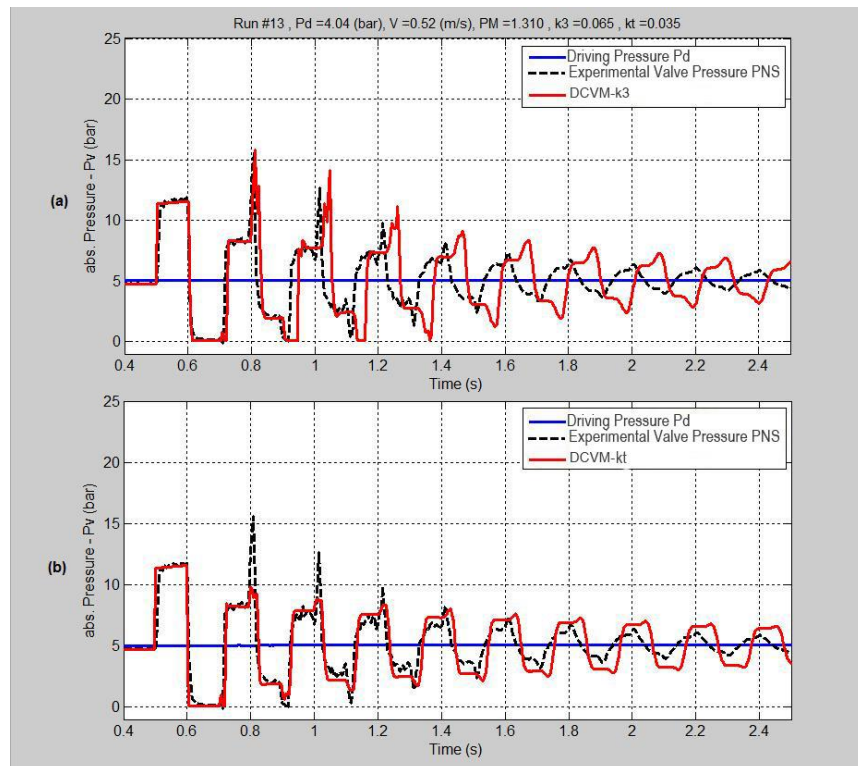
chose between methods if DVCM is used, but if DGCM is used then  $k_t$  is more likely to be better.

**Table(6.1) Qualitative assessment of best unsteady friction model (Section 6.2.2):  $k_3$  denotes the model of Section(3.2),  $k_t$  denotes the new full MOC model (Section 3.3).**

Criteria (Figures)	2 <sup>nd</sup> peak amplitude		Response overall shape		Response overall phase	
	DVCM	DGCM	DVCM	DGCM	DVCM	DGCM
(6.10) and (6.15)	similar	similar	$k_3$	similar	$k_t$	similar
(6.11) and (6.16)	similar	$k_3$	similar	$k_t$	$k_t$	$k_t$
(6.12) and (6.17)	$k_t$	$k_t$	$k_t$	$k_3$	$k_t$	$k_t$
(6.13) and (6.18)	similar	$k_t$	$k_3$	$k_3$	$k_t$	$k_t$
(6.14) and (6.19)	$k_3$	$k_t$	$k_3$	$k_3$	$k_3$	$k_t$

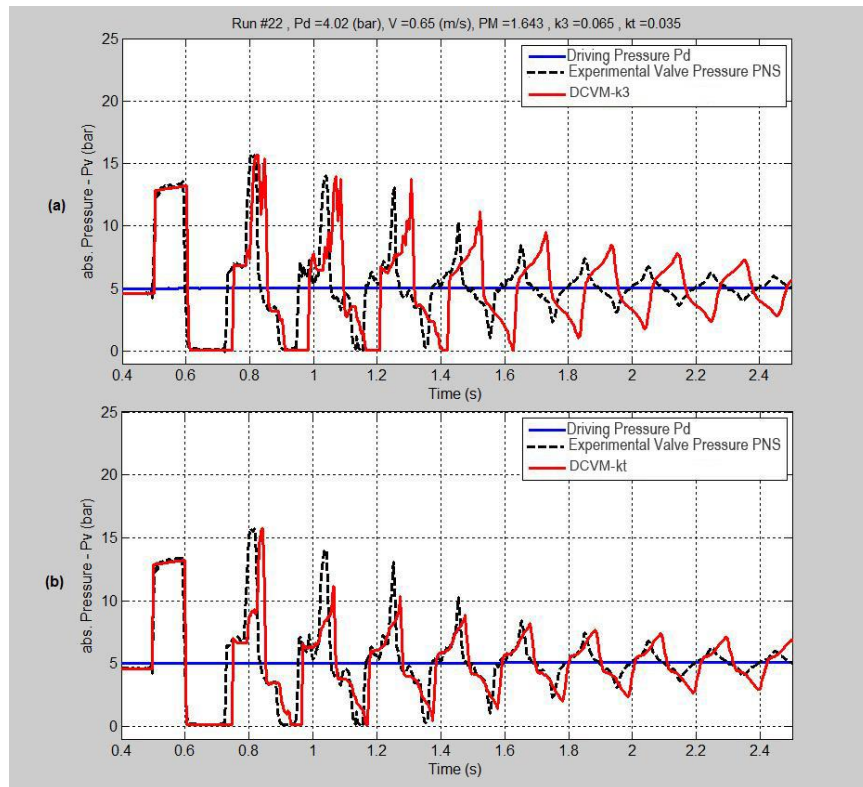


Figure(6.10) Transient behaviour of 1<sup>st</sup> transition zone, (run 9) vs prediction of both (a) DVCM-k3, (b) DVCM-kt.

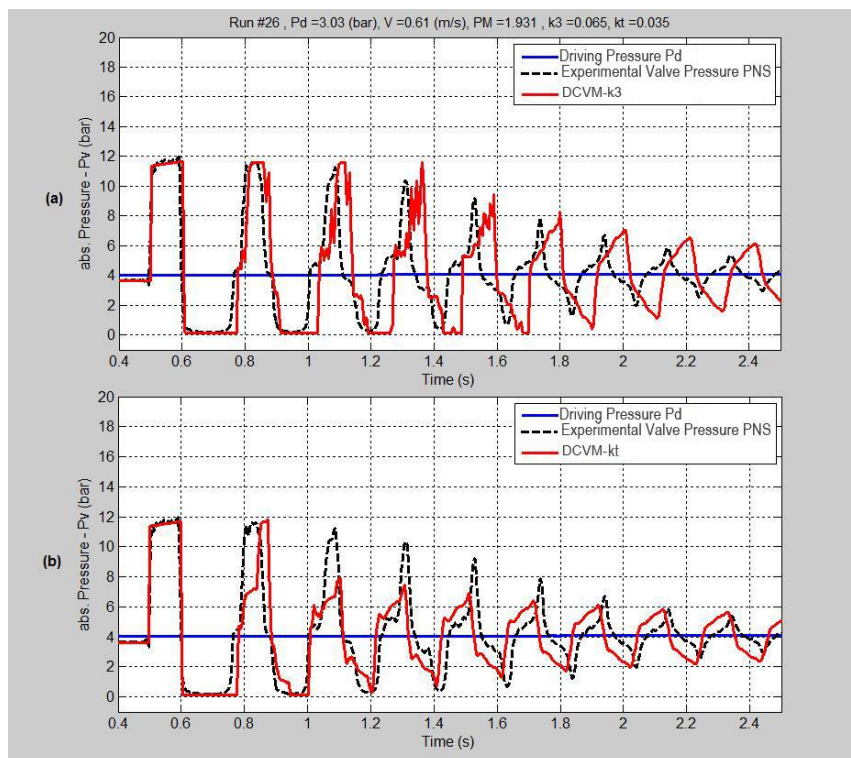


Figure(6.11) Comparison of Limited column separation (run 13) vs prediction of both (a) DVCM-k3, (b) DVCM-kt.

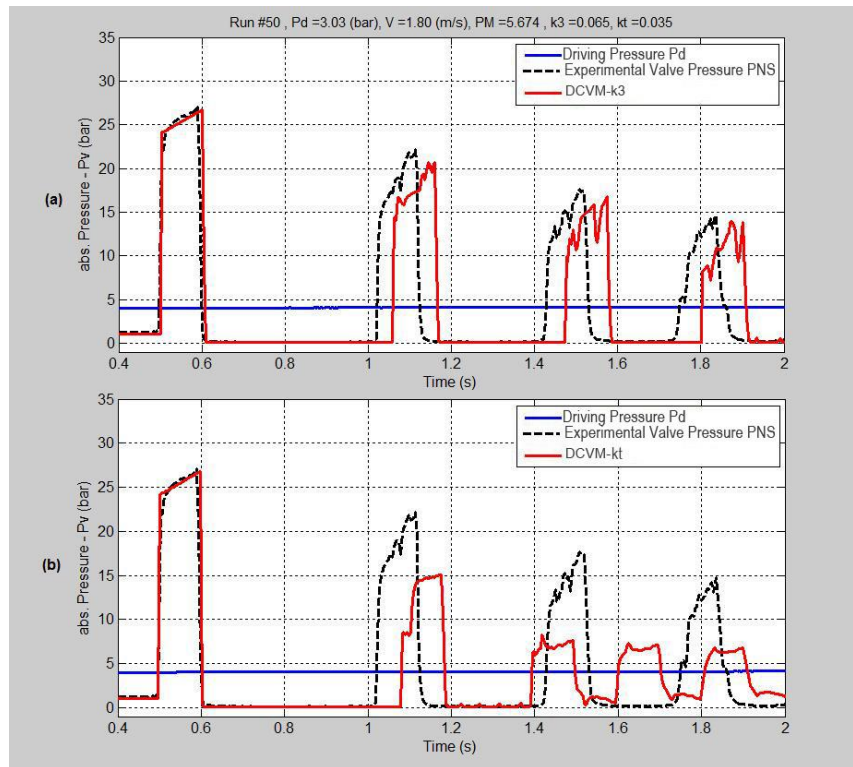




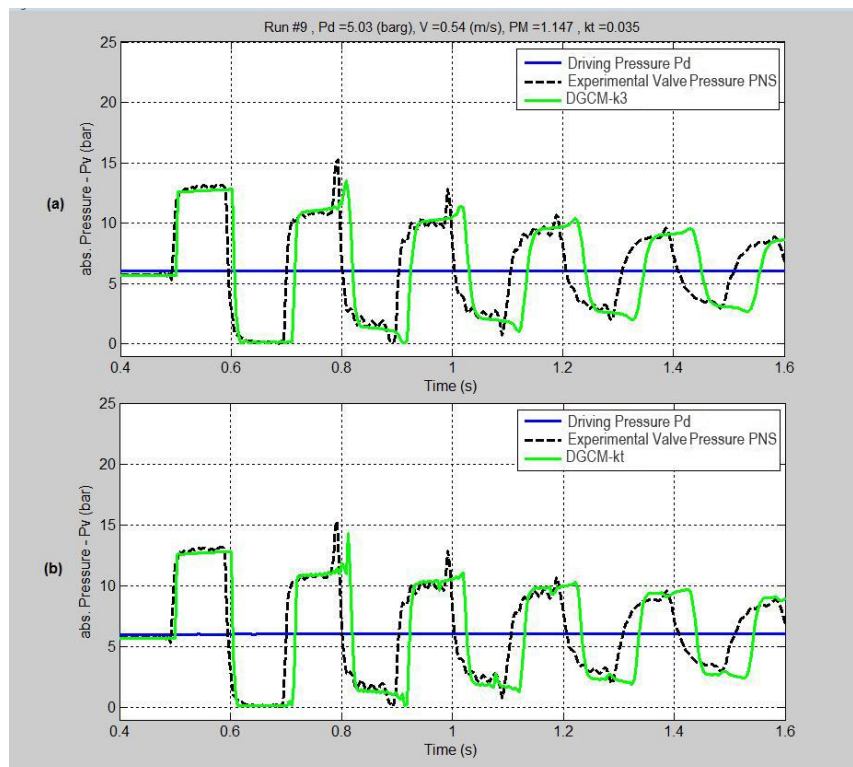
Figure(6.12) Comparison of Limited column separation (run 22) vs prediction of both (a) DVCM-k3, (b) DVCM-kt.



Figure(6.13) Transient behaviour of 2<sup>nd</sup> transition zone, (run 26) vs prediction of both (a) DVCM-k3, (b) DVCM-kt.

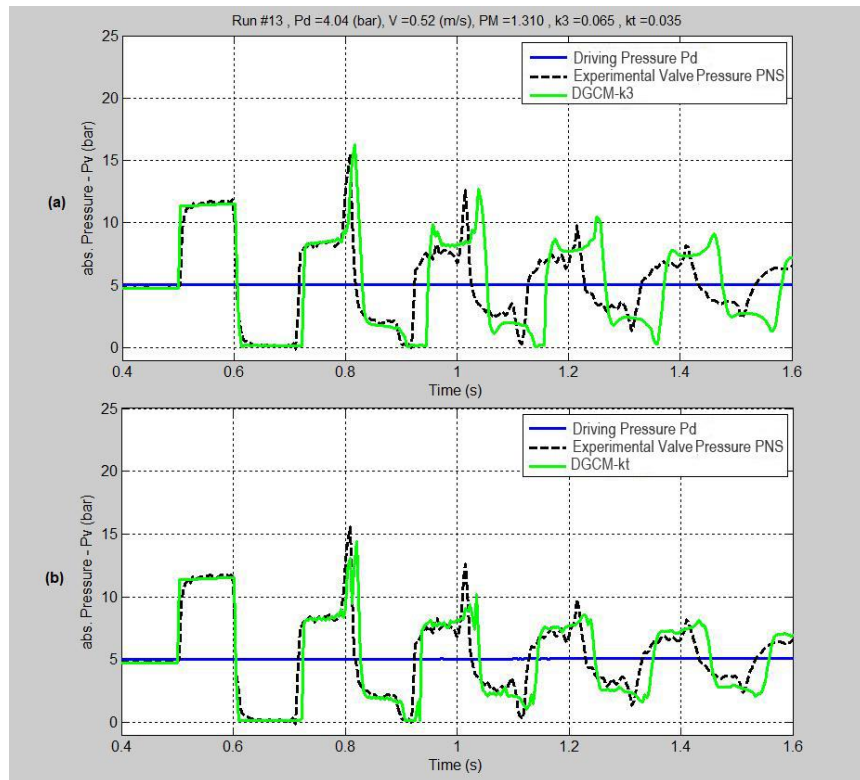


Figure(6.14) Comparison of Typical column separation (run 50) vs prediction of both (a) DVCM-k3 , (b) DVCM-kt.

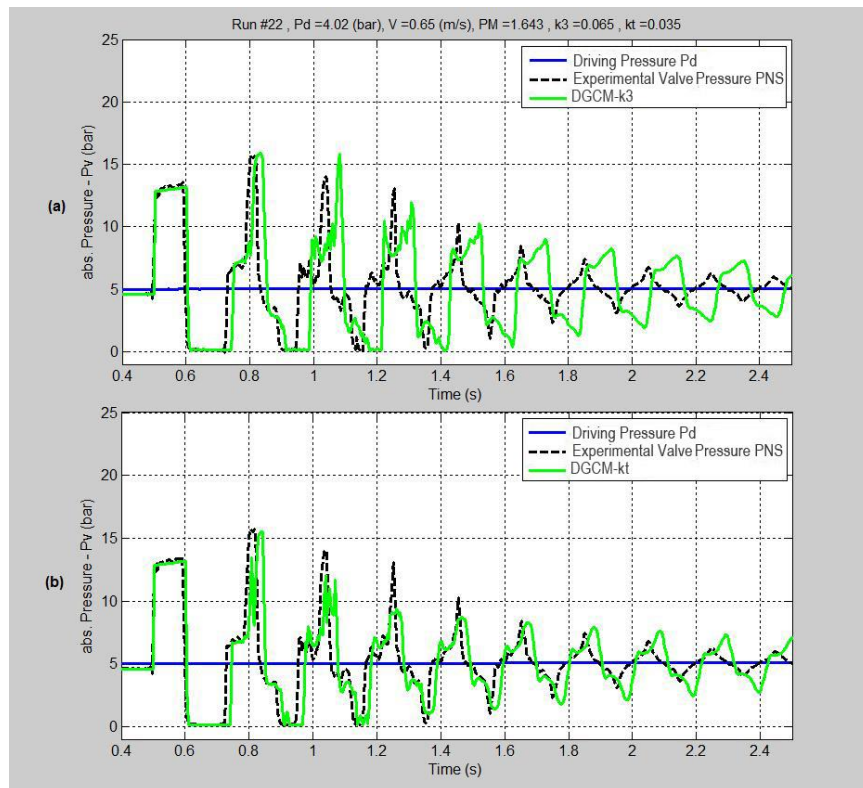


Figure(6.15) Transient behaviour of 1<sup>st</sup> transition zone (run 9), vs prediction of both (a) DGCM-k3 , (b) DGCM-kt.

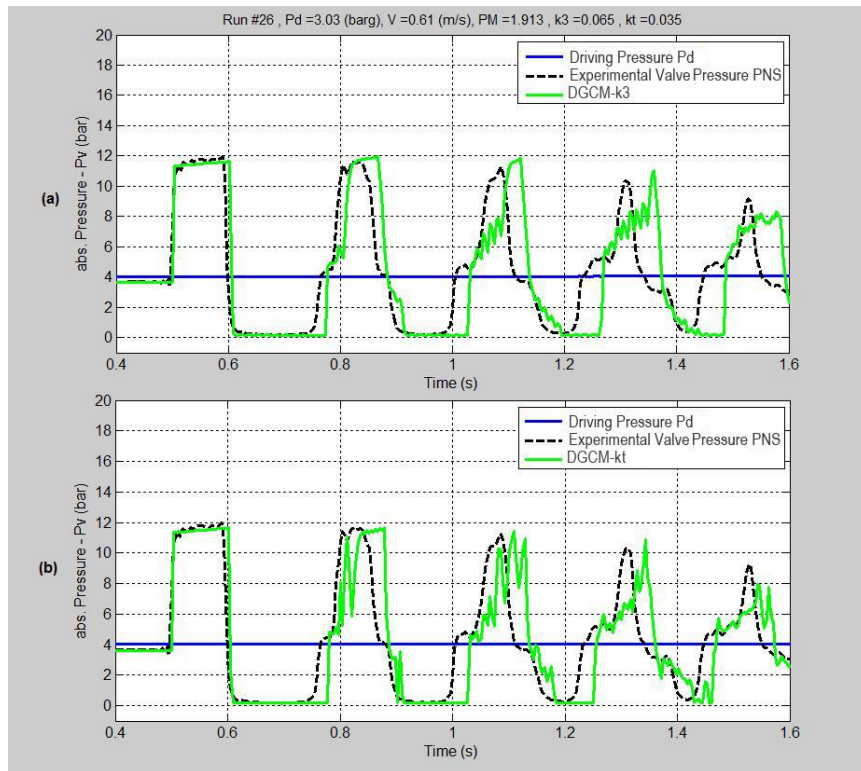




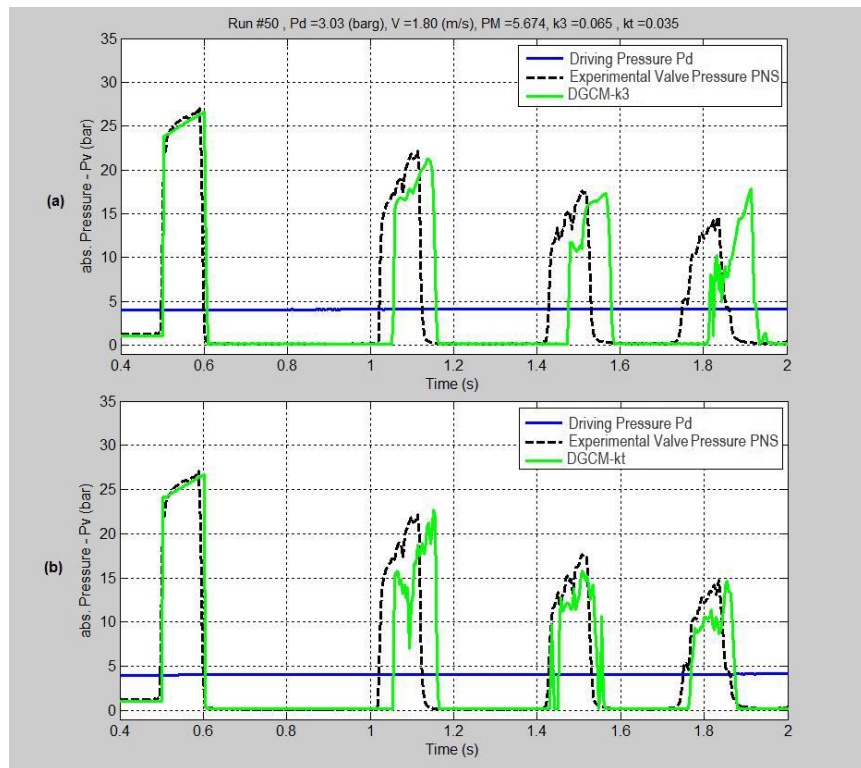
Figure(6.16) Comparison of Limited column separation (run 13) vs prediction of both (a) DGCM- $k_3$ , (b) DGCM- $k_t$ .



Figure(6.17) Comparison of Limited column separation (run 22) vs prediction of both (a) DGCM- $k_3$ , (b) DGCM- $k_t$ .



Figure(6.18) Transient behaviour of 2<sup>nd</sup> transition zone, (run 26) vs prediction of both (a) DGCM-k3, (b) DGCM-kt.



Figure(6.19) Comparison of Typical column separation (run 50) vs prediction of both (a) DGCM-k3, (b) DGCM-kt.

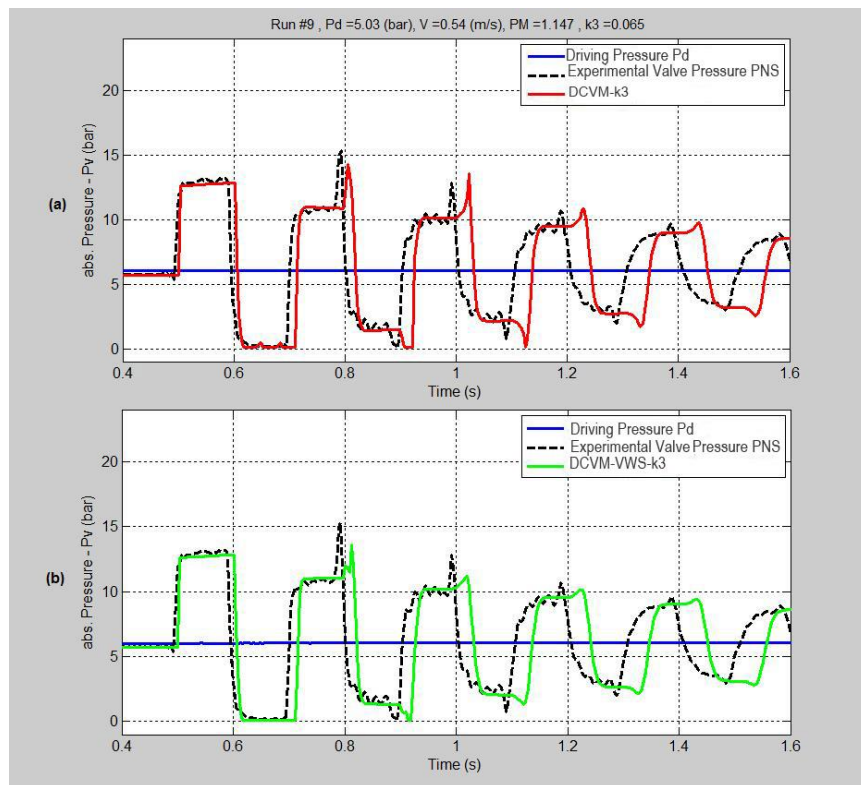
### **6.2.3 Comparison of internal boundary condition models for DVCM**

This section compares the conventional Wylie and Streeter and “improved” Arfaie transient internal cavity interface models for the DVCM, essentially repeating the work of Arfaie (1989) with new experimental results. In keeping with his other recommendation, the Bughazem and Anderson (2000) unsteady friction model is used with  $k_3 = 0.065$  (and vapour pressure at 2kPa). The results are shown over a range of modes of behaviour as he suggested:

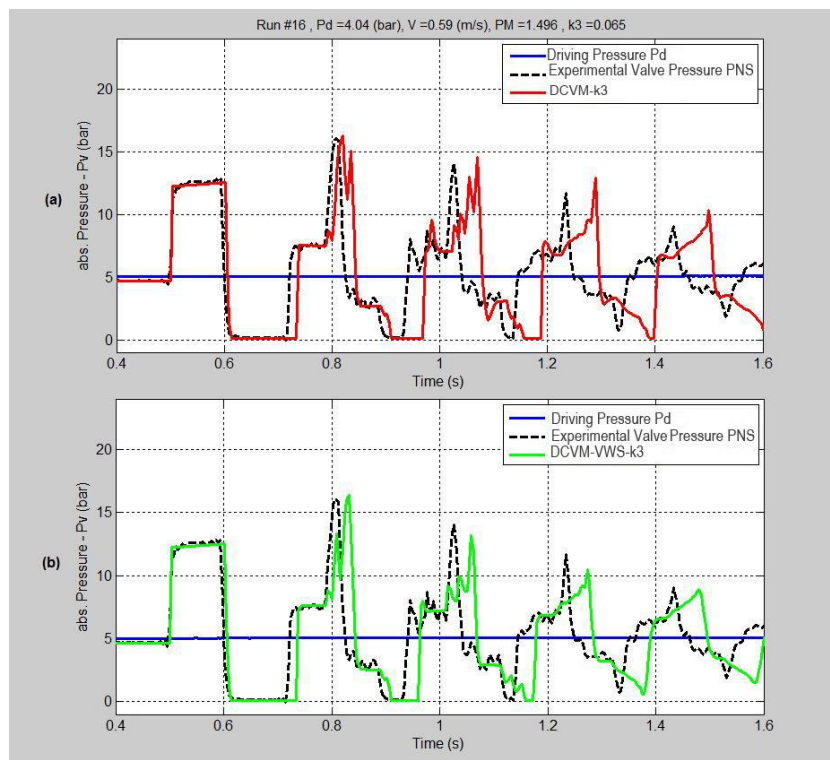
- Figure(6.20) shows the first transient from waterhammer to limited column separation.
- Figure(6.21) to Figure(6.23) show limited cavitation, with the second (post first cavity) peak higher than Joukowsky pressure.
- Figure(6.24) and Figure(6.25) show classic severe cavitation.

Across all modes of behaviour, all the results show both boundary conditions fail to maintain phase, with cavity duration over-predicted, but the Arfaie boundary condition gives improving performance through limited cavitation, e.g. Figure(6.23), and for severe cavitation, e.g. Figure(6.25). In terms of predicting the second (post-cavity) peak there is little to choose between the boundary conditions, with the conventional Wylie and Streeter better for Figure(6.20) and Figure(6.21) but Arfaie better as cavitation becomes more severe.

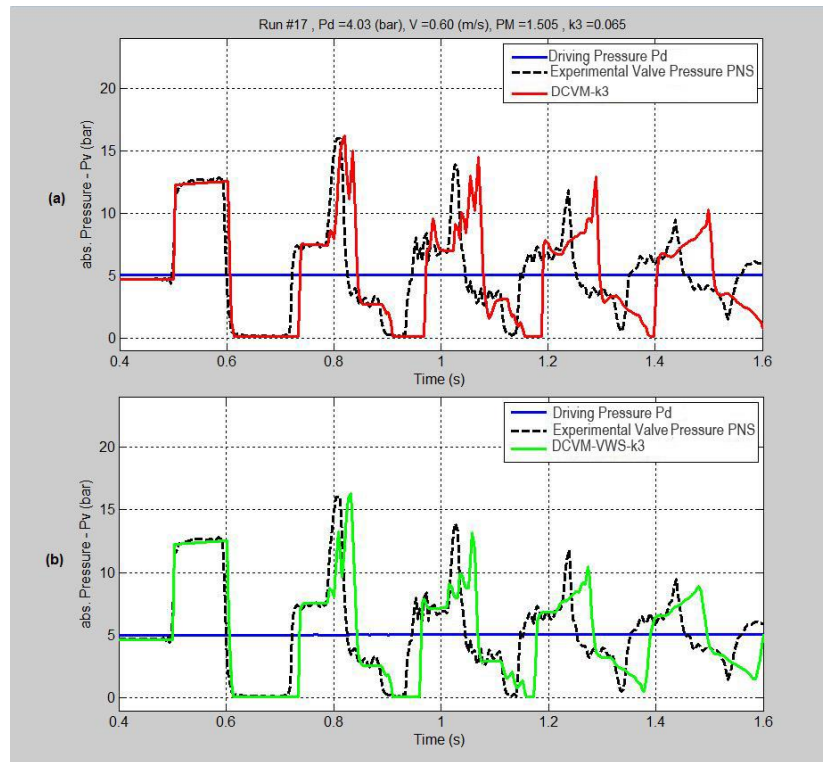
However, from this set of results it is hard to draw any firm conclusions, because all of the results are influenced by using an unsteady friction model. Therefore it would be useful to repeat them all, but with quasi-steady friction. That would still have tested only DVCM, so the process would also have to be repeated for DGCM.



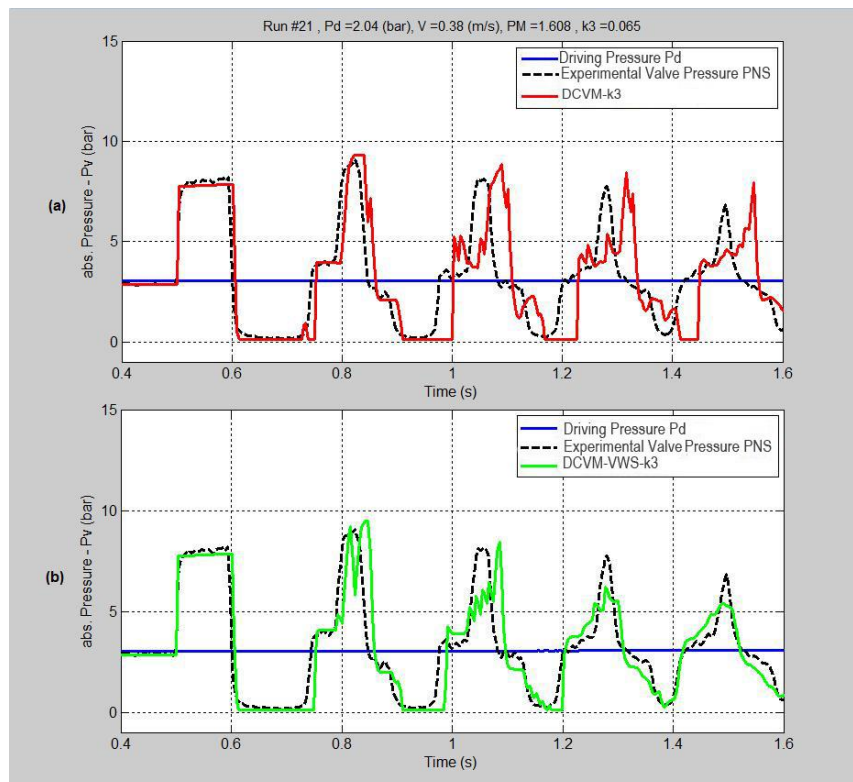
Figure(6.20) Transient behaviour of 1<sup>st</sup> transition zone (run 9), vs prediction of both (a) DVCM-k3, (b) DVCM-VWS-k3.



Figure(6.21) Comparison of Limited column separation (run 16) vs prediction of both (a) DVCM-k3, (b) DVCM-VWS-k3.

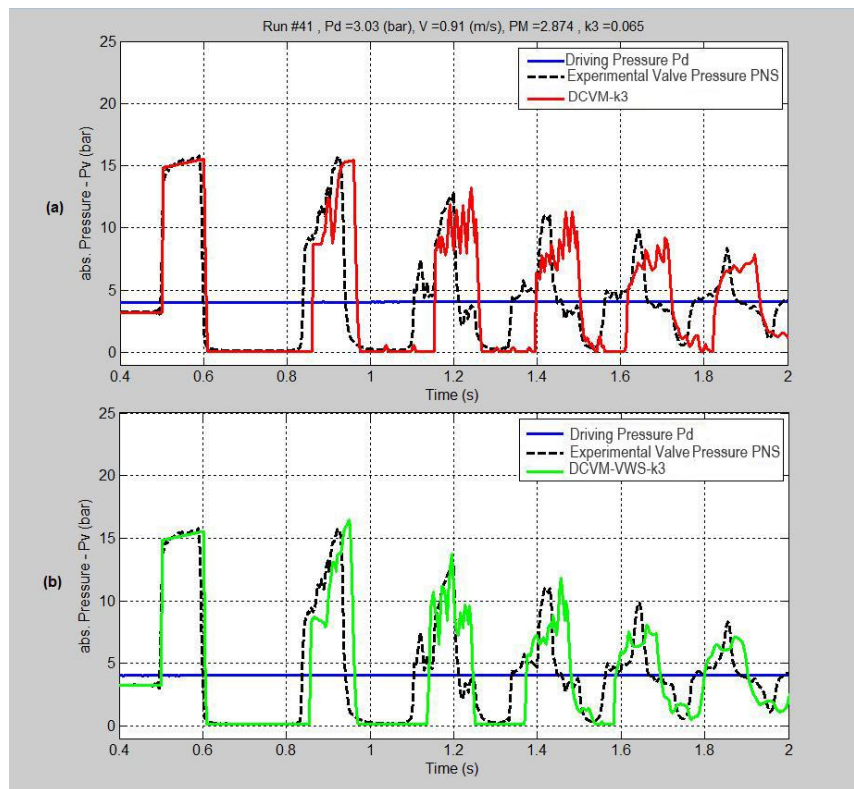


Figure(6.22) Comparison of Limited column separation (run 17) vs prediction of both (a) DVCM-k3 , (b) DVCM-VWS-k3.

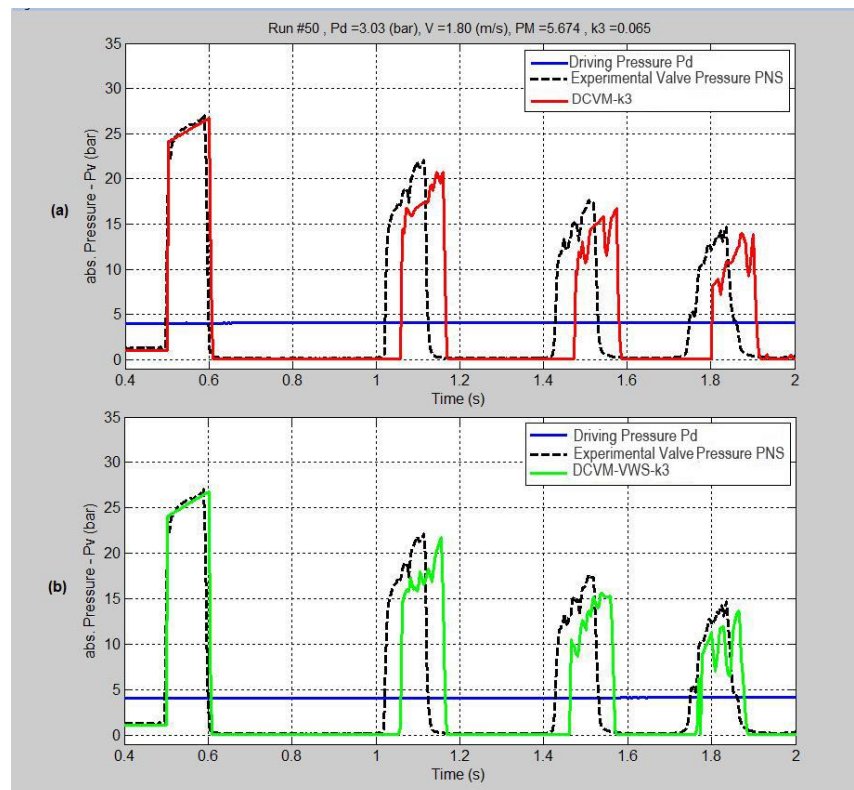


Figure(6.23) Comparison of Limited column separation (run 21) vs prediction of both (a) DVCM-k3 , (b) DVCM-VWS-k3.





Figure(6.24) Comparison of Typical column separation (run 41) vs prediction of both (a) DVCM-k3 , (b) DVCM-VWS-k3.

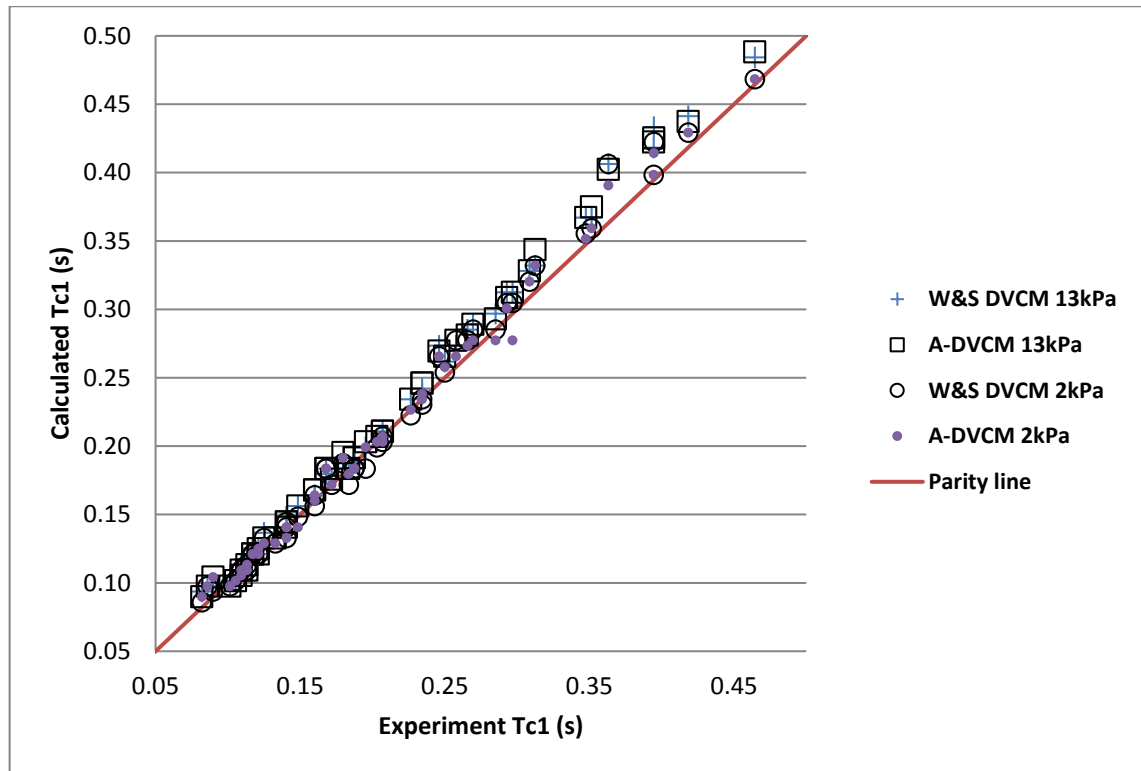


Figure(6.25) Comparison of Limited column separation (run 50) vs prediction of both (a) DVCM-k3 , (b) DVCM-VWS-k3.

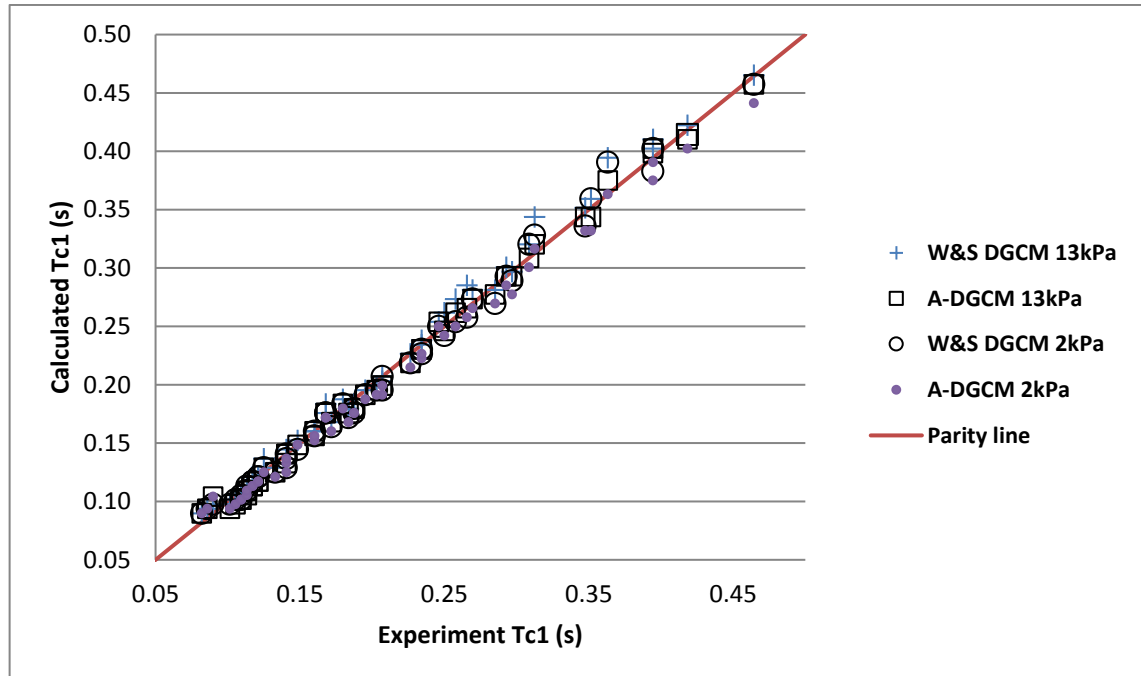
### 6.3 Quantitative assessment

To overcome the issues indicated above with qualitative assessment and with having a range of modelling aspects to consider (not just basic model, but also boundary condition, friction, mode of column separation and now also the data value for vapour pressure), as well as being able to incorporate all of the experimental runs (not just a selection as in Section 6.2 or Appendix B), a new approach was attempted. This focused on the two specific criteria defined in Section(6.1), either comparing computed model with experimental value, Figure(6.26) and Figure(6.27) or the relative error % of Equation(6.2), Figure(6.28) to Figure(6.35). Each of these figures compares two model aspects while holding the others fixed. For example, Figure(6.26) compares the effects of boundary condition and  $P_v$  value for DVCM with quasi-steady friction, and Figure(6.27) makes the same comparison but for DGCM rather than DVCM.

Comparing Figure(6.26) (DVCM) with Figure(6.27) (DGCM), while both methods give similar patterns of performance at low cavity durations (i.e. limited column separation), at larger cavity durations (tending to classic column separation), DVCM tends to (but not always) overestimate this criterion whereas DGCM tends to (but not always) underestimate it. However, even when these plots are presented at much larger sizes than herein, it is very difficult to identify any behaviour trends associated with the choices for BC or  $P_v$ .



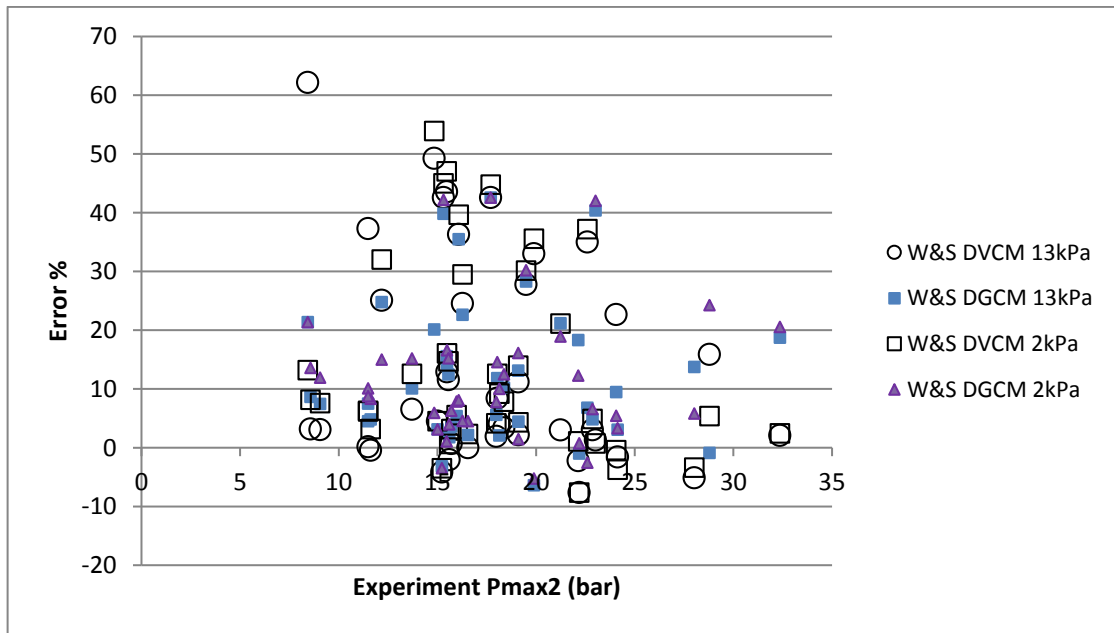
Figure(6.26) The 1st cavity duration calculated by DVCM with change of two factors (BC &  $P_v$ ) versus measurements (quasi-steady friction).



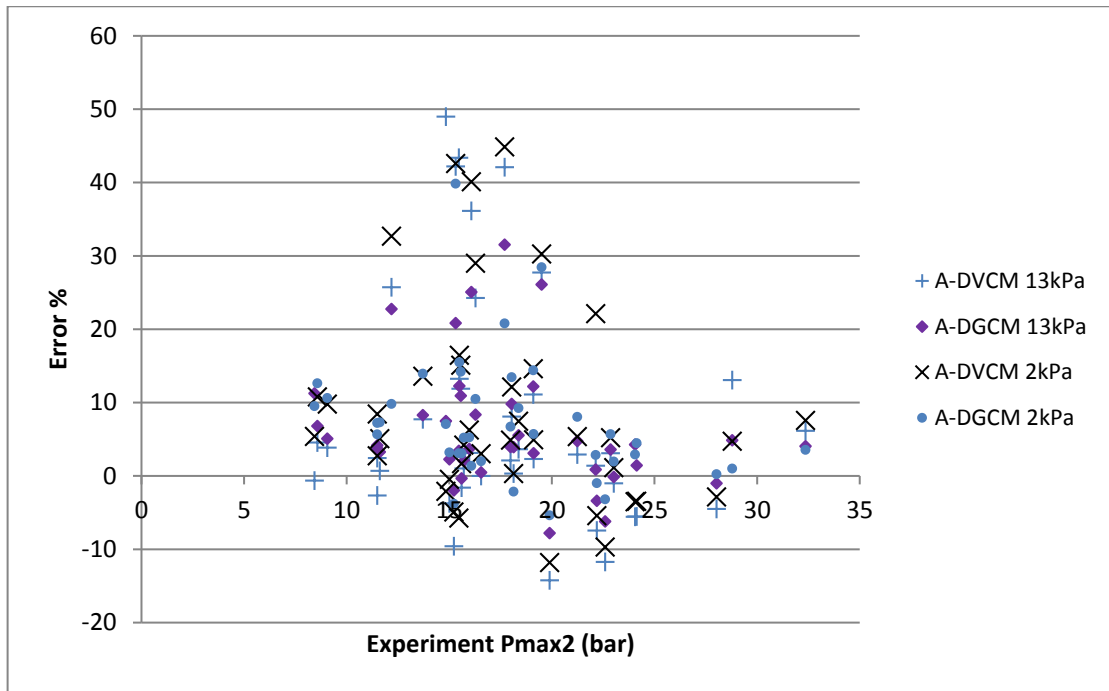
Figure(6.27) The 1st cavity duration calculated by DGCM with change of two factors (BC &  $P_v$ ) versus measurements (quasi-steady friction).



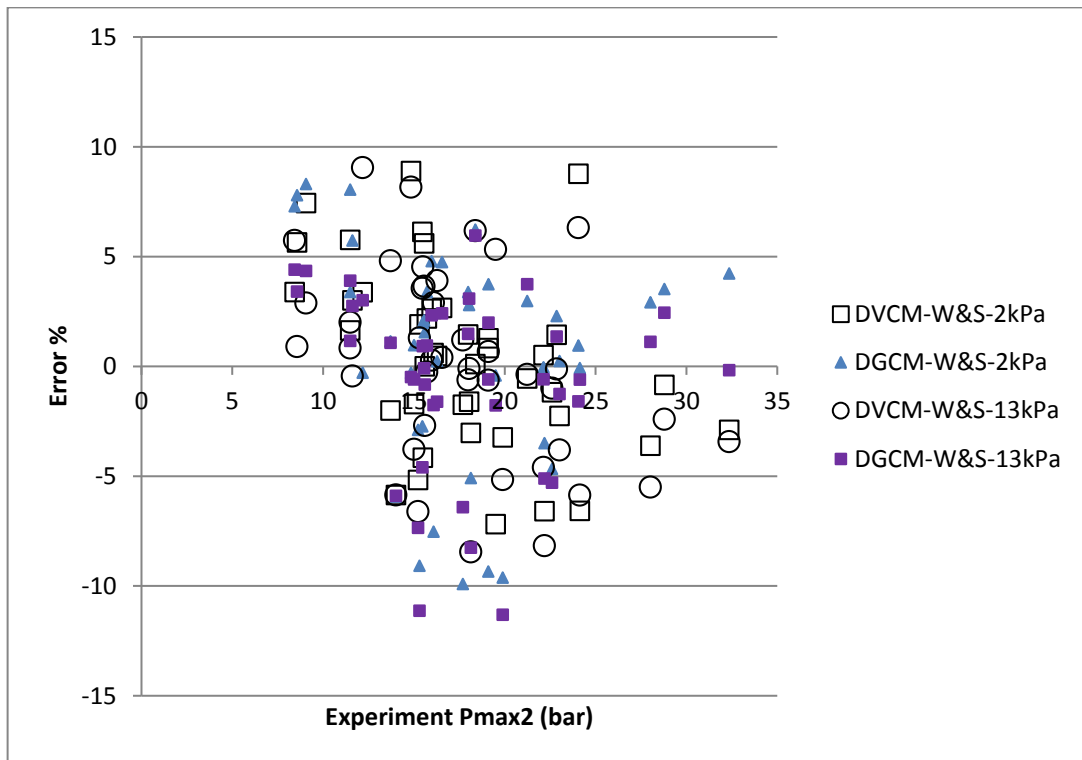
Figures(6.28) to (6.35) plot relative errors (against response magnitude, either amplitude or duration). Figure(6.28) to Figure(6.31) compared with Figure(6.32) to Figure(6.35) show that both the magnitude of and scatter in the errors for amplitude  $P_{max2}$  are greater than for cavity duration  $T_{c1}$ , with the scatter explained by the probable greater uncertainty in  $P_{max2}$  error (especially for limited cavitation). Note that for cavity duration  $T_{c1}$  the magnitude of the error (irrespective of its sign) is the criterion, whereas for peak amplitude  $P_{max2}$  the sign of the error has to be important for engineering design purposes. Figure(6.30) and Figure(6.31) compared with Figure(6.28) and Figure(6.35) show that both the magnitude and the scatter in the errors for amplitude  $P_{max2}$  are less when unsteady friction is used instead of quasi-steady friction. However, this reduction in error magnitude is accompanied by an increase in negative (and thus un-conservative) errors.



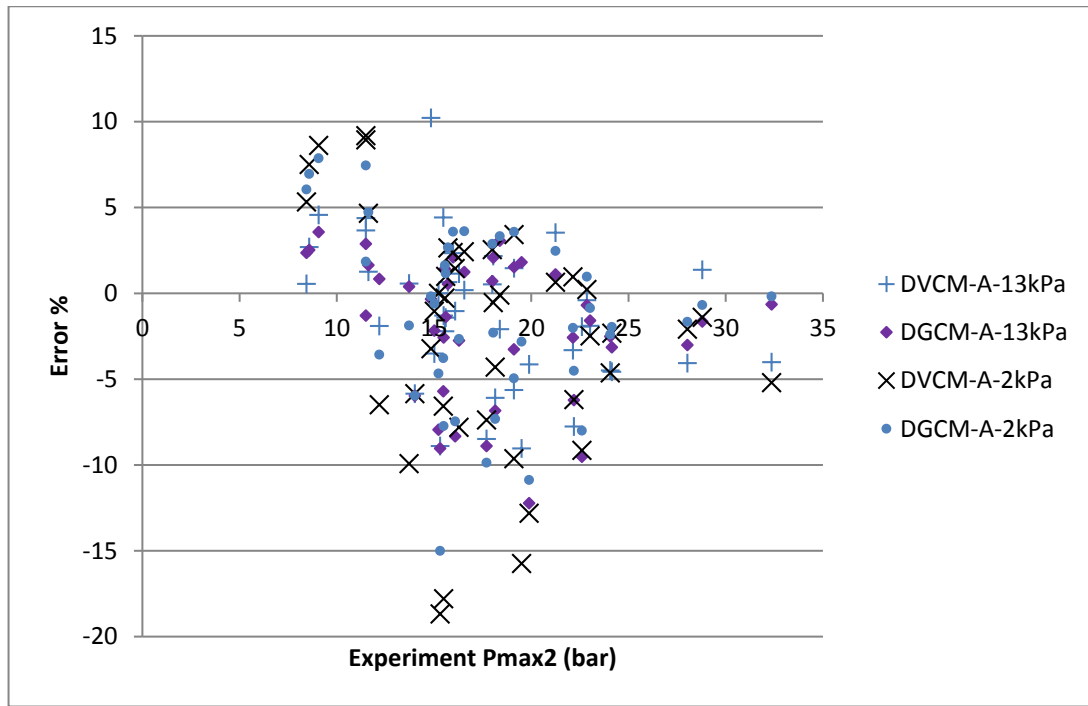
**Figure(6.28) Error (%) in Post-cavity pressure amplitude with conventional (W&S) boundary condition calculated by both DVCM & DGCM, with change of  $P_v$ , versus measurements (quasi-steady friction).**



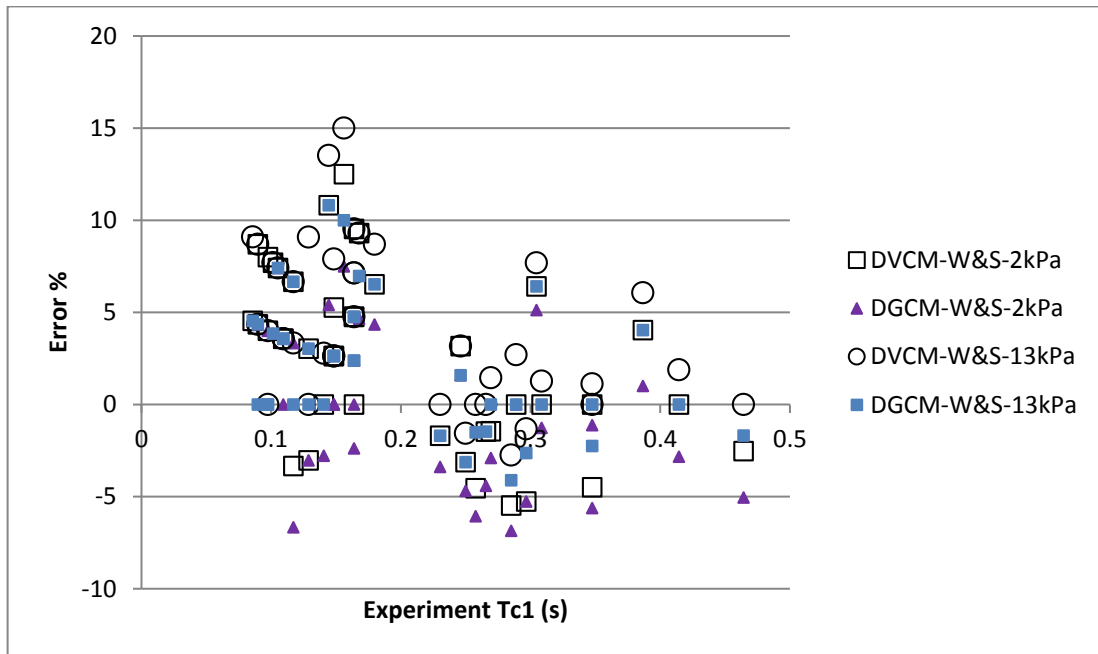
Figure(6.29) Error (%) in Post-cavity pressure amplitude with Arfaie (1989) boundary condition calculated by both DVCM & DGCM, with change of  $P_v$ , versus experiments (quasi-steady friction).



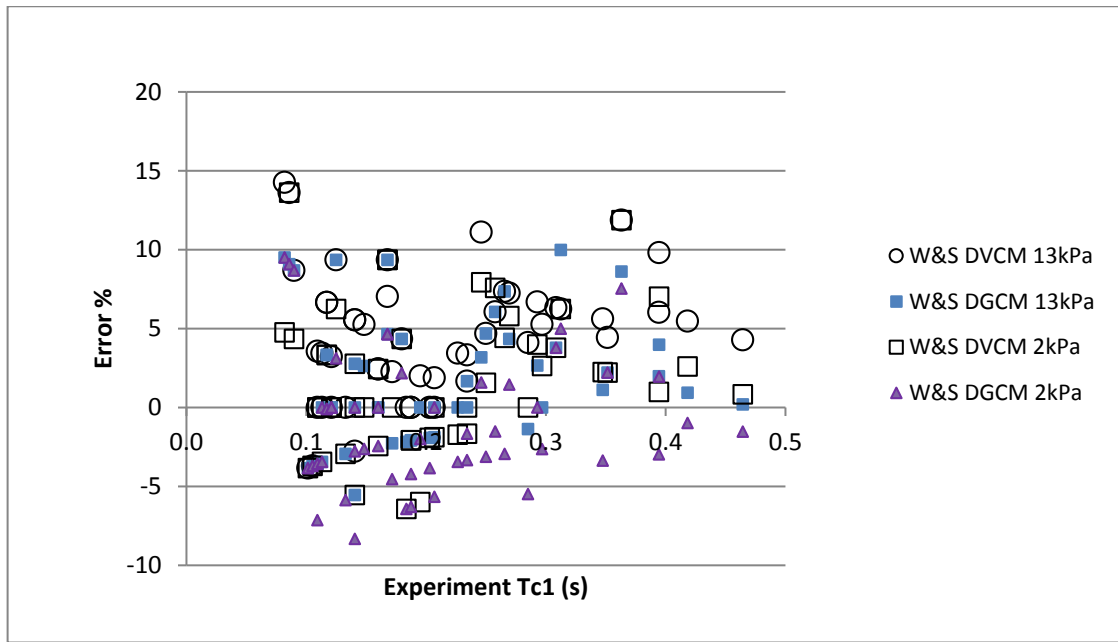
Figure(6.30) Error (%) in post-cavity pressure amplitude with conventional (W&S) boundary condition calculated by both DVCM & DGCM with unsteady friction ( $k_3 = 0.065$ ) with change of  $P_v$ , versus experiments.



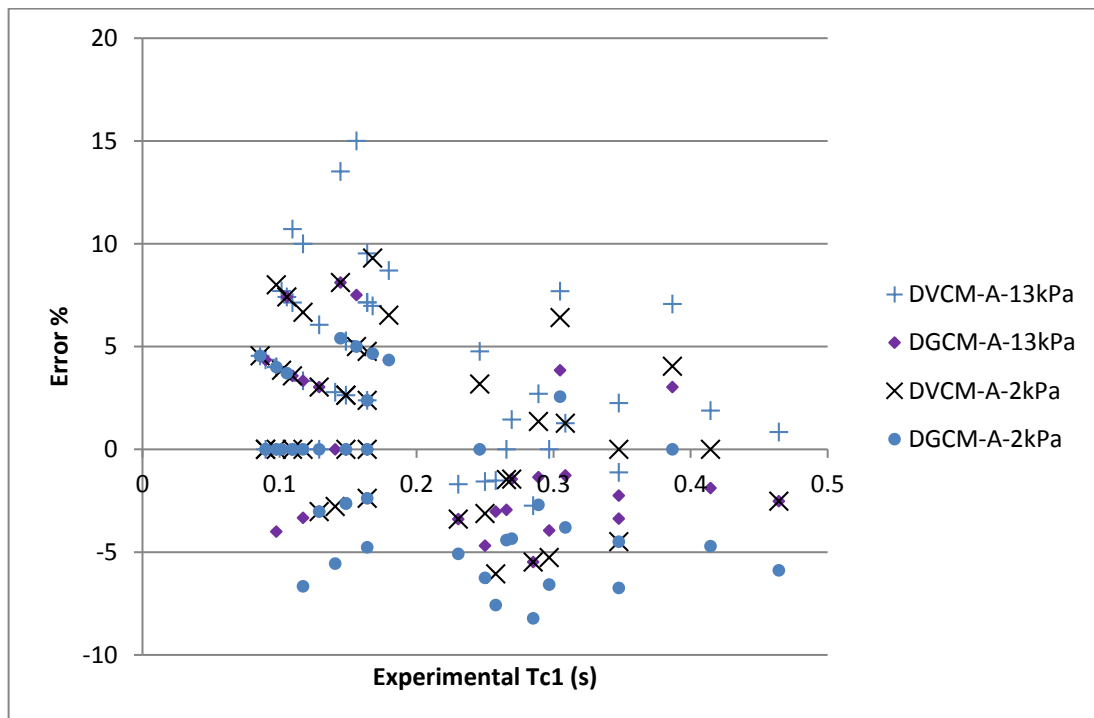
Figure(6.31) Error (%) in post-cavity pressure amplitude with Arfaie (1989) boundary condition calculated by both DVCM & DGCM with effect of transient friction ( $k_3 = 0.065$ ) with change of  $P_v$ , versus experiments.



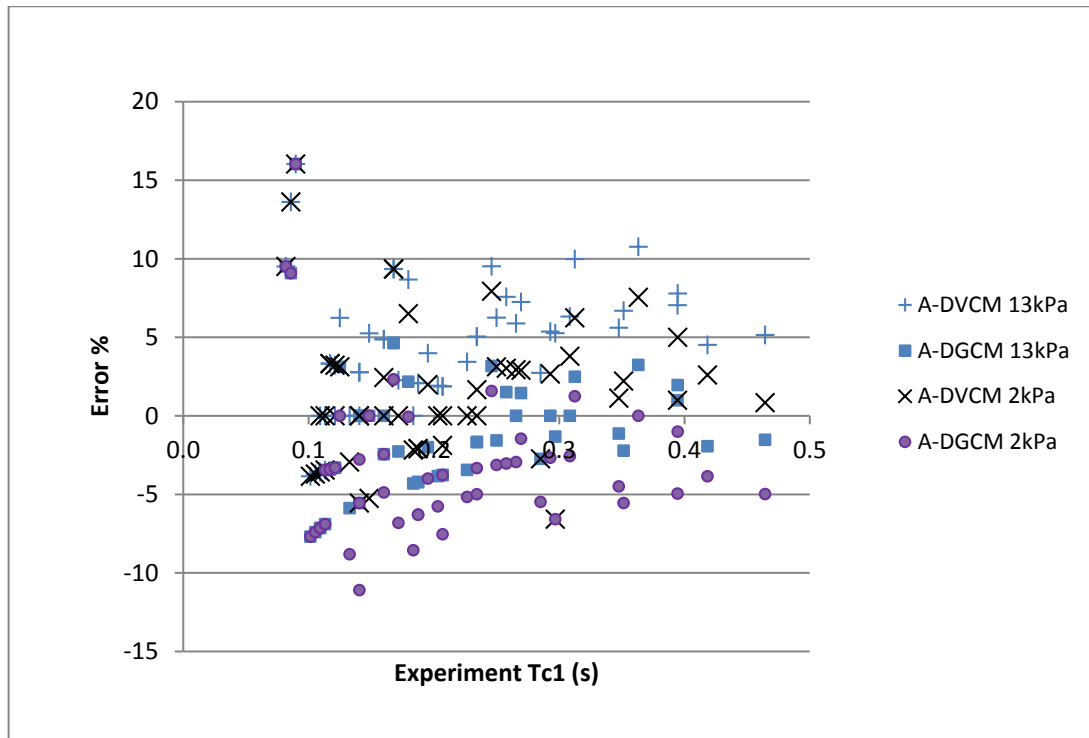
Figure(6.32) Error (%) in cavity duration with conventional (W&S) boundary condition calculated by both DVCM & DGCM with transient friction  $k_3 = 0.065$  with change of  $P_v$ , versus experiments.



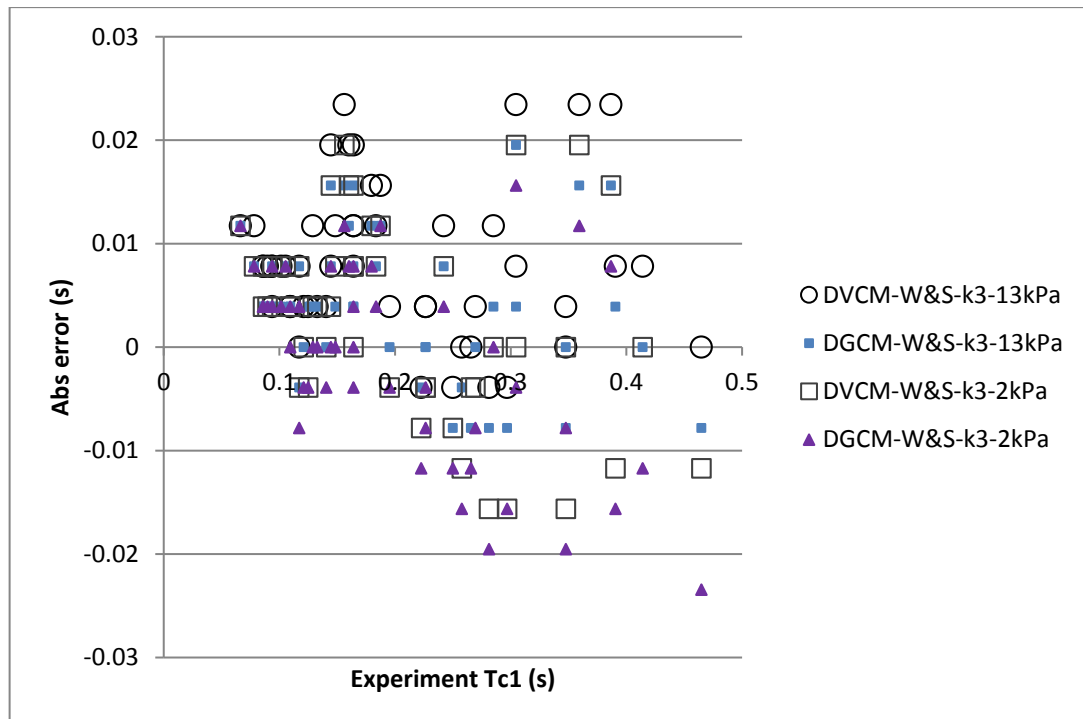
**Figure(6.33) Error (%) in cavity duration with conventional (W&S) boundary condition calculated by both DVCM & DGCM with quasi-steady friction with change of  $P_v$ , versus experiments.**



**Figure(6.34) Error (%) in cavity duration with Arfaie (1989) boundary condition calculated by both DVCM & DGCM with transient friction  $k_3 = 0.065$  with change of  $P_v$ , versus experiments.**



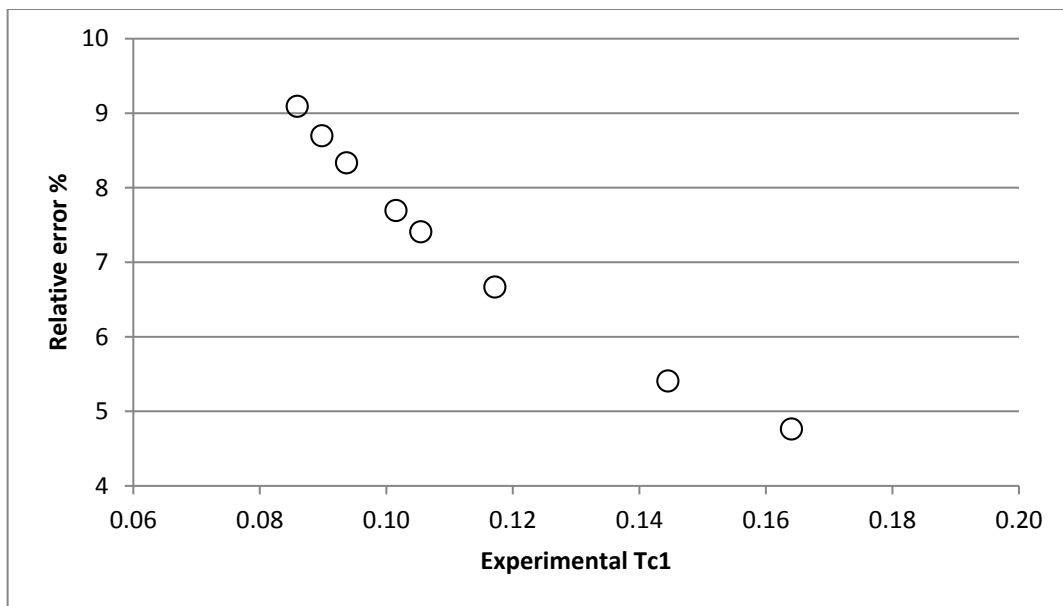
Figure(6.35) Error (%) in cavity duration with Arfaie (1989) boundary condition calculated by both DVCM & DGCM, with quasi-steady friction with change of  $P_v$ , versus experiments.



Figure(6.36) Absolute error in cavity duration with conventional (W&S) boundary condition calculated by both DVCM & DGCM with transient friction  $k_3 = 0.065$  with change of  $P_v$ , versus experiments.

Figure(6.36) shows exactly the same results as on Figure(6.32), but plotting absolute Eq.(6.1) instead of relative Eq.(6.2) error. For all the cavity duration  $T_{c1}$  relative error

plots, Figure(6.32) to Figure(6.35), the data fall into a distinctive pattern which is different to the pattern on an absolute error plot such as Figure(6.36). From Figure(6.32), the experimental runs have been identified for one of the apparent curves (Figure(6.37)) and the error calculations for these are in Table(6.2). This shows that the pattern of the trend lines is an artefact related to multiples of the time step  $\Delta t = 0.0039\text{s}$  (at **256 Hz**) at which both experimental and calculated values are recorded. As all recorded times (whether experimental or computational) are integer multiples of the time step  $\Delta t$ , then the cavity duration will be an integer multiple of the time step and thus the absolute error (difference in experimental and computational cavity durations) will be some integer multiple of the time step, as is seen on Figure(6.36). Relative error, therefore, will be inversely proportional to cavity duration magnitude, thus producing the hyperbolic curves of results shown (one for each integer multiplier occurring over the set of results).



Figure(6.37) Error (%) in cavity duration of a sample of DVCM-W&S (Table(6.2)) from Figure(6.32)

Table(6.2) Sample for highlighted values (Figure(6.37)) of DVCM-W&amp;S in Figure(6.32)

Run	Experimental Tc1 (s)	DVCM-W&S-k3-13kPa		
		Absolute error (s) Figure(6.36)	Relative error % Figure(6.32)	n*Δt
9	0.0859	0.0078	9.09	2
11	0.0898	0.0078	8.70	2
13	0.0938	0.0078	8.33	2
15	0.1016	0.0078	7.69	2
16	0.1055	0.0078	7.41	2
22	0.1172	0.0078	6.67	2
26	0.1445	0.0078	5.41	2
32	0.1641	0.0078	4.76	2

This more systematic approach is better at distinguishing the effects of a number of model changes than the qualitative approach of Section(6.2). Various general observations become possible, e.g.:

- Figures(6.26 and 6.27) give no evidence of changes in model performance over the full range of column separation modes of behaviour that they include. However, these Figures also do not show up any obvious patterns of differences between the model choices additional to the basic method (DVCM or DGCM), W&S vs A(rfaie), or Pv value (2kPa vs 13kPa).
- Relative error magnitudes appear to decrease as pressure peak and cavity duration amplitudes increase, because the actual errors (and their uncertainties) remain more or less constant, so the larger responses give smaller relative error (%) values.
- There is some evidence that the Arfaie column separation boundary condition is possibly better than the conventional W&S, though the latter may be more conservative. This can be seen by comparing Figure(6.28) v Figure(6.29) and Figure(6.30) v Figure(6.33).
- Expected results emerge when comparing unsteady with quasi-steady friction, e.g. Figure(6.28) and Figure(6.29) against Figure(6.30) and Figure(6.31):
  - Quasi-steady is mostly conservative (i.e. model over-predicts peak pressure).
  - Unsteady gives fairly even distribution between positive and negative error (as expected from increased damping) and reduces error magnitude. However, for peak amplitude the former reduces the benefit of the latter.

Though more systematic than Section(6.1), this approach also clearly has its limitations, again being effectively a “one factor at a time” approach, which also cannot easily distinguish any interactions between factors. This leads to consideration of an alternative statistical approach to comparison utilising the methods adopted by Ahmeid (1997), which does not appear to have previously been applied to pressure transients.



## 6.4 Statistical design of experiments approach

Statistics (Design of Experiments with ANOVA) has been used before at Newcastle University to explore different modelling aspects in CFD (Computational Fluid Dynamics) (Ahmeid 1997). However, this previous work did not involve direct comparison with experiment (involving an uncertainty in the quantified response) as in this present study. The statistical literature and methods are fully discussed in Ahmeid (1997). Minitab-17 (Ryan et al, 2005) has been used to generate the series of ANOVA results listed in Appendix F.

The Design Of Experiment (DOE) is set to assess the two responses, i.e. absolute error in calculated  $T_{c1}$  &  $P_{max2}$ , Eq.(6.1), for a range of model factors each with two levels as listed in Table(6.3). These factors are the basic numerical method, to repeat the work of Bergant and Simpson (1999) by including the DGCM method as suggested (but not implemented) by Arfaie (1989), with the internal boundary condition at the column separation interface, mode of behaviour and unsteady friction as suggested by Arfaie (1989) that could influence the modelling. In addition, a fifth factor (the value of vapour pressure used in the calculated model data) is incorporated following the qualitative review in Section(6.2.1). With reference to the Aims and the Objectives (Section 1.2), for the comparisons of computational with experimental results some factors have not been taken into account computationally that might have an effect on smoothing pressure waves; experimental valve closure occurs over finite time ( $11 - 16ms$ ) which was assumed to be instant (zero closure time) in the analysis, the effect of local mechanical vibration at valve as a result of closure impact and Fluid-Structure Interaction.

Table(6.4) provides a summary of the ANOVA analyses undertaken for both responses ( $T_{c1}$  and  $P_{max2}$ ). To investigate the effect of the mode of behaviour, only the experiments leading clearly to limited cavitation with  $P_{max} > \text{Joukowsky}$  or “classic” column separation could be selected to give two distinct levels for this factor. With this reduction in the data, testing for all five factors (Appendix F.2) does not give significant outcomes for all of the five factors, Table(6.4), whereas testing for only four (Appendix F.4) or only three (Appendix F.1 and F.3) does give more significant outcomes for the main factors tested. Where friction is not included as a factor itself, two separate ANOVA analyses were undertaken, using quasi-steady and

unsteady friction, respectively (Appendix F.4 and Appendix F.3 for comparison with F.1(a))

**Table(6.3) DOE for ANOVA analyses with quantified responses Tc1 and Pmax2**

Factors	Levels (two)	Comment	Objectives
(1) Method	DVCM	Bergant & Simpson (1999) comparison	Done by Arfaie
	DGCM		Suggested by Arfaie(1989)
(2) Boundary condition	Wylie & Streeter	Wylie & Streeter (1993)	Aim
	Arfaie	Arfaie (1989) Thesis	
(3) Vapour pressure	Theoretical 2kPa	Steam Tables	Outcome from qualitative comparison (Section 6.2)
	Observed 13kPa	Observed from pressure traces	
(4) Friction	Quasi-steady friction	Arfaie (1989) suggestion	Aim
	Unsteady friction		
(5) Mode	Limited (with spike)	Arfaie (1989) suggestion	
	Classic		

**Table(6.4) Summary of ANOVA analyses undertaken (Appendix F).**

Friction Model	Conventional quasi-steady				Unsteady			
Data set (Appendix)	Full				Selected		Full	Selected
	F.1(a)	F.1(b)			F.4(a)	F.2	F.3	F.4(b)
Factors:	3	1 at a time			4	5	3	4
Method	√	√	×	×	√	√	√	√
BC	√	×	√	×	√	√	√	√
Pv	√	×	×	√	√	√	√	√
Mode	×	×	×	×	√	√	×	√
Friction	×	×	×	×	×	√	×	×

Table(6.5) summarises the ANOVA outcomes in term of significance (taken for  $p \leq 0.005$ , i.e. 99.5% probability) and importance ranking (1<sup>st</sup>, 2<sup>nd</sup>, etc) for significant results as indicated by the relative F-values. Where main factors are NS (not significant) in one ANOVA (Appendix F.2) for the Tc1 response, main factors close to significance have second-order interactions that are significant and these are noted (I). At this stage interactions between factors are not further considered (it is typical for significant main factors to also have significant interactions). Simple dot-line plots (Appendix F) identify which of the two levels for each factor gives the better overall result in terms of the magnitude of the mean error across all the tests.

**Table(6.5) Summary of significant factors from ANOVA (1,2, etc. = ranking for significant factors, NS = Not Significant, I = Significant Interactions if main factor NS, – = Not tested**

Response	Factor	Data set (Appendix F)					
		F.1(a)	F.1(b)	F.4(a)	F.2	F.3	F.4(b)
Tc1	Method	1	1	1	1	1	1
	Pv	2	2	3	2	2	2
	BC	3	3	4	3	NS	NS
	Mode	–	–	2	I	–	3
	Friction	–	–	–	I	–	–
Pmax2	Method	NS	NS	NS	NS	NS	NS
	Pv	NS	NS	NS	NS	NS	NS
	BC	1	1	NS	2	1	2
	Mode	–	–	NS	NS	–	1
	Friction	–	–	–	1	–	–

The normal probability plots in Appendix F for the Tc1 responses always lie very close to the Normal Probability Lines, whereas the Pmax2 responses are always less satisfactory in this respect. This probably reflects the higher uncertainty and greater variability in the error (Eq.(6.1)) for the pressure peak, especially where a “spike” occurs (with discrete data recording). This in turn suggests why Table(6.5) shows a good level of significant outcomes for the Tc1 response, but with far fewer for the Pmax2 response.

From these ANOVA analyses (Table(6.5) and Appendix F) the results for each of the five factors can be evaluated:

**(a) Method:**

For the duration of first cavity ( $T_{c1}$ ), all of the ANOVA analyses (Table 6.4) show that the Method is significant and the most important factor, with DGCM giving the lower error magnitude. In some analyses that error is negative, i.e. the calculation slightly under-predicts the cavity duration.

For the second peak amplitude ( $P_{max2}$ ), none of the ANOVA analyses (Table 6.4) gives a significant difference between the two methods, DVCM and DGCM. Though the outcomes are not significant, with unsteady friction there is a possibility that DVCM may give lower errors (Appendix F.4(b)).

**(b) Value used for vapour pressure ( $P_v$ ):**

For  $T_{c1}$ , all of the ANOVA analyses (Table 6.4) show that  $P_v$  is significant and all but one give it as the second most important factor (with the other giving third). Perhaps surprisingly (but usefully for analysts) the Steam Tables value of 2kPa gives the best outcome despite the actual experimental value being 13kPa. In terms of determining the response (cavity duration), with such a small difference in level values compared with the pressure wave amplitudes, any differences in duration are likely to be within the uncertainty for this discretely recorded response.

For  $P_{max2}$ , none of the ANOVA analyses (Table 6.4) gives a significant difference between the two  $P_v$  values (2kPa or 13kPa). Though the outcomes are not significant, again with unsteady friction there is a possibility that the experiment actual value of 13kPa may give lower errors (Appendices F.3 and F.4(b)).

**(c) Boundary conditions (BC):**

For  $P_{max2}$ , three ANOVA analyses give this as the most important factor, with two giving second most important and only one not significant. In all but one analysis, the Arfaie (1989) improvement is confirmed. The one exception (Appendix F.3) has unsteady friction over-damping the response to make it more negative (and thus not conservative), so that the conventional Wylie & Streeter boundary condition works better.

For  $T_{c1}$ , three ANOVA analyses give this as only third most important factor (behind Method and  $P_v$ ) with another making it fourth (behind Mode also) and two (with unsteady friction) not significant at all. In three of these significant outcomes,

the Arfaie's improvement is better, with conventional Wylie & Streeter better only in one ANOVA calculated for unsteady friction (Appendix F.3),

**(d) Mode of column separation behaviour:**

This was tested in only three ANOVA analyses (Appendix F.2 and F.4), all with selected (i.e. reduced) data and giving contradictory outcomes. For Pmax2 two give not significant, but the third (Appendix F.4(b)) gives it as significant and the most important factor (more important than significant BC and not significant Method and Pv). For Tc1 two give it as significant (second and third in importance, respectively) with the other giving it as not significant but with significant interactions (and less important than Method, Pv or BC). Similarly the identification of the best level is equally confused. The Appendix F.4 analyses are identical, except (a) was with quasi-steady friction and the other (b) with unsteady friction. The former gives smaller error in Tc1 with limited cavitation (not significant for Pmax2) but the latter gives smaller error for classic column separation (both responses). The Appendix F.2 analysis includes friction as well as mode as factors and, though the outcomes are not significant, suggests that limited cavitation might give smaller error in Tc1 but classic cavitation might give smaller error in Pmax2.

**(e) Friction:**

Friction was included as a factor in only one ANOVA analysis (which had the selected data set as Mode was also included as a factor), Appendix F.2. For Pmax2 it was the most important of only two significant factors (ahead of BC), with unsteady friction giving smaller average error magnitudes than conventional quasi-steady friction. However, the increased damping gives a tendency towards negative (and thus non-conservative) error. For Tc1 there is no significant difference between unsteady and quasi-steady friction, though an interaction involving this factor is significant, Table(6.6).

In addition, though, two sets of ANOVA analyses were repeated for quasi-steady and then unsteady friction: Appendix F.1(a) with F.3 (full data), then Appendix F.4(a) with (b) (selected data). These pairs can be compared for the differences between them. With the full dataset (and only 3 factors) unsteady friction gives generally similar outcomes to quasi-steady (Table 6.4 comparing F1(a) with F3).

Unsteady friction reduces error for DVCM but has little effect on DGCM,  $P_v$  is better at 2kPa in both and BC at Arfaie (but this is not significant with unsteady friction). For  $P_{max2}$  only BC is significant in both, but while Arfaie improvement is better for quasi-steady friction, the increased damping of unsteady friction actually increased the magnitude of the largely negative (and thus non-conservative) error, so conventional Wylie & Streeter becomes best.

As would be expected with the selected (reduced) data set (and 4 factors) the comparison of  $F4(a)$  with (b) is less clear in terms of significance and ranking, Table(6.5). Unsteady friction seems to moderate the effect of uncertainties on error and shows two significant factors for  $P_{max2}$  compared to none with quasi-steady friction. As above the increased damping of unsteady friction increases negative (and thus non-conservative) error magnitudes.

The comments above relate to only the factor main effects, but the benefit of DOE over the “one factor at a time” approach is that possible significant interactions between the factors can be identified, Table(6.5). With these sets of data there are no significant interactions:

- for the second peak  $P_{max2}$ , and
- no 3<sup>rd</sup> order for the cavity duration  $T_{c1}$ , though there are a limited number of significant 2<sup>nd</sup> order interactions for cavity duration  $T_{c1}$ , Table(6.6).

Bearing in mind that there is only one ANOVA in which friction (quasi-steady or unsteady) is actually a factor, there is a significant interaction in this for Friction with Mode and the interaction dot-line plot suggests that using unsteady friction has an opposite effect for the limited and classic modes of behaviour:

- Two of the three ANOVA which include Mode with  $P_v$ , suggest that classic is more influenced than limited and DVCM more than DGCM by mode of behaviour.
- Three ANOVA give a significant interaction for Method with BC, all agreeing that DGCM is more influenced by BC than DVCM.

These tend to reinforce Arfaie (1989) in that his contentions about the importance of mode of behaviour on best method and use of unsteady friction are supported, as is his suggestion that his study should be extended to include DGCM as well as DVCM. However, they do not in themselves lead to any definite conclusions at this stage.

**Table(6.6) Summary of significant 2nd order interactions from ANOVA (Appendix F) for Tc1 (cavity duration).**

	Method	Pv	Friction
BC	F.1(a), F.2		
Mode	F.2, F.4(a)	F.2, F.4(a)	F.2

## **Chapter 7**

### **Conclusions and Suggestions for Further Study**



## 7.1 Limitation of experimental results and apparatus

The experimental apparatus described in Chapter 4 had apparently been used successfully in previous research (e.g. Arfaie 1989, Bughazem 1997) and was improved in number of minor respects, including moving the pressure transducer to improve column separation visualization, strengthening the support of the quick closure valve and improving the upstream reservoir to give observable stability during transient runs. Nevertheless, in retrospect (highlighted particularly by the normal probability plots for pressure peak from the statistical analysis in Appendix F), the experimental results had limitations resulting from deficiencies in the apparatus which restricted the ability to draw meaningful results from the comparison between experimental and computed results in Chapter 6.

The key limitation of the rig was the difficulty in producing consistently repeatable test runs:

- (a) The pressurised upstream reservoir made it easy, in principle, to set up a range of driving pressures in conjunction with the downstream initial flow control valve. However, in practice the combination of downstream valve, reservoir inlet flow and reservoir free surface pressure settings made it extremely difficult to exactly replicate initial steady states for a series of test runs.
- (b) The relatively short pipe length needed a fast downstream valve closure that was genuinely “rapid” with respect to the waterhammer wave reflection period ( $2L/a$ ). Initial trials with actuated valves either failed to produce the advertised closure rate or led to issues with completeness of valve closure (leakage) at the closure required rate. The manually actuated closure valve used did not suffer from either of these limitations, but in retrospect was also an issue for repeatability (with actual measured closure times in the range 11 – 16ms) and the vigorous manual closure process required possibly caused support structure movement.

Another significant limitation for the rig relates to the use of a coiled pipe to save space. Though this coiling had been shown to affect the waterhammer wavespeed, since an actual measured value was used that was not an issue for this study. However, on a number of experimental traces (and with experience during the actual testing) there is evidence of probable fluid structure interaction, notwithstanding

efforts to increase the restraint of the pipe coils and support of the downstream closure valve. This raises the question of additional wave systems within the experimental results which were not taken into account in the various models tested, notwithstanding the fact that in some comparisons the computed result can appear “noisier” than the experimental traces. This would also impact on the issue of repeatability, above.

Finally, some other less significant deficiencies of the rig were also noted:

- (i) For visualisation of the transient cavitation region at the downstream closure valve, there will always be issues associated with the length of the cavitation region compared with pipe diameter (filming “aspect ratio”) and with being able to detect the actual length (growth and decay) of that region (for a phenomenon leading to scattered small bubbles as observed). However, a real practical issue is being able to visualise conditions right up to the valve closure disc (where cavitation is, in principle, initiated) because of the valve body itself and the support for this.
- (ii) Even with the small pipe bore of this apparatus, it was difficult to get the flow velocities for a full range of hydraulic transient behaviours from just waterhammer to severe column separation at Reynolds numbers well into the fully turbulent flow regime. Even though the measured steady flow Darcy friction factors did not indicate smooth turbulent flow, nevertheless the evidence is that even quasi-steady friction factor varied with Reynolds number, so that the flows were not fully turbulent.
- (iii) The coiled pipe arrangement provided a reasonably uniform pipe slope as well as avoiding reflections from pipe bends, but in this apparatus possibly there was insufficient upslope to ensure transient cavitation occurred only at the closed valve (as hoped). Additional pressure transducers along the pipe, as in Martin (1983), could compensate for this by providing information to help in identifying other transient cavitation locations.

As a consequence of all of the above, subsequent to this study a decision was taken to retire and scrap this apparatus because of its limitations for progressing this research.

## 7.2 Column separation-induced pressure spikes exceeding Joukowsky pressure

One aim of this study was to attempt to identify simple criteria for designers and fluid transient analysts to indicate whether the issue of column separation pressure spikes exceeding Joukowsky pressure (usually regarded as an upper limit) might need investigation. Another related aim, responding to the view of Arfaie (1989) that best prediction method choice might be influenced by the mode of column separation behaviour, was to investigate if there were any obvious differences of physical mechanism between the limited column separation causing these Martin (1983) pressure spikes, compared with classic severe column separation where they are not apparent. In retrospect, both these aims were compromised by the limitations of the apparatus.

The range of experiments conducted suggested that there are three principle modes of fluid transient behaviours for this simple single pipe system with downstream flow closure initiation of the transient:

- 1) Single-phase waterhammer.
- 2) Limited column separation (transient cavitation) where the pressure peaks following the first cavitation event (duration  $\geq 2L/a$ ), feature a pressure spike which may exceed Joukowsky pressure (Martin 1983).
- 3) Classic severe column separation, where the pressure peaks following the first cavitation event do not appear to feature this pressure spike and are lower than Joukowsky pressure, decreasing in amplitude with time.

In addition, there are two transient behaviours between these:

- (1-2) a first transient from single-phase waterhammer (1) to limited column separation (2), with extremely limited cavity durations ( $\approx 2L/a$ ) leading to a series of pressure peaks essentially corresponding to waterhammer but with pressure spikes (possibly greater than Joukowsky) from the second peak on.
- (2-3) A second transition from limited (2) to classic severe (3) column separation, featuring a gradual broadening (in time) of the pressure spike accompanied by reduction in its magnitude (to below Joukowsky) until it merges into the classic severe column separation response.

Two simple criteria have been identified with the possibility to indicate potential limited cavitation behaviour leading to pressure spikes exceeding Joukowsky pressure Table(5.3):

(a) The Martin ratio  $P_M$ , Eq.(5.1) and Figure(5.1), in the range:

$$\sim 1.2 \leq P_M \leq \sim 1.9 \quad (7.1)$$

(b) The cavity duration ratio  $T_{cr}$ , Eq.(5.2) and Figure(5.3), in the range:

$$\sim 1.2 \leq T_{cr} \leq \sim 1.9 - 2 \quad (7.2)$$

However, for prediction purposes (b) is not practical as the cavity duration is not known without modelling, though an estimate (which under-predicts it by up to 20%) is given by Eq.(D.7). Nevertheless (a) does provide a simple index without the need for modelling of the transient, though further work on an apparatus with better repeatability and lower experimental uncertainty remains necessary to clarify both criteria.

Using a combination of visualisation of the transient cavitation region adjacent to the closure valve (time linked to the recorded pressure) and the wave reflection tracing method of Arfaie (1989) suggests there is no physical mechanism difference between the two column separation behaviour modes (2) and (3) above (Section 4.5). The transition behaviour (2 – 3) described above suggests that behaviour (2) progressively matches into behaviour (3), with the greater dispersion due to more reflections over longer durations smearing out the characteristic pressure step-up / spike / step-down of behaviour (2), e.g. Figure(5.15), with the transition to behaviour (3), e.g. Figure(5.16). Apart from the increase in distributed bubble/cavity size (and occasional coalescence) afforded by the longer time duration available for behaviour (3), there was nothing else from the visualisations to indicate a difference in physical mechanism.

### 7.3 Criteria for assessment of computational models

In order to evaluate different computational models against measured results (from either field tests, e.g. at plant commissioning, or from laboratory experiments, as in

this study), criteria are needed to enable the comparisons to be assessed. In this study two approaches to choosing these criteria have been illustrated, each with strengths but also limitations.

In Section(6.2) a qualitative approach to comparison was adopted, with the criteria used explicitly defined in Section(6.2.2) (e.g. Table(6.1)). Following Arfaie (1989), two of these (general shape of response and ability to maintain time phase of oscillation) can be, and possibly most easily are, applied to extended periods of transient behaviour. The third of these (amplitude of first post-cavity peak) is for a single specific occurrence, which should characterise the phenomenon except that on occasion, e.g. Figure(5.10) and Figure(5.11), the maximum pressure may not occur at that point.

This single specific item leads itself to a quantitative criterion, as defined in Eq.(6.1) and Eq.(6.2) and applied to the first post-cavity peak amplitude (as above) and the duration of the first cavity (Sections 6.3 and 6.4). The former occurs at a single specific time, whereas the latter is a single specific occurrence with a finite duration. There is an obvious relationship between the latter and the above qualitative assessment of ability to maintain time phase of oscillation, though they are not the same thing. Quantitative criteria could, in principle, be applied at more than one specific occurrence, e.g. a series of pressure peaks (perhaps used to look at damping rate), but this raises the issue of how they would be compared quantitatively to give an overall assessment (as above), e.g., multi-objective optimisation.

The qualitative criteria used can work well for an assessment of the overall model success, but where multiple criteria are applied, e.g. Table(6.1), it is apparent that the criteria are as likely to disagree as to agree for a particular comparison, which then raises issues of prioritisation between or combination of them. A particular case in point is the second row of Table(6.1) for DGCM, where both the overall criteria (general shape and phase) favour one model, but the maximum pressure amplitude (probably the item of greatest importance to the designer) disagree and favour the other model.

A significant issue for this study emerged from the attempt to adopt a statistical approach where a number of different aspects of modelling were investigated (basic

method, friction, internal cavitation interface boundary, data used for vapour pressure). This was adopted because of the difficulty in using the qualitative approach in these circumstances (Section 6.4), but it demands quantitative criteria. However, the associated normal probability plots (Appendix F) flagged up the unreliability of the quantified post-cavity amplitudes (as mentioned previously in Section 7.1). Thus, though Arfaie (1989) suggested that mode of column separation behaviour could influence the choice of model, with more runs available in Table(6.1) Rows 2, 3 and 4 (which are all for limited cavity with spike > Joukowsky) show varying assessments for the same mode, probably highlighting the deficiencies of the experimental rig.

It is believed that the statistical comparison of Section(6.4) is innovative in the field of pressure transients. It has two significant benefits, but at the cost of being restricted to single quantified responses:

- it can identify whether observed differences are significant or not (ANOVA); and
- with a properly designed experiment (Design of Experiment) it can handle a number of factors simultaneously more effectively (economically) than a series of “one factor at a time” comparisons, as well as identifying whether there are any significant interactions between factors (which would not be apparent at all from “one factor at a time” comparison).

It is believed that both of these benefits have been demonstrated, but unfortunately only for one of the quantified criteria (first cavity duration), because the post-cavity peak amplitude data of greatest interest were not of sufficiently good quality to give significant results. In these circumstances there was little point in extending the statistical investigations further for these particular data to clarify the conclusions of Section(6.4), but the methodology has future potential.

Its limitation is the requirement for quantifiable criteria. It may be possible to devise ways of quantifying the qualitative criteria previously used, e.g.:

- The ability to maintain phase of oscillation is readily defined by a quantified phase lag or gain after a specific feature on the experimental trace, e.g. the nth pressure peak.

- The quality of the overall response could be the sum (possibly weighted) of a series of qualitative numerical score estimates for a series of specific response features including amplitudes and durations (as for the quantified criteria of Section 6.1) but also spurious (or missing) pressure spikes, rate of damping of successive peaks, etc.

## 7.4 Other issues investigated

### 7.4.1 *Properties of water (including vapour pressure)*

The unusual properties of water noted in the discussion at the end of Section(4.5) are reflected in the potential difficulty observed in Section(6.2) of obtaining reliable data for water properties, especially its vapour pressure in an actual operational situation. For liquid water its properties important to fluid transients (density, viscosity, bulk modulus, vapour pressure) are influenced more by temperature than pressure (though temperature changes during waterhammer are orders of magnitude less than pressure changes). Data on these properties are readily available for water (ASME 2006), but for vapour pressure these have to be treated with caution.

The published properties are for pure  $H_2O$ , but the unusual properties of water include its high solubility and thus propensity to hold “non-condensable” gases, in particular air, in solution. At normal concentrations (up to saturation) these have negligible impact on most properties (e.g. density, viscosity, bulk modules), but they do on the value of vapour pressure, as observed and explained in Section(6.2). Consequently, the published values for water vapour (or saturation) pressure are the minimum, with the practical value likely to exceed these.

Fortunately, though, the comparisons in Section(6.4) suggest that though this definitely does have a significant effect on the modelled results, that effect seems relatively small, so unless there are unusually high quantities of dissolved gas, getting a precise value for the effective vapour pressure is not especially important.

### 7.4.2 *IAB unsteady friction models*

The study of unsteady friction was not an objective of this study. However, it was necessary to adopt an unsteady friction model of some kind to test the proposition

(Arfaie 1989) that additional damping could improve column separation modelling. The choice of an unsteady friction model for this purpose from those available was essentially arbitrary but informed by the knowledge that for this particular experimental rig the implementation by Bughazem (1997) had been proved to work.

Bughazem and Anderson (2000) had tested one version of this and an implementation was used. However Bughazem and Anderson (2000) had also suggested but not actually implemented a full MOC version (including a suggestion from Vitkovsky). This was fully implemented (but only as a single coefficient model) (Section 3.3), applied in some comparisons (Appendix B) and tested against the previous implementation (Section 6.2.2).

The essential practical limitation of both these models is that the single unsteady friction coefficient ( $k_3$  or  $k_t$ , respectively) has not been predicted but obtained by “tuning” its value for a good comparison with measured single-phase waterhammer traces from the apparatus. While, within the context of this study, such a process (applied also to waterhammer wavespeed  $a$  and Darcy friction factor  $f$ ) removes issues which may detract from or confuse the evaluation of column separation models, it is simply not a practical procedure for design or any measurements from outside a laboratory environment.

In terms of the two versions, the results of Section(6.2.2) suggest there is little to choose between them in terms of results as well as that the good fit they provide for purely single-phase waterhammer does not seem to be carried over to column separation (though that could be attributed to deficiencies in column separation models). The new full MOC implementation has been tedious to derive (Section 3.3) but no more difficult to implement in code. It modifies the characteristic lines on the fixed  $x - t$  grid (which possibly explains suggestions of better performance for phase), but this introduces a need for interpolations for non-grid points which may introduce not only additional numerical dispersion but also unwanted noise in the response.

### **7.5 Suggestion for further study**

It is believed that the original simple experimental rig design philosophy remains valid, but to obtain experimental results of sufficient quality to accomplish the original



aims of this study it is important that the apparatus is capable of producing repeatable results free from non-modelled disturbances and with a controlled experimental uncertainty, particularly for peak pressure amplitudes. The two key features are:

- (i) mechanical fast closure valve actuation to give consistent closure time, and
- (ii) pipe and component restraint sufficient to eliminate fluid structure interaction and any additional mechanical disturbance due to valve closure, etc.

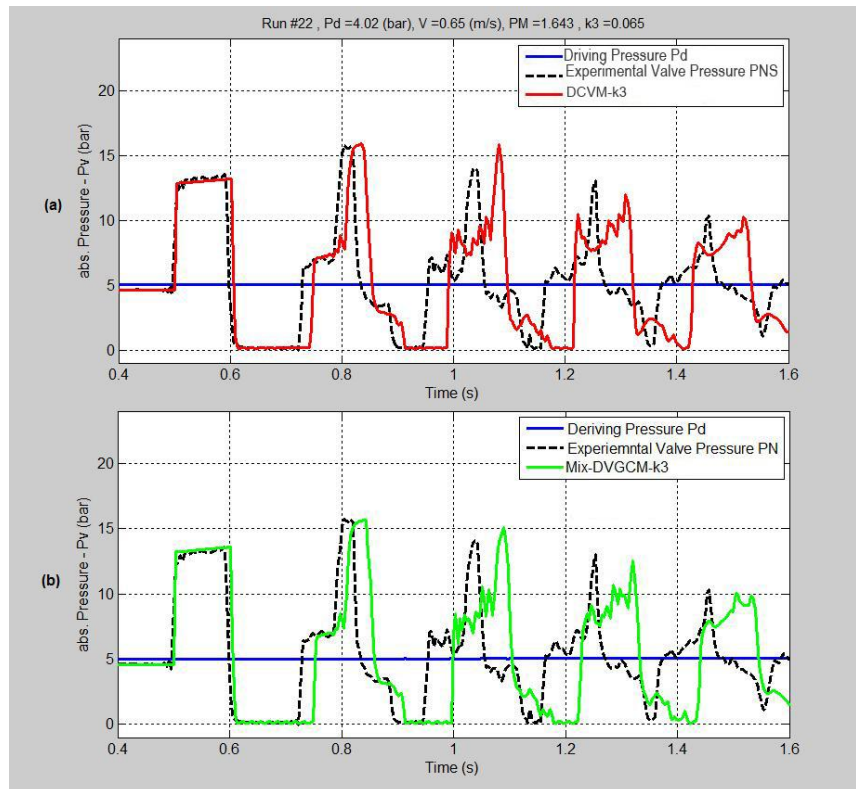
Desirable features would also include:

- (a) A longer pipe, giving a large reflection period ( $2L/a$ ), to facilitate (i) above.
- (b) Water supply at a sufficient pressure to give initial flow velocities close to, if not actually at, fully turbulent flow, but combined with prior deaeration of the supply to repeatably regulate dissolved gas content.
- (c) Additional pressure transducers, as in Martin (1983), at the quarter and mid-points.

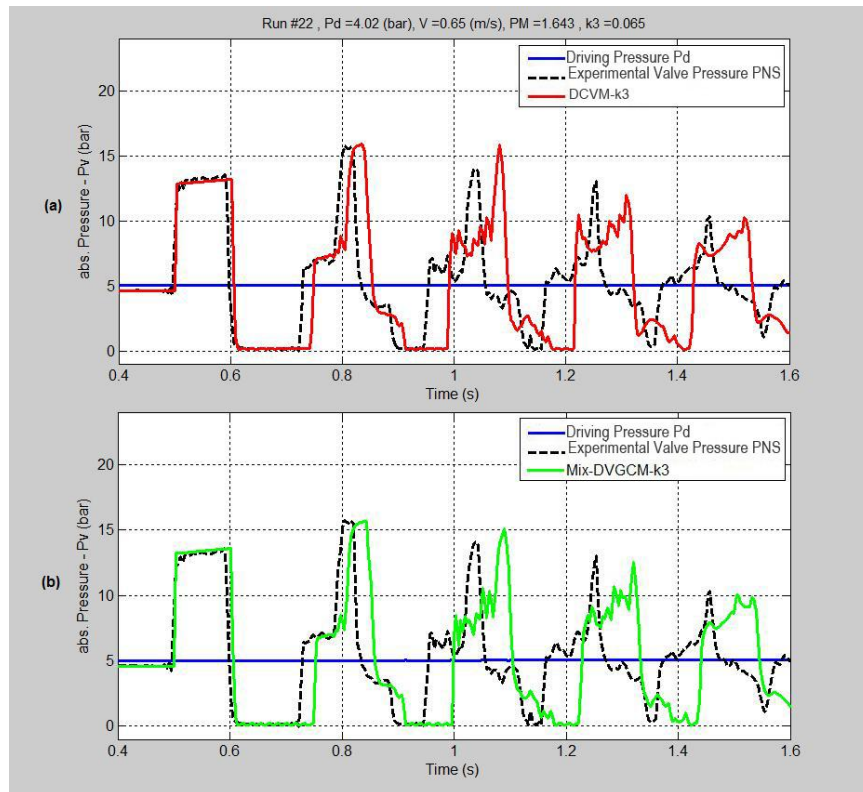
Finally, if cavity visualisation is intended, consideration should be given to a pipe layout where a high point would give column separation not at the closure valve, because of the practical difficulty of arranging transparent tube up to the valve face (the cavitation initiation point).

If a suitable apparatus is, or becomes, available, then if the statistical approach is to be pursued (for the benefits it offers) a sufficient range (believed to have been achieved in this study) but also number of experimental test runs needs to be completed, particularly to give balanced and sufficient numbers of runs in each principle mode of behaviour being studied (that being a limitation in this study). With multi-factor studies in particular, attention has to be paid to this requirement. In retrospect, the original aims of this study were over-ambitious. It would have been better to start with fewer factors, as in Bergant and Simpson (1999) who focussed simply on comparing two basic methods. Increasing the number of factors greatly complicates the assessment of comparisons, unless the statistical approach can be implemented (and suitable criteria found for that). Whether or not the statistical approach is adopted (it is probably not practical for field studies), attention needs to be given to the definition of criteria for model comparison, a topic which has had surprisingly little discussion in the literature.

In terms of the models to be tested, during this research an attempt was made to combine the features of DVCM and DGCM into a single mixed DVGCM model, e.g. Figure(7.1) and Figure(7.2), which covers a wider range of the physical phenomena involved in column separation than either separate model currently does, but without requiring an additional differential equation (for energy) or more data than are likely to be available (e.g. for heat transfer). There was insufficient time available to progress this concept adequately.



Figure(7.1) Comparison of Limited column separation (run 22) vs prediction of both models, (a) DVCM-k3, (b) Mix-DVGCM-k3.



Figure(7.2) Comparison of Limited column separation (run 22) vs prediction of both models, (a) DVCm-k3 , (b) Mix-DVGCM-k3.

## **References.**

Adamkowski, A. (1996), "Investigations of waterhammer phenomenon with column separation." *Sci. Bull.Lodz Tech. Univ.: Turbomachinery*, 110, pp11–22 (in Polish).

Adamkowski, A., Lewandowski, M., (2004), "Unsteady Friction Modelling in Transient Pipe Flow Simulation," *Transactions of the Institute of Fluid-Flow Machinery*, 115. pp83-97.

Adamkowski, A., and Lewandowski, M., (2009), "A new Method for Numerical prediction of liquid column separation accompanying hydraulic transients in pipelines," *Journal of Fluid Engineering*, 131(7), [DOI 10.1115/1.3153365].

Adamkowski, A., and Lewandowski, M., (2012). "Investigation of hydraulic transients in a pipeline with column separation," *Journal of Hydraulic Engineering*, 138(11), pp935–944.

Ahmeid, M.A., (1997), "*Investigation of a statistical approach to benchmarking software for computational fluid dynamics*," MPhil. Thesis, Newcastle University, School of Mechanical and System Engineering.

Anderson, A., (1976), "Menabrea's note on waterhammer: 1858," *ASCE Journal of the Hydraulics Division*, 102, pp29–39.

Anderson, A., (1979), "Column separation in a pumping main, Merz and McLellan," Newcastle upon Tyne (Unpublished notes).

Anderson, A., (1988), "Normalisation as a teaching in fluid mechanics," *International Journal of Mechanical Engineering Education*, 16(3), pp177–187.

Anderson, A., (2000), "Celebrations and challenges – waterhammer at the start of the 20<sup>th</sup> and 21<sup>st</sup> Centuries," *Proceedings, 8<sup>th</sup> International Conference on Pressure Surges*, Professional Engineering Publishing, Bury St Edmunds, pp317–322.

Anderson, A., (2008), "Towards integrating fluid transient issues into pipe system design through a risk management approach," *10<sup>th</sup> International Conference on*

*Pressure Surges: Surge analysis - system design, simulation, monitoring and control*, Conference Proceedings, BHR Group, pp5–20.

Anderson, A., and Arfaie, M., (1991), "Variable waterhammer wavespeed in column separation," *Proceedings, International meeting on hydraulic transients with water column separation, Valencia*, Universidad Politecnica de Valencia, pp183–199.

Anderson, A., and Johnson, G.R., (1990), "Effect of tube ovaling on pressure wave propagation speed," *Journal of Engineering in Medicine*, Proceedings, Institution of Mechanical Engineers, Part H. 204, pp245–251.

Anderson, A., Sandoval-Pena, R., and Arfaie, M., (1991), "Column separation behaviour modes in a simple test rig," *Proceedings, International meeting on hydraulic transients with water column separation, Valencia*, Universidad Politecnica de Valencia, pp33–50.

Angus, R.W., (1935), "Simple graphical solution for pressure rise in pipes and discharge lines," *Journal of the Engineering Institute of Canada*, 18(2), pp72–81.

Angus, R.W., (1937), "Water hammer in pipes, including those supplied by centrifugal pumps: graphical treatment," *Proceedings of the Institution of Mechanical Engineers*, 136, pp245–331.

Arfaie, M., (1989), "*Pressure transient analysis including column separation and behaviour of long pipelines*," PhD. Thesis, Newcastle University, School of Mechanical and Systems Engineering.

Arfaie, M., Suwan, K., and Anderson, A., (1993), "Stability and accuracy of pipe friction approximations in method of characteristics solutions for water hammer," *Mathematical Engineering in Industry*, 4(1) pp265–281.

ASME, (2006), *Compact edition properties of saturated and superheated steam in U.S customary and SI units from the IAPWS-IF97 International Standard for Industry Use*, ASME Research and Technology Committee on Water and Steam in Thermal Systems, New York.

Autrique, R., Rodal, E., Sanchez, A., and Carmona, L., (2012), "Physical model studies of water column separation," *26th IAHR Symposium on Hydraulic Machinery and Systems, IOP Conference Series: Earth and Environmental Science*. 15.

Bahadori, A., and Vuthaluru, B.H., (2009), "Prediction of bulk modulus and volumetric expansion coefficient of water for leak tightness test of pipelines," *International Journal of Pressure Vessels and Piping*, 86, pp. 550–554.

Baltzer, R.A., (1967a), "Column separation accompanying liquid transients in pipes," *ASME Journal of Basic Engineering*, 89, pp837–846.

Baltzer, R.A., (1967a). "A study of column separation accompanying transient flow of liquids in pipes," PhD Thesis, The University of Michigan, Ann Arbor, Michigan, USA.

Bergant, A., and Simpson, A.R., (1992), "Interface model for transient cavitating flow in pipelines," In: Bettess, R., Watts, J. (Eds.), *Unsteady Flow and Fluid Transients*. A. A. Balkema, Rotterdam, pp333–342.

Bergant, A., and Simpson, A.R., (1999), "Pipeline column separation flow regimes," *ASCE Journal of Hydraulic Engineering*, 125, pp835 – 848.

Bergant, A., Simpson, A.R., and Tijsseling, A.S., (2006), "Water hammer with column separation: A historical review," *Journal of Fluid and Structures*, 22(2), pp135–171.

Bergant, A., Simpson, A.R., and Tijsseling, A.S., (2008a), "Parameters affecting water-hammer wave attenuation, shape and timing—Part 1: Mathematical tools," *Journal of Hydraulic Research. IAHR* 39(3), pp373–381.

Bergant, A., Simpson, A.R., and Tijsseling, A.S., (2008b), "Parameters affecting water-hammer wave attenuation, shape and timing—Part 2: Case studies," *Journal of Hydraulic Research. IAHR* 46(3), pp382–391.

Bergant, A., Simpson A.R., and Vitkovsky, J., (2001), "Developments in Unsteady Pipe Flow Friction Modelling," *Journal of Hydraulic Research*, 39(3), pp249–25.

Bergant, A., and Tijsseling, A., (2001), "Parameters affecting water hammer wave attenuation, shape and timing," *Proceedings of the 10<sup>th</sup> International Meeting of IAHR Group on The Behaviour of Hydraulic Machinery Under Steady Oscillatory Conditions*, Trondheim, Norway, June, pp26–28.

Bergeron, L., (1939), Discussion of "Experiments and calculations on the resurge phase of water hammer," by J.N. LeConte and discussion of "Air chambers for discharge lines," by L. Allievi. *Transactions of the ASME*, 61, pp441–445.

Bergeron, L., (1950), *Du Coup de Be'l'ier en Hydraulique—Au Coup de Foudre en Electricite´*. (Waterhammer in hydraulics and wave surges in electricity) Dunod, Paris (in French). (English translation by ASME Committee, Wiley, New York, 1961)

Binnie, A.M., and Thackrah, D.G., (1951), "Water hammer in a pumping main and its prevention," *Proceeding, Institution of Mechanical Engineers*, London, 165, pp43–52

Blind, H., (1956), "Nichtstationa're Stro'mungen in Unterwasserstollen, (Unsteady flow in tailrace tunnels)," In: To'like, F. (Ed.), *Vero'ffentlichungen zur Forschung der DruckstoXprobleme in Wasserkraftanlagen und Rohrleitungen*, 2<sup>nd</sup> ed. Springer, Berlin, pp67–108 (in German).

Brown, R.J., (1968), "Water-column separation at two pumping plants," *ASME Journal of Basic Engineering*, 90, pp521–531.

Brunone, B., and Golia, U.M., (1990), "Improvements in modelling of water hammer and cavitating flow in pipes. Experimental verification," *Proceeding 22<sup>nd</sup> Convegno Nazionale di Idraulica e Costuzioni Idrauliche*, 4, Italian Group of Hydraulics (GII), pp147–160 (in Italian).

Brunone, B., Golia, U.M., and Greco, M., (1991a), "Some Remarks on the Momentum Equation for Fast Transients," *Proceedings International Conference on Hydraulic Transients with Water Column Separation, IAHR*, Valencia, Spain, pp201–209.



Brunone, B., Golia, U.M., and Greco, M., (1991b), "Modelling of fast transients by numerical methods," *Proceeding International Conference on Hydraulic Transients with Water Column Separation*, IAHR, Valencia, Spain, pp273–280.

Brunone, B., Golia, U.M., and Greco, M., (1995), "The Effects of Two-Dimensionality on Pipe Transients Modeling," *Journal of Hydraulic Engineering*, 121(12), pp906–912.

Bughazem, M.B., (1997), "*Investigation of a simple unsteady friction model for waterhammer and column separations*," MPhil. Thesis, Newcastle University, School of Mechanical and System Engineering.

Bughazem, M.B., and Anderson, A., (1996), "Problems with simple models for damping in unsteady flow," In: Boldy, A. (Ed.), *Pressure Surges and Fluid Transients in Pipelines and Open Channels*, Mechanical Engineering Publications, Burry St. Edmunds, pp537–548.

Bughazem, M.B., and Anderson, A., (2000), "Investigation of an unsteady friction model for waterhammer and column separation," *Pressure Surges. Safe design and operation of industrial pipe systems* (Ed. Anderson, A.), pp483–498, Bury St. Edmunds: Professional Engineering Publishing Ltd.

Bunt, E.A., (1953), "Preliminary study of valve cavitation in pipelines," *Journal of the South African Institution of Mechanical Engineers*, 2, pp235–260.

Carmona, L., (2012), "Physical model studies of water column separation," *IOP Conference Series: Earth and Environmental Science*, 15(2), pp022014 (2012).

Carstens, M.R., and Roller, J.E., (1959), "Boundary-shear Stress in Unsteady Turbulent Pipe Flow," *Journal of Hydraulics Division*, ASCE, 95, pp67–81.

Carstens, M.R., and Hagler, T.W., (1964), "Water hammer resulting from cavitating pumps," *Proceeding ASCE*, 90(HY6), pp161–184.

- Chang, H., (2007), The Myth of the Boiling Point, [www.hps.cam.ac.uk/people/chang/boiling/index.htm](http://www.hps.cam.ac.uk/people/chang/boiling/index.htm) (Accessed 13 May 2015)
- Chaplin, M., (2015), Water Structure and Science, [www1.lsbu.ac.uk/water/water\\_structure\\_science.html](http://www1.lsbu.ac.uk/water/water_structure_science.html) (Accessed 13 May 2015)
- Chaudhry, M.H., (1987), *Applied hydraulic transients*, New York: Van Nostrand Reinhold, US.
- Chaudhry, M.H., (2014), *Applied hydraulic transients*, 3<sup>rd</sup> ed., Springer, New York. ISBN 978-1-4614-8538-4 (eBook)
- Coulson, C.A. and Jeffrey, A., (1977), *Waves: A mathematical approach to the common types of wave motion*, 2<sup>nd</sup> Rev. EDN, Longman. London and New York.
- Duc, J., (1959), "Negative pressure phenomena in a pump pipeline," *Sulzer Technical Review*, 41(3), pp3–11.
- Ellis, J., (2008), "*Pressure transients in water engineering: a guide to analysis and interpretation of behaviour*," London: Thomas Telford, UK.
- Feather, N., (1961), *An introduction to the physics of vibration and waves*, Edinburgh University press, Edinburgh.
- Franc, J., and Michel, J., (2004), *Fundamentals of cavitation*, 76, Springer, Berlin.
- Ghidaoui, M.S., Zhao, M., McInnis, D.A., and Axworthy, D.H., (2005), "A review of water hammer theory and practice," *ASME Applied Mechanics Reviews*, 58(1), pp49–76.
- GUM (2008), Evaluation of measurements data – Guide to the expression of uncertainty in measurement, Joint Committee for Guides in Metrology: 100, [www.bipm.org](http://www.bipm.org) (Accessed 13 May 2015)

## References

---

- Himr, D., (2015), "Investigation and numerical simulation of a water hammer with column separation," *Journal of Hydraulic Engineering*, 141(11), 935–944.
- Journal of Pressure Vessels and Piping, 80, pp187–195.
- Kagawa, T., Lee, I., Kitagawa, A., and Takenaka, T., (1983), "High speed and accurate computing method of frequency-dependent friction in laminar pipe flow for characteristic method," *Nippon Kikai Gakkai Ronbunshu*, Ahen, 49(447), pp2638–2644 (in Japanese).
- Kamel, M.Y.M., (1954), "*Cavitation produced by fast velocity changes in pipes*," M.Sc. Thesis, Cairo University, Faculty of Engineering, Cairo, Egypt.
- Kaye & Laby, (2015), [www.kayelaby.npl.co.uk](http://www.kayelaby.npl.co.uk) (Accessed 13 May 2015)
- Lighthill, M.J., (1978), *Waves in Fluids*, Cambridge University Press, Cambridge.
- Liou, J.C.P., (2000), "Numerical properties of the discrete gas cavity model for transients," *ASME Journal of Fluids Engineering*, 122(3), pp636–639.
- Lomax, W., and Saul, A., (1979), *Laboratory work in hydraulics*, 1<sup>st</sup> Ed., London, Granada Publishing.
- Malekpour, A., and Karney, W.B., (2014), "Profile-induced column separation and rejoining during rapid pipeline filling," *Journal of Hydraulic Engineering*, ASCE, 140(11), pp04014054-1–12.
- Martin, C.S., (1983), "Experimental investigation of column separation with rapid closure of downstream valve," In: *Proceedings of the 4<sup>th</sup> International Conference on Pressure Surges*, BHRA, Bath, UK, pp77–88.
- O'Neill, I.C., (1959), "*Water-hammer in simple pipe systems*," M.Sc. Thesis, University of Melbourne, Melbourne, Australia.
- Parmakian, J., (1963), *Waterhammer Analysis*, New York: Dover Publications, INC.

Pejovic, S., Boldy, A.P., and Obradovic, D., (1987), *Guidelines to hydraulic transient analysis*, Aldershot, Hants, England: Technical Press; Brookfield, Vt., USA. : Gower Pub. Co.

Pezzinga, G., (1999), "Quasi-2D Model for Unsteady Flow in Pipe Networks," *Journal of Hydraulic Engineering*, 125(7), pp676–685.

Pothof, I., and Karney, B., (2012), "*Guidelines for transient analysis in water transmission and distribution systems*," Pothof and Karney, licensee InTech., 22 p.  
<http://dx.doi.org/10.5772/53944>

Priddin, K.G., (1978), "A theoretical study of two pressure surge phenomena: cavity collapse and surge tank oscillations," Technical Note TN1495, *BHRA*, Cranfield, Sept.

Provoost, G.A., and Wylie, E.B., (1981), "Discrete gas model to represent distributed free gas in liquids," *Proceeding of 5<sup>th</sup> International Symposium on Column Separation, International Association for Hydraulic Research*, Delft, The Netherlands, pp249–258.

Ramos, H., Covas, D., Borga, A., and Loureiro, D., (2004), "Surge damping analysis in pipe systems: modelling and experiments," *Journal of Hydraulic Research*, 42(2), pp413–425.

Reddy, H.P., Silva-Araya, W., and Chaudhry, M.H., (2012), "Estimation of Decay Coefficients for Unsteady Friction for Instantaneous, Acceleration Based Models," *Journal of Hydraulic Engineering*, 138(3), pp260–271.

Richards, R.T., (1956), "Water-column separation in pump discharge lines," *Transactions of ASME*, 78, pp1297–1306.

Ryan, B., Joiner, B., and Cryer, J., (2005), *Minitab Handbook (Updated for Release 14)*, 5<sup>th</sup> ed., Thomson Learning, Canada.

## References

---

Safwat, H.H., and De Kluyver, J.P., (1972), "Digital computations for water hammer-column separation," *In: Proceedings of the 1<sup>st</sup> International Conference on Pressure Surges*, BHRA, Canterbury, pp53–68.

Safwat, H.H., and Van Den Polder J., (1973), "Experimental and analytic data correlation study of water column separation," *ASME Journal of Fluids Engineering*, 95(1), pp91–97.

Schohl, G.A., (1993), "Improved approximate method for simulating frequency-dependant friction in transient laminar flow," *Journal of Fluids Engineering*, 115(3), pp. 420–424.

Sharp, B.B., and Sharp, D.B., (1996), *Water hammer: practical solutions*, Arnold, London.

Shu, J.-J., (2003), "Modelling vaporous cavitation on fluid transients," *International Journal of Pressure Vessels and Piping*, 80, pp187–195.

Siemons, J., (1967), "The phenomenon of cavitation in a horizontal pipe-line due to a sudden pump-failure," *IAHR Journal of Hydraulic Research*, 5, pp135–152.

Silva-Araya, W.F., and Chaudhry, M.H., (1997), "Computation of Energy Dissipation in Transient Flow," *Journal of Hydraulic Engineering*, 123(2), pp108 –115.

Simpson, A.R., and Bergant, A., (1994a), "Numerical comparison of pipe column-separation models," *Journal of Hydraulic Engineering*, 120(3), pp361–377.

Simpson, A.R., and Bergant, A., (1994b), "Developments in pipeline column separation experimentation," *IAHR Journal of Hydraulic Research*, 32, pp183–194.

Simpson, A.R., and Wylie, E.B., (1989), "Towards an improved understanding of waterhammer column separation in pipelines," *Civil Engineering Transactions, The Institution of Engineers*, Australia, CE 31(3), pp113–120.

- Simpson, A.R., and Wylie, E.B., (1991), "Large water-hammer pressures for column separation in pipelines," *Journal of Hydraulic Engineering*, 117(10), pp1310–1316.
- Storli, P.-T., and Nielsen, T.K., (2011), "Transient friction in pressurized pipes. II: Two-Coefficient Instantaneous Acceleration–Based Model," *Journal of Hydraulic Engineering*, 137(6), pp679–695.
- Streeter, V.L. and Lai, C., (1962), "Waterhammer Analysis Including Fluid Friction," *Journal of Hydraulics Division*, ASCE, 88(HY3), May, pp79–112.
- Streeter, V.L., and Wylie, E.B., (1967), *Hydraulic Transients*, McGraw-Hill, New York.
- Suwan, K., (1989), "*The 'Method of Lines' Applied to waterhammer Computation*," PhD. Thesis, University of Newcastle upon Tyne.
- Suzuki, K., Taketomi, T., and Sato, S., (1991), "Improving Zielke's method of simulating frequency-dependent friction in laminar liquid pipe flow," *ASME Journal of Fluids Engineering*, 113(4), pp569–573.
- Swaffield, J.A. (1970), "A study of column separation following valve closure in pipeline carrying aviation kerosene," *Proceedings of the Institution of Mechanical Engineers*, 184(3G), pp57–64.
- Swaffield, J.A., and Boldy A.P., (1993), "*Pressure surge in pipe and duct systems*," Avebury Technical, Aldershot.
- Szymkiewicz, R., and Mitosek, M., (2007), "Numerical aspects of improvement of the unsteady pipe flow equations," *International Journal of Numerical Methods in Fluids*, 55, pp1039–1058.
- Thibessard, G., (1961), "La simulation du coup de bélier sur calculateur numérique. (The simulation of water hammer on a numerical calculator.)," *In: Proceedings of the Ninth IAHR Convention*, Dubrovnik, Yugoslavia, pp881–890 (in French).

Thorley, A.R.D., (2004), *Fluid Transients in Pipeline Systems*, 2<sup>nd</sup> Ed., Professional Engineering Publishing, Bury St Edmunds.

Tijsseling, A.S., and Anderson A., (2004), "A precursor in waterhammer analysis – rediscovering Johannes von Kries," *Proceeding, of the 9<sup>th</sup> International Conference on Pressure Surges* (Editor S.J. Murray), Chester, United Kingdom, *BHR Group*, pp739–751.

Tijsseling, A.S., and Anderson, A., (2007), "Johannes von Kries and the history of water hammer," *ASCE Journal of Hydraulic Engineering*, 133, pp1–8.

Tijsseling, A.S., and Anderson, A., (2008), "Thomas Young's research on fluid transients: 200 years on," *Proceeding, of the 10<sup>th</sup> International Conference on Pressure Surges* (Editor S Hunt), Edinburgh, United Kingdom, *BHR Group*, May, pp21–33.

Trikha, A.K., (1975), "An Efficient Method for Simulating Frequency-Dependent Friction in Transient Liquid Flow," *ASME Journal of Fluids Engineering*, 97(1), pp97–105.

Tullis, J.P., (1989), *Hydraulics of pipelines, pumps, valves, cavitation, transients*, New York, John Wiley & Sons.

Vardy, A.E., and Brown, J.M.B., (1995), "Transient turbulent smooth pipe friction," *Journal of Hydraulic Research*, Delft, The Netherlands, 33(4), pp435–456.

Vardy, A.E., and Brown, J.M.B., (2003), "Transient turbulent friction in smooth pipe flows," *Journal of Sound and Vibration*, 259(5), pp1011–1036.

Vardy, A.E., and Brown, J.M.B., (2004), "Transient turbulent friction in fully rough pipe flows," *Journal of Sound and Vibration*, 270 (1–2), pp233–257.

Vardy, A.E. and Hwang, K.L. (1991), "A Characteristics model of transient friction in pipes," *Journal of Hydraulic Research*, 29(5), pp669–684.

## References

---

- Vitkovsky, J.P., Bergant, A., Simpson, A.R., and Lambert, M.F., (2006a), "Systematic evaluation of one-dimensional unsteady friction models in simple pipelines," *Journal of Hydraulic Engineering*, 132(7), pp696–708.
- Vitkovsky, J.P., Lambert, M.F., Simpson, A.R., and Bergant, A., (2000), "Advances in unsteady friction modelling in transient pipe flow," *Proceeding, 8<sup>th</sup> International Conference on Pressure Surges*, BHR Group, Bedford, UK, pp471–482.
- Vitkovsky, J.P., Stephens, M., Bergant, A., Simpson, A.R. and Lambert, M.F., (2006b), "Numerical error in weighing function based unsteady friction models for pipe transients," *Journal of Hydraulic Engineering*, 132(7), pp709–721.
- Vreugdenhil, C.B., (1964), "Digital computations of water-hammer," *Delft Hydraulics Laboratory*, Report S 103-I, Delft, The Netherlands.
- Siemons, J., (1967), "The phenomenon of cavitation in a horizontal pipe-line due to a sudden pump-failure," *IAHR Journal of Hydraulic Research* 5, pp135–152. (Also: Delft Hydraulics Laboratory, Publication No. 53)
- Weyler, M.E., (1969), "*An investigation of the effect of cavitation bubbles on momentum loss in transient pipe flow*," PhD Thesis, The University of Michigan, Ann Arbor, USA
- Weyler, M.E., Streeter, V.L., and Larsen, P.S., (1971), "An Investigation of Cavitation Bubbles on the Momentum loss in Transient Pipe flow," *ASME Journal of Basic Engineering*, 93(1), pp1–7.
- White, F.M. (1986), *Fluid mechanics*, 2<sup>nd</sup> edition, McGraw-Hill, New York.
- Wiggert, D.C., and Sundquist, M.J., (1979), "The effect of gaseous cavitation on fluid transients," *ASME Journal of Fluids Engineering*, 101, pp 79–86.
- Williams, D.J., (1977), "Waterhammer in non-rigid pipes: precursor waves and mechanical damping," *IMechE Journal of Mechanical Engineering Science*, 19, pp237–242.



Wylie, E.B., (1984), "Simulation of vaporous and gaseous cavitation," *ASME Journal of Fluids Engineering*, 106(9), pp307–311.

Wylie, E.B., and Streeter, V.L., (1984), *Fluid transients*, Tomson-Shore, Dexter, MI.

Wylie, E.B., and Streeter, V.L., (1993), *Fluid transients in systems*, Prentice Hall, Englewood Cliffs, NJ.

Zhao, M., and Ghidaoui, M.S., (2004), "Review and analysis of 1D and 2D energy dissipation models for transient flows," *Proceeding, International Conference on Pressure Surges*, BHR Group, Bedford, UK, pp477–492.

Zielke, W., (1968), "Frequency-dependent friction in transient pipe flow," *ASME Journal of Basic Engineering*, 90, pp109–115.

**Appendix A.**

## **Uncertainty Calculations**

## A.1 WATERHAMMER WAVESPEED

### A.1.1 Evaluation of theoretical value

The theoretical value given by Eq.(4.1) has to be evaluated using data from Table(4.1) and Table(4.2) that are subject to tolerance (e.g. pipeline dimensions  $d$ ,  $e$ ), environmental temperature variation (e.g. water properties  $K$ ,  $\rho$ ) and measurement uncertainties (e.g. pipeline material properties  $E$ ,  $\nu$ ).

In principle, experimental uncertainty should always be calculated by the GUM (Guide to Uncertainty in Measurement) (JCGM, 2008) approach, but in this example using the quoted manufacturing tolerance on the pipe wall thickness  $e$  in Table(4.2) leads to an unrealistically high probable uncertainty of around  $\pm 183$  m/s. Consequently, following Anderson and Johnson (1990) a different approach has been adopted, in which the direction of the uncertainty or tolerance is chosen to give the range of likely maximum and minimum values from Eq.(4.1), with the average of these identifying the nominal value.

Following Anderson and Johnson (1990), the waterhammer wavespeed  $a$  in Eq.(4.1) is decomposed into its fluid compressibility ( $a_s$ ) and pipeline elasticity ( $a_y$ ) components to illustrate this process numerically:

$$\frac{1}{a^2} = \frac{1}{a_s^2} + \frac{1}{a_y^2} \quad \text{where} \quad a_s = \sqrt{\frac{K}{\rho}} \quad \text{and} \quad a_y = \sqrt{\frac{Ee}{\rho d}} \quad (\text{A.1})$$

Then using the data from Table(4.1) and Table(4.2) for the  $a_s$  component only:

(a) GUM approach:

$$\begin{aligned} a_s &= \sqrt{\frac{2.18 * 10^9}{999}} = 1477 \text{ m/s} \\ \pm \Delta a_s &= a_s \sqrt{\left(\frac{\Delta K}{K}\right)^2 + \left(\frac{\Delta \rho}{\rho}\right)^2} \\ &= 1477 \sqrt{\left(\frac{0.02}{2.18}\right)^2 + \left(\frac{2}{999}\right)^2} = 14 \text{ m/s} \end{aligned} \quad (\text{A.2})$$

(b) Maximum and minimum values approach.

$$\text{Maximum } a_s \quad a_s = \sqrt{\frac{2.20 * 10^9}{997}} = 1485 \text{ m/s.}$$

$$\text{Minimum } a_Y \quad a_s = \sqrt{\frac{2.16 * 10^9}{1001}} = 1469 \text{ m/s.}$$

$$\begin{aligned} \text{Nominal } a_s \quad a_s &= \frac{1}{2} (\text{Max} + \text{Min}) \pm \frac{1}{2} (\text{Max} - \text{Min}) \text{ m/s.} \quad (\text{A.3}) \\ &= 1477 \pm 8 \text{ m/s} \end{aligned}$$

Following the same procedure through for the  $a_Y$  component and then final waterhammer wavespeed  $a$  gives the values summarised in Table(A.1).

The values in Table(A.1) have not been rounded to an appropriate number of significant figures taking the uncertainties into account, so the theoretical value of wavespeed  $a$  could finally be given as:

$$a = 1355 \pm 27 \text{ m/s} \quad (\text{A.4})$$

**Table(A.1) Comparison of uncertainty for calculated theoretical wavespeed**

Approach	Unconfined $a_s$	Young $a_Y$	Waterhammer $a$ Eq.(A.1)
GUM uncertainty Eq.(A.2)	$1477 \pm 14 \text{ m/s}$	$3397 \pm 458 \text{ m/s}$	$1355 \pm 183 \text{ m/s}$
Max/Min Eq.(A.3)	$1477 \pm 8 \text{ m/s}$	$3399 \pm 338 \text{ m/s}$	$1355 \pm 27 \text{ m/s}$

### A.1.2 Experimental value from Joukowsky pressure rise

On Figure(4.8) the points plotted have experimental uncertainty bars:

- For initial flow velocity  $V_o$ :

$$V_o = \frac{\text{volume}}{\text{time} \cdot \text{area}} \quad (\text{A.5})$$

The data in Table(4.2) give the uncertainty in pipe internal cross-section area as about 3.3%. If a sufficiently large volume is collected in a graduated container (of the order of 500ml) then the measured uncertainty in volume is small, but the uncertainty in time is relatively large, not just because of human reaction but also because of moving the container to and from the pipe steady discharge. Therefore, this time uncertainty dominates the uncertainty in the initial flow velocity, increasing as flow velocity increases because the volume collection time becomes shorter for a graduated container of a given size. Typically for  $V_o$  this will range from 5 to 15%.

- For Joukowsky pressure rise  $P_j$ :

The uncertainty in the observed Joukowsky pressure rise  $P_j$  results from:

- (i) The pressure transducer calculation shown in Figure(4.4).
- (ii) The scale resolution of the transient recorder for any particular reading.
- (iii) Identification of the Joukowsky first pressure rise event on the pressure trace.

The third of these dominates the uncertainty, being an order of magnitude larger than the first two for two reasons:

- Judging the starting deviation from steady state pressure for valve closure over finite time (see Section 4.3).
- Judging the completion of the Joukowsky pressure rise due to the “noise” created by the superimposed precursor waves, e.g. Figure(4.6).

Because of these issues, the uncertainty  $\Delta P_j$  is more or less uniform over the range of  $P_j$  values at about  $\Delta P_j \cong \pm 0.05 \text{ bar}$ .

With these uncertainty bars marked on an enlarged version of Figure(4.8), then the likely range of gradients for the straight-line graph can be assessed, giving an indication of the uncertainty in the wavespeed  $a$  evaluated from:

$$a = \text{graph gradient}/\rho \quad (\text{A.6})$$

As the uncertainty in water density is much smaller than the uncertainty in the graph gradient, the latter is dominant and gives a result  $a = 1280 \pm 40 \text{ m/s}$ .

### **A.1.3 Experimental value from wave period and frequency**

Using Eq.(4.4), in principle the greater the number of wave cycles used to measure the experimental time duration of the waterhammer cycle then the greater the accuracy of the result, since for results recorded at  $256\text{Hz}$  the time discrimination is  $1/256 = 3.91 \times 10^{-3} \text{ s}$ . However, as Figure(4.5), Figure(4.9) and Figure(5.6) show, wave damping and dispersion (the latter related to the finite valve closure times achieved) alter the time domain form of the pressure cycle over time, causing practical issues with identifying appropriate corresponding cycle start and end times. As indicated on Figure(4.8), successive pressure maxima and minima are most easily identified, with uncertainties introduced by pressure waves at the start and dispersion at the end of the time measurement. A best estimate for these suggests that the time discrimination is a multiple (taken as 3) of the instrumentation discrimination, with the number of cycles used judged to be 3 or 4 depending on the wave amplitude, as in Figure(4.5).

Using the GUM (JCGM 2008) approach to uncertainty, the average measured period of a single-phase waterhammer cycle is  $0.1968 \pm 0.0117/n$  seconds, where  $n$  is the number of wave cycles counted. Taking a minimum  $n = 3$ , the uncertainty in the wavespeed  $a$  evaluated from Eq.(4.4) with the pipe length  $L$  from Table(4.2) is:

$$a = \frac{4(62.75)}{(0.1968)} = 1275 \text{ m/s}$$

$$\pm \Delta a = a \sqrt{\left(\frac{\Delta L}{L}\right)^2 + \left(\frac{\Delta T}{T}\right)^2}$$

$$\pm\Delta a = 1275 \sqrt{\left(\frac{0.25}{62.75}\right)^2 + \left(\frac{0.0117}{3 * 0.1968}\right)^2} = 25.8 \text{ m/s}$$

Selecting significant figures appropriate to this uncertainty suggests  $a = 1275 \pm 25 \text{ m/s}$ .

Using the alternative frequency domain approach with Eq.(4.4) has two significant differences. Firstly, it is easier to identify the peaks on the frequency response of Figure(4.7) but, secondly, that frequency response summaries the whole transient recorded, as that while it is not necessary to identify the wave cycles to measure from, nor is it possible to eliminate the heavily dispersed later cycles. For the uncertainty calculation, the fundamental frequency can be picked up at  $5.08 \pm 0.05 \text{ Hz}$ , giving:

$$a = 4(62.75)(5.08) = 1275 \text{ m/s}$$

$$\begin{aligned} \pm\Delta a &= a \sqrt{\left(\frac{\Delta L}{L}\right)^2 + \left(\frac{\Delta f_n}{f_n}\right)^2} \\ &= 1275 \sqrt{\left(\frac{0.25}{62.75}\right)^2 + \left(\frac{0.05}{5.08}\right)^2} = 13.5 \text{ m/s} \end{aligned}$$

Selecting significant figures appropriate to this uncertainty suggests  $a = 1275 \pm 13 \text{ m/s}$ .

## A.2 DARCY FRICTION FACTOR

For the uncertainty bars shown on Figure(4.14) with pipe flow Reynolds Number  $Re$  defined as in Eq.(4.9), then its probable relative uncertainty is given by:

$$\left(\frac{\Delta Re}{Re}\right) = \sqrt{\left(\frac{\Delta \rho}{\rho}\right)^2 + \left(\frac{\Delta \mu}{\mu}\right)^2 + \left(\frac{\Delta d}{d}\right)^2 + \left(\frac{\Delta V_o}{V_o}\right)^2} \quad (A.7)$$

From Table(4.2) all of:

$$\left(\frac{\Delta \rho}{\rho}\right) = 2 * 10^{-3} \quad \left(\frac{\Delta \mu}{\mu}\right) = 26 * 10^{-3} \quad \left(\frac{\Delta d}{d}\right) = 24 * 10^{-3}$$

are an order of magnitude less than the uncertainty estimated before in Section(4.4.2) for  $V_o$ , so the uncertainties in Reynolds Number  $Re$  for the points in Figure(4.14) are effectively the same as for steady flow velocity  $V_o$  and hence increase as  $Re$  increases (as shown).

For the measured friction factor  $f$  values on the vertical axis of Figure(4.14) then from Eq.(4.11) the probable relative uncertainty is given by:

$$\left(\frac{\Delta f}{f}\right) = \sqrt{\left[\left(\frac{\Delta \rho}{\rho}\right)^2 + \left(\frac{\Delta d}{d}\right)^2 + \left(\frac{\Delta L}{L}\right)^2 + \left(\frac{\Delta K_e}{K_e}\right)^2 + \left(\frac{\Delta H_{NS}}{H_{NS}}\right)^2\right] + \left[\left(\frac{\Delta P_R}{P_R}\right)^2 + \left(\frac{\Delta P_{NS}}{P_{NS}}\right)^2 + 2 \cdot \left(\frac{\Delta V_o}{V_o}\right)^2\right]} \quad (A.8)$$

With for the constant quantities in addition to the values above:

$$\left(\frac{\Delta L}{L}\right) = 4 * 10^{-3} \quad \left(\frac{\Delta K_e}{K_e}\right) \cong 100 * 10^{-3} \quad \left(\frac{\Delta H_{NS}}{H_{NS}}\right) \cong 20 * 10^{-3}$$

As shown in Section(4.2), of the varying measurement values the uncertainty in the two pressures  $P_R$  and  $P_{NS}$  is of a similar order of magnitude as for pipe length  $(\Delta L/L)$ , with the uncertainty in flow velocity (doubled with sensitivity 2 for  $V^2$ ) again being dominant. Hence, the friction factor uncertainty also increases as  $Re$  increases (as shown).



## **Appendix B.**

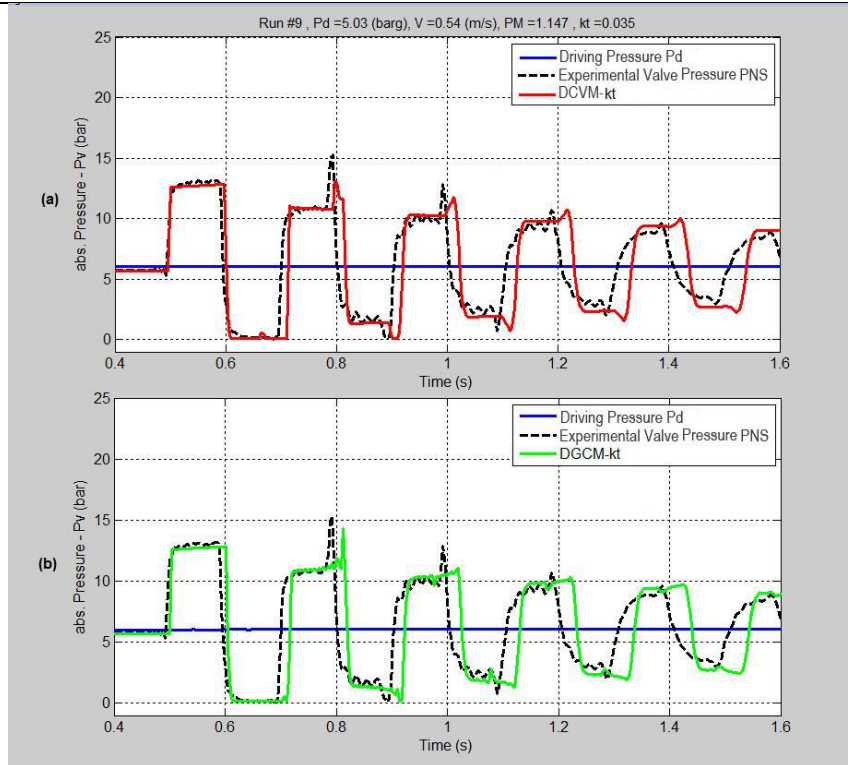
**Pilot Study: Initial Visual Comparison of Column Separation Using  
Modified Unsteady Friction Model.**

The original intention had been to adopt the qualitative comparison methodology of Arfaie (1989) and others. This Appendix outlines that pilot study, comparing only DVCM and DGCM, with the Wylie and Streeter (1993) (W&S) internal cavity boundary condition and the steam tables data value of  $P_v = 2\text{kPa}$  (ASME 2006).

The unsteady friction model suggested by Bughazem and Anderson (2000) (Section 3.3.1) was tested with the best value for this apparatus of  $k_t = 0.035$  adopted for both DVCM and DGCM to investigate their predictions for the range of transient behaviours mentioned earlier (Section 5.2): first transition zone, limited column separation with spike higher than Joukowski pressure, the 2<sup>nd</sup> transition zone and the typical classic column separation.

The first transition zone is presented in Figure(B.1)) which shows the experimental transient behaviour at valve successfully predicted by both models (DVCM- $k_t$  & DGCM- $k_t$ ). In general appearance, plot (b), of DGCM- $k_t$  provides better estimation of the pressure spike at the top of the second pressure peak than DVCM- $k_t$  (a), despite the small phase shift. Figure(B.1)) can be compared with Figure(6.3) for the same experimental run 9. Both use a Brunone et al type of unsteady friction with the optimum unsteady friction coefficients ( $k_t$  and  $k_x$ , respectively) determined from experiments on the apparatus. Following this pilot study using the new implementation of this (Section 3.3.1), it was decided that its additional complexity did not lead to any improvement over the original published version so the latter was adopted for all further comparisons in Chapter 6.

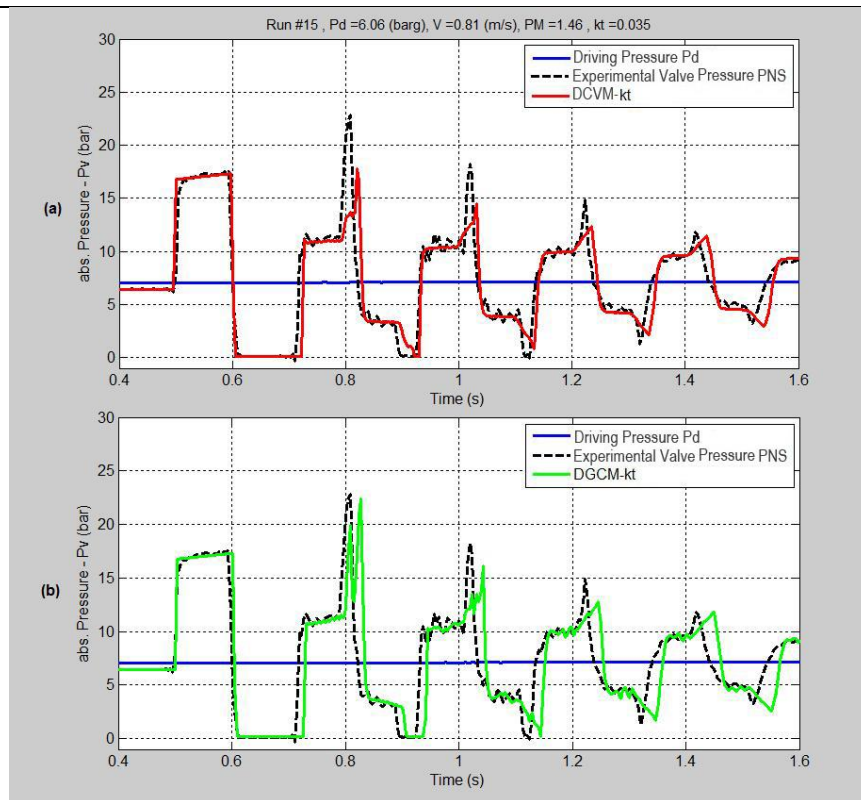
**Appendix B. Pilot study: Initial visual comparison of column separation using modified unsteady friction model.**



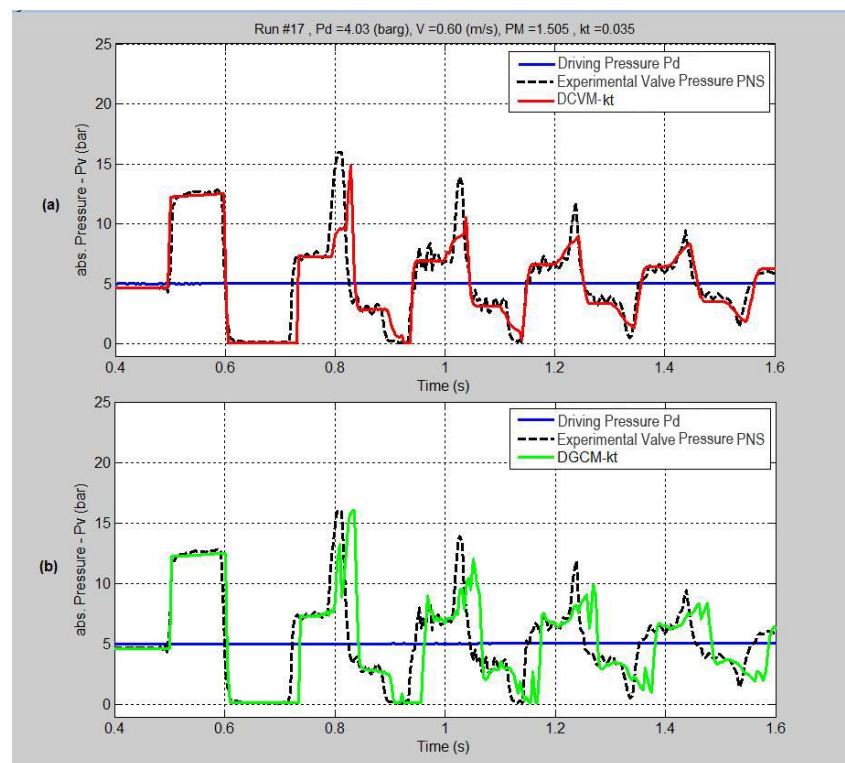
**Figure(B.1) Transient behaviour of first transition zone (run 9) vs prediction of both models, (a) DVCM-kt , (b) DGCM-kt.**

Figure(B.2), Figure(B.3) and Figure(B.4) represent limited column separation with the pressure spikes higher than Joukowski pressure. The general appearance for limited column separation with spike at the top of the second pressure-peak and corresponding reflections are predicted. In two Figure(B.2) & Figure(B.3) DVCM-kt maintains the wave phase better than DGCM-kt but in two (Figure(B.3) and Figure(B.4) DGCM-kt represents the shape of the pressure spike better.

**Appendix B. Pilot study: Initial visual comparison of column separation using modified unsteady friction model.**

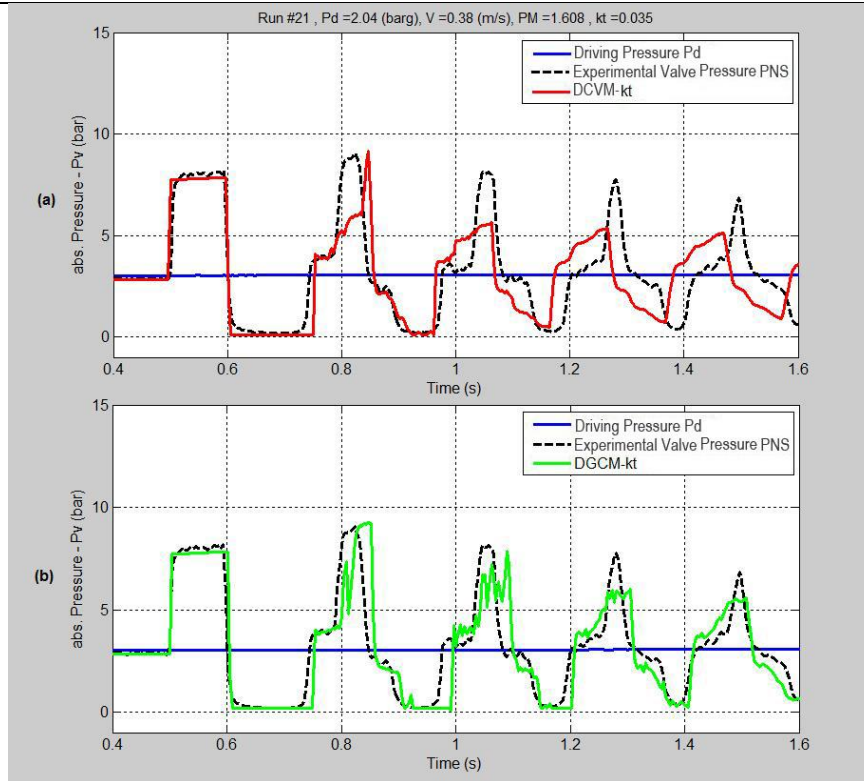


**Figure(B.2) Comparison of Limited column separation (run 15) and prediction of both models, (a) DVCM-kt, (b) DGCM-kt.**



**Figure(B.3) Comparison of Limited column separation (run 17) and prediction of both models, (a) DVCM-kt, (b) DGCM-kt.**

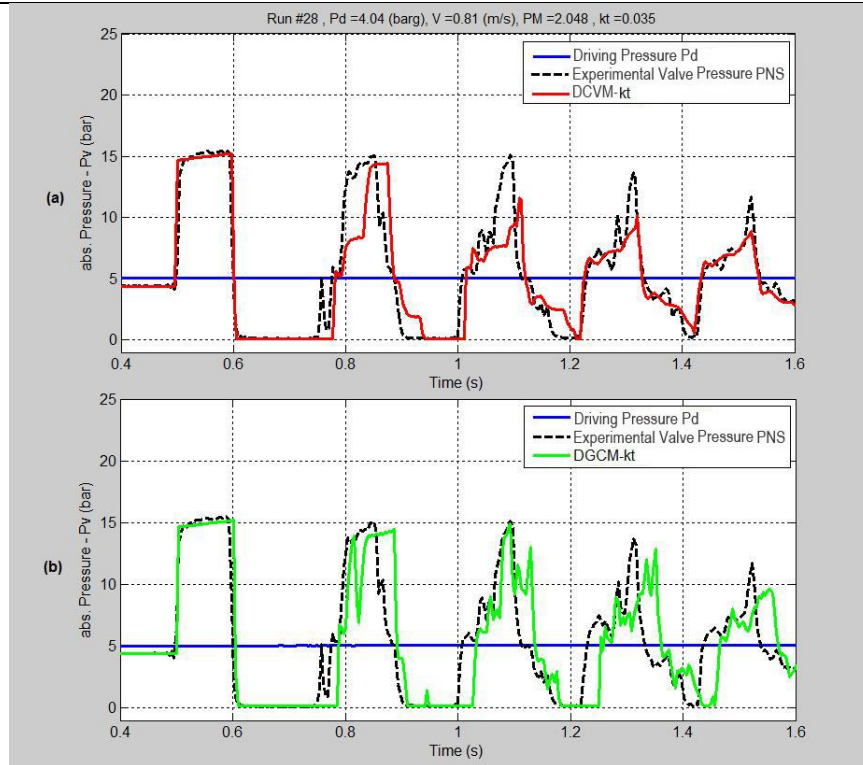
**Appendix B. Pilot study: Initial visual comparison of column separation using modified unsteady friction model.**



**Figure(B.4) Comparison of Limited column separation (run 21) and prediction of both models, (a) DVCM-kt, (b) DGCM-kt.**

Figure(B.5) shows the second transition zone between limited and classic column separation. DGCM-kt has provided a better estimation than DVCM-kt for predicting the general form of this transient behaviour (i.e. long cavity duration getting shorter as time progresses and pressure peak wave shorter in time and lower in magnitude than Joukowski pressure) but the DVCM-kt model has succeeded in predicting the cavity durations and wave phase better.

**Appendix B. Pilot study: Initial visual comparison of column separation using modified unsteady friction model.**

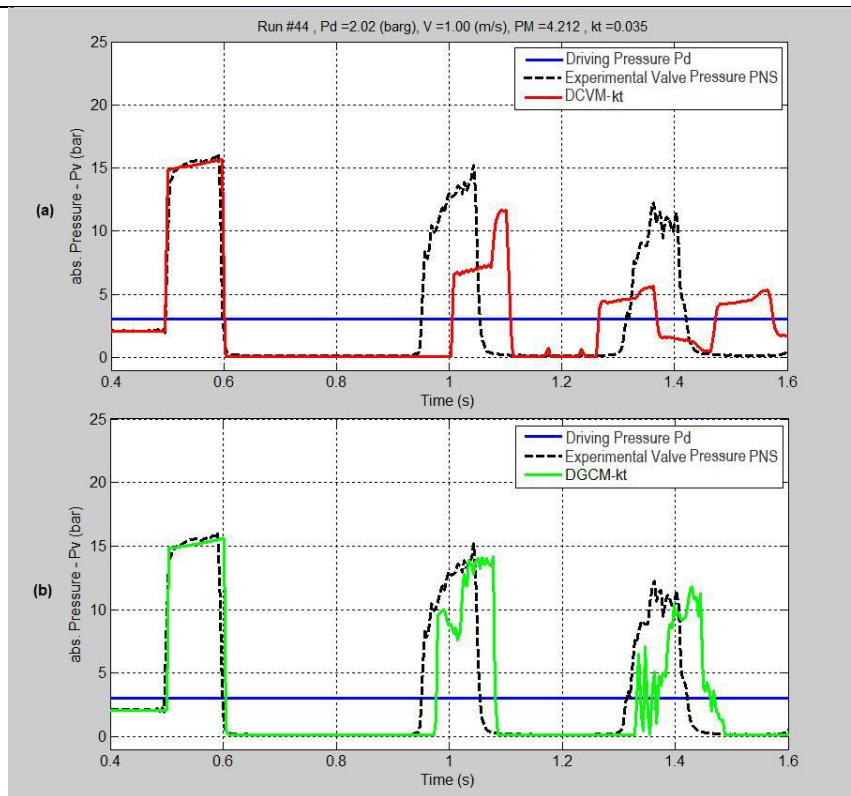


**Figure(B.5) Transient behaviour of second transition zone, (run 28) and prediction of both models, (a) DVCM-kt , (b) DGCM-kt.**

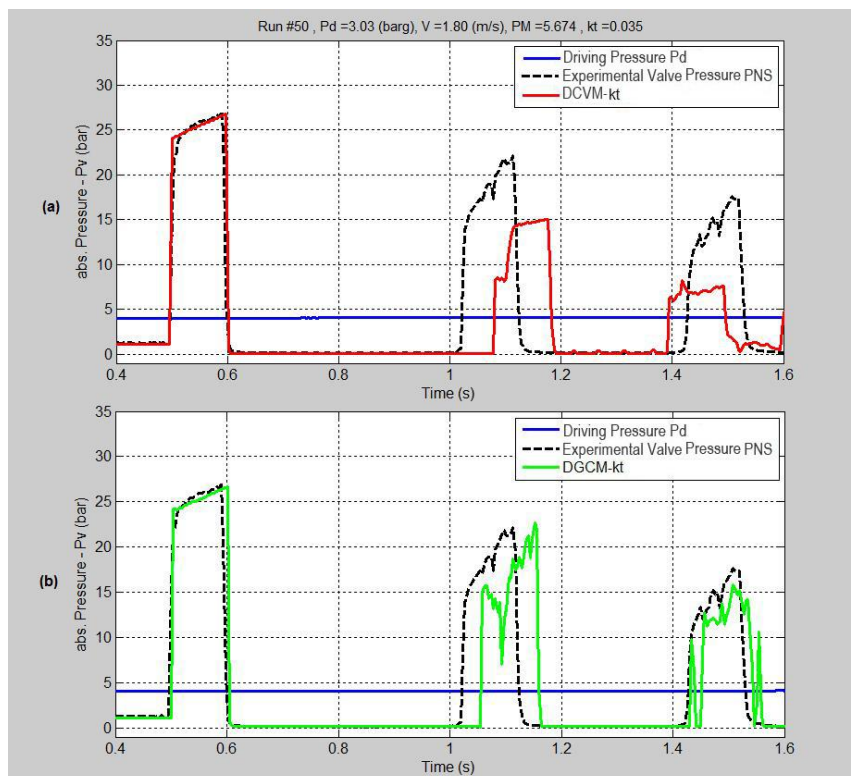
Finally, Figure(B.6) and Figure(B.7) show typical “classic” column separation characterised by long cavity duration getting shorter with decreasing pressure amplitudes lower than Joukowski pressure. In both cases DGCM-kt appears to provide a better overall representation than DVCM-kt, as well as better prediction of the second peak amplitude.

Overall this appears to support the opinion of Arfaie (1989) that the mode of column separation behaviour influences the choice of best method. Section(6.1) repeats this pilot study using the published Bughazem and Anderson (2000) unsteady friction model, but for a different selection of runs (with the one exception previously noted).

**Appendix B. Pilot study: Initial visual comparison of column separation using modified unsteady friction model.**



**Figure(B.6) Comparison of Typical column separation (run 44) and prediction of both models, (a) DVCM-kt , (b) DGCM-kt.**



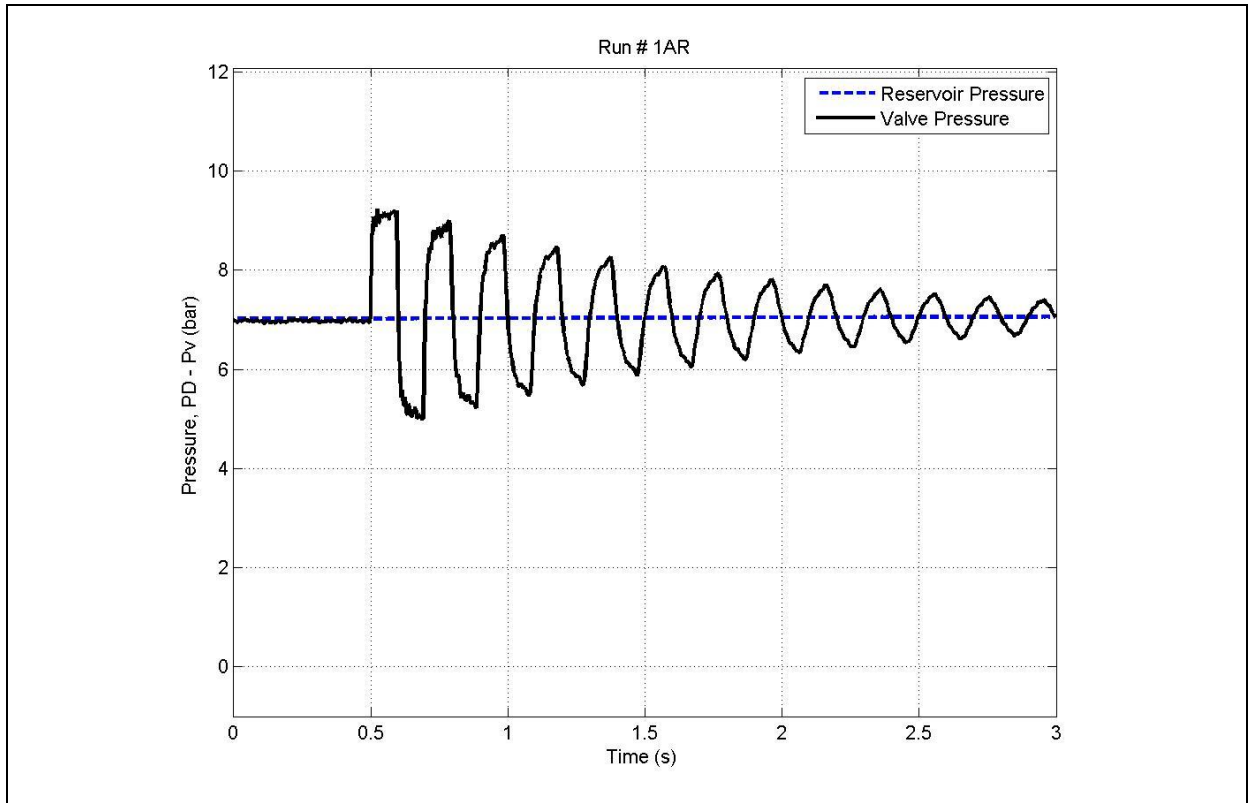
**Figure(B.7) Comparison of Typical column separation (run 50) and prediction of both models, (a) DVCM-kt , (b) DGCM-kt.**

## **Appendix C.**

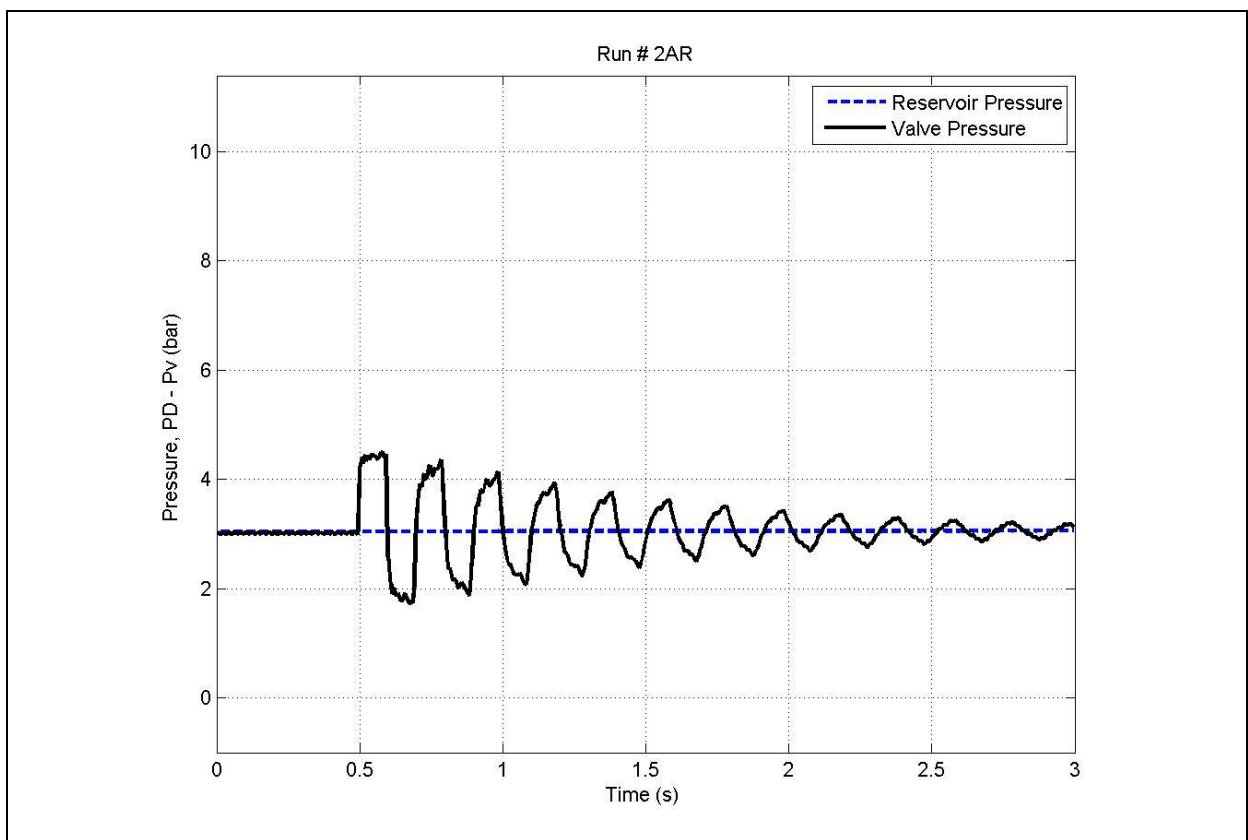
### **Experiments of All Pressure Transient Behaviours.**



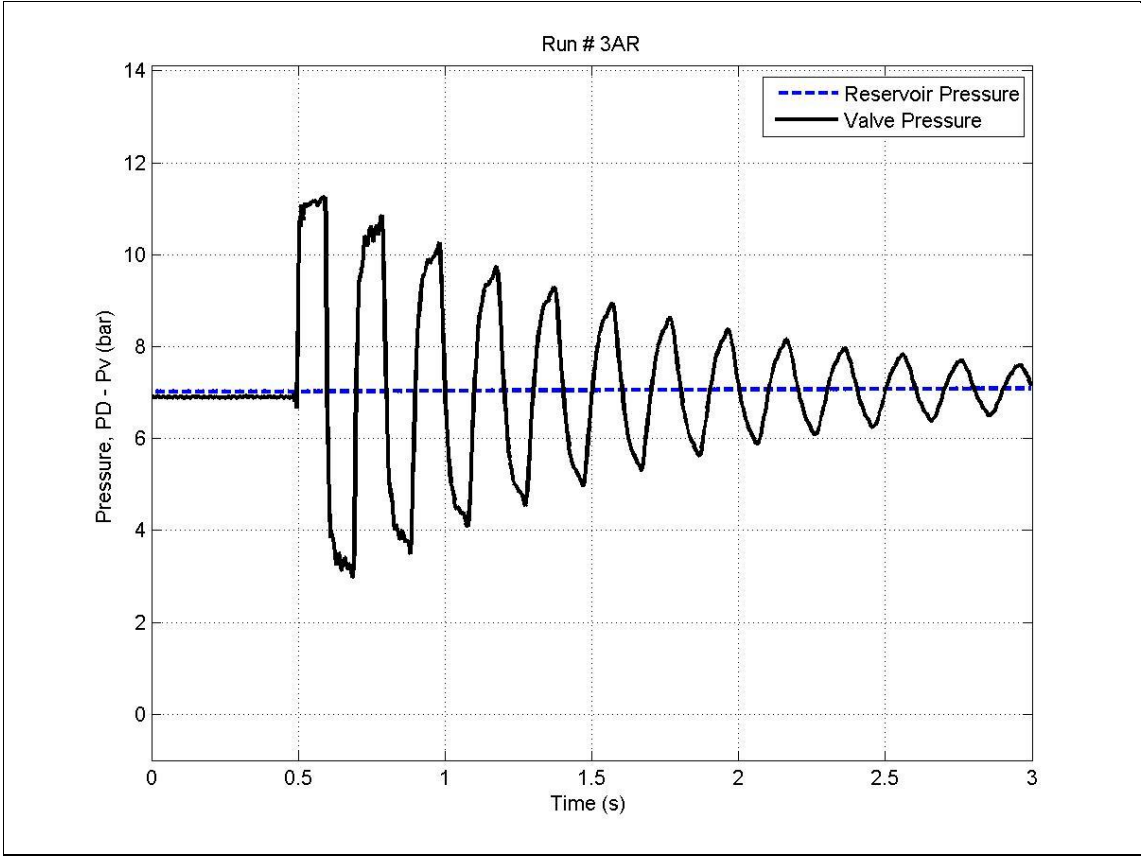
C.1 Experiments of Single-phase waterhammer, runs[1-6].



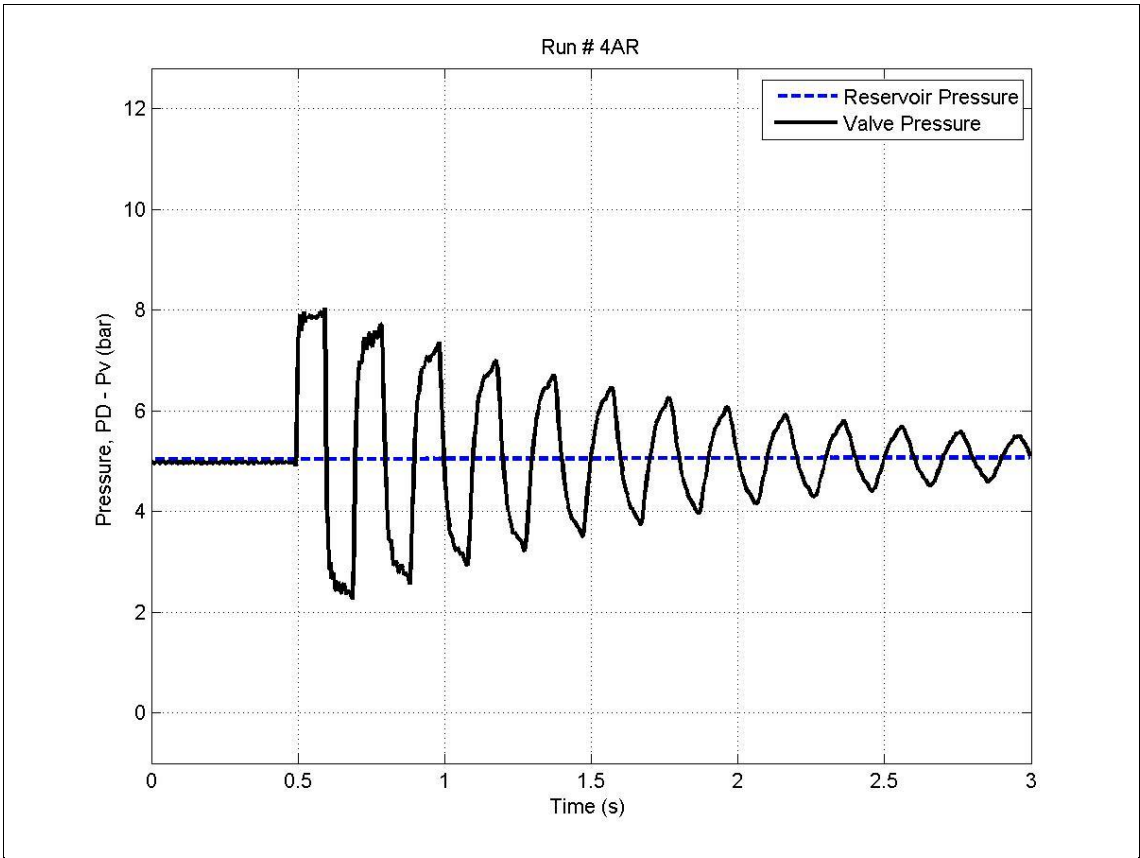
Figure(C.1) Experiment No. 1.



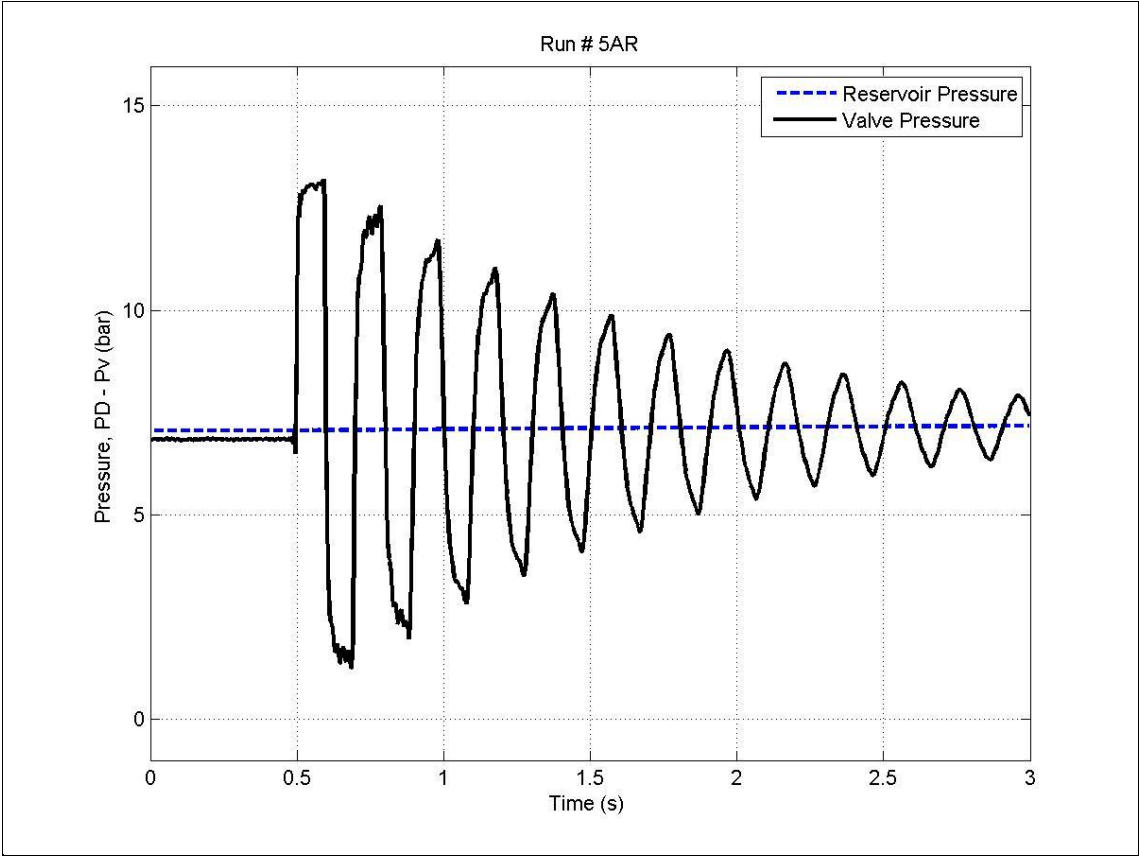
Figure(C.2) Experiment No. 2.



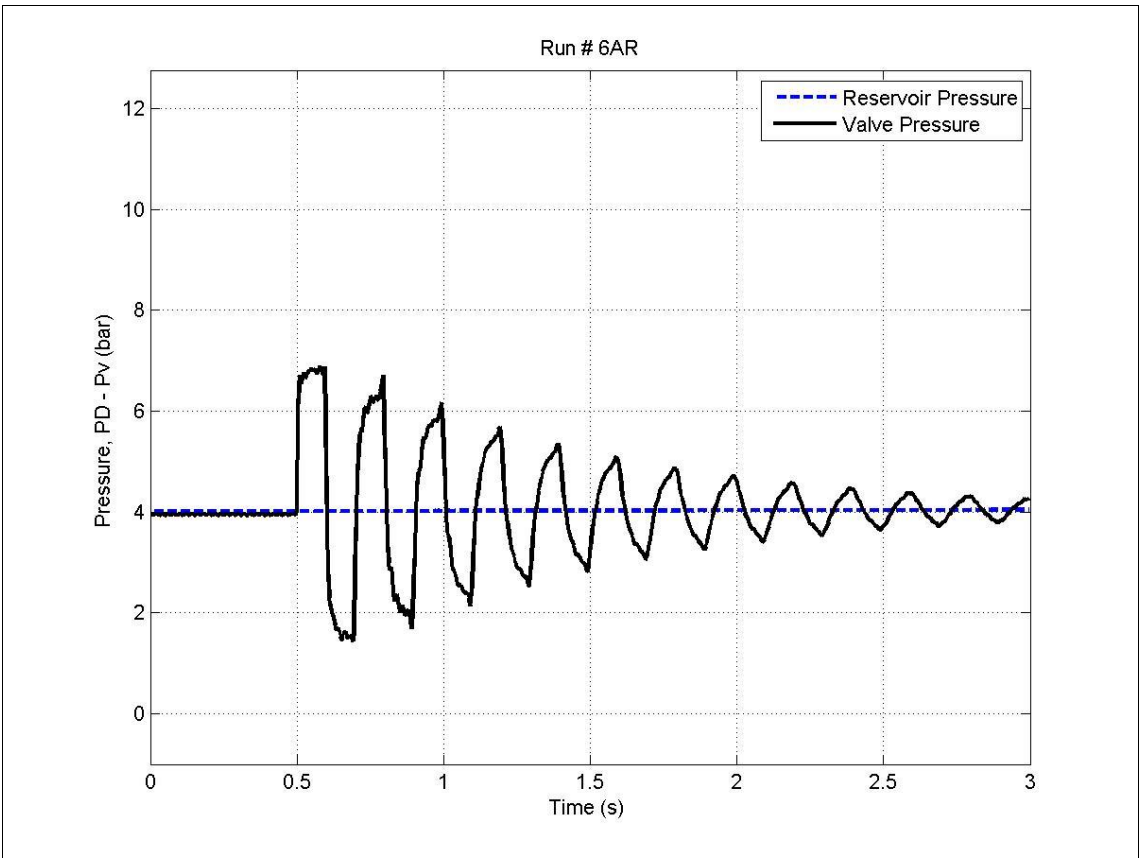
Figure(C.3) Experiment No. 3.



Figure(C.4) Experiment No. 4.

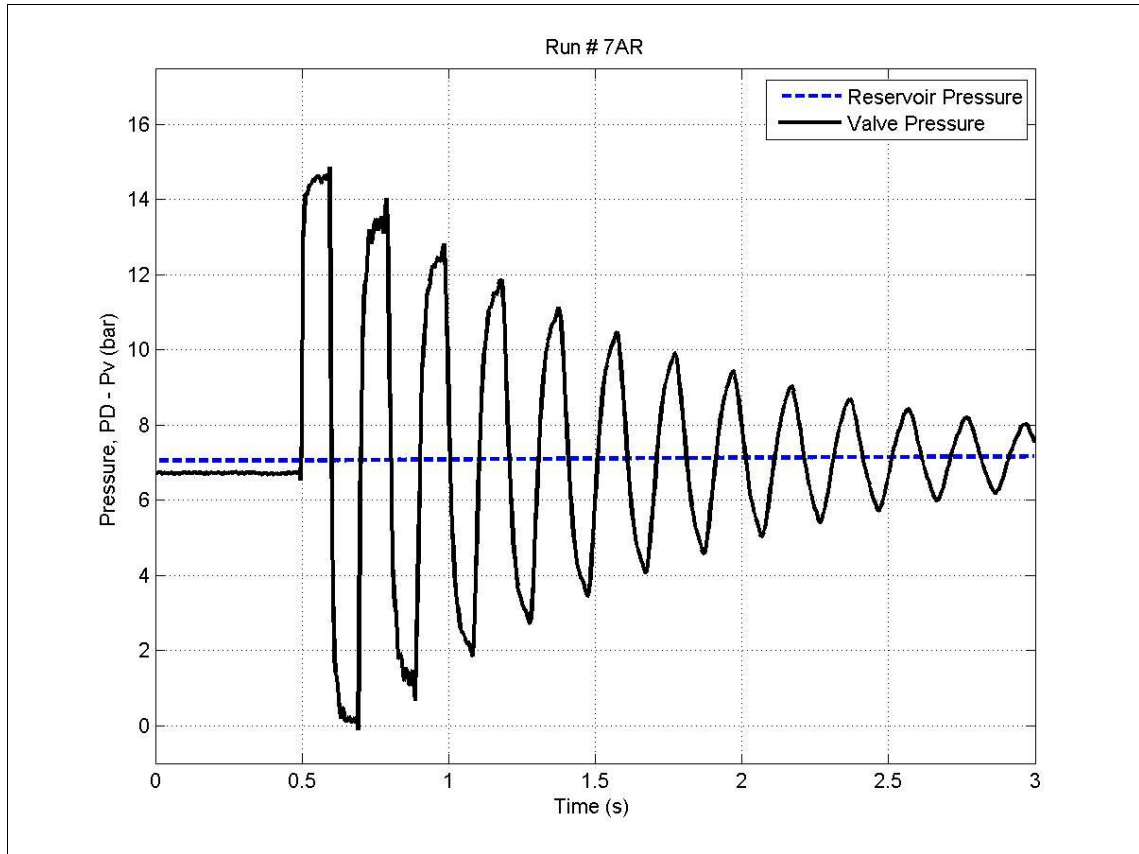


Figure(C.5) Experiment No. 5.

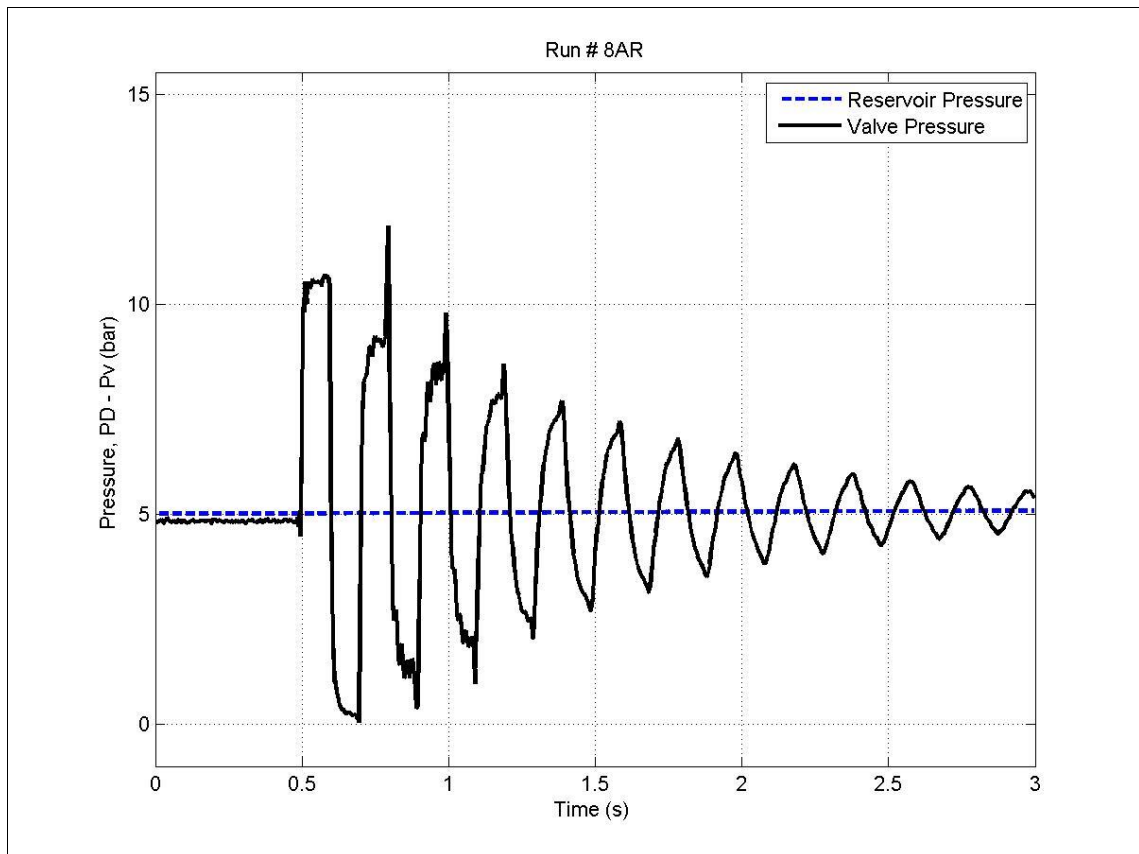


Figure(C.6) Experiment No. 6.

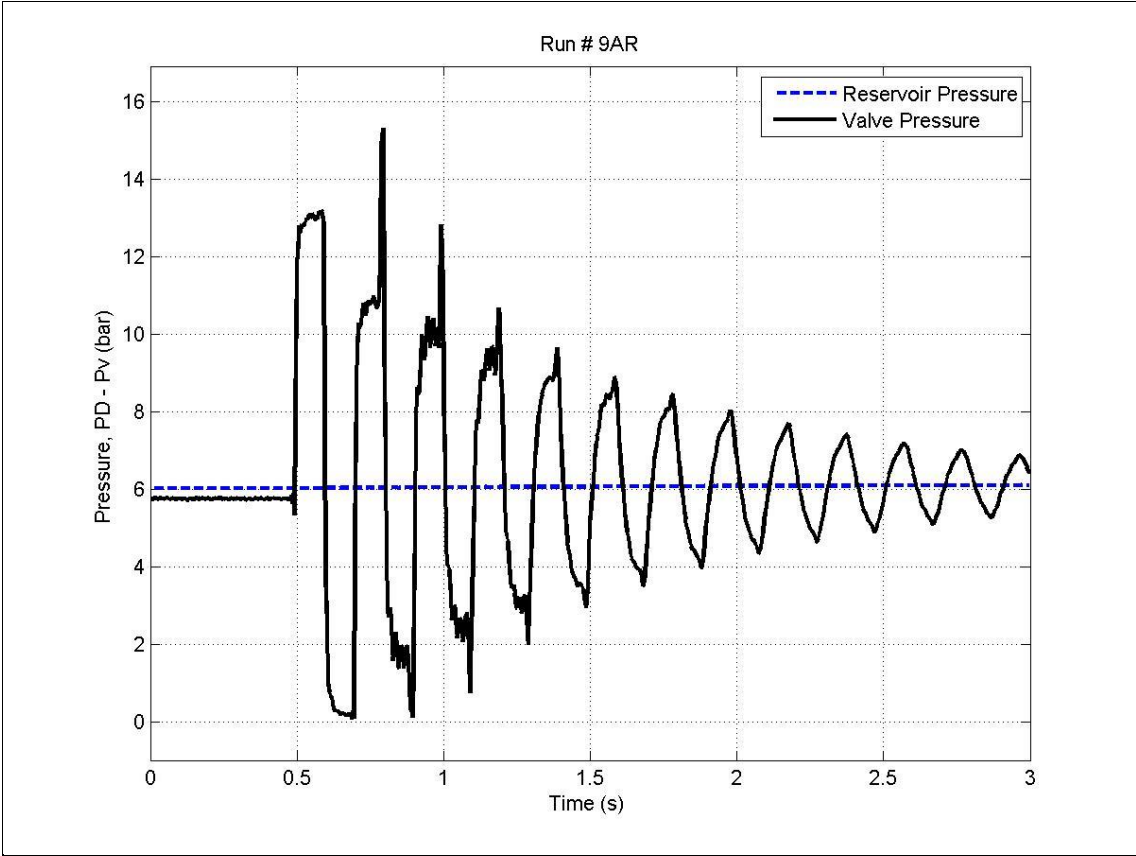
C.2 Experiments of 1st transition zone, runs[7-10]



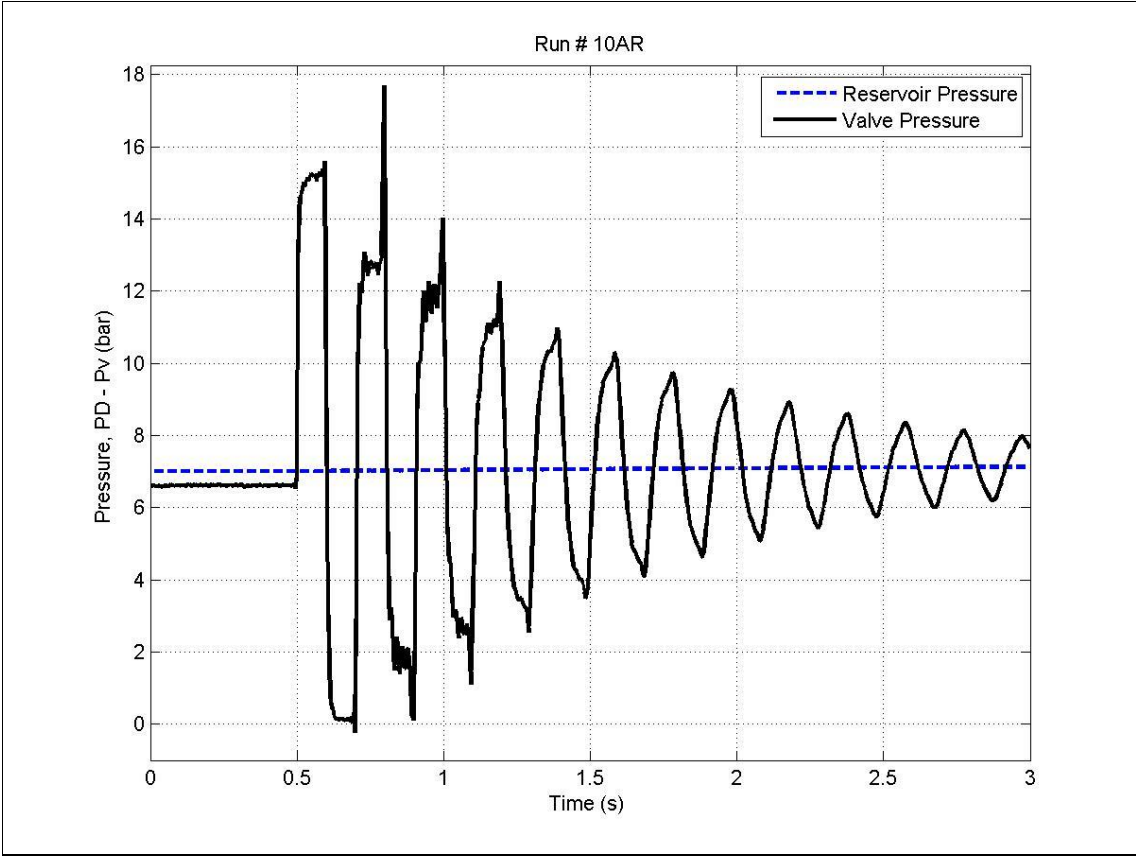
Figure(C.7) Experiment No. 7.



Figure(C.8) Experiment No. 8.

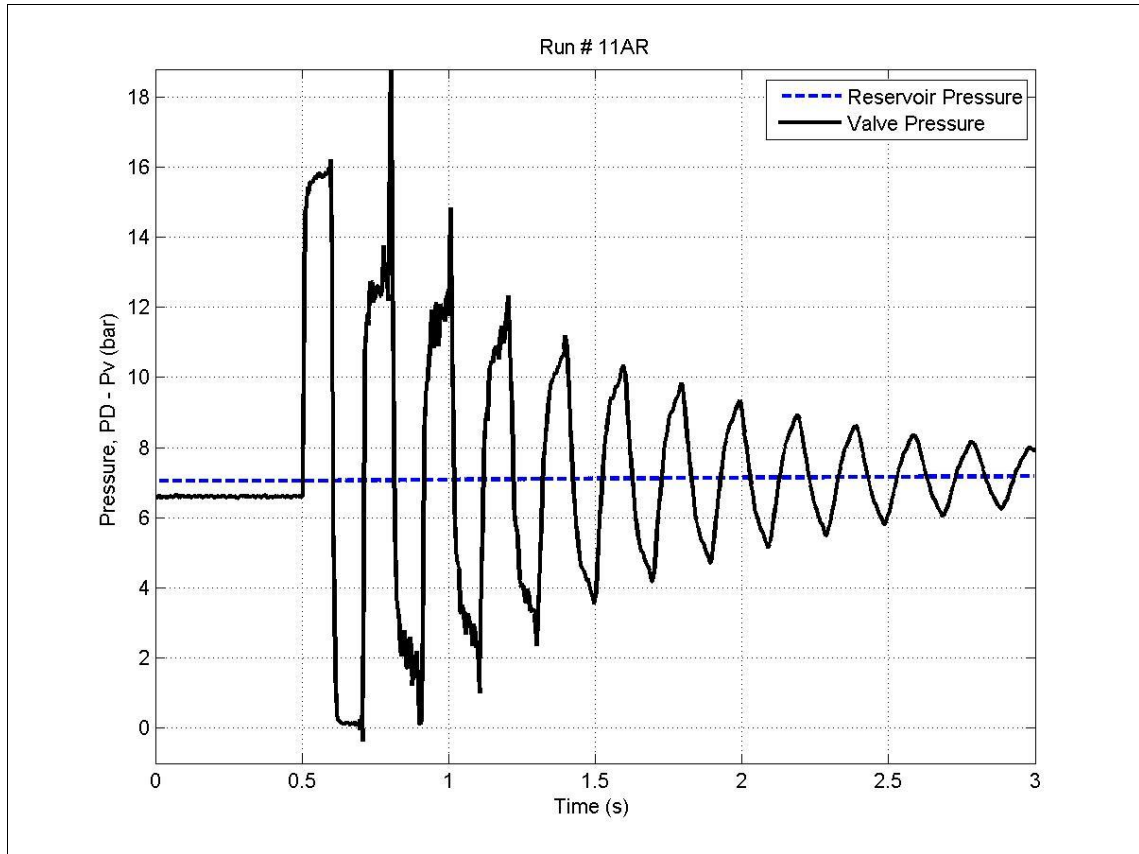


Figure(C.9) Experiment No. 9.

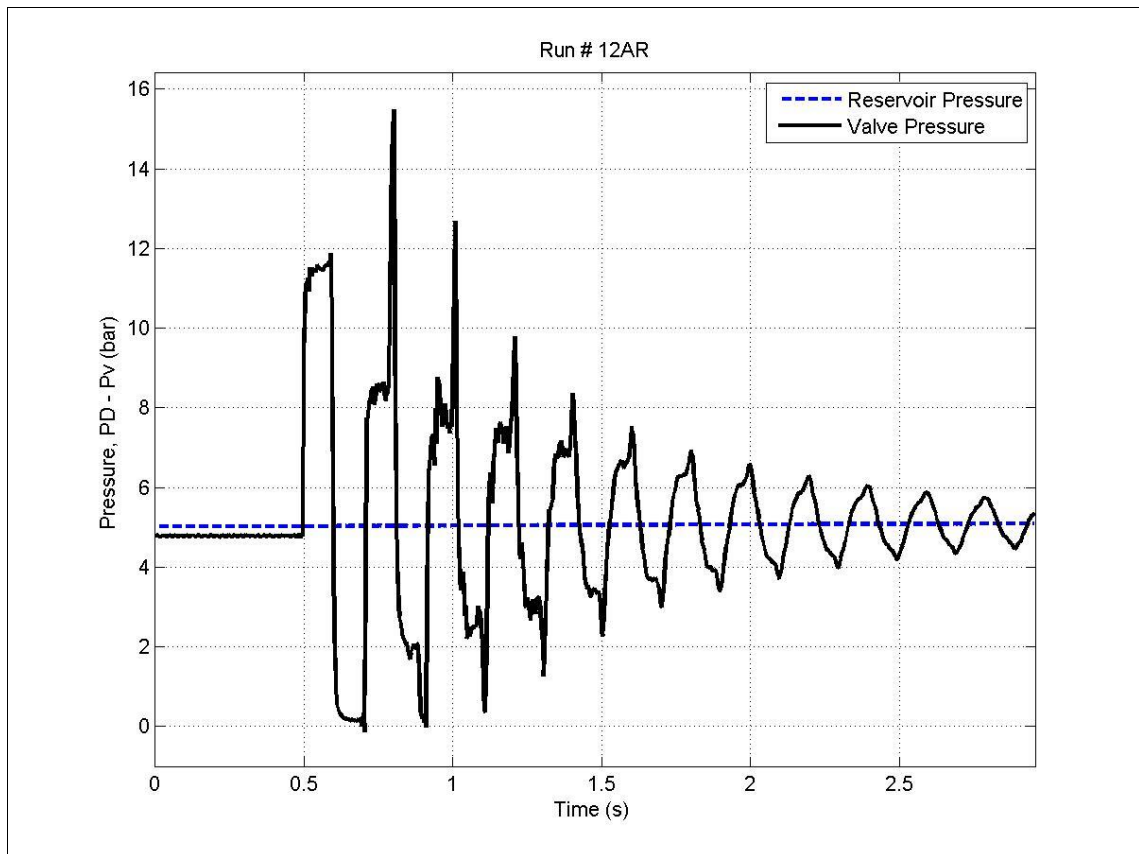


Figure(C.10) Experiment No. 10.

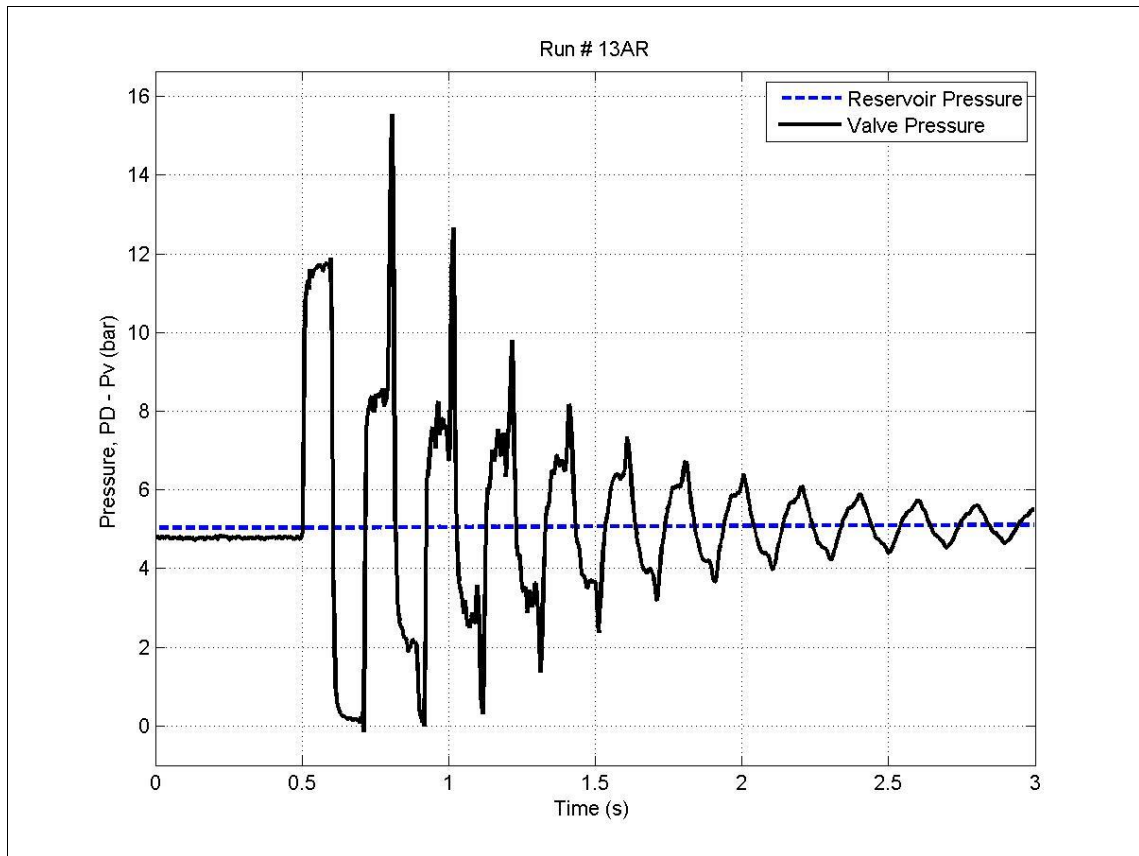
C.3 Experiments of Limited column separation, runs[11-25].



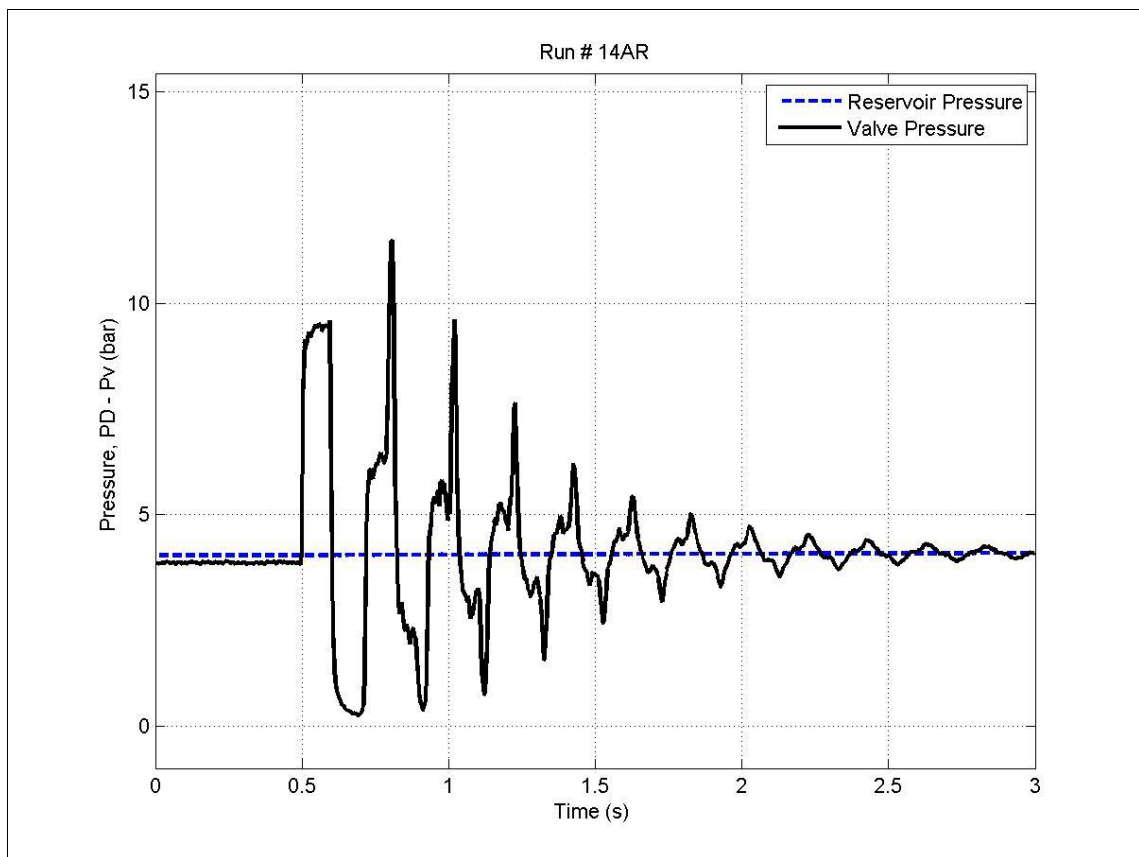
Figure(C.11) Experiment No. 11.



Figure(C.12) Experiment No. 12.

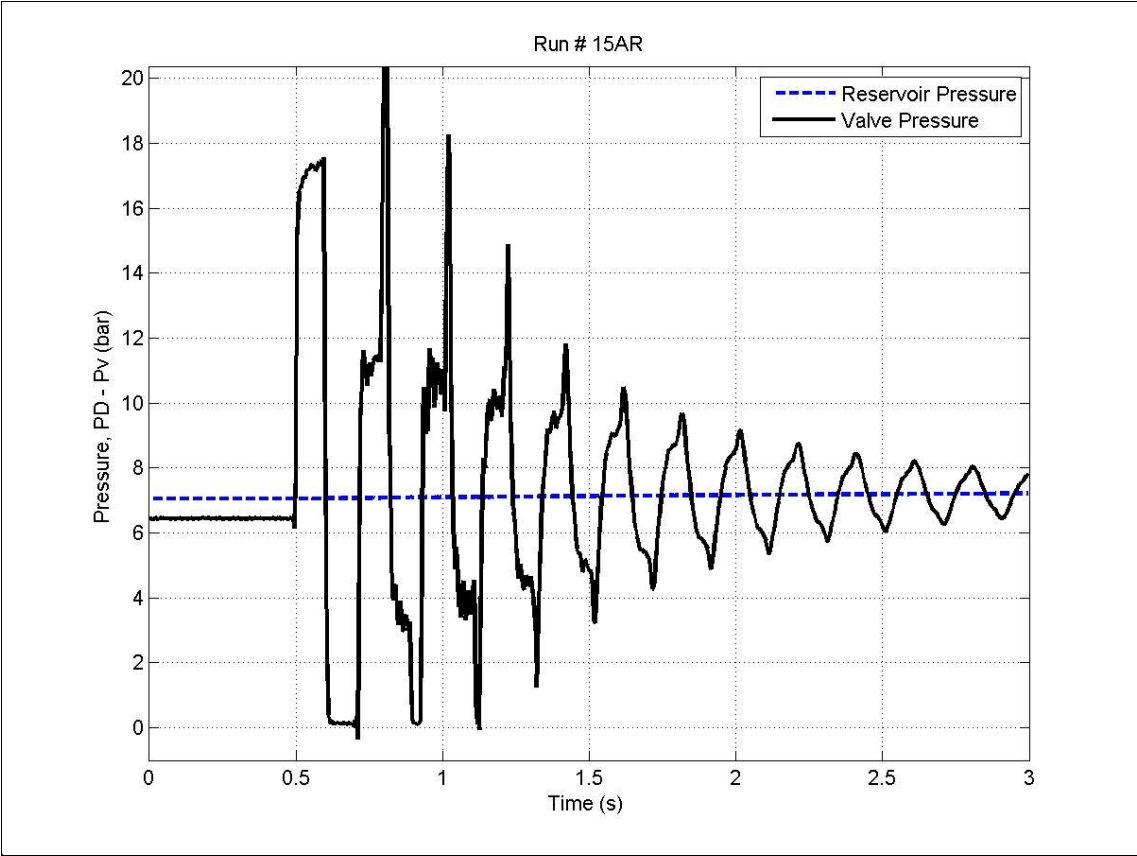


Figure(C.13) Experiment No. 13.

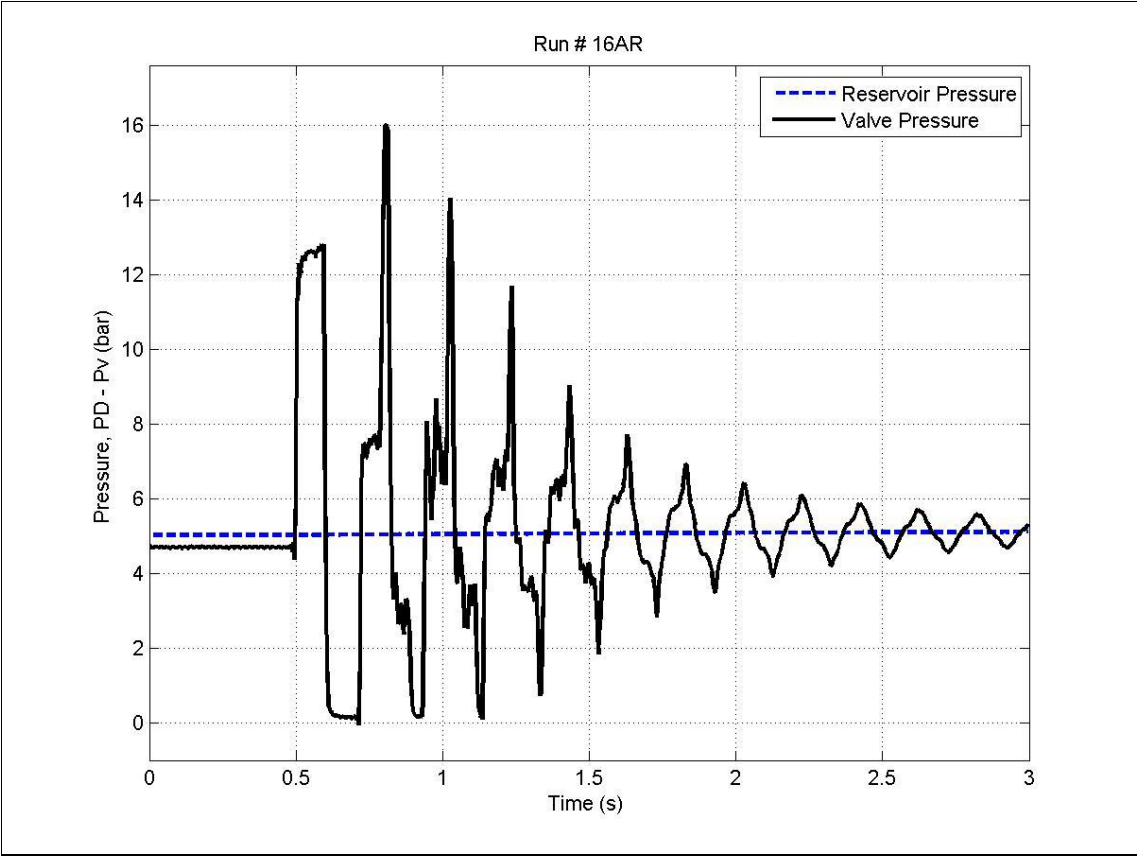


Figure(C.14) Experiment No. 14.



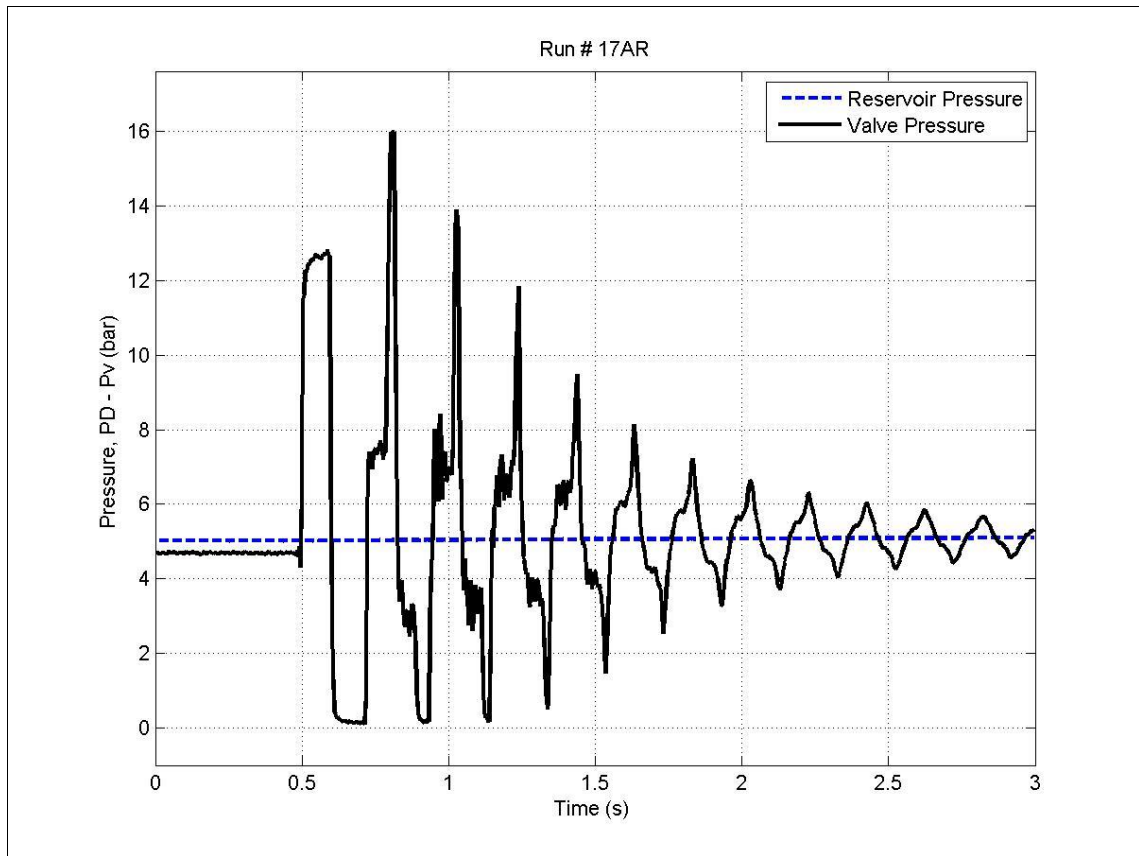


Figure(C.15) Experiment No. 15.

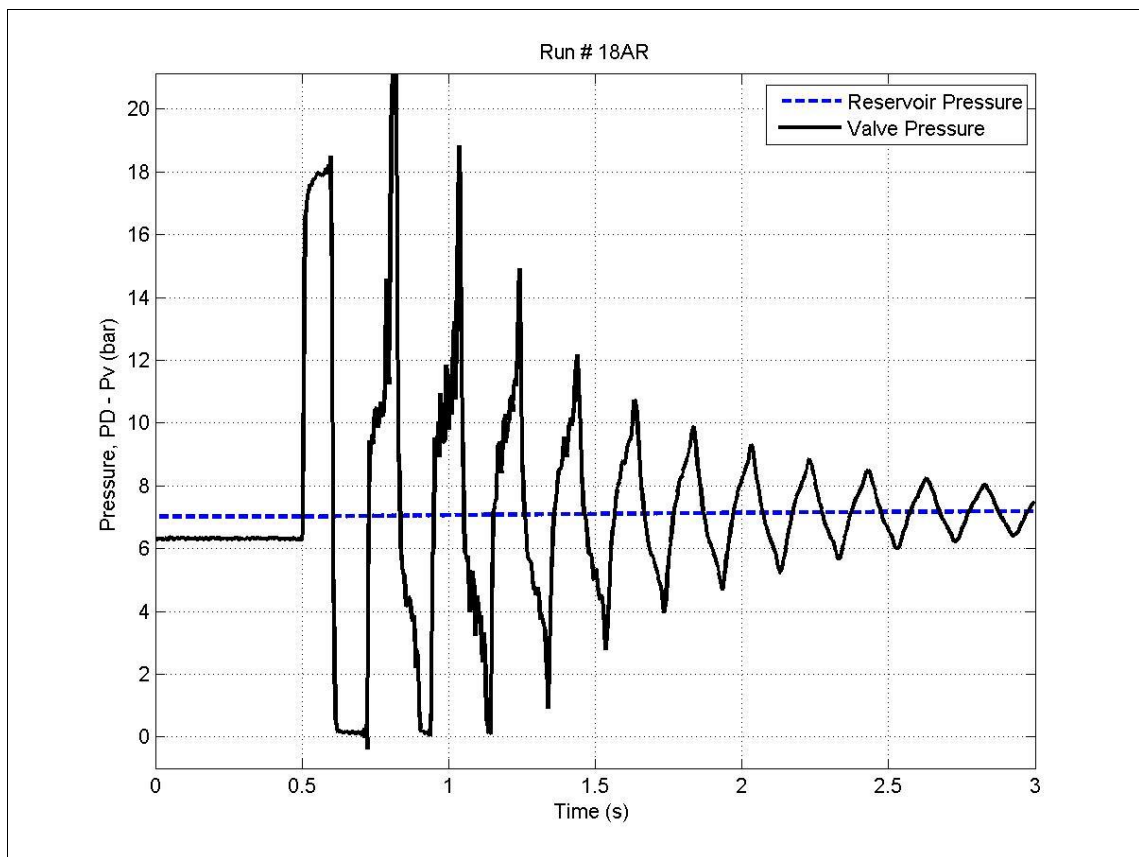


Figure(C.16) Experiment No. 16.

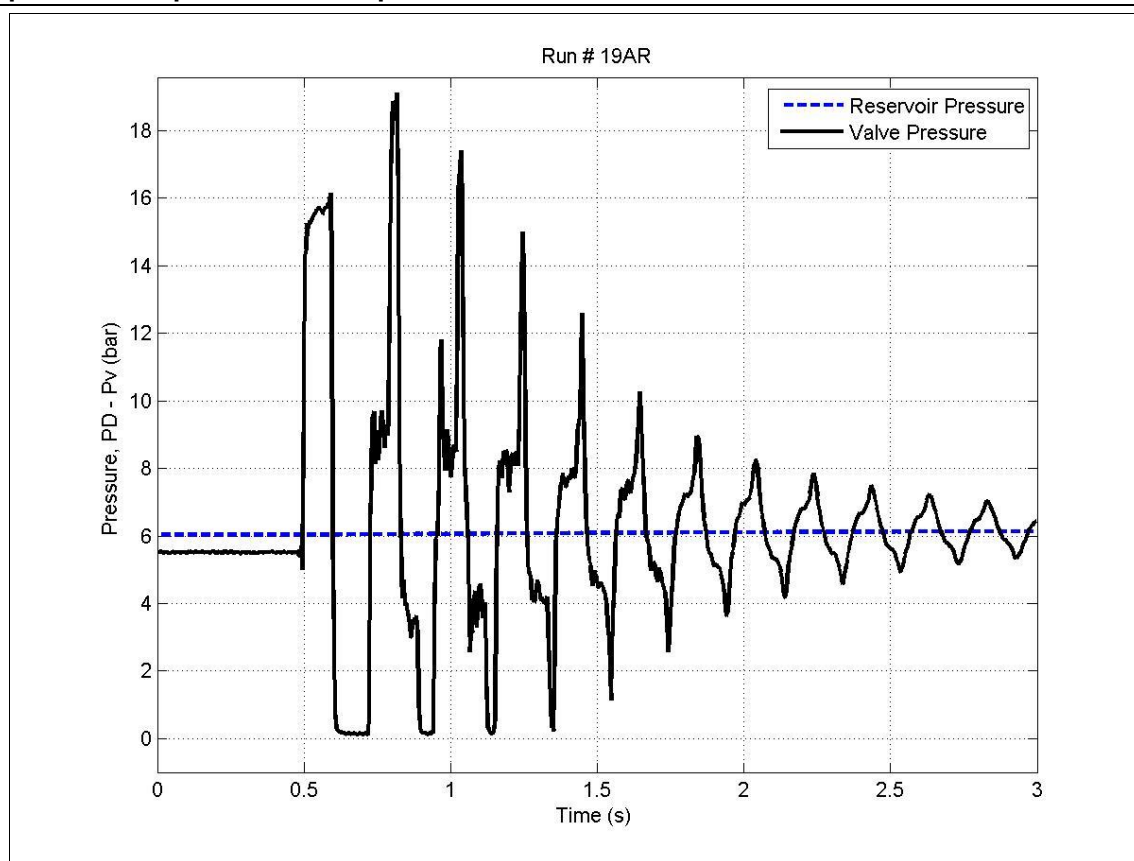




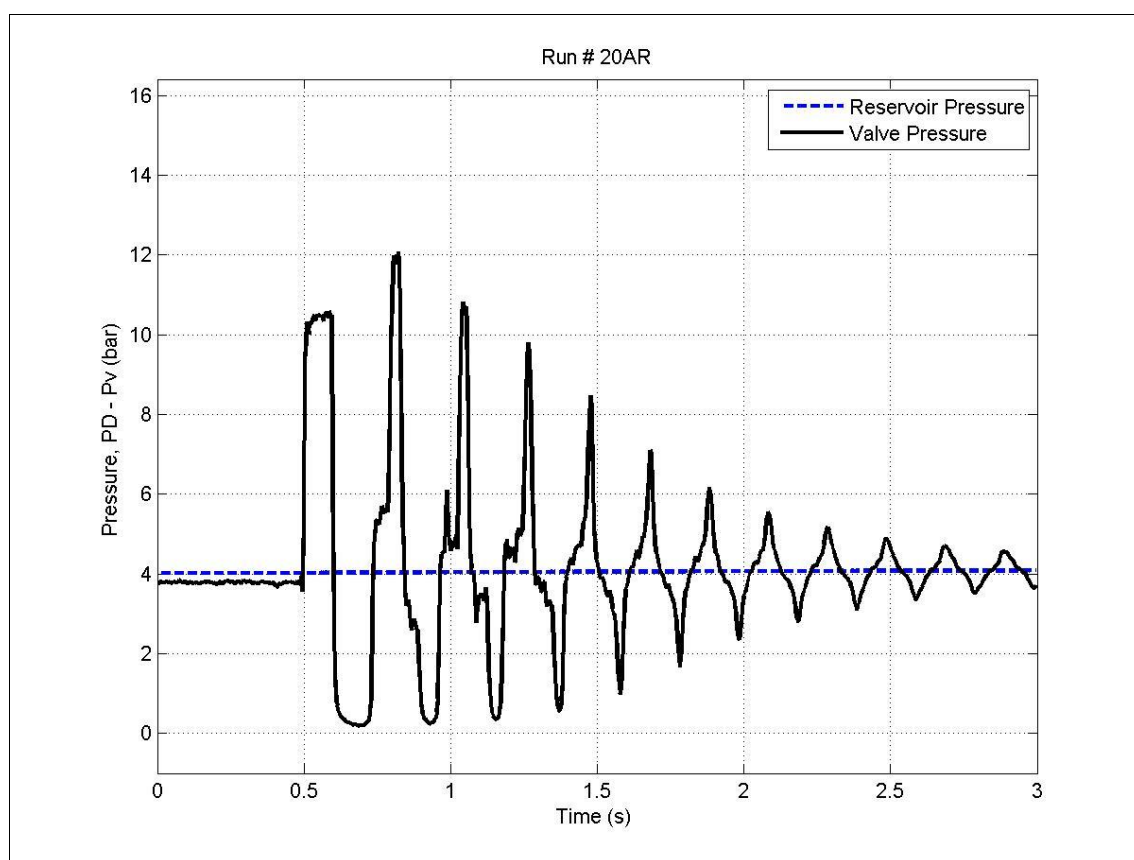
Figure(C.17) Experiment No. 17.



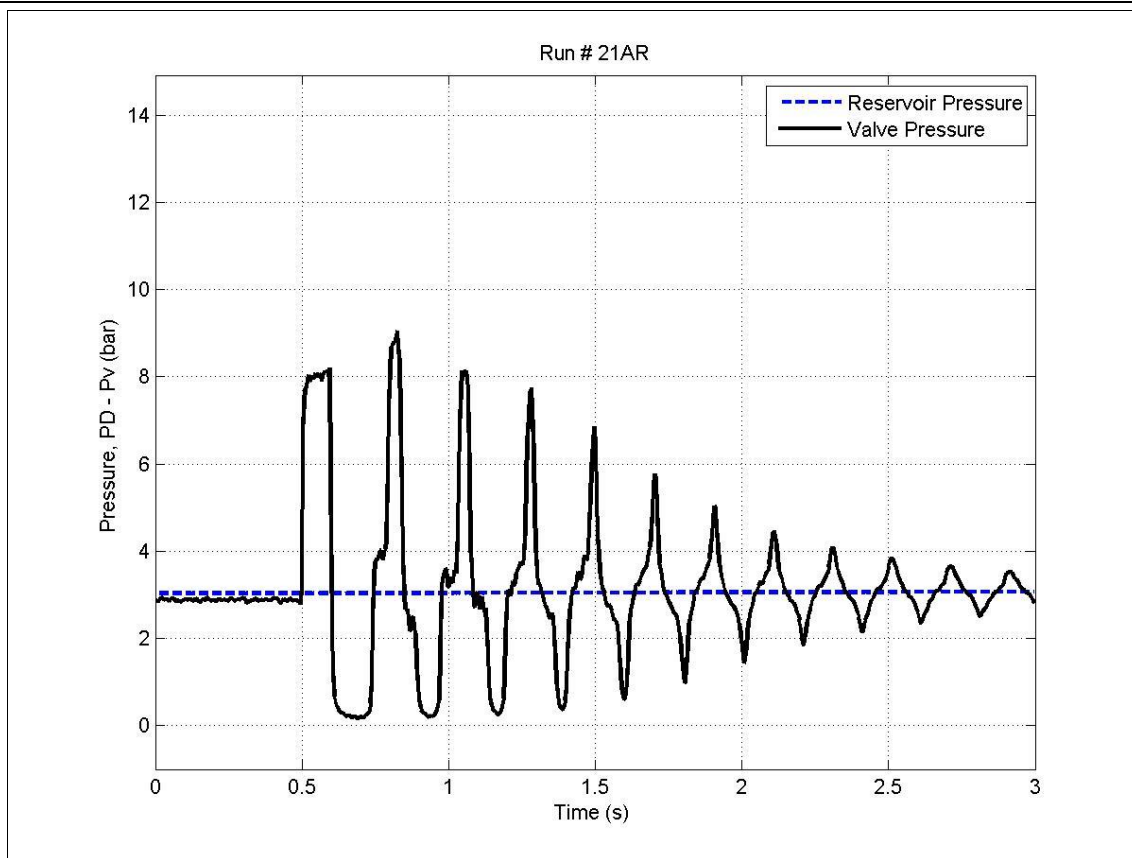
Figure(C.18) Experiment No. 18.



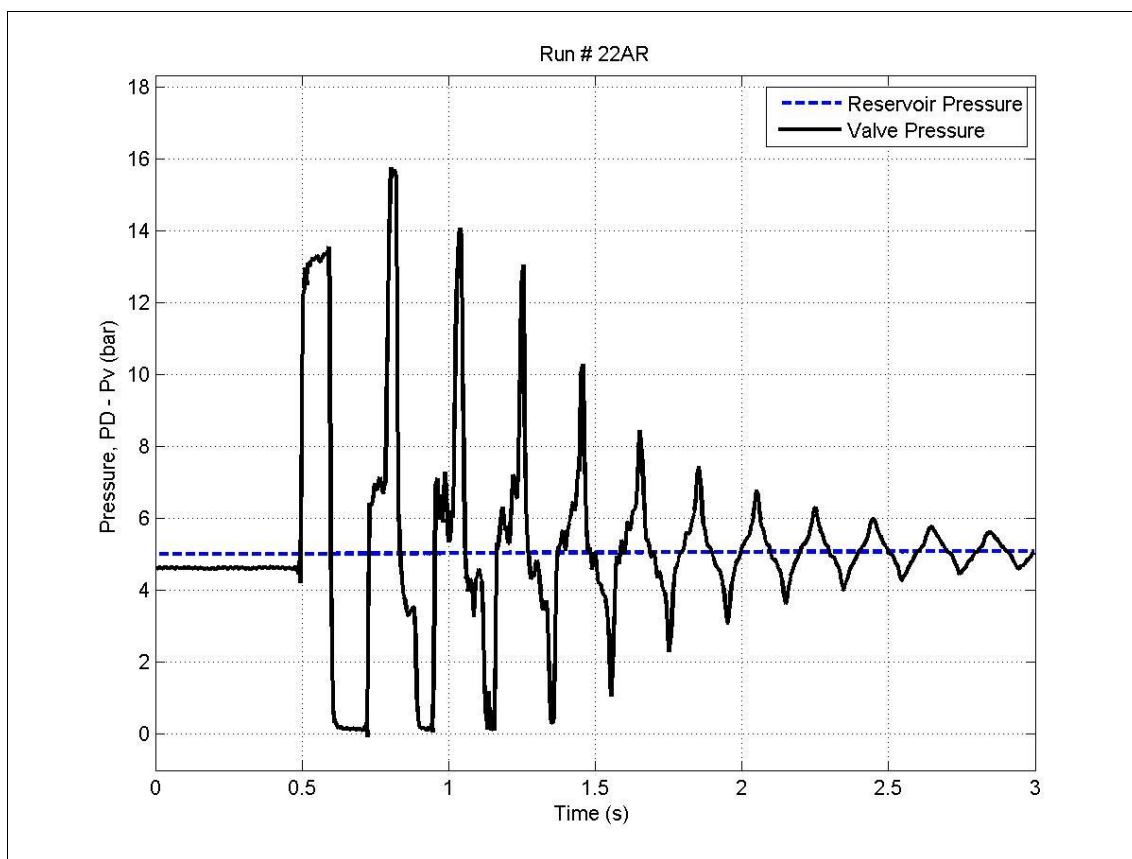
Figure(C.19) Experiment No. 19.



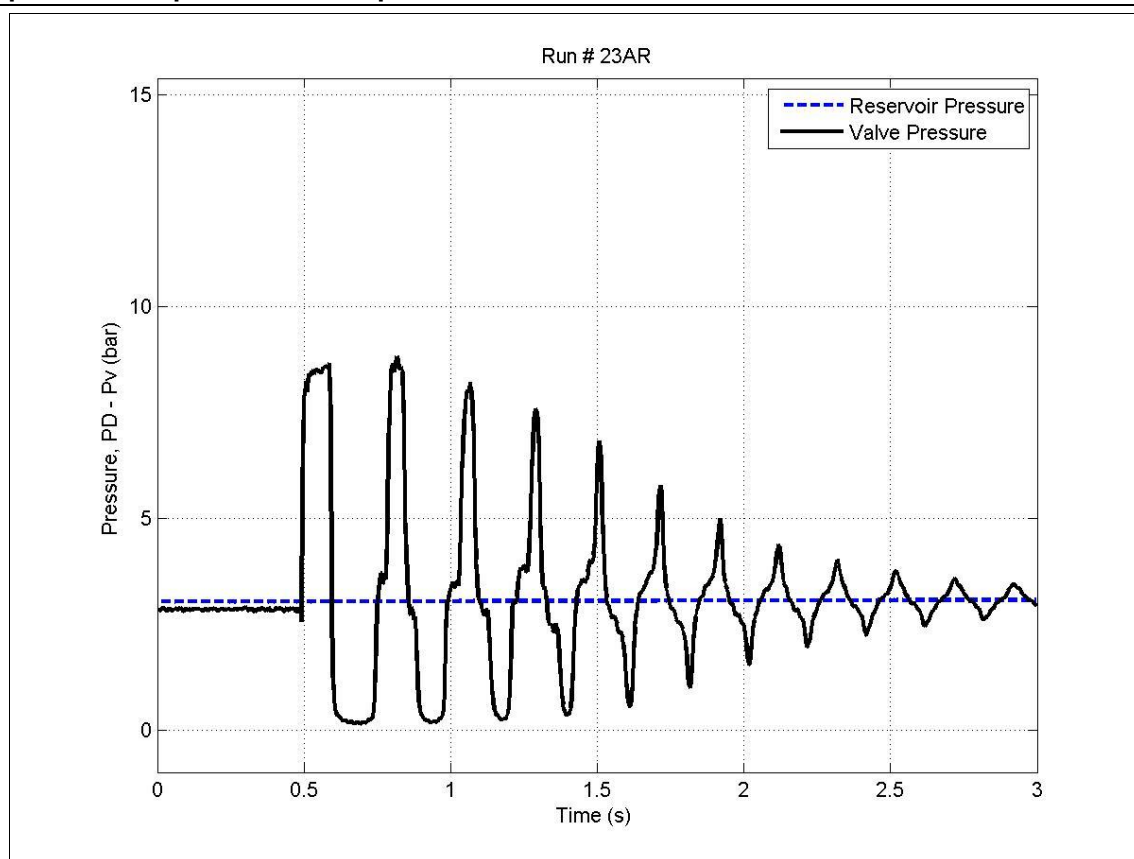
Figure(C.20) Experiment No. 20.



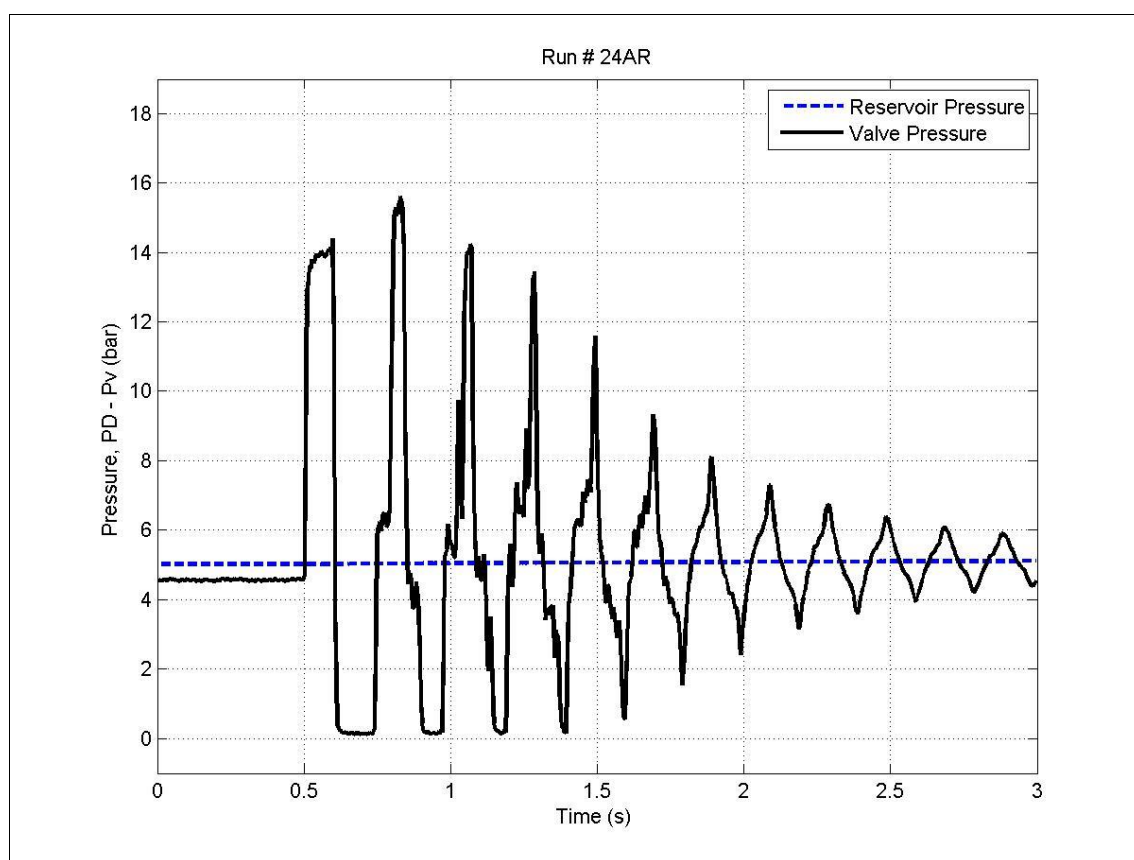
Figure(C.21) Experiment No. 21.



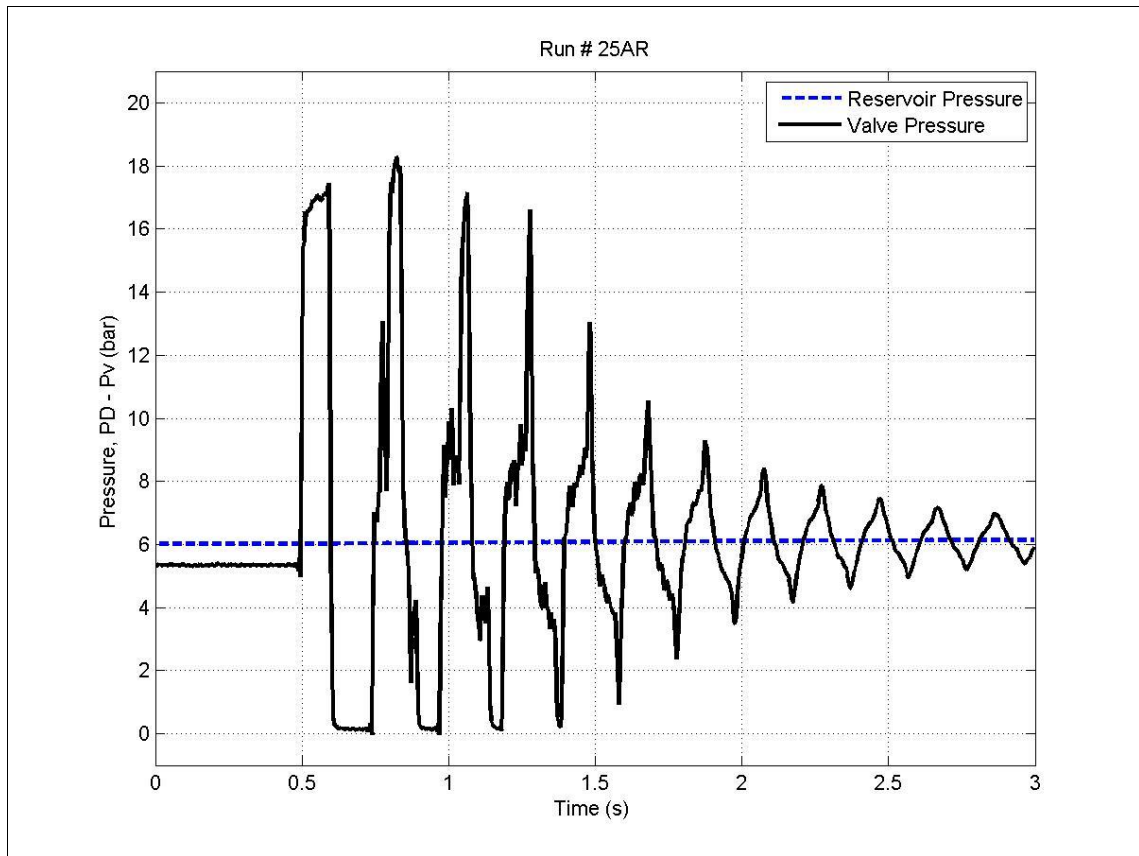
Figure(C.22) Experiment No. 22.



Figure(C.23) Experiment No. 23.

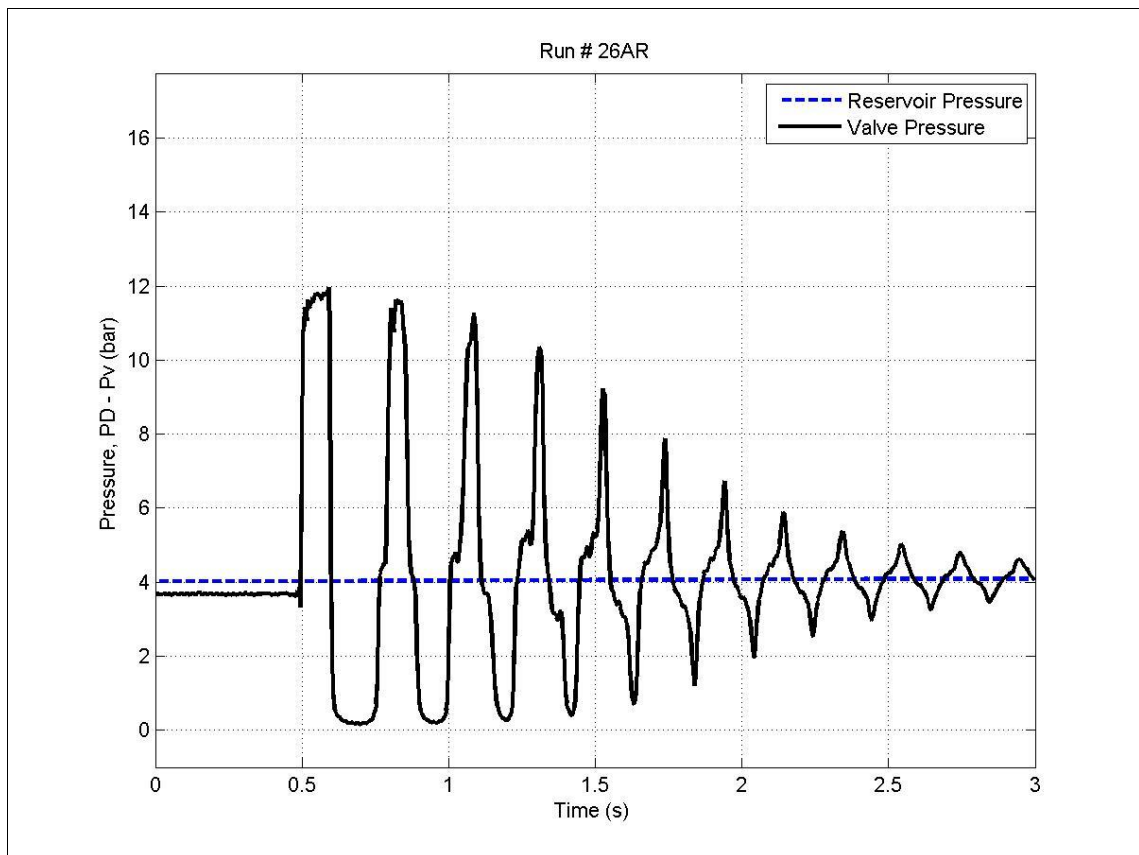


Figure(C.24) Experiment No. 24.

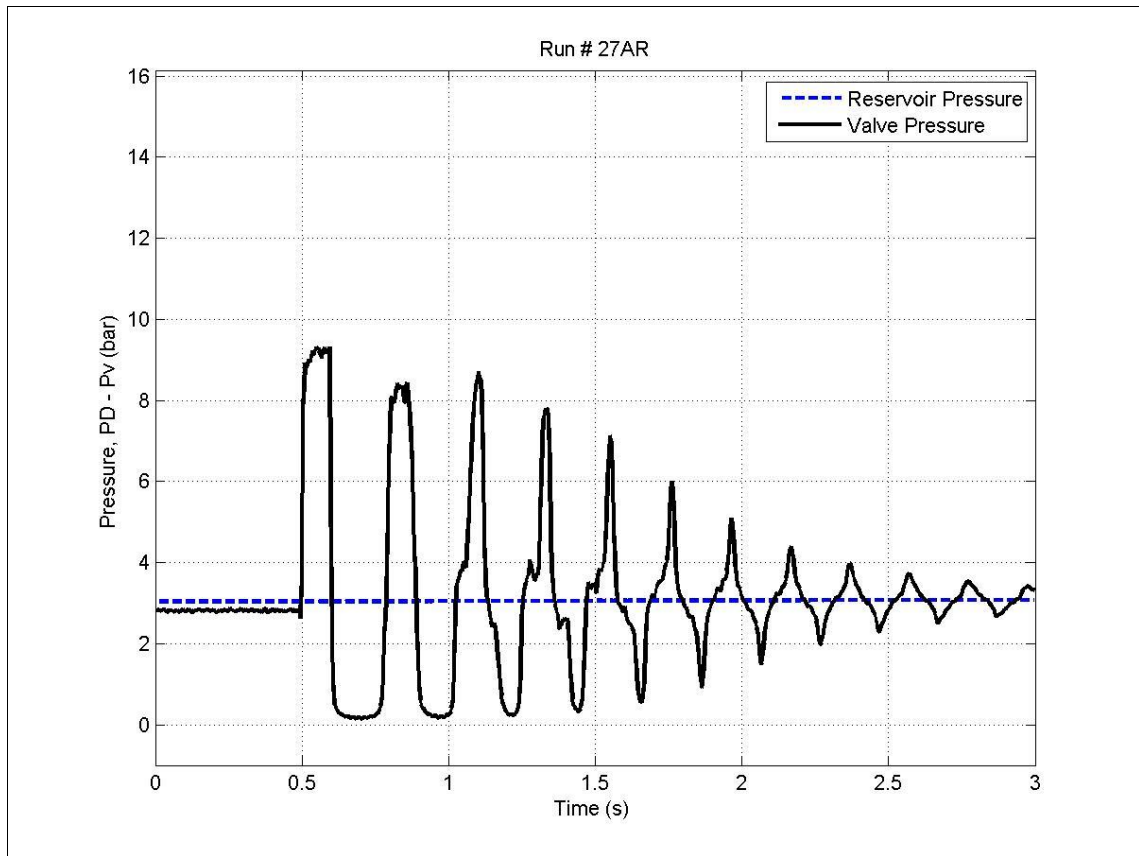


Figure(C.25) Experiment No. 25.

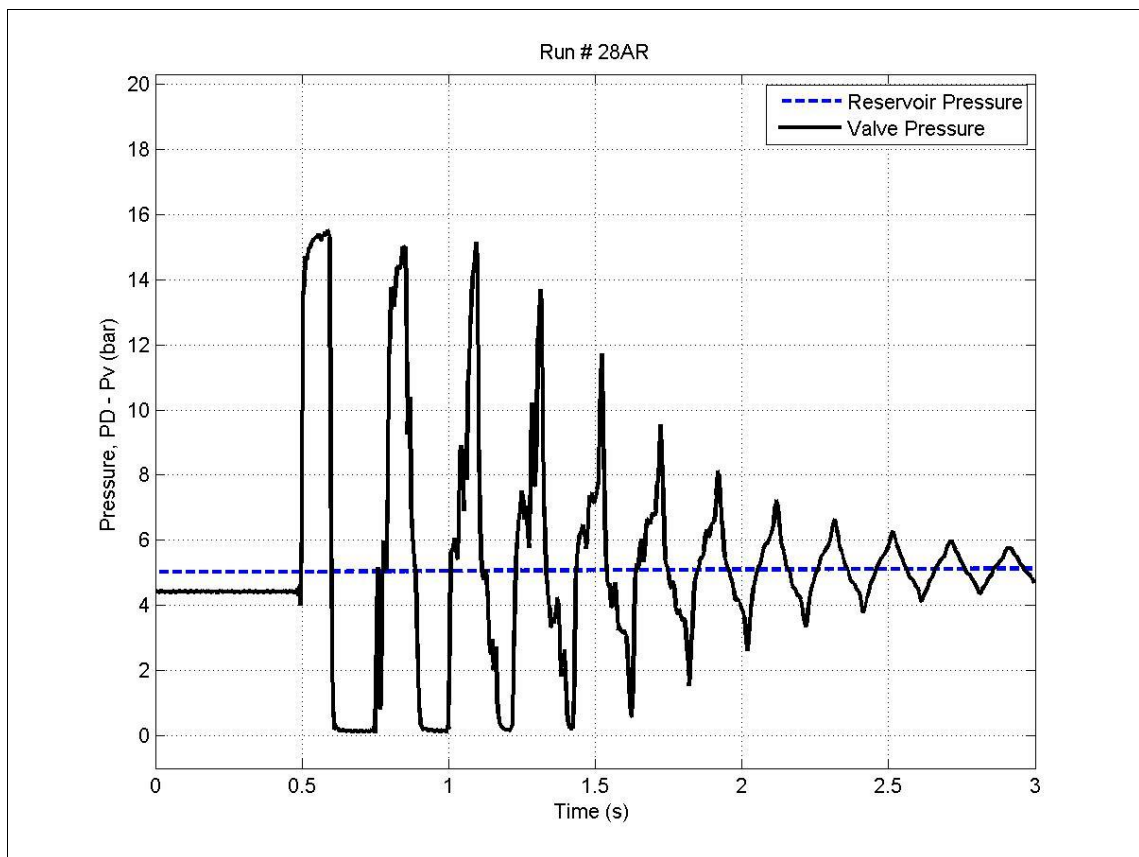
#### C.4 Experiments of 2nd transition zone, runs[26-36].



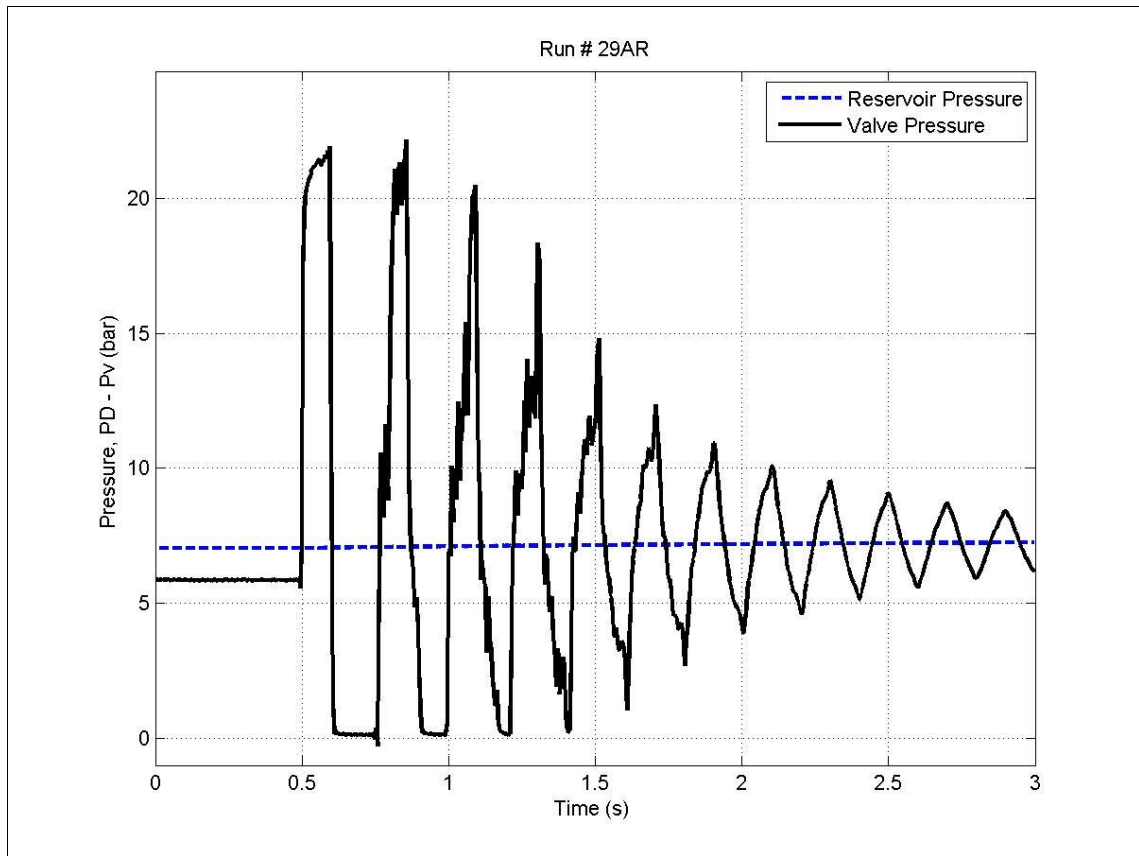
Figure(C.26) Experiment No. 26.



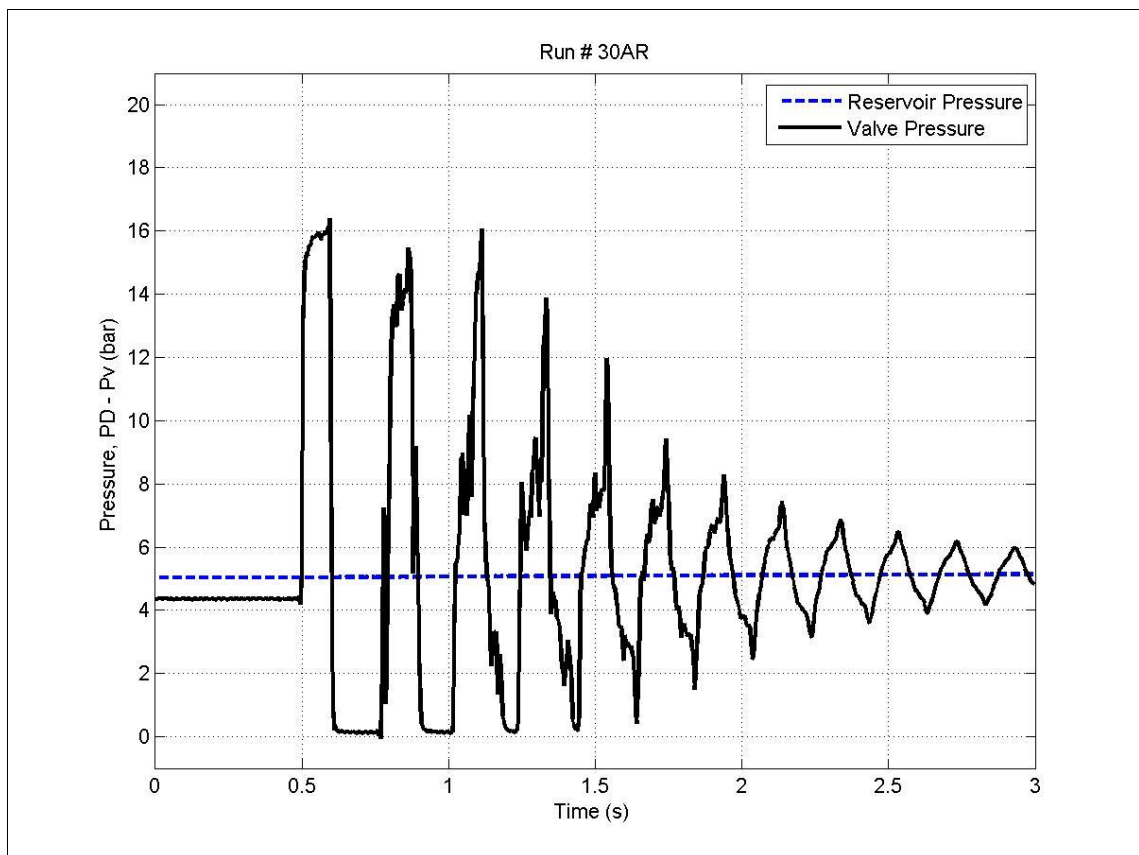
Figure(C.27) Experiment No. 27.



Figure(C.28) Experiment No. 28.

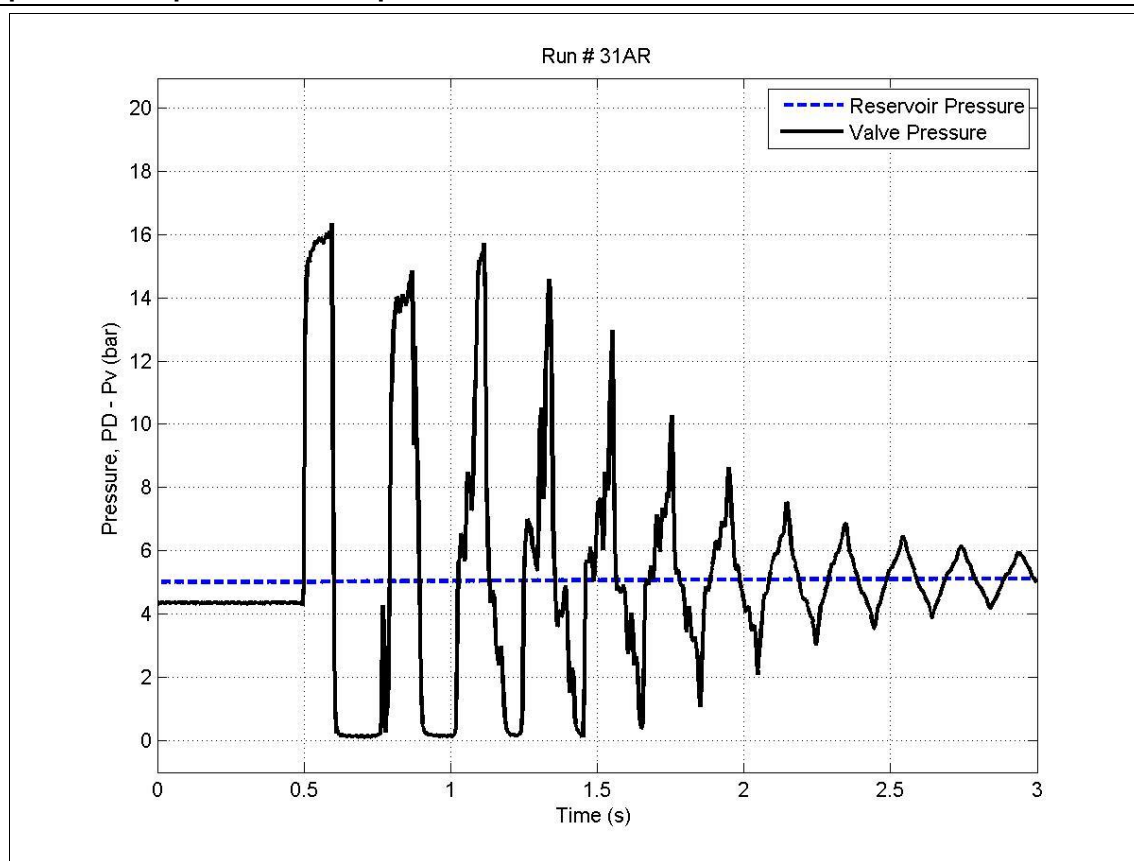


Figure(C.29) Experiment No. 29.

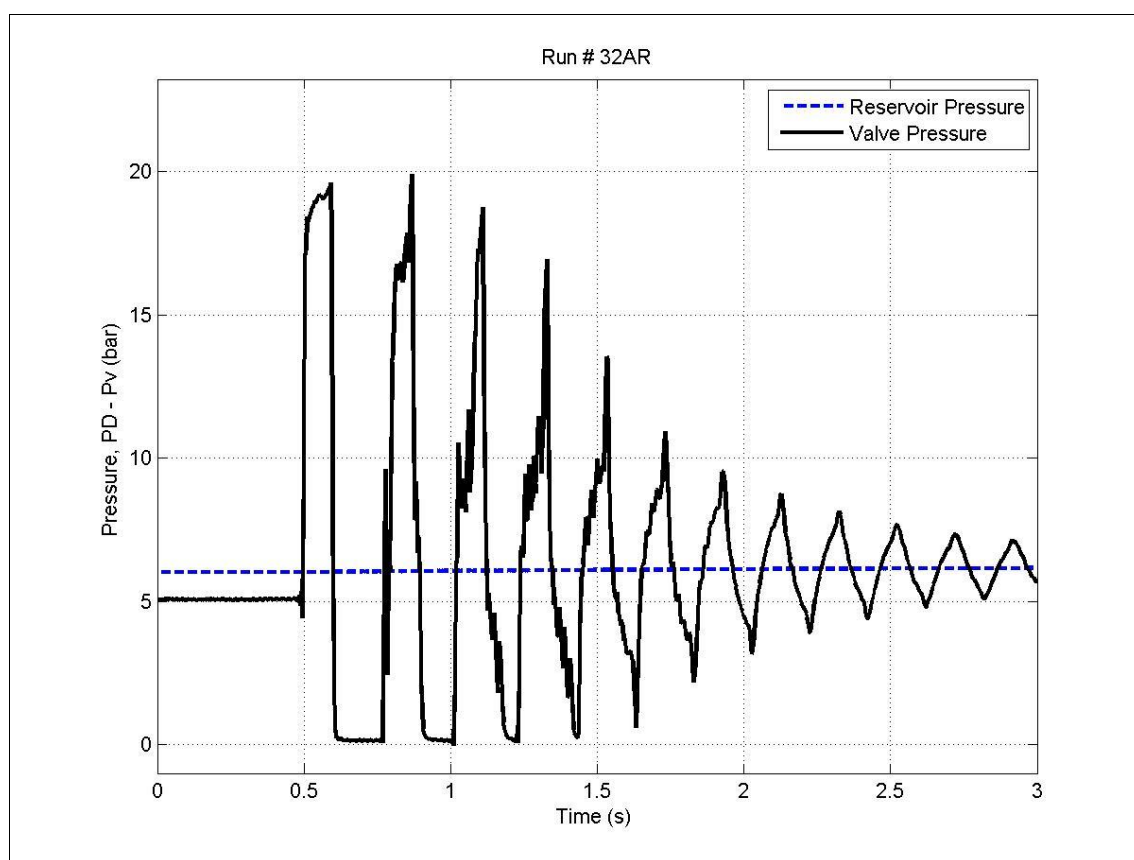


Figure(C.30) Experiment No. 30.



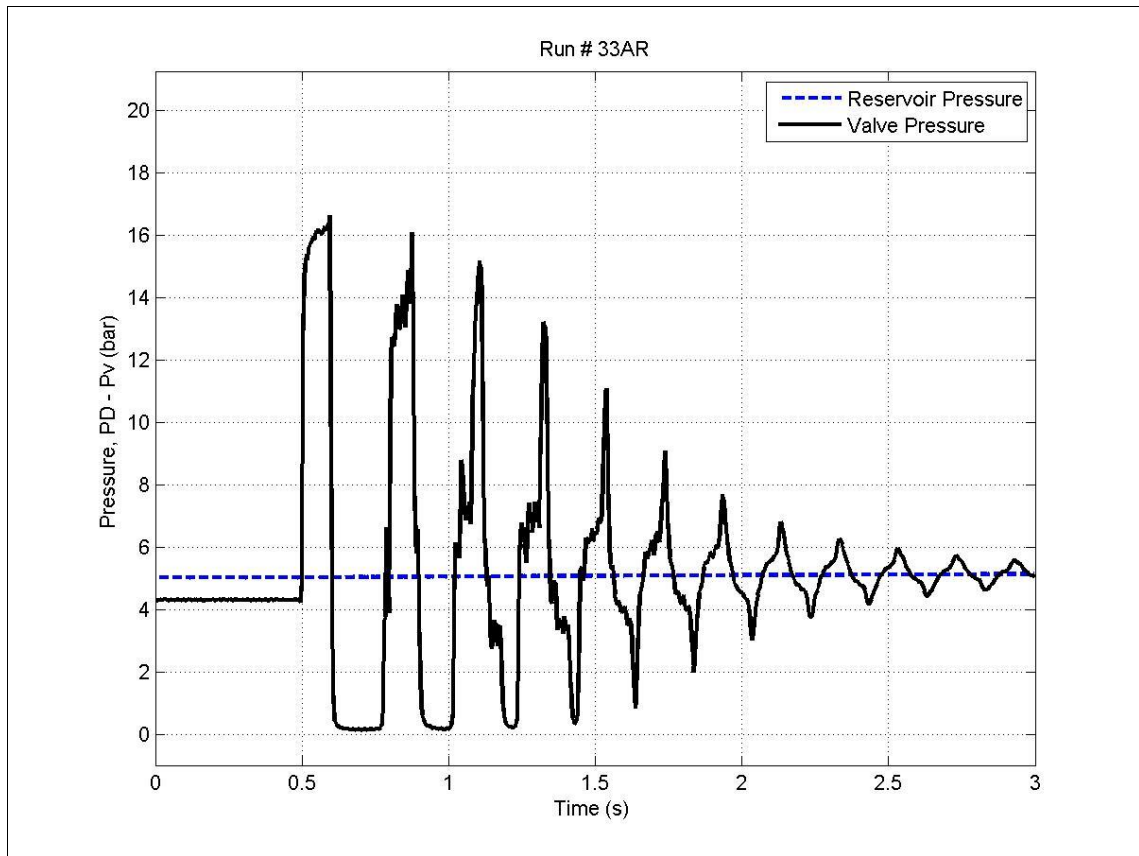


Figure(C.31) Experiment No. 31.

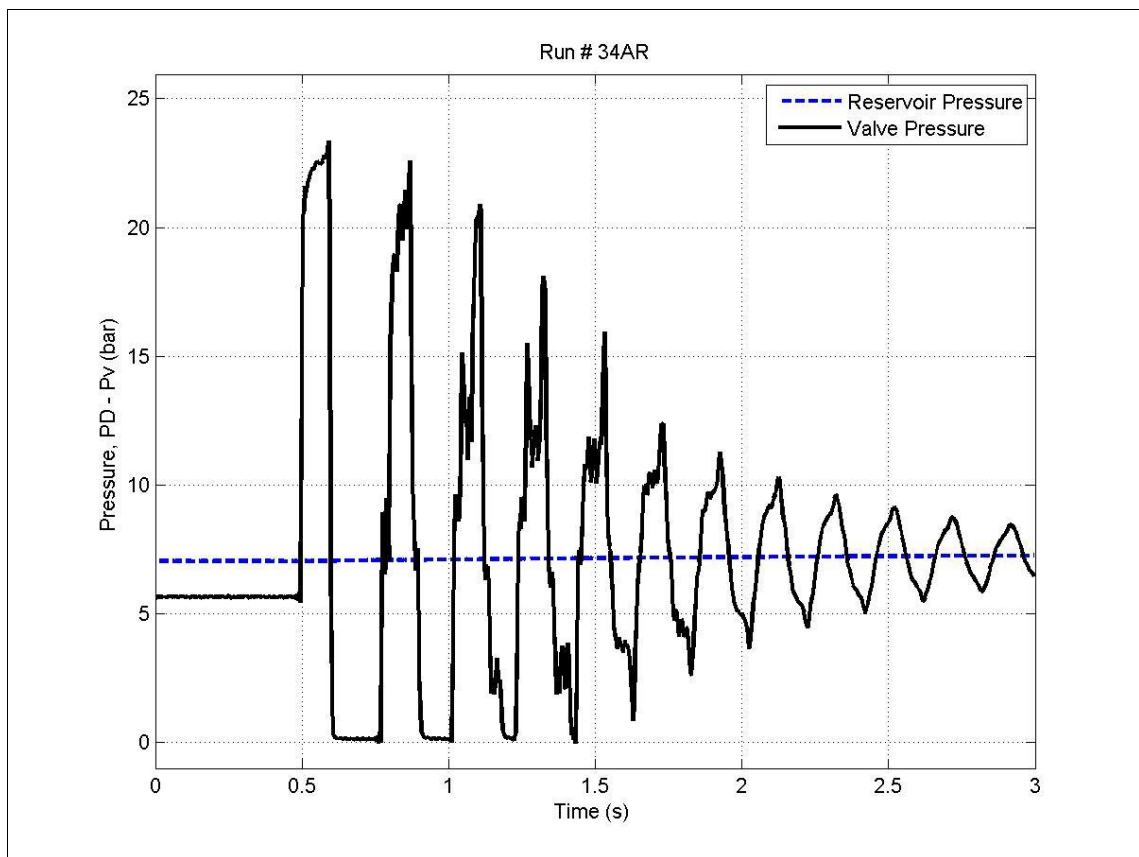


Figure(C.32) Experiment No. 32.

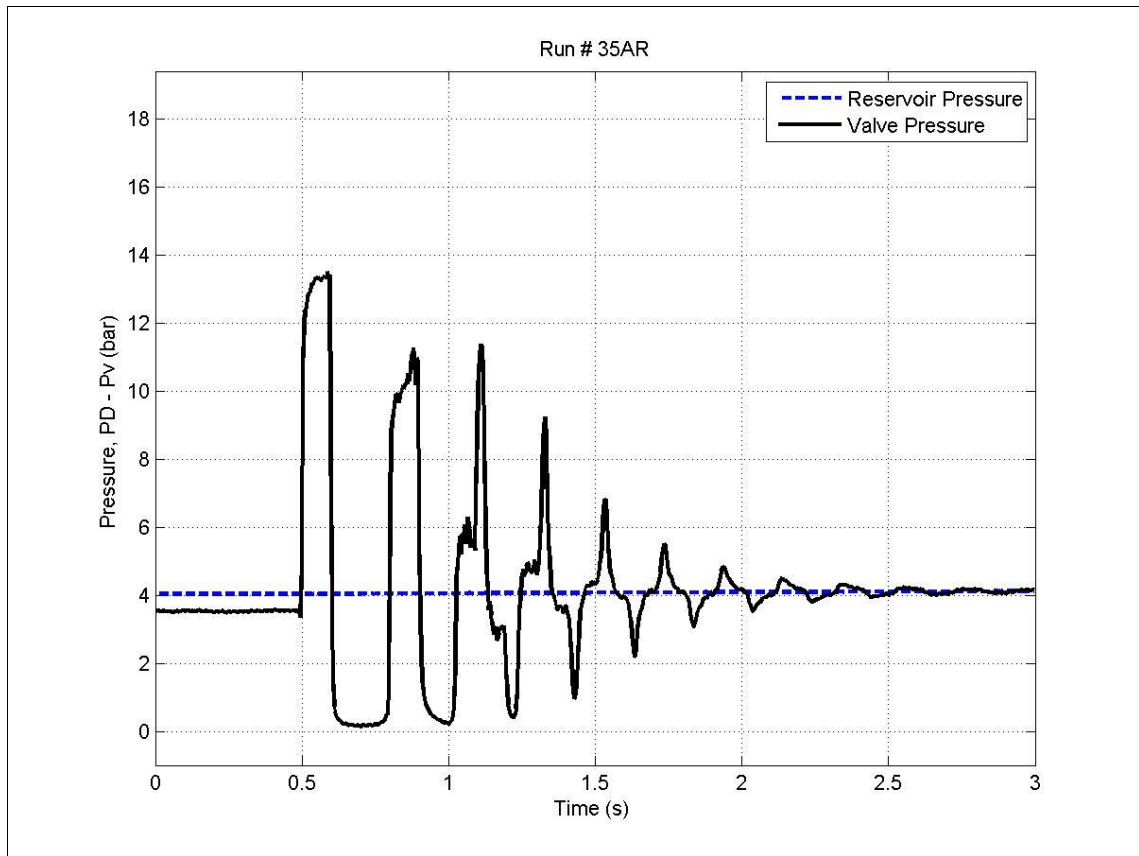




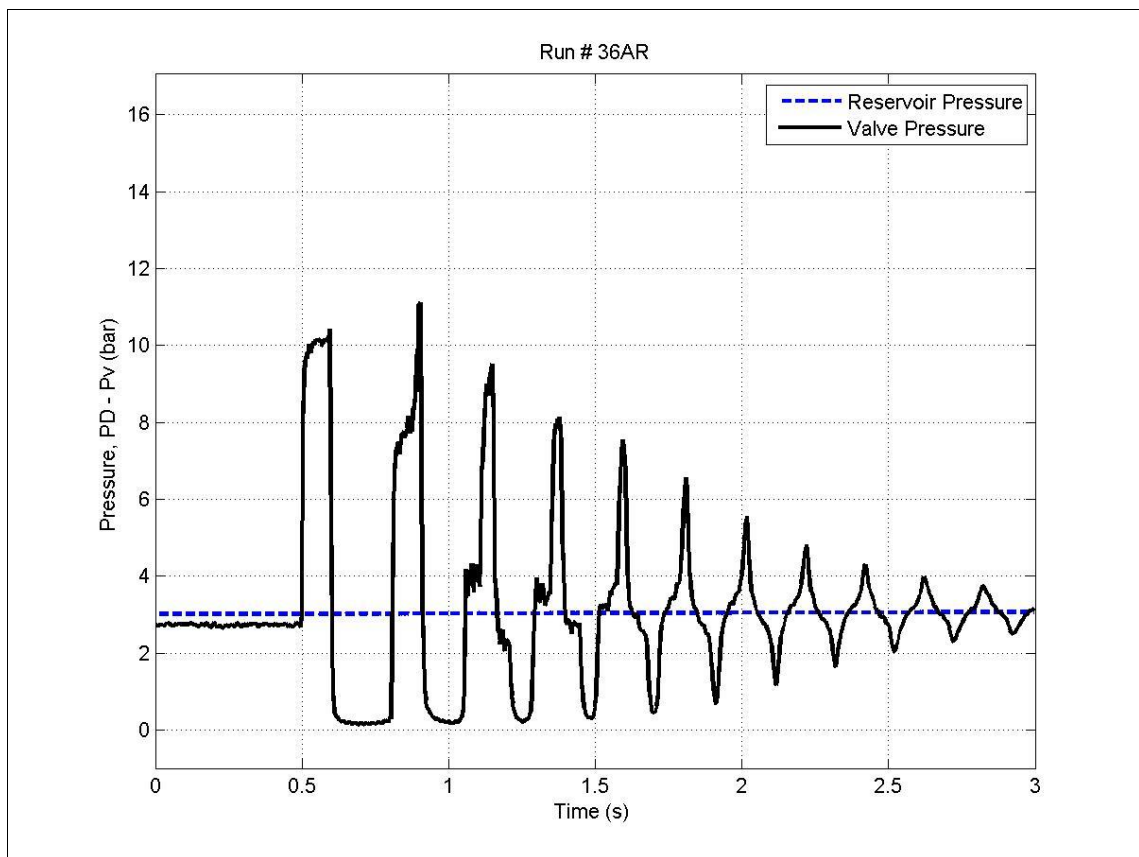
Figure(C.33) Experiment No. 33.



Figure(C.34) Experiment No. 34.

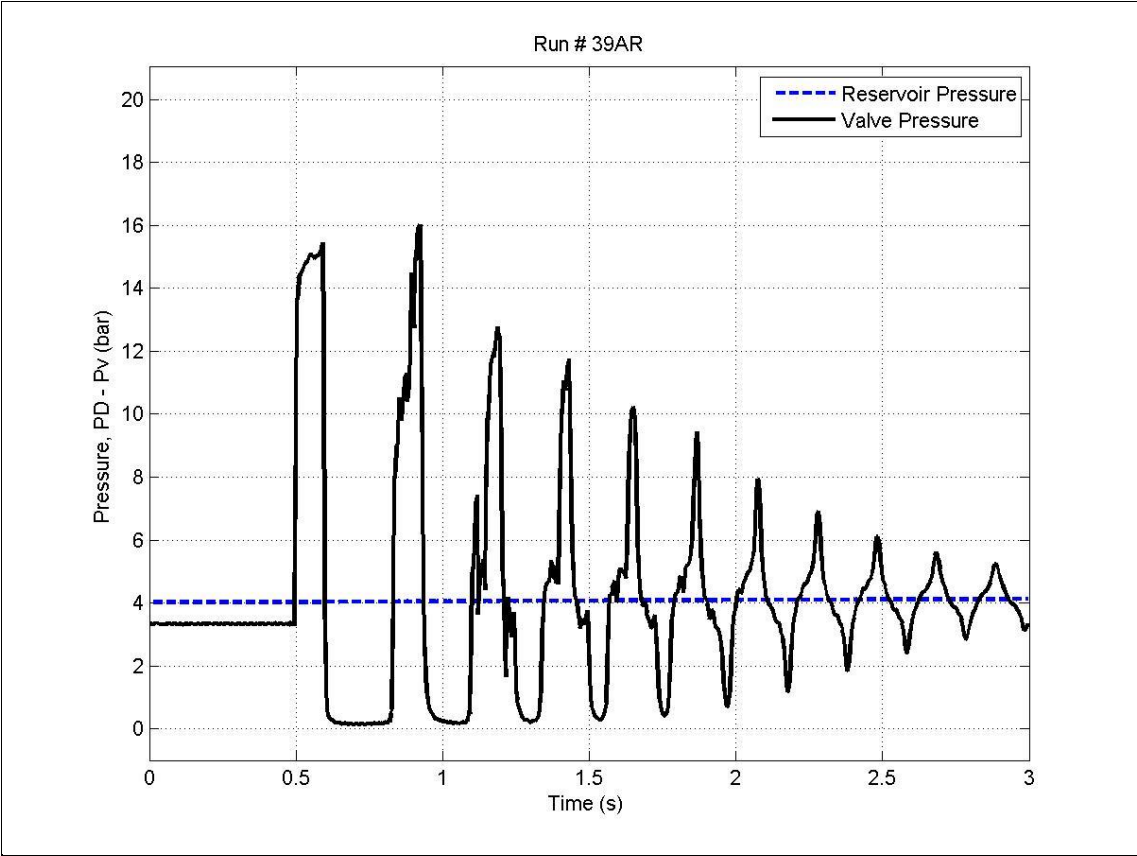


Figure(C.35) Experiment No. 35.

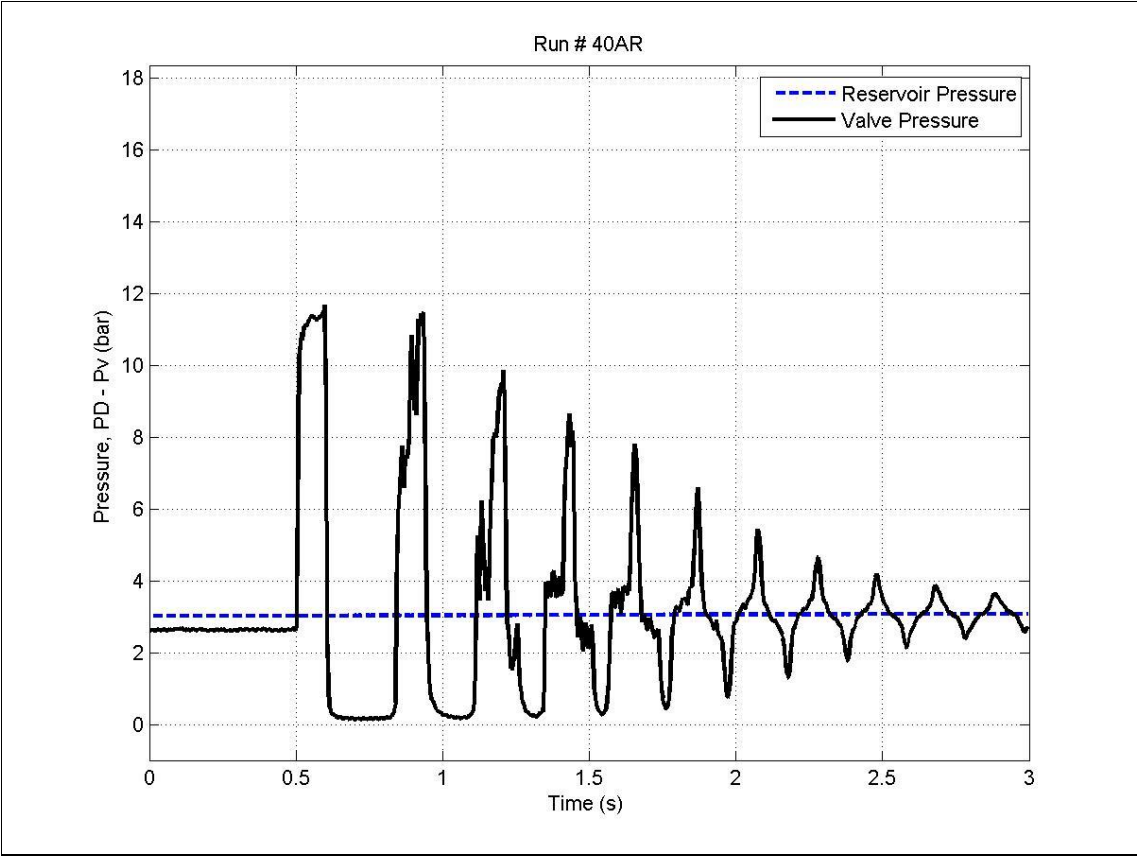


Figure(C.36) Experiment No. 36.

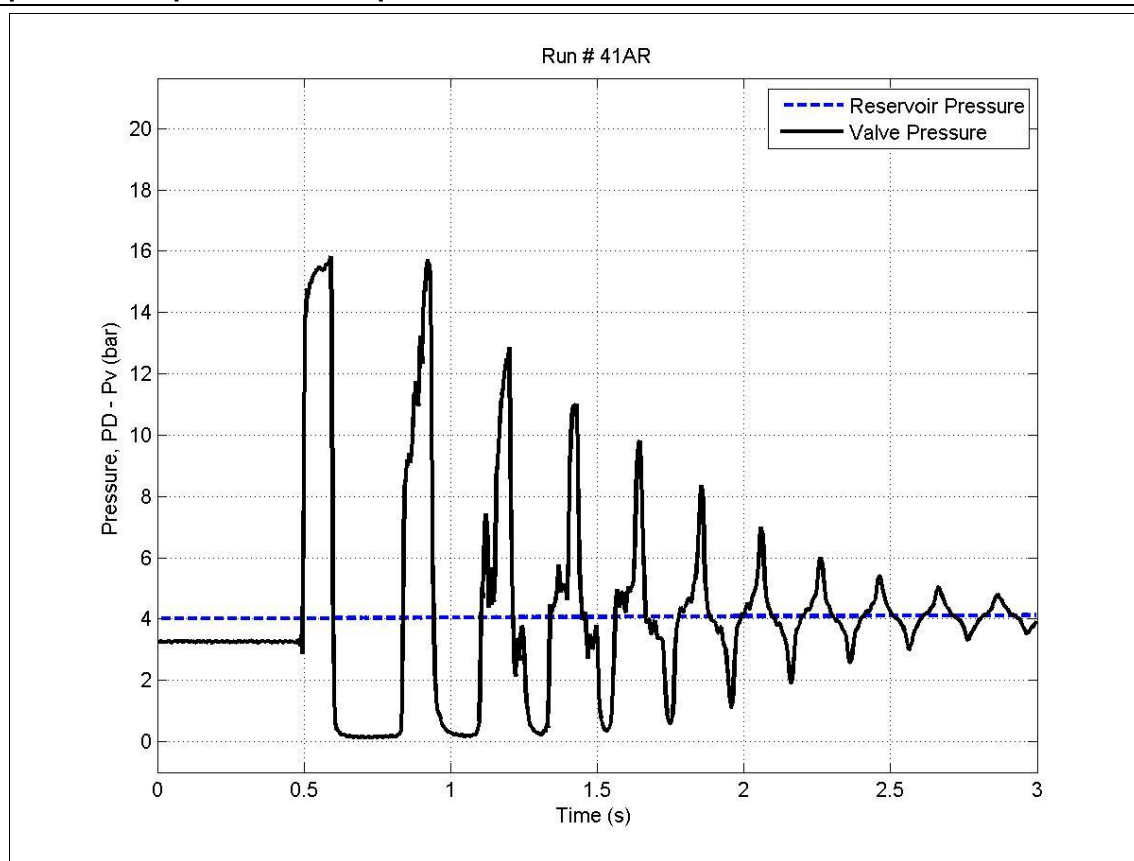




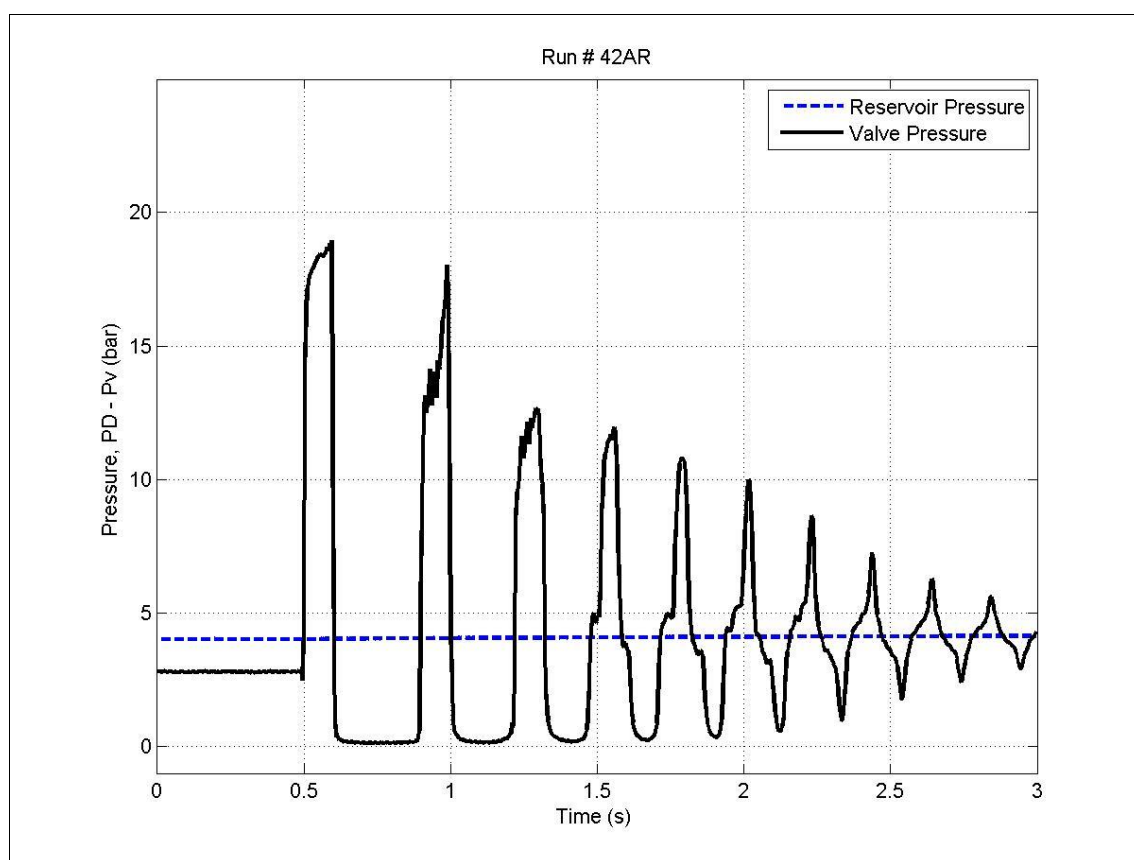
Figure(C.39) Experiment No. 39.



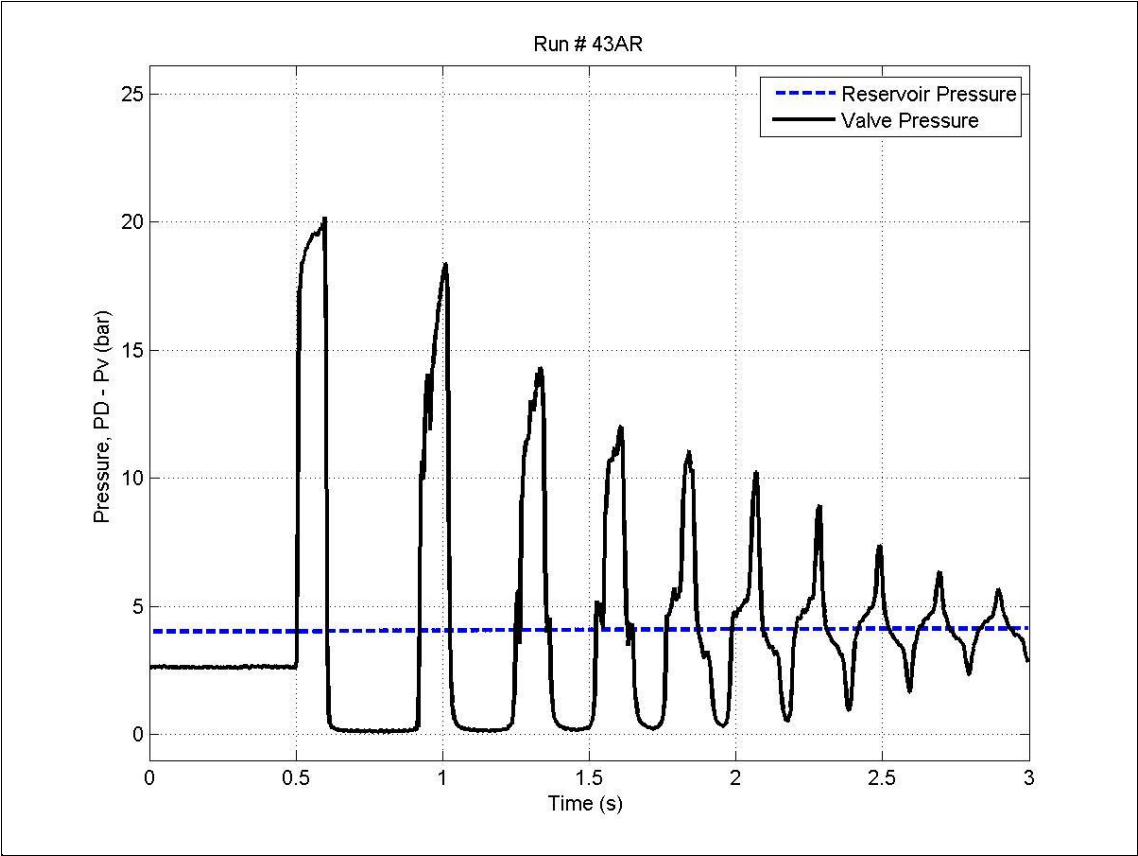
Figure(C.40) Experiment No. 42.



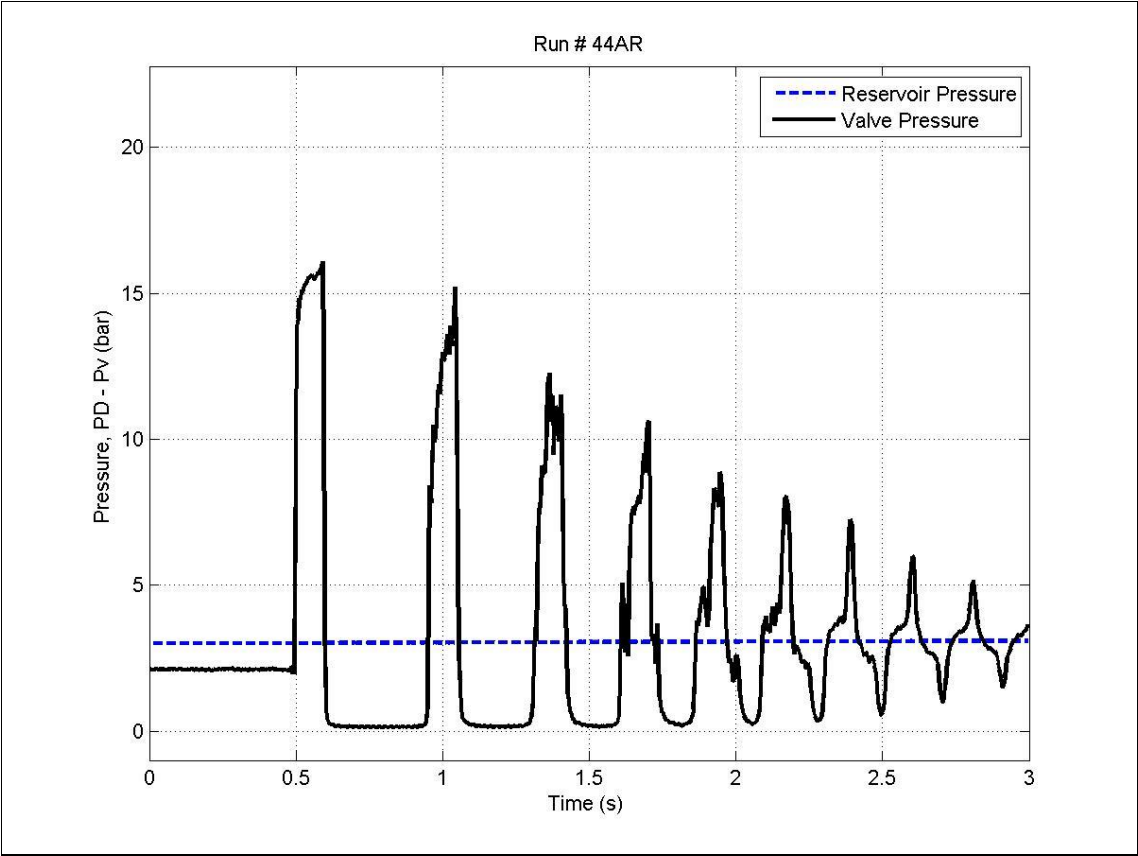
Figure(C.41) Experiment No. 41.



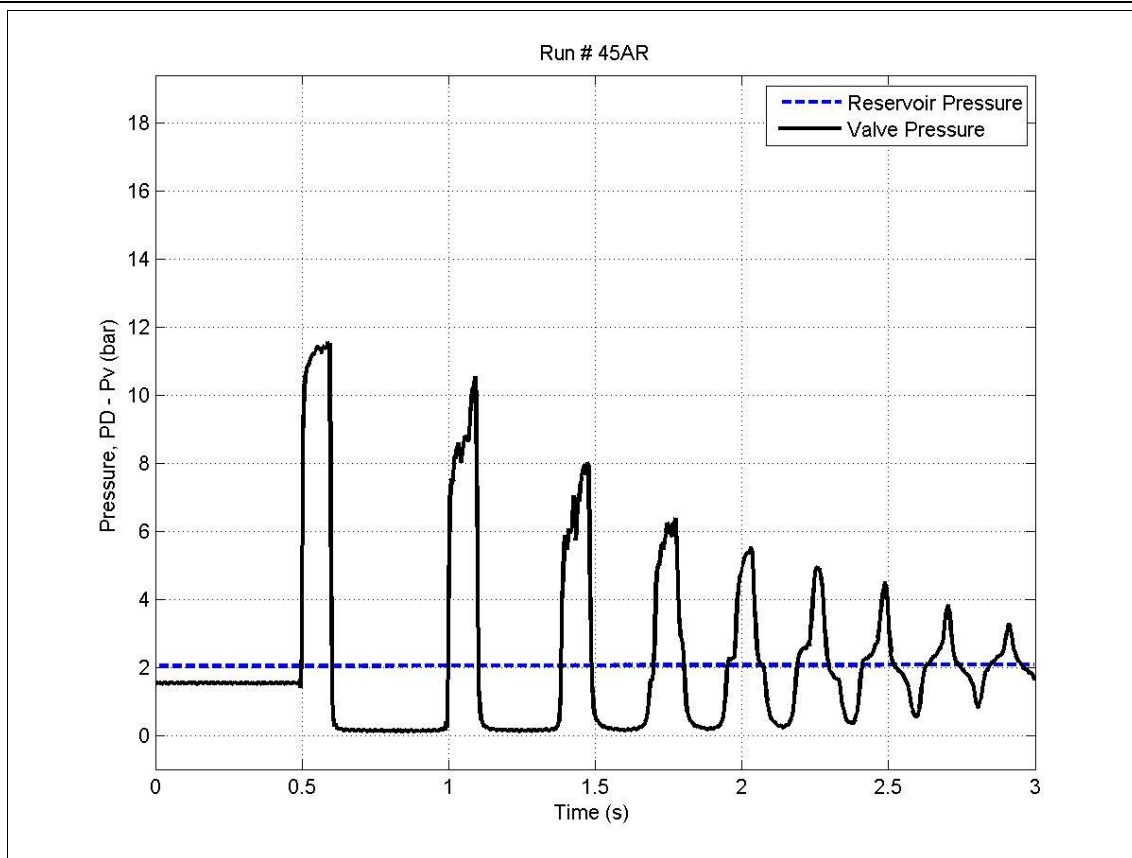
Figure(C.42) Experiment No. 42.



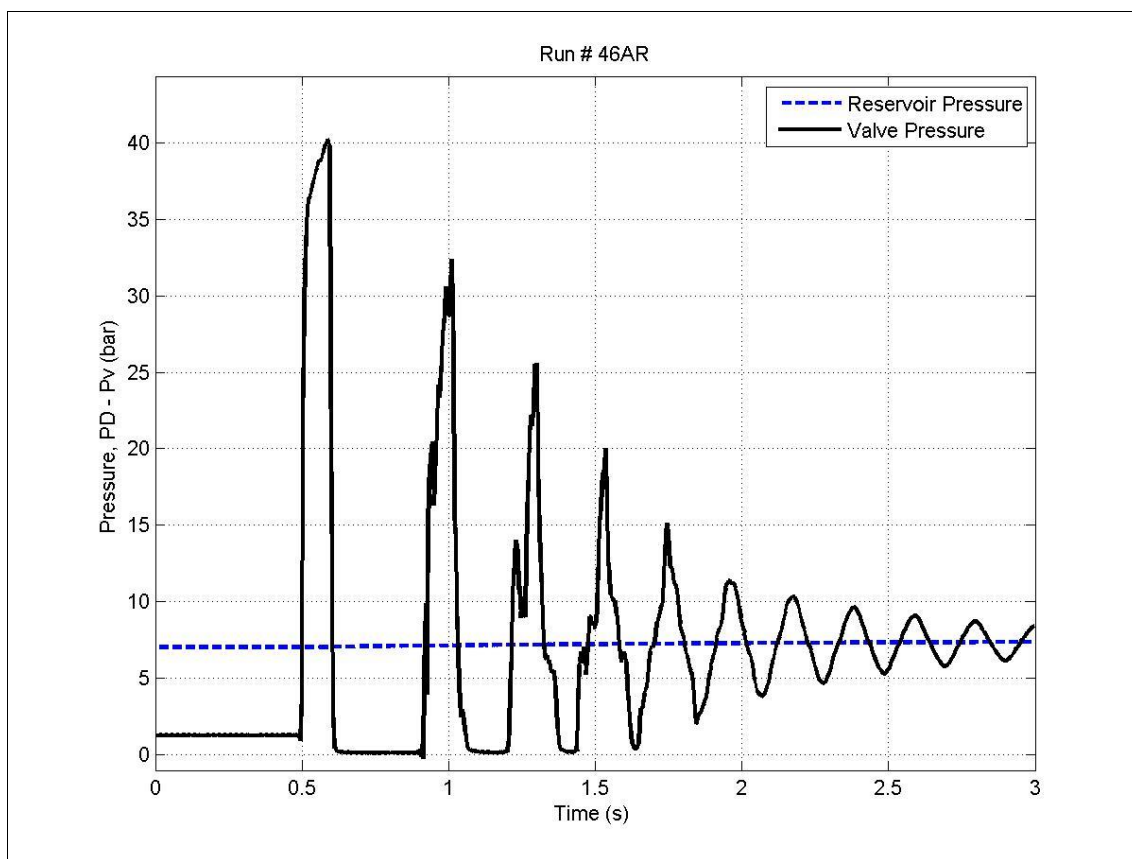
Figure(C.43) Experiment No. 43.



Figure(C.44) Experiment No. 44.

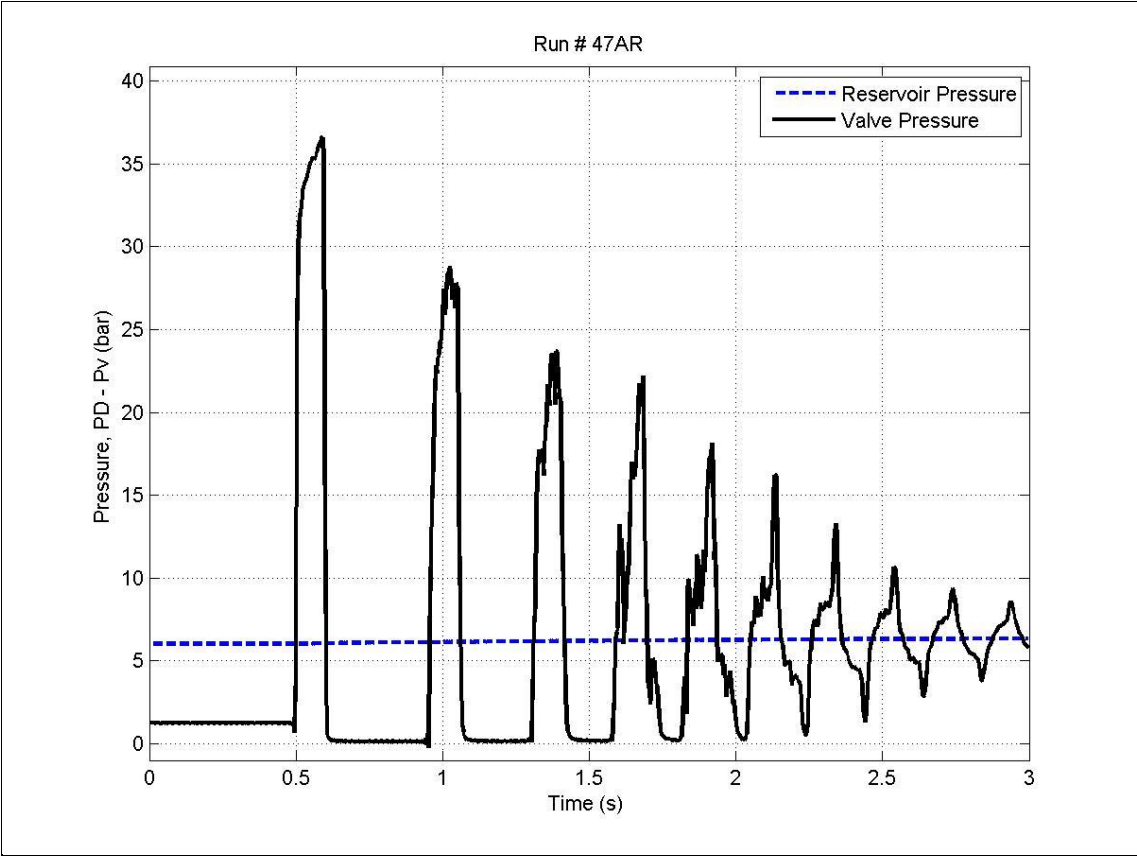


Figure(C.45) Experiment No. 45.

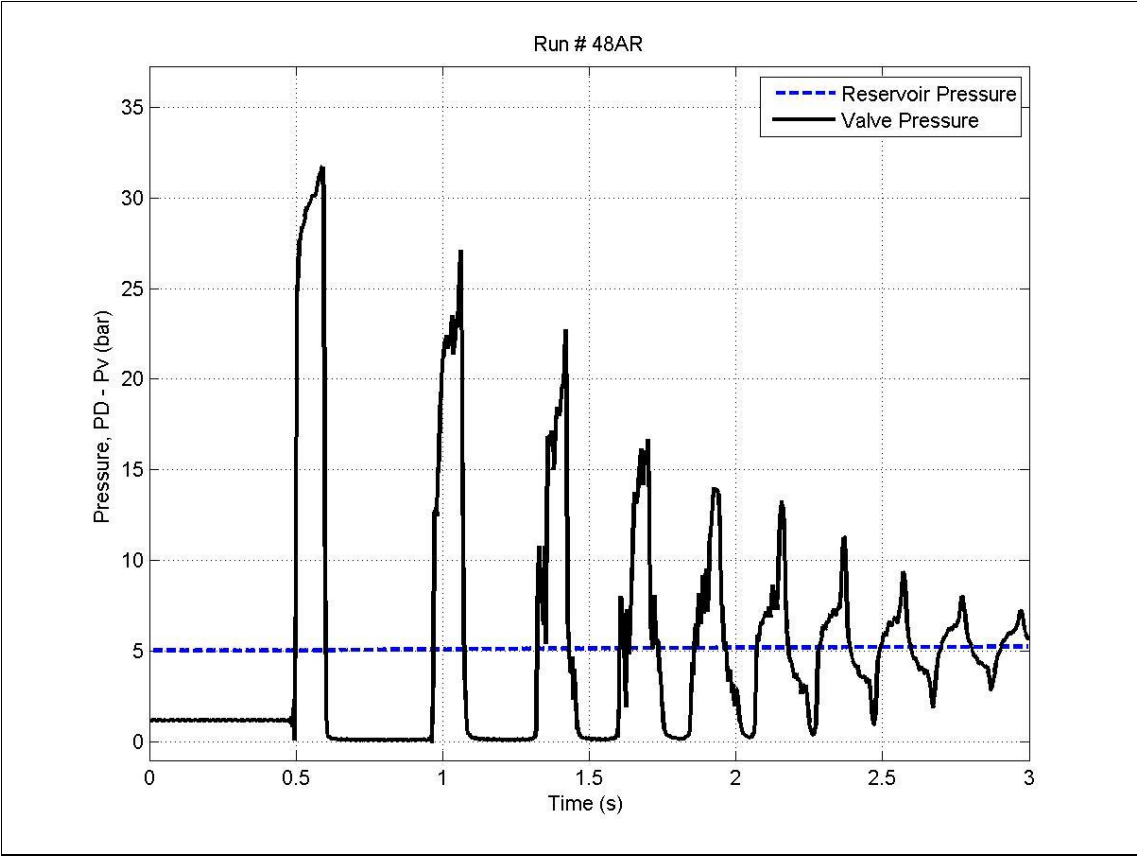


Figure(C.46) Experiment No. 46.



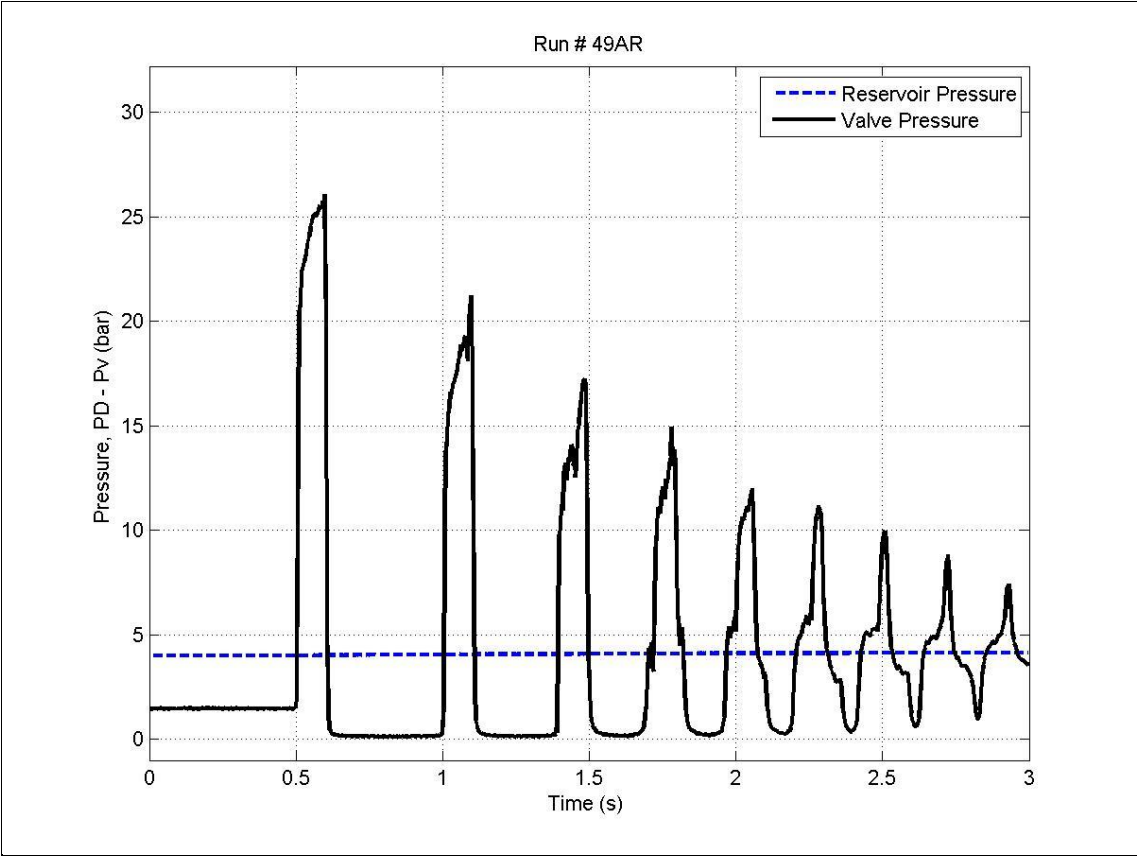


Figure(C.47) Experiment No. 47

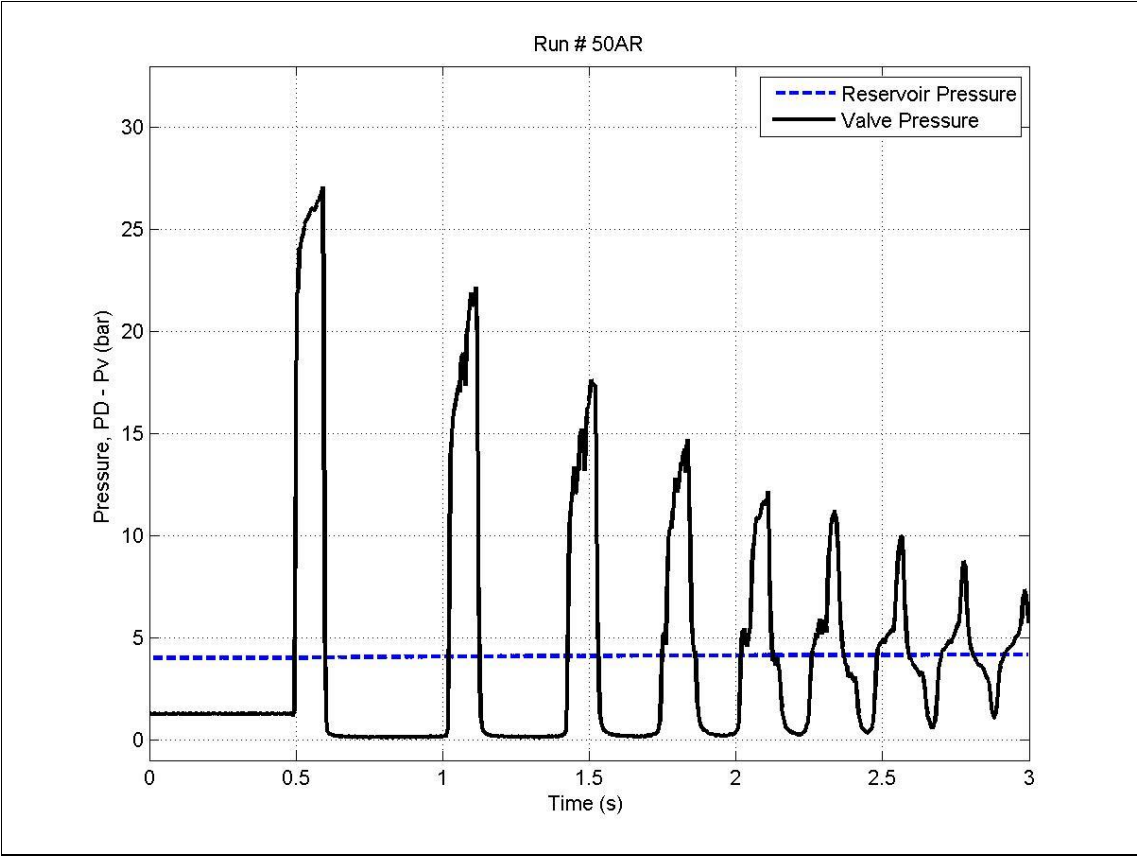


Figure(C.48) Experiment No. 48.

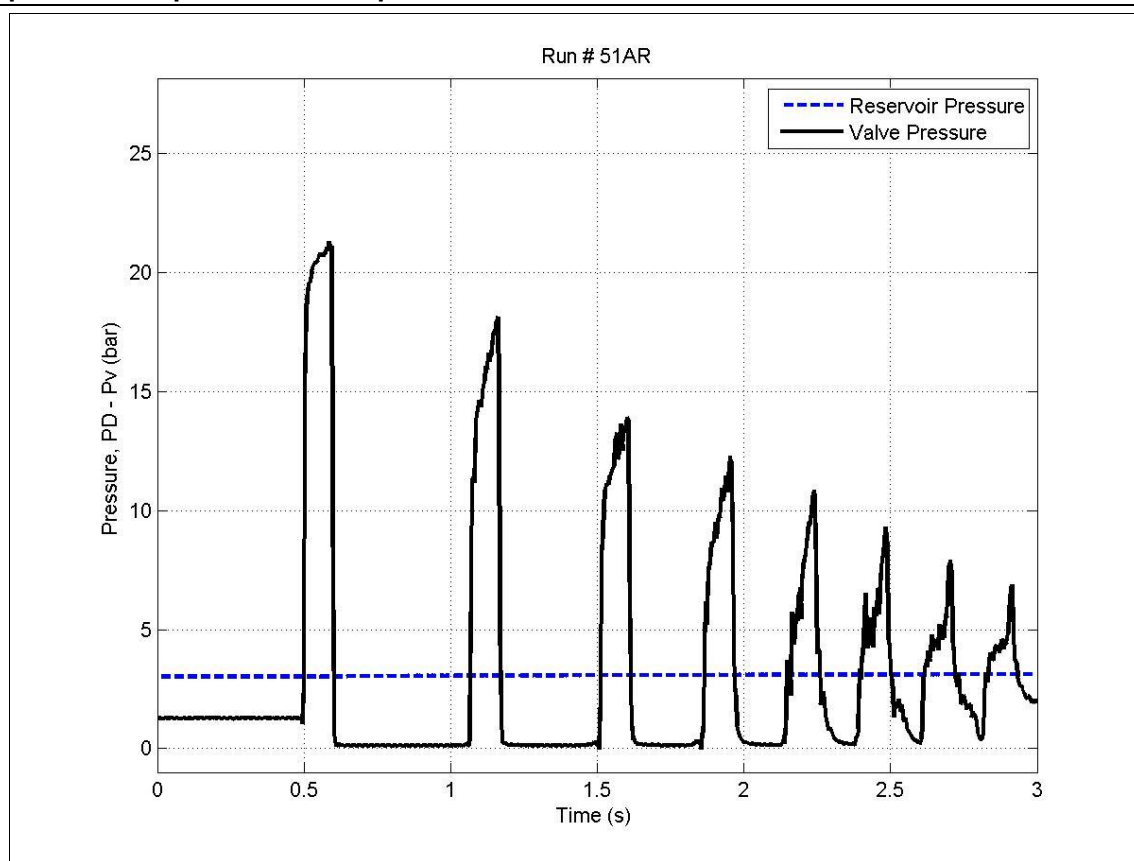




Figure(C.49) Experiment No. 49.



Figure(C.50) Experiment No. 50.



Figure(C.51) Experiment No. 51.

**Appendix D.**

**Analytical Model for Column Separation and  
First Cavity Time Duration**

In unpublished work Anderson (1979) had developed an analytical solution for a simple model of column separation due to rapid pumped flow stoppage based on previous studies by Binnie and Thackrah (1951) and Priddin (1978), Figure(D.1a). For comparison with the experimental work in this study (Chapter 4), this model can be adapted to the present delivery valve closure apparatus, Figure(D.1b).

Considering the idealised case of instantaneous valve closure in a frictionless horizontal pipeline, e.g. Figure(1.1), the first pressure wave reflection at the closed valve occurs at time  $= (2L/a)$  after the instantaneous closure, at which point the flow along the entire pipe is at a velocity  $V_0$  away from the valve and towards the reservoir. If the Joukowsky waterhammer wave magnitude  $(\rho \cdot a \cdot V_0)$  is less than  $(P_a - P_v)$ , where  $P_a$  is the atmospheric pressure and  $P_v$  is the pipe fluid vapour pressure, i.e.  $(\rho \cdot a \cdot V_0) < (P_a - P_v)$ , then the idealised waterhammer cycle continues. However, when  $(\rho \cdot a \cdot V_0) > (P_a - P_v)$ , then column separation occurs at the shut valve at the vapour pressure  $P_v$  and the fluid column is no longer restrained at the closed valve, allowing it to move away from the valve so that the vapour cavity grows, Figure(D.2). Under the action of the external pressure, the initial separating column velocity will decelerate (from  $V_0$  to zero at maximum cavity size) and then start to accelerate towards the valve as the cavity collapses, leading to renewed waterhammer when the column is again brought to rest at the closed valve, Figure(D.2).

To compare this model with the experimental results, the key assumption will be that over the first  $(2L/a)$  of waterhammer resulting from rapid valve closure, with relatively low system damping, the change from the initial pipe flow velocity  $V_0$  before closure is negligible. This somewhat exaggerates the initial flow velocity at flow reversal, so should give slightly higher theoretical as compared with experimental cavity duration. The key assumption in the Binnie and Thackrah (1951) model is that the pipe length  $(L) \gg$  maximum cavity size  $(x_{\max})$  so that:

- Change in the moving fluid column length is small so that a reasonable approximation is that the column is always of length  $L$ ; and
- If the pipe is not horizontal the static head at the valve is always  $H_s$ , Figure(D.1).

The Binnie and Thackrah (1951) model also assumes that once column separation is initiated, the pipe fluid behaves as a “rigid column”, ignoring the waterhammer

(compressibility) waves that the experiments show still continue to propagate along it. In addition, during the cavity existence, the pressure at the valve remains constant at the vapour pressure  $P_v$ , Figure(D.3) and the net flow resistance/driving pressure  $P_d$  due to the surface pressure at the reservoir  $P_s$  and the valve submergence  $H_s$  is also constant at:

$$P_d = P_s + \rho \cdot g \cdot H_s \quad (D.1)$$

The unsteady rigid column Bernoulli equation including the inertia pressure  $\rho \cdot L(dV/dt)$  is then (where  $\rho$  is the liquid density,  $K$  is the overall pipe loss coefficient and noting the changes in signs due to the velocity reversal where  $V$  is positive towards the reservoir):

Separating Figure(D.3a)	$\left  \right.$	Collapsing Figure(D.3b)
$\rho L \frac{dV}{dt} + (P_d - P_v) + K \frac{1}{2} \rho V^2 = 0$		$\rho L \frac{dV}{dt} - (P_d - P_v) + K \frac{1}{2} \rho V^2 = 0 \quad (D.2)$

Due to the assumption above that the liquid rigid column length  $L$  is constant, the cavity front displacement  $x(t)$  away from the valve does not occur in these equations, but can be introduced through:

$$x = \int V \cdot dt \Rightarrow dx = V \cdot dt \quad (D.3)$$

Then Eq.(D.2) can be rearranged to give an integral of the form  $\int dU/U$ , where  $dU = \pm K \cdot \rho \cdot d\left(\frac{1}{2} V^2\right) = \pm K \cdot \rho \cdot V \cdot dV$  and  $x_{\max}$  is the maximum cavity length occurring when  $V = 0$ :

Decelerating Figure(D.3a)

$$\frac{\rho \cdot K \cdot V \cdot dV}{\left[ (P_d - P_v) + K \frac{1}{2} \rho V^2 \right]} = \frac{-K}{\rho \cdot L} \cdot dx$$

i.e.  $[\ln(U)]_{V=V_0}^{V=0} = \frac{-K}{L} [x]_0^{x_{\max}}$

Accelerating Figure(D.3b)

$$\frac{-\rho \cdot K \cdot V \cdot dV}{\left[ (P_d - P_v) - K \frac{1}{2} \rho V^2 \right]} = \frac{-K}{\rho \cdot L} \cdot dx$$

i.e.  $[\ln(U)]_{V=0}^{V=V_1} = \frac{-K}{L} [x]_{x_{\max}}^0$

$$\Rightarrow x_{\max} = \frac{-L}{K} \ln \left\{ \frac{(P_d - P_v)}{(P_d - P_v) + K \frac{1}{2} \rho V_0^2} \right\} \quad \Rightarrow x_{\max} = \frac{-L}{K} \ln \left\{ \frac{(P_d - P_v) - K \frac{1}{2} \rho V_1^2}{(P_d - P_v)} \right\} \quad (D.4)$$

Equating these two solutions for  $x_{\max}$  in Eq.(D.4) to eliminate  $x_{\max}$  gives the final velocity at cavity collapse  $V_1$  that gives rise to a Joukowsky waterhammer pressure rise ( $\rho \cdot a \cdot V_1$ ) as in Figure(D.2):

$$V_1 = V_0 / \sqrt{1 + \frac{K \frac{1}{2} \rho V_0^2}{(P_d - P_v)}} \quad (D.5)$$

Note that  $V_1 < V_0$ , so this pressure rise after column separation will be less than that after the initial valve closure ( $\rho \cdot a \cdot V_0$ ), as in “classical” sever column separation, e.g. Figure(4.18). In the limiting frictionless case ( $K = 0$ ) then  $V_1 = V_0$  and the cycle repeats endlessly.

However, as noted in Section(4.5), in this study the cavity length cannot be measured or inferred, whereas the cavity time duration  $T_{\text{cav}}$  can be measured from the transient pressure trace, e.g. Figure(4.18). It is therefore necessary also to integrate Eq.(D.2) with respect to time ( $t$ ) as well as space ( $x$ ) as above, again using standard integral forms (with  $\tan^{-1}(0) = \tanh^{-1}(0) = 0$ ):

Cavity growth Figure(D.3a)

$$\frac{dV}{\left[(P_d - P_v) + K \frac{1}{2} \rho V^2\right]} = \frac{-dt}{\rho \cdot L}$$

Cavity collapse Figure(D.3b)

$$\frac{dV}{\left[(P_d - P_v) - K \frac{1}{2} \rho V^2\right]} = \frac{dt}{\rho \cdot L}$$

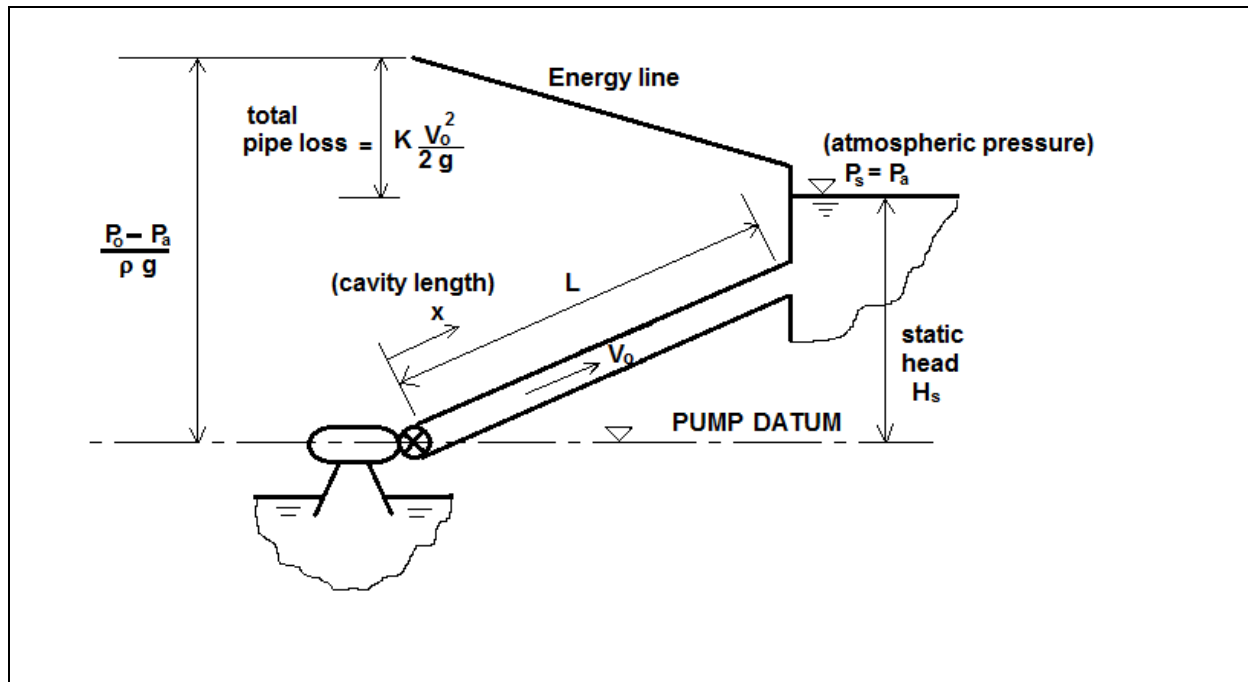
i.e.

$$\int_0^{t_{\max}} \frac{dV}{a+by^2} = \frac{1}{\sqrt{ab}} \tan^{-1} \left[ V \sqrt{b/a} \right]_{V_0}^0 \quad \left| \quad \int_{t_{\max}}^{T_{\text{cav}}} \frac{dV}{a-by^2} = \frac{1}{\sqrt{ab}} \tanh^{-1} \left[ V \sqrt{b/a} \right]_0^{V_1} \quad (D.6)$$

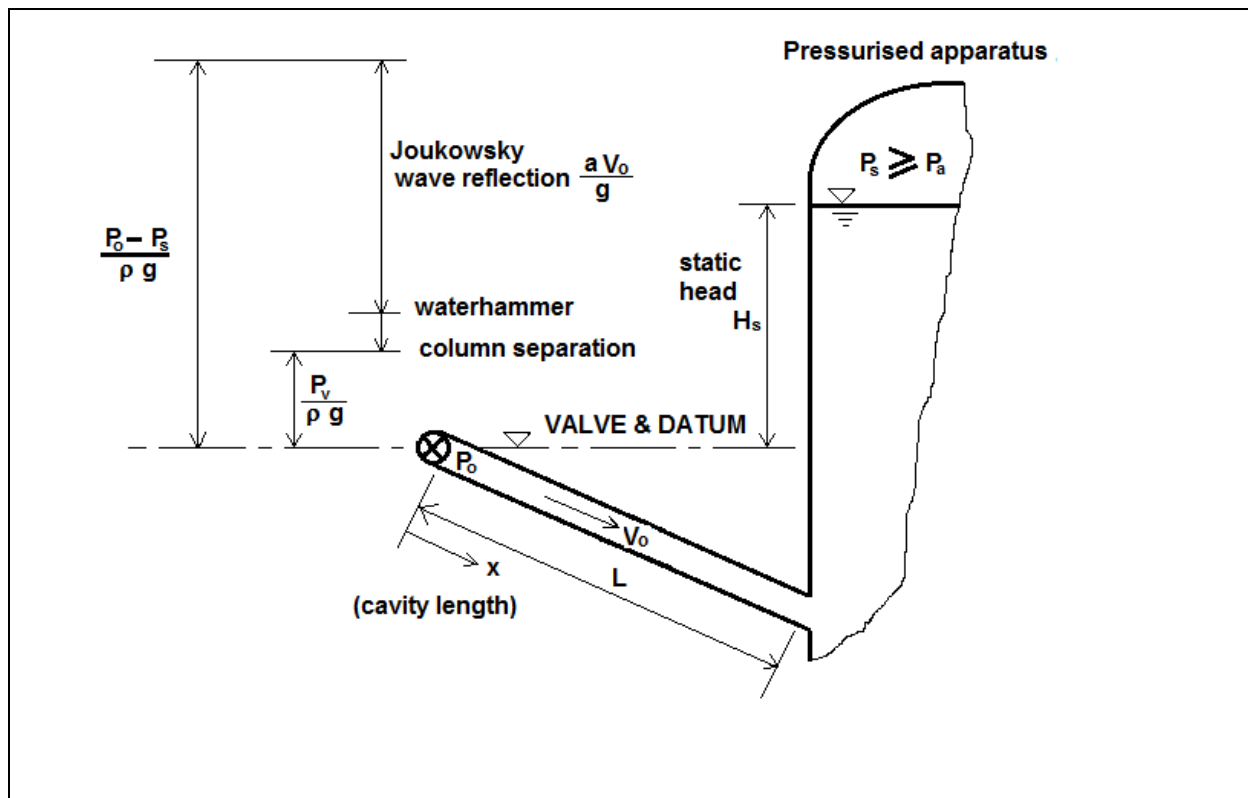
Combining these two to give the cavity duration  $T_{\text{cav}} = (T_{\text{cav}} - t_{\max}) + t_{\max}$  by eliminating  $V_1$  using Eq.(D.5) obtained above gives:

$$T_{\text{cav}} = \frac{\rho \cdot L}{\sqrt{\frac{1}{2} \rho \cdot K(P_d - P_v)}} \left\{ \tanh^{-1} \sqrt{\frac{K \frac{1}{2} \rho \cdot V_0^2}{(P_d - P_v) + K \frac{1}{2} \rho \cdot V_0^2}} + \tan^{-1} \sqrt{\frac{K \frac{1}{2} \rho \cdot V_0^2}{(P_d - P_v)}} \right\} \quad (D.7)$$

Table(5.1) uses the experimental results from Arfaie (1989) to calculate the ratio of the Eq.(D.7) calculation to the measured value. For perfect agreement these ratios should have the value = 1, but all are somewhat > 1, reflecting the assumption that there is no damping in the initial waterhammer pressure rise before column separation



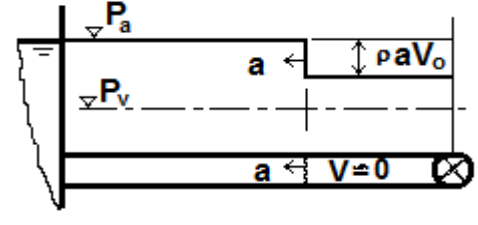
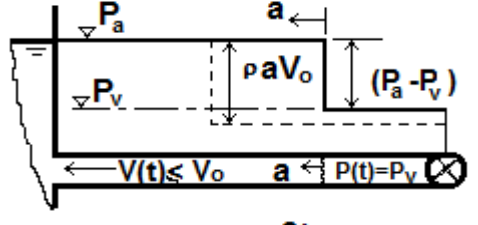
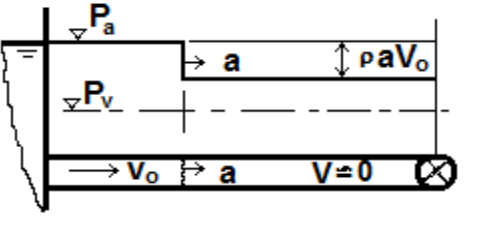
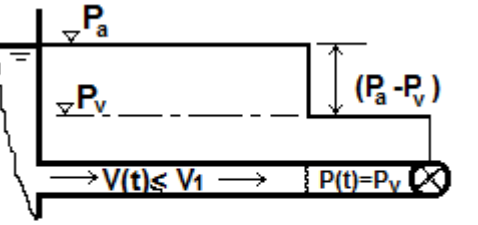
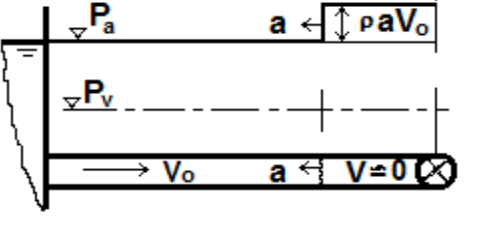
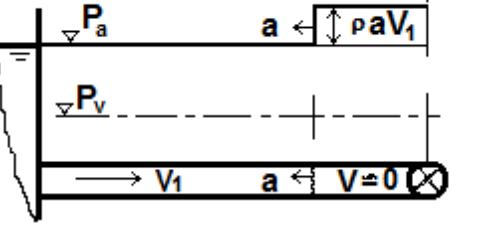
(a) Pump system as analysed by Binnie and Thackrah (1951).



(b) Experimental rig at instant of first Joukowski wave reflection at closed valve, when all pipe flow is towards reservoir at velocity  $V_0$ .

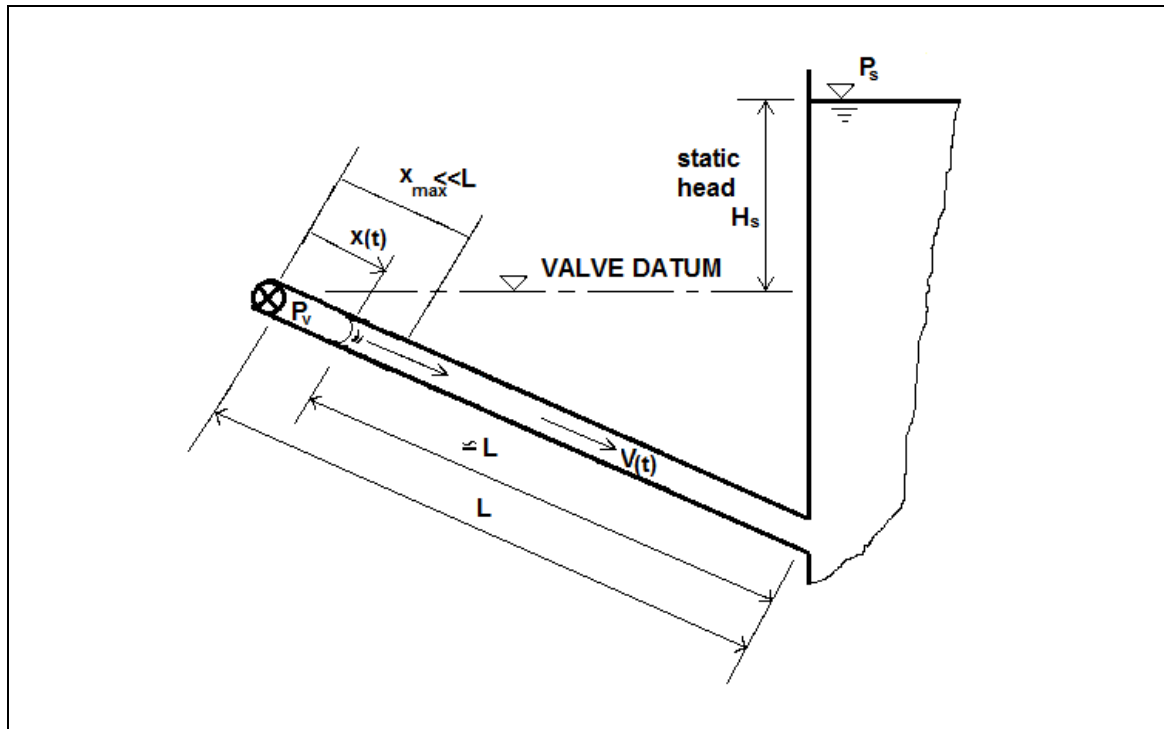
Figure(D.1) System definition schematic for analytical column separation model: comparison of (a) Binnie and Thackrah (1951), pump stoppage with (b) present experimental rig at flow reversal.



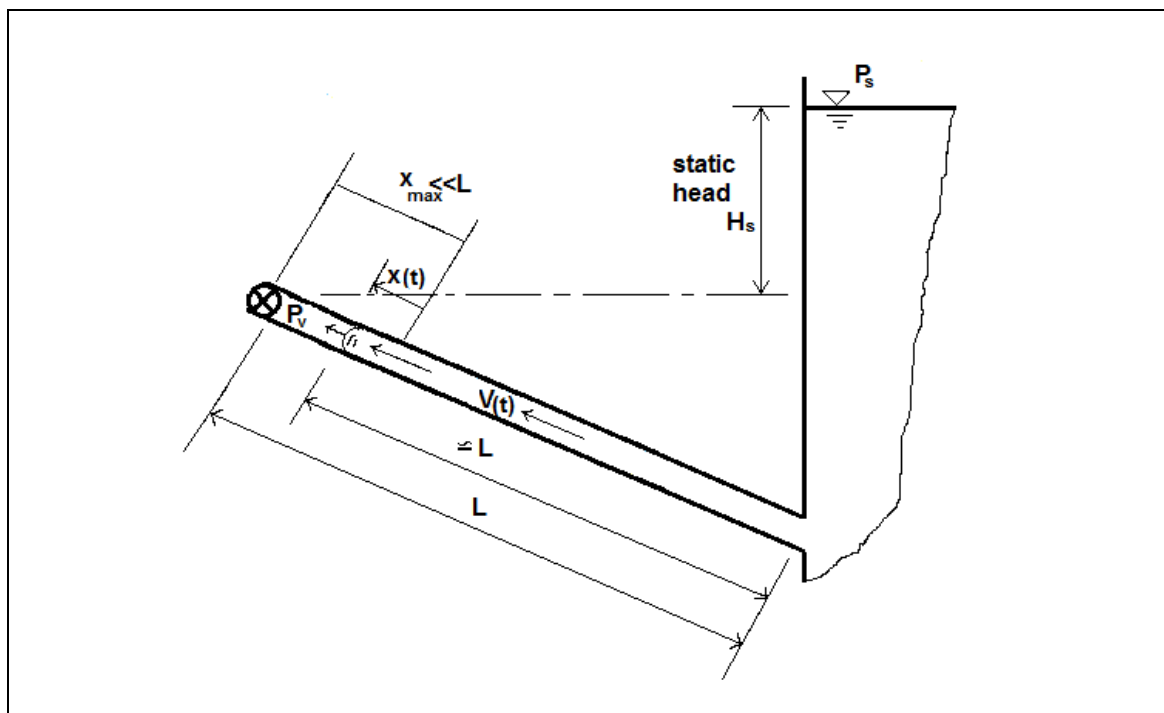
<p>Elastic column (waterhammer): fluid column restrained at shut valve (Wylie and Streeter, 1993)</p> <p><math>\rho \cdot a \cdot V_o &lt; (P_a - P_v)</math></p>	<p>Rigid column (column separation): fluid column no longer restrained at moving cavity boundary</p> <p><math>\rho \cdot a \cdot V_o &gt; (P_a - P_v)</math></p>
 <p><math>\frac{2L}{a} &lt; t &lt; \frac{3L}{a}</math></p>	 <p><math>\frac{2L}{a} &lt; t &lt; (\frac{2L}{a} + t_{max})</math></p>
 <p><math>\frac{3L}{a} &lt; t &lt; \frac{4L}{a}</math></p>	 <p><math>(\frac{2L}{a} + t_{max}) &lt; t &lt; (\frac{2L}{a} + T_{cav})</math></p>
 <p><math>\frac{4L}{a} &lt; t &lt; \frac{5L}{a}</math></p>	 <p><math>T_{cav} &lt; t &lt; (T_{cav} + \frac{L}{a})</math></p>

Figure(D.2) Classical frictionless waterhammer cycle (left column) compared with waterhammer leading to cavitation at valve (right column).

NB:  $T_{cav}$  = cavity duration,  $t_{max}$  = time for cavity growth to its maximum size.



(a) Separation (decelerating) flow (from  $t = 2L/a$ ) with cavity growth to maximum size  $x_{\max}$  when  $V(t) \rightarrow 0$  (growth duration  $t_{\max}$ )



(b) Collapsing (accelerating) flow (from  $t = 2L/a + t_{\max}$ ) with cavity collapse to zero size when  $V(t) \rightarrow V_1$  (collapse duration  $T_{\text{cav}} - t_{\max}$ )

Figure(D.3) Rigid column model during (a) cavity growth and (b) cavity collapse

## **Appendix E.**

**MATLAB Code for Systematic Identification of 1<sup>st</sup> Column  
Separation Duration and 2<sup>nd</sup> Pressure Peak Amplitude**

A systematic identification has been set for acquiring both the first column separation duration Tc1 and second pressure peak amplitude Pmax2 this consistent procedure has be put in place to be applied to all runs. Table(E.1) shows the MATLAB code

**Table(E.1) MATLAB code**

```
%% Function Analytic (dt,trigger,t,pn,Pmodel_1,Pmodel_2)
clear;
Pmin_level = 0.8; % Level of minimum pressure to be censored for cavitation duration.
for K = 7:58 %46:51
    U = xlsread('data_out.xlsx',K);
    t=U(:,2);
    TC1_Mark = 0;
    TC2_Mark = 0;
    for W = 2:4 % forloop to cove analysis
        if (W == 2)
            W = 1;
        end
        pn = U(:,W); %<---
        disp(['K =', num2str(K),'& W=',num2str(W)]);
        disp(['Max(pn)',num2str(max(pn))]);
        disp(['Min(pn)',num2str(mean(pn))]);
    }
    %% Cavity finder
    for J = 133:length(pn)-1 %Trigger index at 133 (the star of valve closer)
        %% 1st cavity calculation
        if (pn(J) <Pmin_level) && (TC1_Mark <= 1)
            if (TC1_Mark == 0)
                TC1_Mark = 1;
                start_index_TC1 = J;
            elseif ((TC1_Mark == 1) && (pn(J+1) >= Pmin_level))
                TC1_Mark = 2;
                end_index_TC1 = J;
            end
        end
        %% 2nd cavity calculation
        if ((TC2_Mark <= 1) && (TC1_Mark == 2) && (pn(J+1) <Pmin_level) ) % && )
            if (TC2_Mark == 0)
                TC2_Mark = 1;
                start_index_TC2 = J;
            elseif ((TC2_Mark == 1) && (TC1_Mark == 2) && (pn(J+1) >= Pmin_level))
                TC2_Mark = 2;
            end
        end
    end
end
```

```
        end_index_TC2 = J;
    end
end
end
TC1(W)= t(end_index_TC1) - t(start_index_TC1);
%% 2nd pressure peak calculation.
JJ = 1;
for J = end_index_TC1:start_index_TC2+1
    Pmax2_List(JJ) = pn(JJ);
    JJ = JJ + 1;
end
Pmax2(W) = max(Pmax2_List);
%% option below, to work out the 2nd cavity measure.
% TC2 = t(end_index_TC2)- t(start_index_TC2+1);
table(K,5+W)= Pmax2(W);
table(K,W)= TC1(W);
TC1_Mark = 0;
TC2_Mark = 0;
end
table(K,2)= K;
end %forloop to cover all sheets of the (Runs) .xls file.
xlswrite('P-data_Analytic_modefide.xlsx',table);
```

## **Appendix F.**

### **Minitab Statistical Computations**

### F.1 Full data: comparison of Method, BC, Pv using quasi-steady friction

All experimental runs including transition between limited and classic column separation:

(a) General linear Model (3 factors):

#### General Linear Model: Tc1 versus Method, Pv, BC

Method

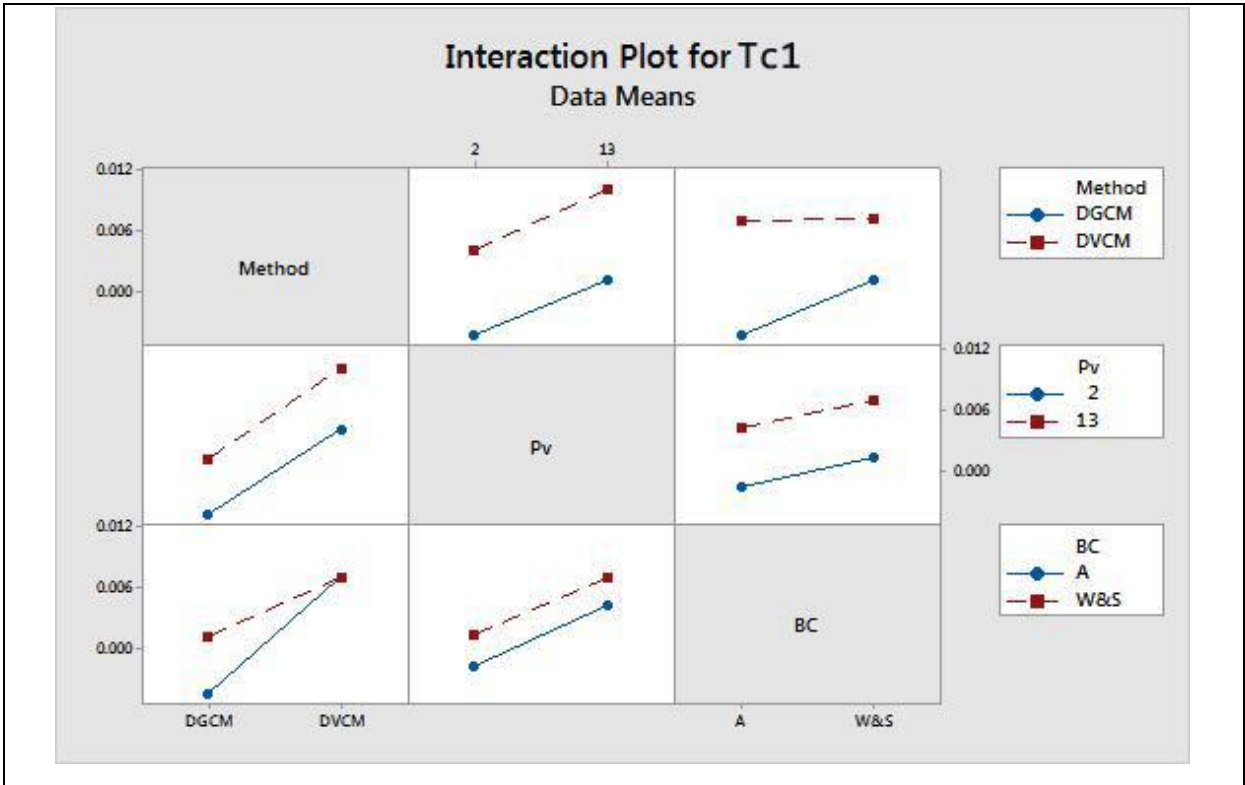
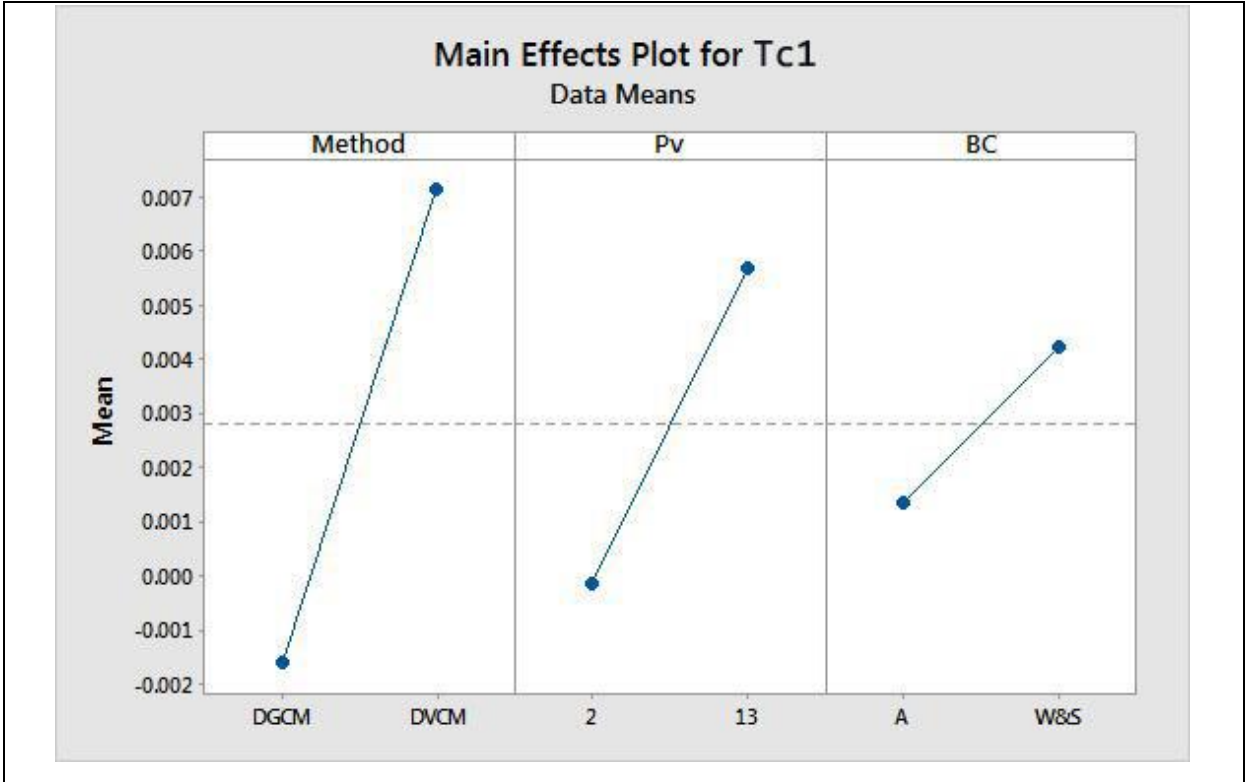
Factor coding (-1, 0, +1)

Factor Information

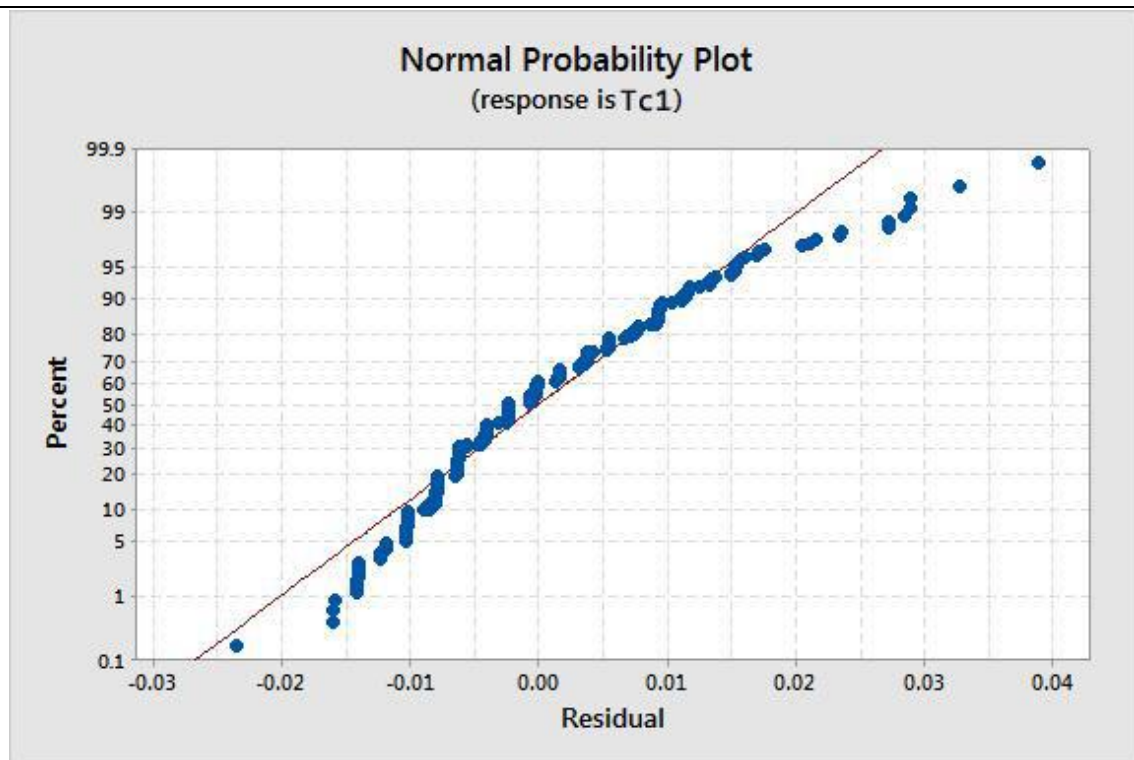
Factor	Type	Levels	Values
Method	Fixed	2	DGCM, DVCM
Pv	Fixed	2	2, 13
BC	Fixed	2	A, W&S

Analysis of Variance

Source	DF	Adj SS	Adj MS	F-Value	P-Value
Method	1	0.007988	0.007988	105.33	0.000
Pv	1	0.003560	0.003560	46.95	0.000
BC	1	0.000856	0.000856	11.29	0.001
Method*Pv	1	0.000008	0.000008	0.11	0.744
Method*BC	1	0.000775	0.000775	10.22	0.001
Error	410	0.031093	0.000076		
Lack-of-Fit	2	0.000026	0.000013	0.17	0.842
Pure Error	408	0.031067	0.000076		
Total	415	0.044280			







### General Linear Model: Pmax2 versus Method, Pv, BC

Method

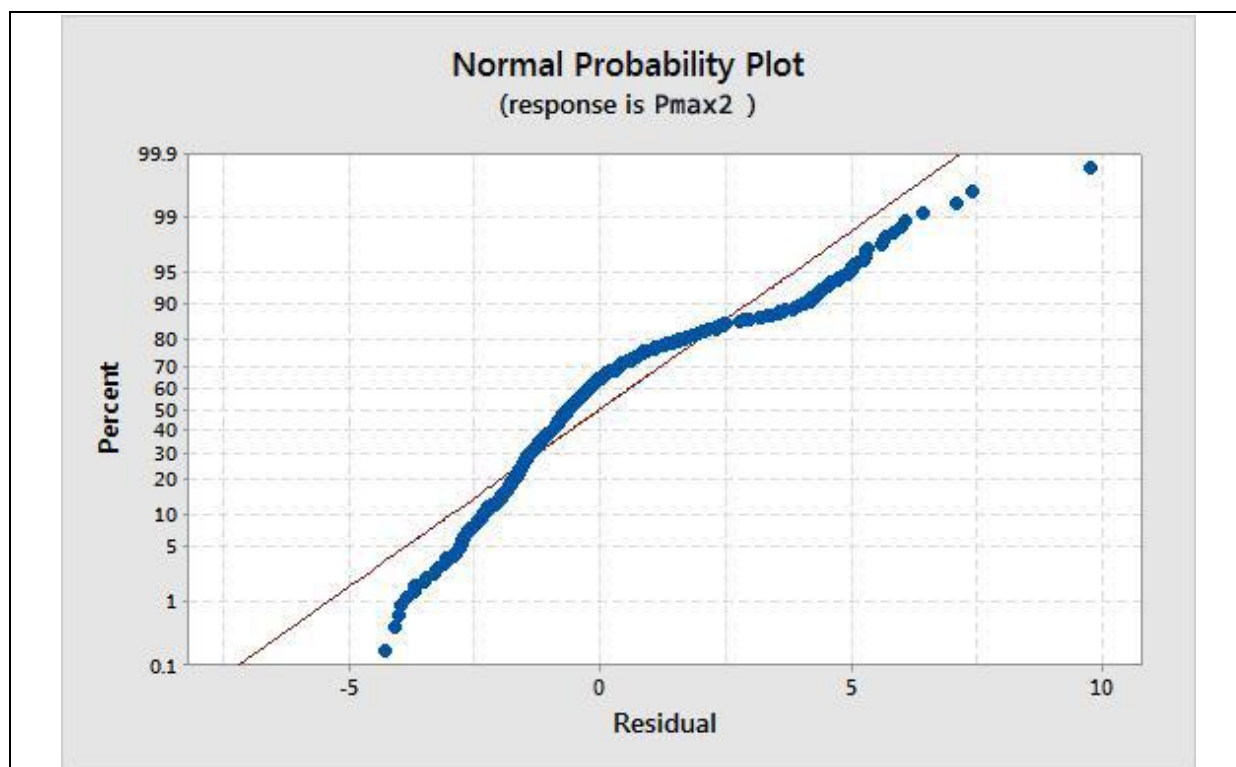
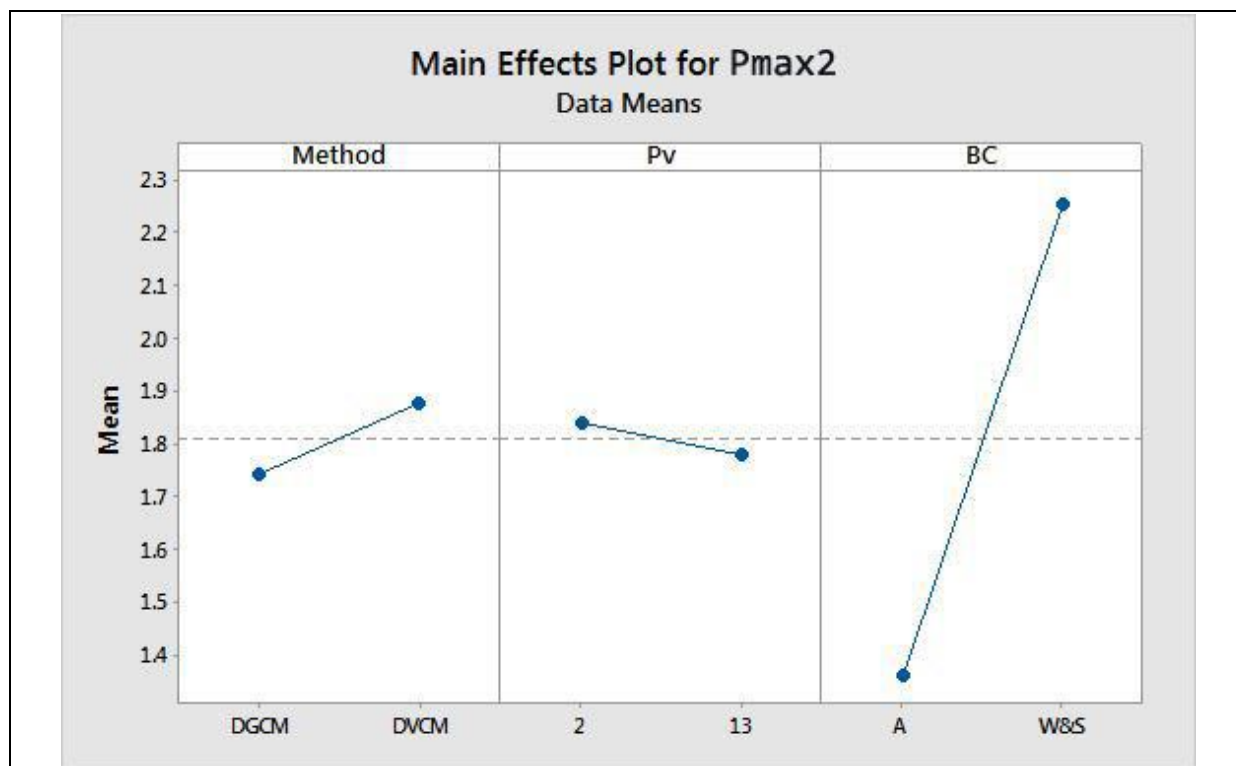
Factor coding (-1, 0, +1)

Factor Information

Factor	Type	Levels	Values
Method	Fixed	2	DGCM, DVCM
Pv	Fixed	2	2, 13
BC	Fixed	2	A, W&S

Analysis of Variance

Source	DF	Adj SS	Adj MS	F-Value	P-Value
Method	1	1.82	1.8223	0.33	0.564
Pv	1	0.34	0.3422	0.06	0.803
BC	1	83.07	83.0666	15.17	0.000
Method*Pv	1	0.00	0.0040	0.00	0.978
Method*BC	1	0.48	0.4823	0.09	0.767
Error	410	2244.92	5.4754		
Lack-of-Fit	2	1.77	0.8842	0.16	0.851
Pure Error	408	2243.15	5.4979		
Total	415	2330.63			



(b) For confirmation, 3 one-way ANOVA for each factor separately:

### One-way ANOVA: Tc1 versus Method

Method

Null hypothesis All means are equal  
Alternative hypothesis At least one mean is different  
Significance level  $\alpha = 0.05$

Equal variances were assumed for the analysis.

Factor Information

Factor	Levels	Values
Method	2	DGCM, DVCM

Analysis of Variance

Source	DF	Adj SS	Adj MS	F-Value	P-Value
Method	1	0.007988	0.007988	91.12	0.000
Error	414	0.036292	0.000088		
Total	415	0.044280			

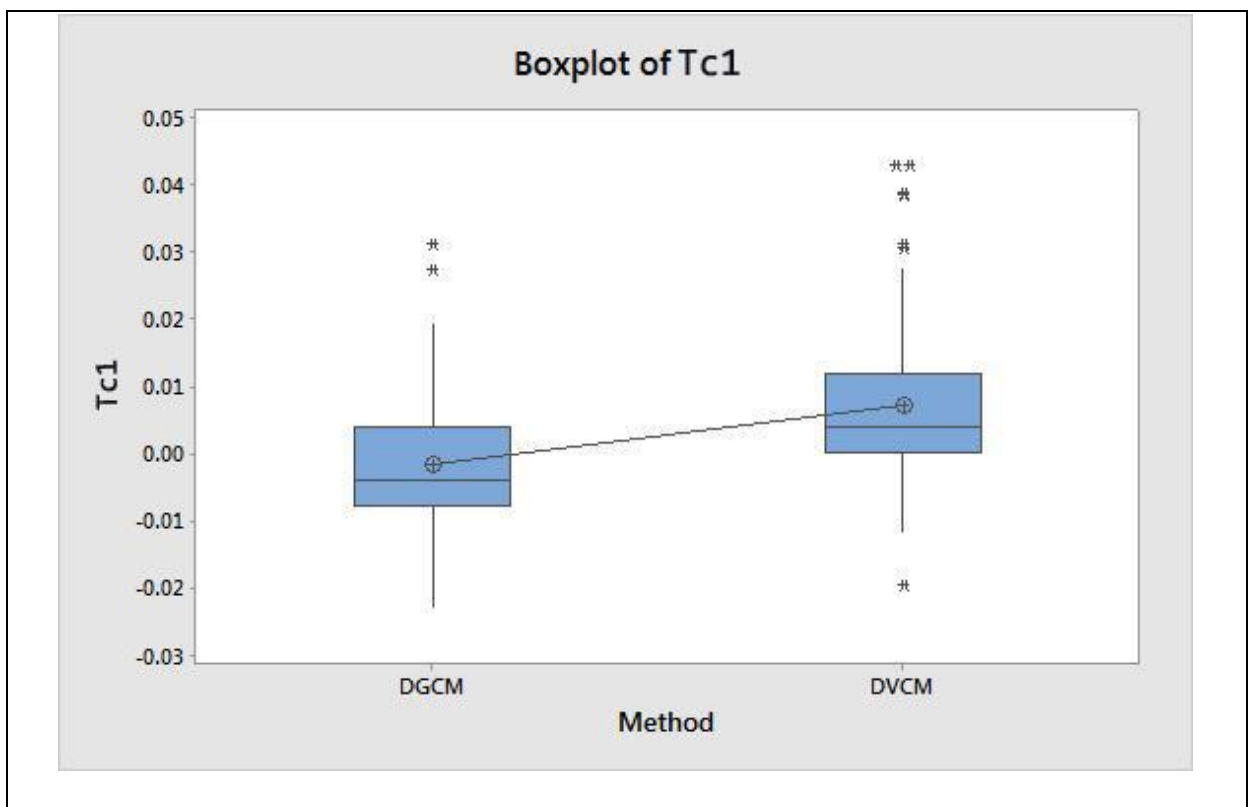
Model Summary

S	R-sq	R-sq(adj)	R-sq(pred)
0.0093628	18.04%	17.84%	17.25%

Means

Method	N	Mean	StDev	95% CI
DGCM	208	-0.001588	0.008579	(-0.002864, -0.000312)
DVCM	208	0.007176	0.010086	(0.005899, 0.008452)

Pooled StDev = 0.00936284



**One-way ANOVA: Tc1 versus Pv**

## Method

Null hypothesis All means are equal  
 Alternative hypothesis At least one mean is different  
 Significance level  $\alpha = 0.05$

Equal variances were assumed for the analysis.

## Factor Information

Factor	Levels	Values
Pv	2	2, 13

## Analysis of Variance

Source	DF	Adj SS	Adj MS	F-Value	P-Value
Pv	1	0.003560	0.003560	36.20	0.000
Error	414	0.040720	0.000098		
Total	415	0.044280			

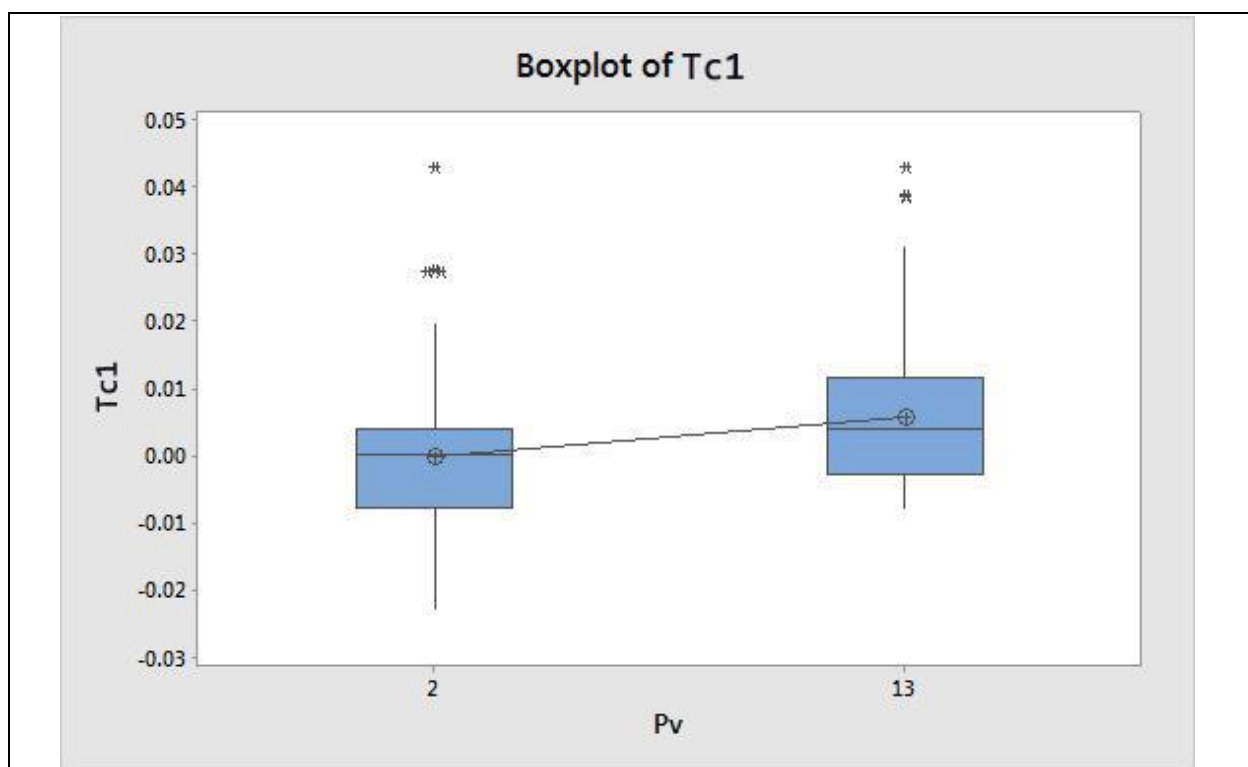
## Model Summary

S	R-sq	R-sq(adj)	R-sq(pred)
0.0099175	8.04%	7.82%	7.15%

## Means

Pv	N	Mean	StDev	95% CI
2	208	-0.000132	0.009733	(-0.001483, 0.001220)
13	208	0.005719	0.010099	( 0.004367, 0.007071)

Pooled StDev = 0.00991754



**One-way ANOVA: Tc1 versus BC**

## Method

Null hypothesis All means are equal  
 Alternative hypothesis At least one mean is different  
 Significance level  $\alpha = 0.05$

Equal variances were assumed for the analysis.

## Factor Information

Factor	Levels	Values
BC	2	A, W&S

## Analysis of Variance

Source	DF	Adj SS	Adj MS	F-Value	P-Value
BC	1	0.000856	0.000856	8.16	0.004
Error	414	0.043424	0.000105		
Total	415	0.044280			

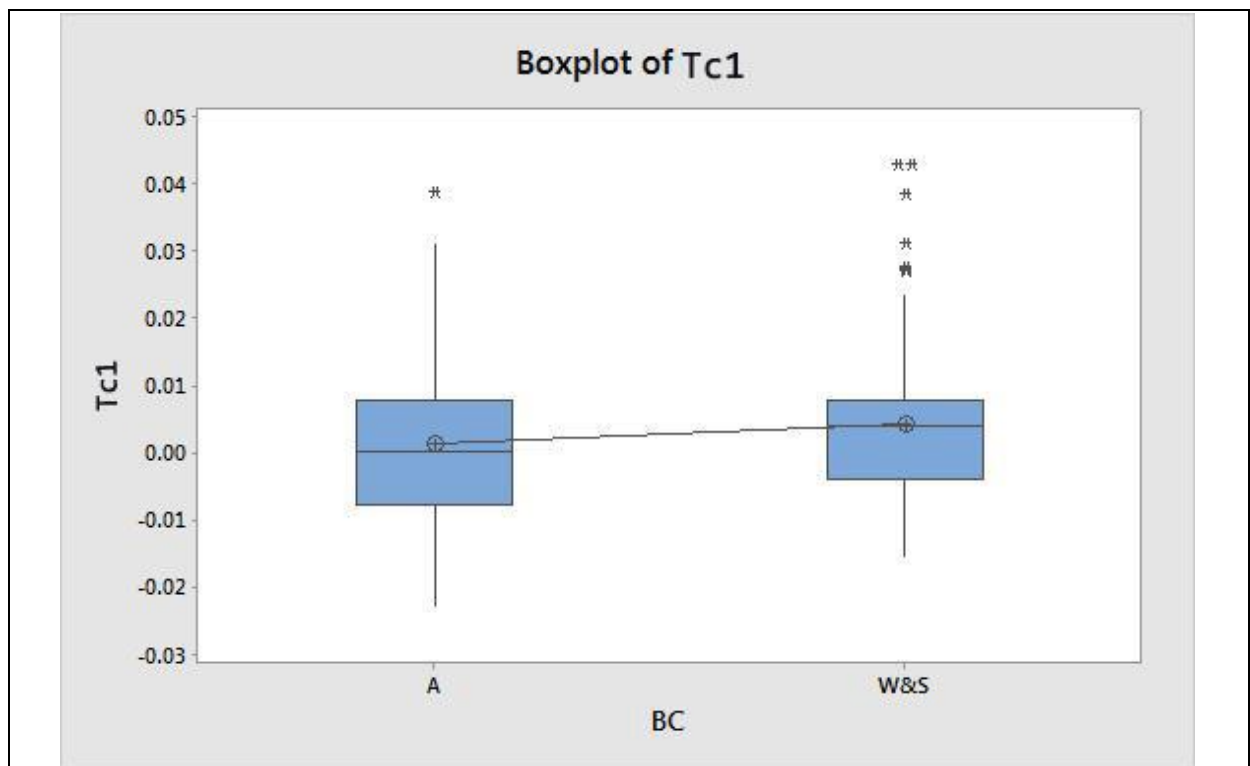
## Model Summary

S	R-sq	R-sq(adj)	R-sq(pred)
0.0102416	1.93%	1.70%	0.98%

## Means

BC	N	Mean	StDev	95% CI
A	208	0.001359	0.010440	(-0.000037, 0.002755)
W&S	208	0.004228	0.010040	( 0.002832, 0.005624)

Pooled StDev = 0.0102416



**One-way ANOVA: Pmax2 versus BC**

## Method

Null hypothesis All means are equal  
 Alternative hypothesis At least one mean is different  
 Significance level  $\alpha = 0.05$

Equal variances were assumed for the analysis.

## Factor Information

Factor	Levels	Values
BC	2	A, W&S

## Analysis of Variance

Source	DF	Adj SS	Adj MS	F-Value	P-Value
BC	1	83.07	83.067	15.30	0.000
Error	414	2247.57	5.429		
Total	415	2330.63			

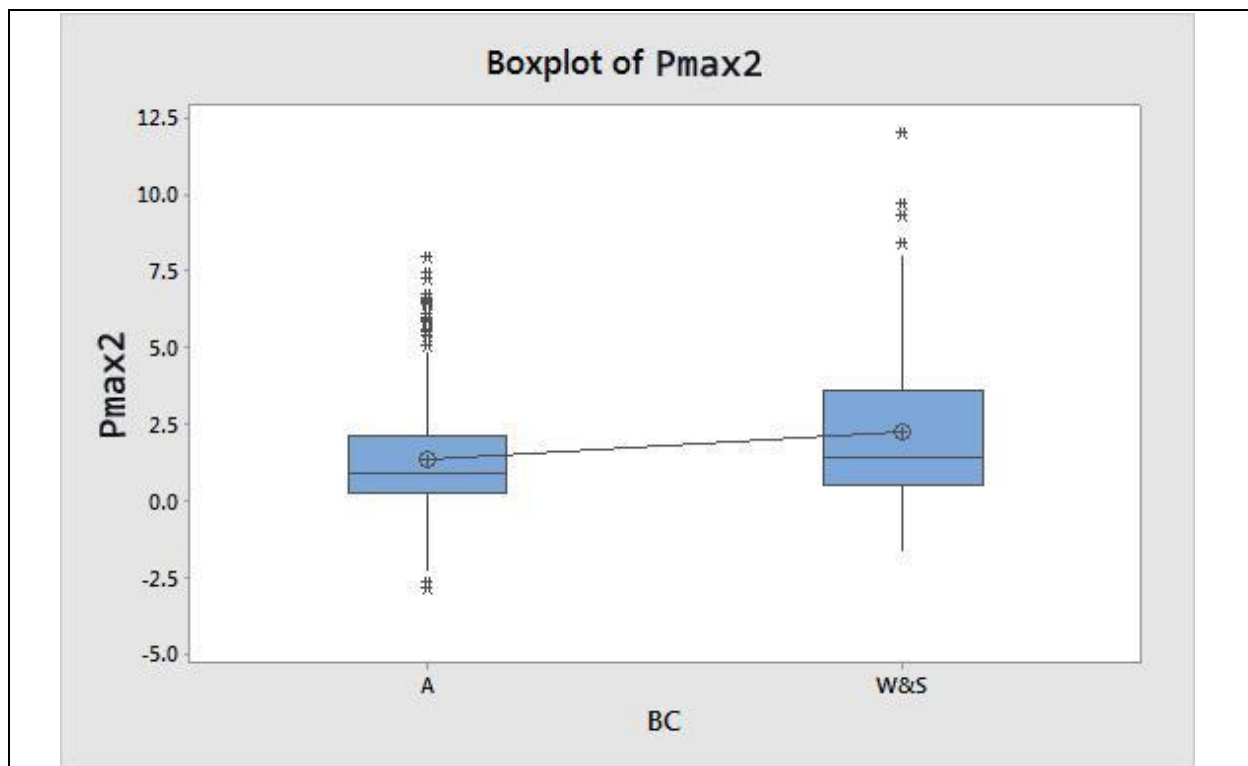
## Model Summary

S	R-sq	R-sq(adj)	R-sq(pred)
2.33000	3.56%	3.33%	2.63%

## Means

BC	N	Mean	StDev	95% CI
A	208	1.363	2.062	(1.045, 1.680)
W&S	208	2.256	2.570	(1.939, 2.574)

Pooled StDev = 2.33000



**One-way ANOVA: Pmax2 versus Pv**

## Method

Null hypothesis All means are equal  
 Alternative hypothesis At least one mean is different  
 Significance level  $\alpha = 0.05$

Equal variances were assumed for the analysis.

## Factor Information

Factor	Levels	Values
Pv	2	2, 13

## Analysis of Variance

Source	DF	Adj SS	Adj MS	F-Value	P-Value
Pv	1	0.34	0.3422	0.06	0.805
Error	414	2330.29	5.6287		
Total	415	2330.63			

## Model Summary

S	R-sq	R-sq(adj)	R-sq(pred)
2.37249	0.01%	0.00%	0.00%

## Means

Pv	N	Mean	StDev	95% CI
2	208	1.838	2.276	(1.515, 2.162)
13	208	1.781	2.465	(1.458, 2.104)

Pooled StDev = 2.37249

## F.2 Data selected for only limited and classic column separation models: comparison of Method, BC, Pv but also Friction and behaviour Mode

The data focusses on the limited cavitation (with  $P_{max2} > \text{Joukowski}$ ) and classic column separation behaviour modes, with transition behaviour runs removed.

### General Linear Model: Tc1 versus Method, Pv, BC, Mode, Friction

Method

Factor coding (-1, 0, +1)

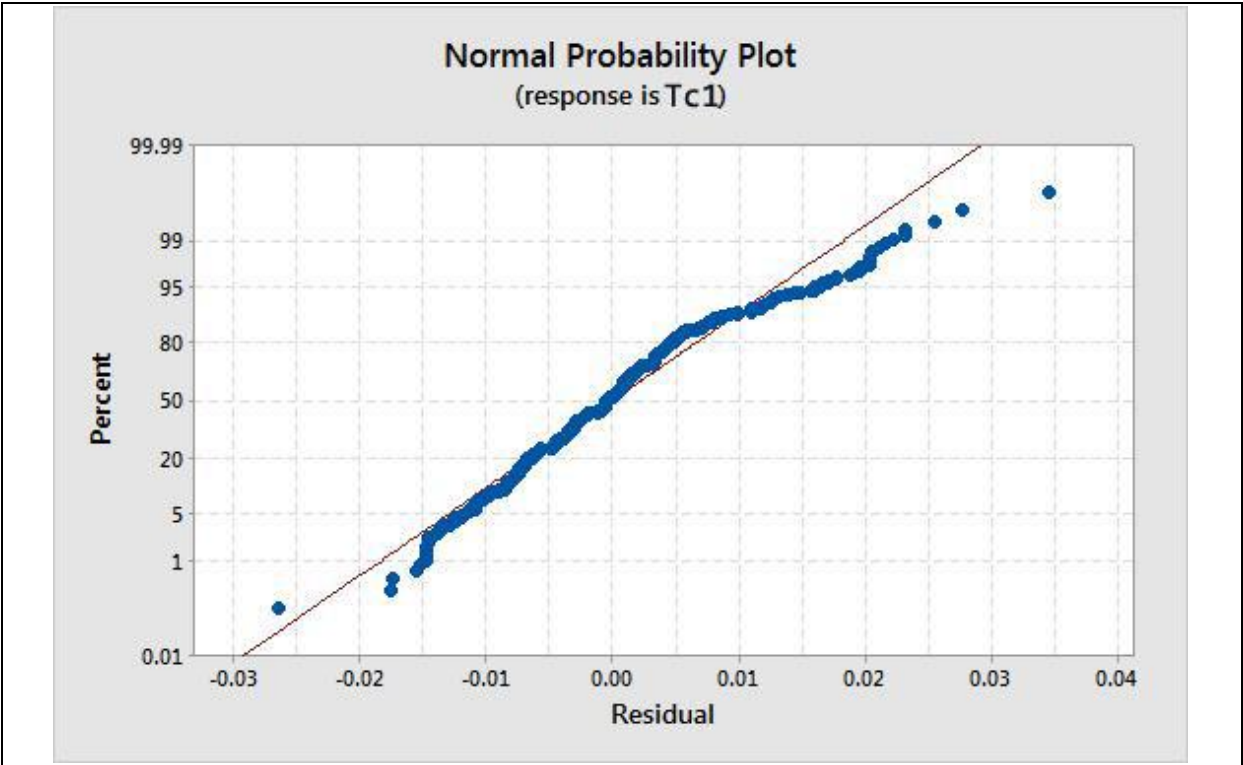
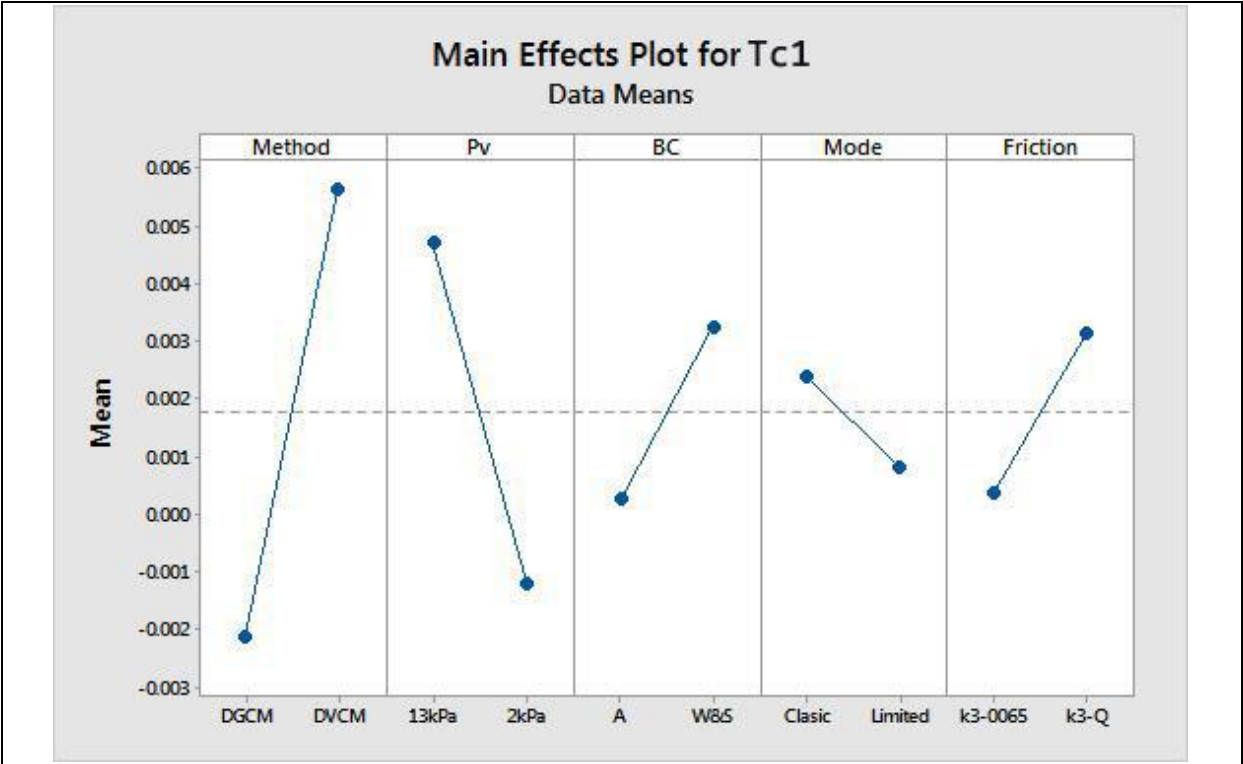
Factor Information

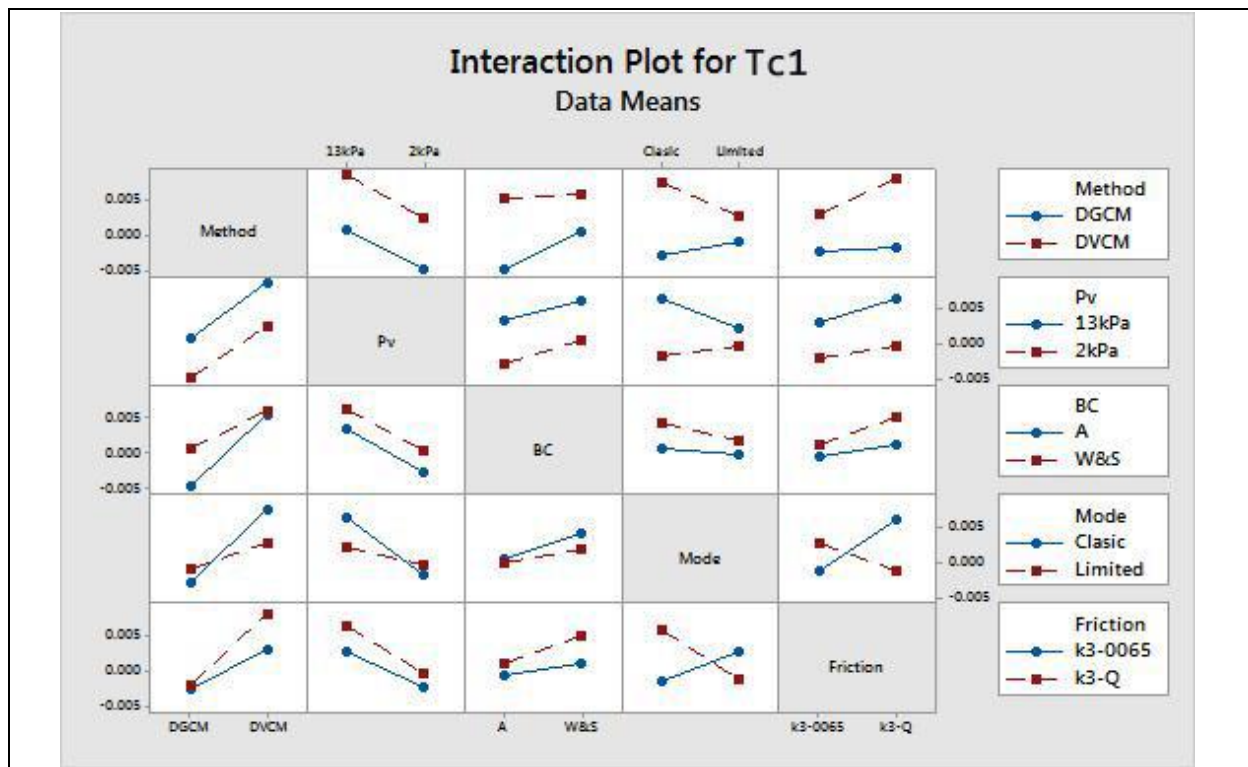
Factor	Type	Levels	Values
Method	Fixed	2	DGCM, DVCM
Pv	Fixed	2	13kPa, 2kPa
BC	Fixed	2	A, W&S
Mode	Fixed	2	Classic, Limited
Friction	Fixed	2	k3-0065, k3-Q

Analysis of Variance

Source	DF	Adj SS	Adj MS	F-Value	P-Value
Method	1	0.007281	0.007281	114.17	0.000
Pv	1	0.004099	0.004099	64.27	0.000
BC	1	0.001147	0.001147	17.99	0.000
Mode	1	0.000365	0.000365	5.72	0.017
Friction	1	0.000416	0.000416	6.52	0.011
Method*Pv	1	0.000009	0.000009	0.14	0.704
Method*BC	1	0.000650	0.000650	10.20	0.001
Method*Mode	1	0.001676	0.001676	26.28	0.000
Method*Friction	1	0.000802	0.000802	12.57	0.000
Pv*BC	1	0.000009	0.000009	0.13	0.715
Pv*Mode	1	0.001188	0.001188	18.64	0.000
Pv*Friction	1	0.000111	0.000111	1.73	0.189
BC*Mode	1	0.000110	0.000110	1.73	0.189
BC*Friction	1	0.000188	0.000188	2.95	0.086
Mode*Friction	1	0.004402	0.004402	69.04	0.000
Method*BC*Mode	1	0.000169	0.000169	2.65	0.104
Method*BC*Friction	1	0.000032	0.000032	0.51	0.478
Pv*BC*Mode	1	0.000005	0.000005	0.07	0.787
Error	573	0.036540	0.000064		
Lack-of-Fit	13	0.000497	0.000038	0.59	0.860
Pure Error	560	0.036043	0.000064		
Total	591	0.063023			







### General Linear Model: Pmax2 versus Method, Pv, BC, Mode, Friction

Method

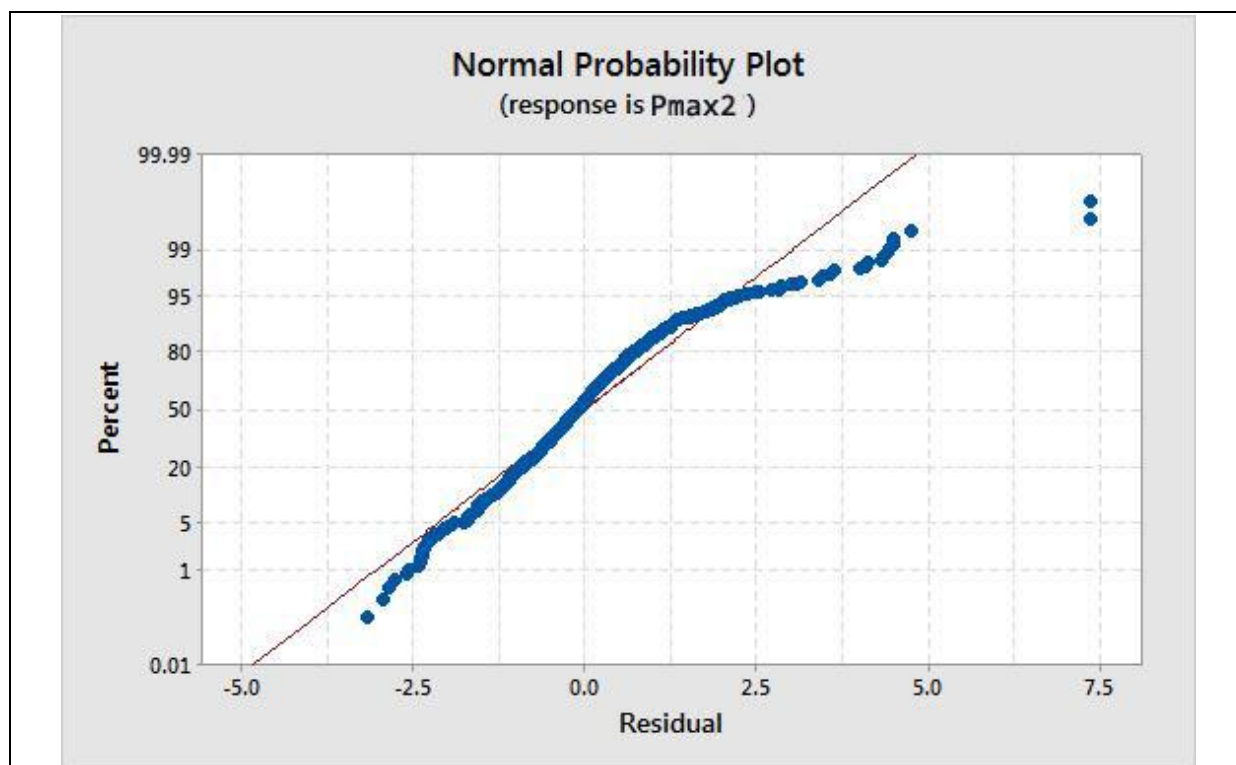
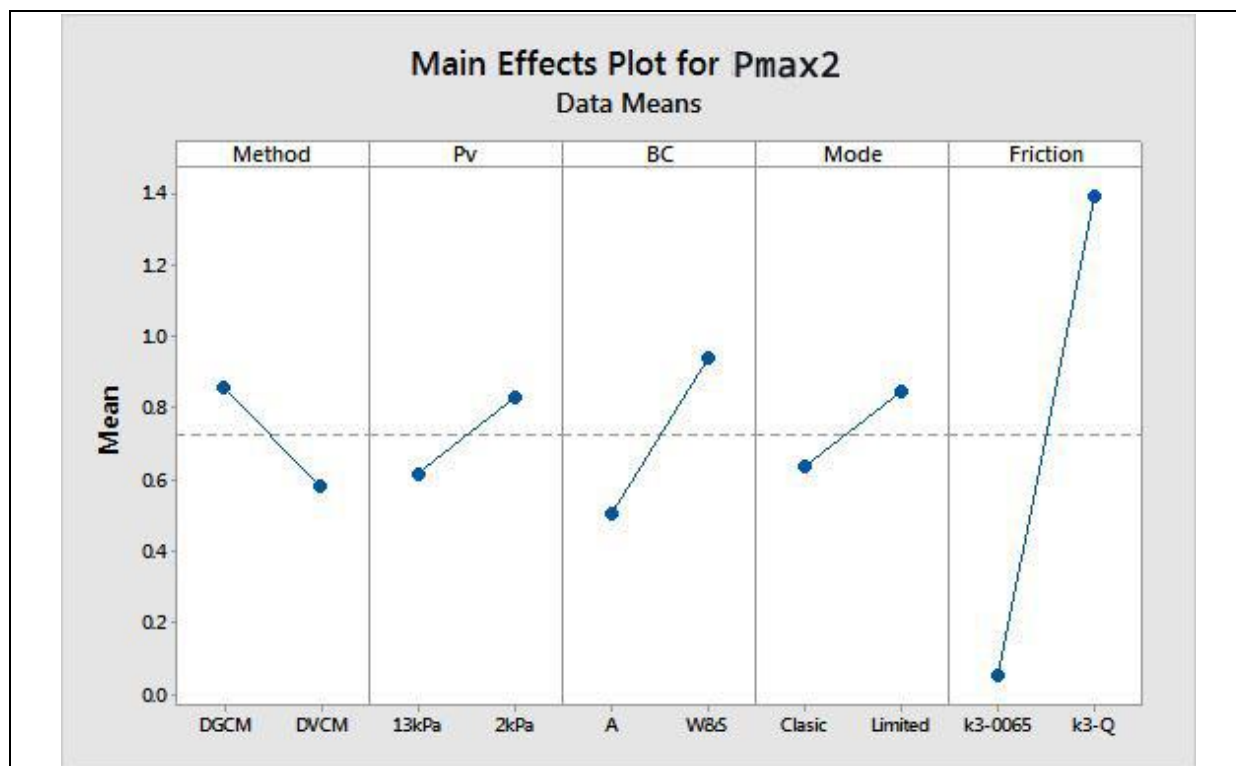
Factor coding (-1, 0, +1)

Factor Information

Factor	Type	Levels	Values
Method	Fixed	2	DGCM, DVCM
Pv	Fixed	2	13kPa, 2kPa
BC	Fixed	2	A, W&S
Mode	Fixed	2	Clasic, Limited
Friction	Fixed	2	k3-0065, k3-Q

Analysis of Variance

Source	DF	Adj SS	Adj MS	F-Value	P-Value
Method	1	11.92	11.918	6.85	0.009
Pv	1	7.30	7.301	4.19	0.041
BC	1	24.21	24.208	13.91	0.000
Mode	1	6.32	6.322	3.63	0.057
Friction	1	249.16	249.164	143.15	0.000
Method*Pv	1	0.00	0.001	0.00	0.986
Method*BC	1	7.29	7.290	4.19	0.041
Method*Mode	1	0.60	0.605	0.35	0.556
Method*Friction	1	2.14	2.142	1.23	0.268
Pv*BC	1	0.01	0.009	0.00	0.944
Pv*Mode	1	0.20	0.200	0.11	0.735
Pv*Friction	1	1.79	1.791	1.03	0.311
BC*Mode	1	2.10	2.096	1.20	0.273
BC*Friction	1	2.07	2.068	1.19	0.276
Mode*Friction	1	2.02	2.023	1.16	0.281
Method*BC*Mode	1	0.07	0.075	0.04	0.836
Method*BC*Friction	1	8.03	8.025	4.61	0.032
Pv*BC*Mode	1	0.05	0.052	0.03	0.863
Error	573	997.32	1.741		
Lack-of-Fit	13	3.68	0.283	0.16	1.000
Pure Error	560	993.64	1.774		
Total	591	1344.30			



**F.3 Full data: comparison of Method, BC, Pv using unsteady Friction**

All experimental runs including transition stages to and between limited and classic column separation.

**General Linear Model: Tc1 versus Method, Pv, BC**

Method

Factor coding (-1, 0, +1)

Factor Information

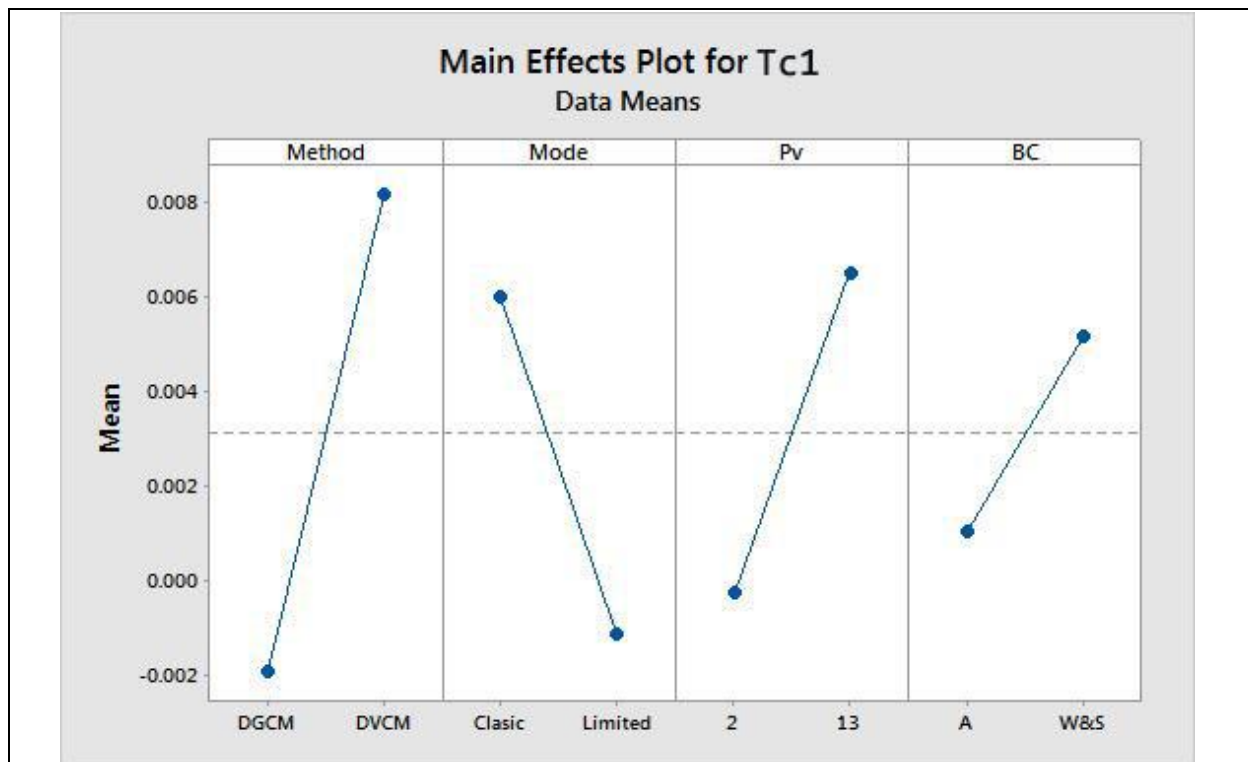
Factor	Type	Levels	Values
Method	Fixed	2	DGCM_k0065, DVCM_k0065
Pv	Fixed	2	13kPa, 2kPa
BC	Fixed	2	A, W&S

Analysis of Variance

Source	DF	Adj SS	Adj MS	F-Value	P-Value
Method	1	0.002714	0.002714	39.86	0.000
Pv	1	0.001907	0.001907	28.01	0.000
BC	1	0.000477	0.000477	7.00	0.008
Method*Pv	1	0.000009	0.000009	0.14	0.711
Method*BC	1	0.000180	0.000180	2.64	0.105
Pv*BC	1	0.000012	0.000012	0.17	0.676
Error	409	0.027843	0.000068		
Lack-of-Fit	1	0.000012	0.000012	0.17	0.677
Pure Error	408	0.027831	0.000068		
Total	415	0.033142			

Model Summary

S	R-sq	R-sq(adj)	R-sq(pred)
0.0082509	15.99%	14.75%	13.09%



**General Linear Model: Pmax2 versus Method, Pv, BC**

Method

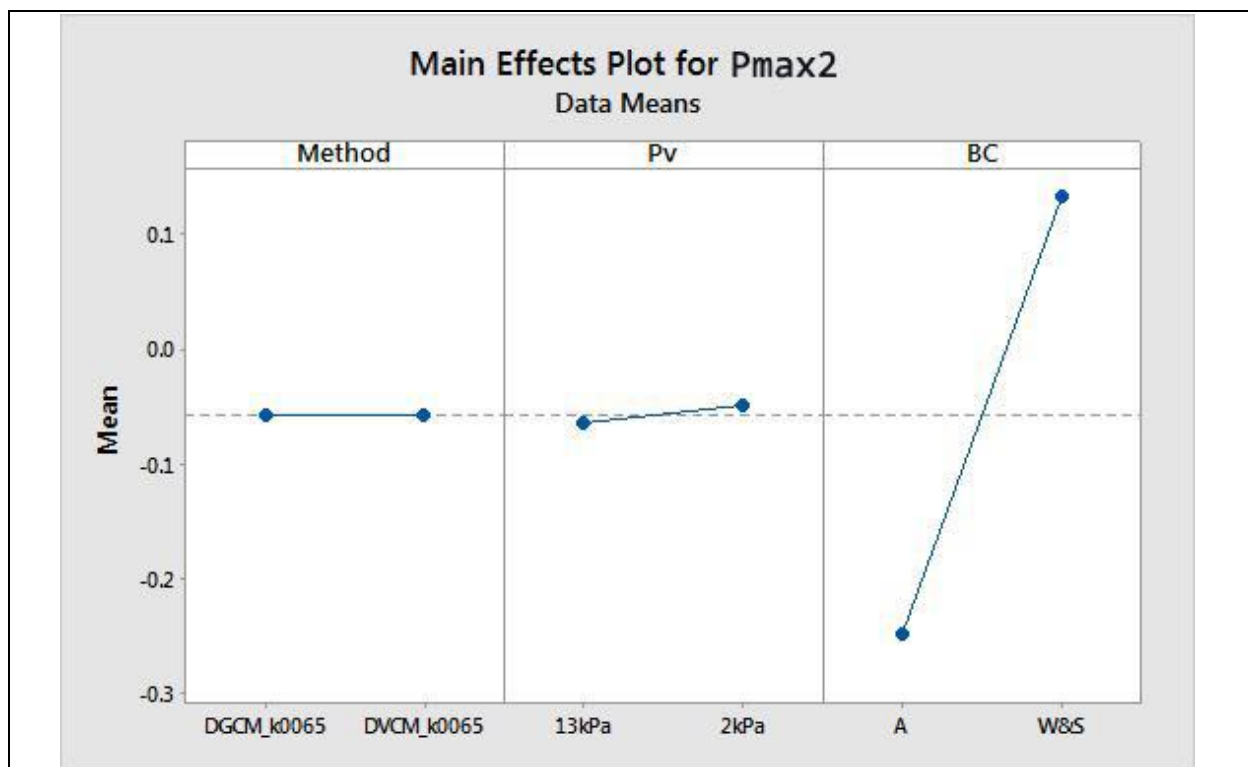
Factor coding (-1, 0, +1)

Factor Information

Factor	Type	Levels	Values
Method	Fixed	2	DGCM_k0065, DVCM_k0065
Pv	Fixed	2	13kPa, 2kPa
BC	Fixed	2	A, W&S

Analysis of Variance

Source	DF	Adj SS	Adj MS	F-Value	P-Value
Method	1	0.000	0.0001	0.00	0.992
Pv	1	0.025	0.0248	0.02	0.881
BC	1	15.230	15.2302	13.72	0.000
Method*Pv	1	0.747	0.7474	0.67	0.412
Method*BC	1	0.670	0.6695	0.60	0.438
Pv*BC	1	0.805	0.8047	0.72	0.395
Method*Pv*BC	1	0.335	0.3348	0.30	0.583
Error	408	453.018	1.1103		
Total	415	470.830			



#### F.4 Data selected for only limited and classic separation modes: comparison of Method, BC, Pv, Mode of behaviour.

The data focuses on the limited cavitation (with  $P_{max2} > \text{Joukowski}$ ) and classic column separation behaviour modes, with transition behaviour runs removed:

(a) Using quasi-steady friction:

##### General Linear Model: Tc1 versus Pv, BC, Method, Mode

Method

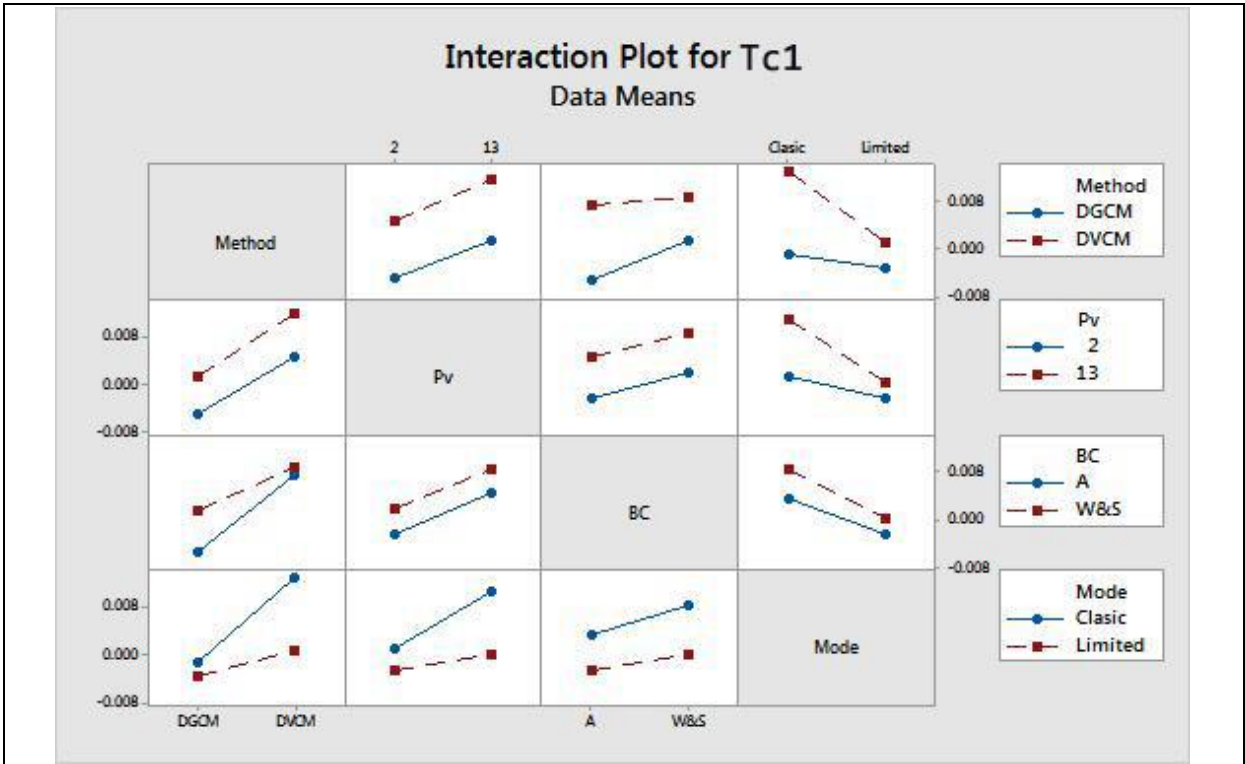
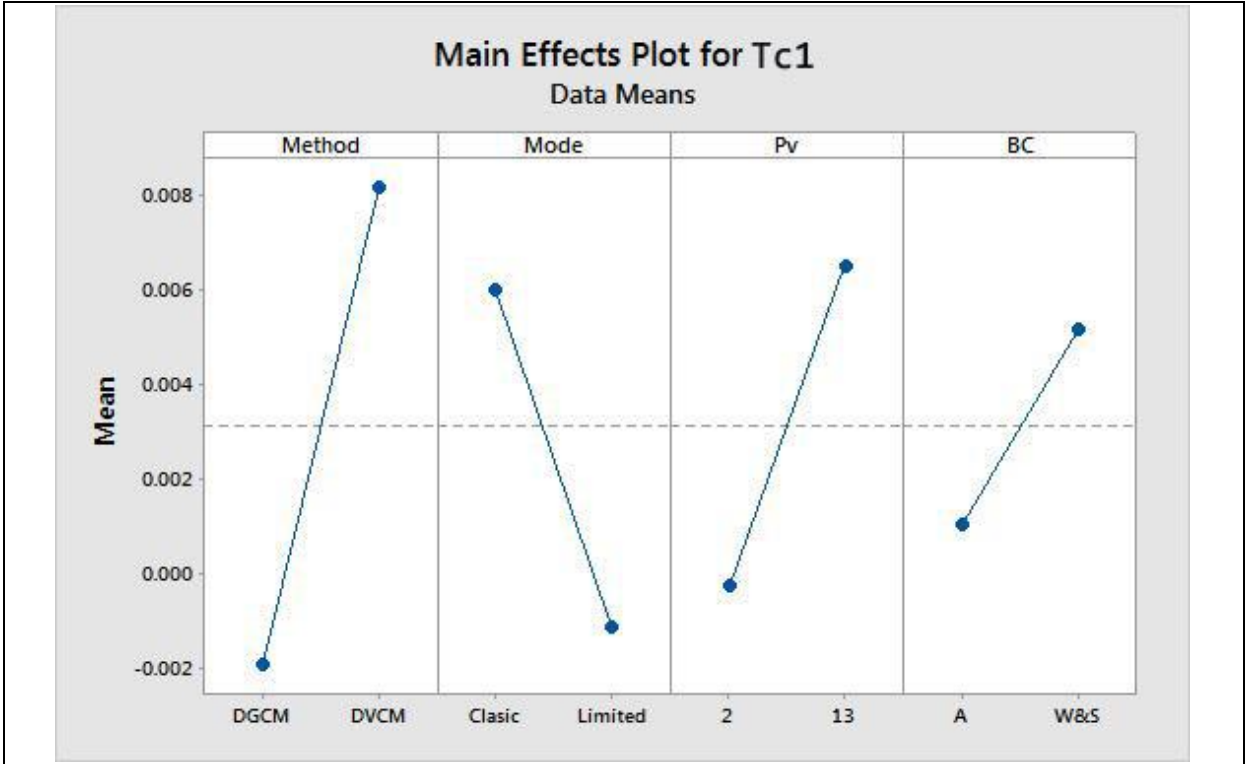
Factor coding (-1, 0, +1)

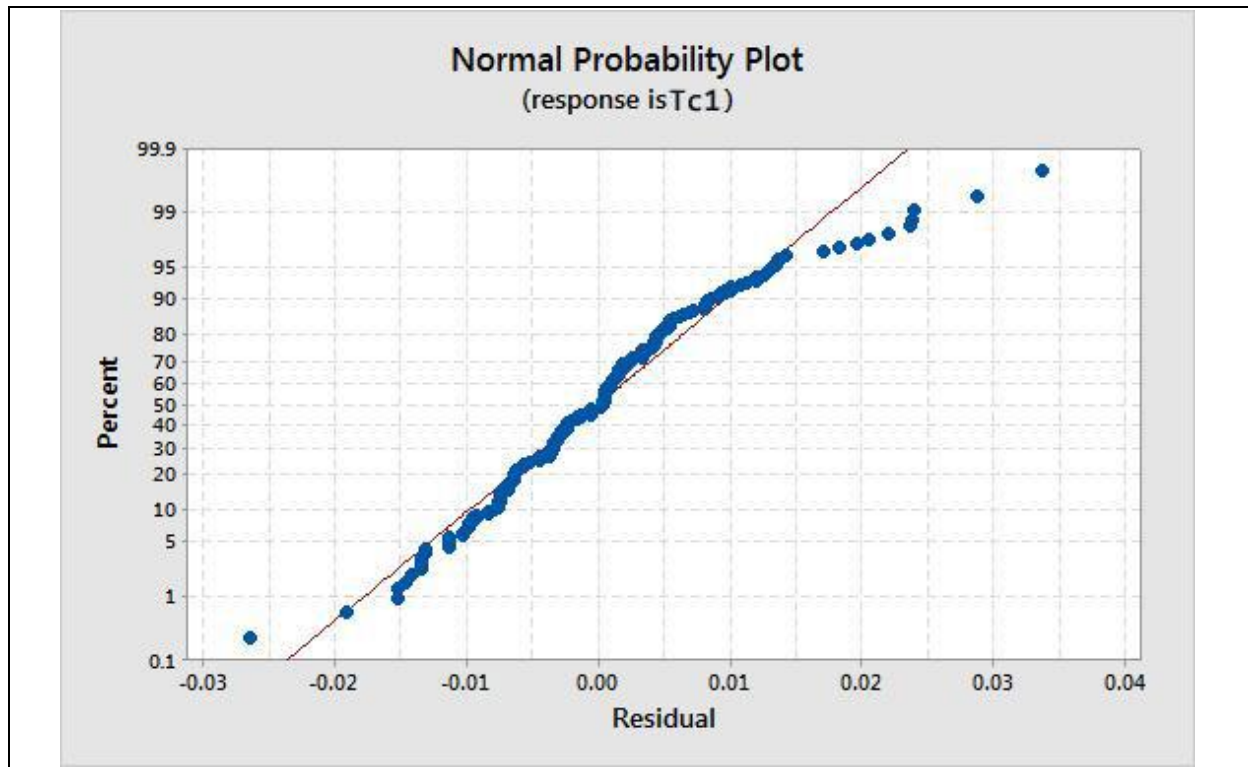
Factor Information

Factor	Type	Levels	Values
Pv	Fixed	2	2, 13
BC	Fixed	2	A, W&S
Method	Fixed	2	DGCM, DVCM
Mode	Fixed	2	Classic, Limited

Analysis of Variance

Source	DF	Adj SS	Adj MS	F-Value	P-Value
Pv	1	0.002679	0.002679	44.47	0.000
BC	1	0.001078	0.001078	17.89	0.000
Method	1	0.006032	0.006032	100.12	0.000
Mode	1	0.003651	0.003651	60.61	0.000
Pv*BC	1	0.000005	0.000005	0.09	0.768
Pv*Method	1	0.000010	0.000010	0.17	0.684
Pv*Mode	1	0.000822	0.000822	13.64	0.000
BC*Method	1	0.000583	0.000583	9.68	0.002
BC*Mode	1	0.000116	0.000116	1.93	0.166
Method*Mode	1	0.001704	0.001704	28.29	0.000
Error	285	0.017169	0.000060		
Lack-of-Fit	5	0.000255	0.000051	0.85	0.518
Pure Error	280	0.016914	0.000060		
Total	295	0.036291			





### General Linear Model: Pmax2 versus Pv, BC, Method, Mode

Method

Factor coding (-1, 0, +1)

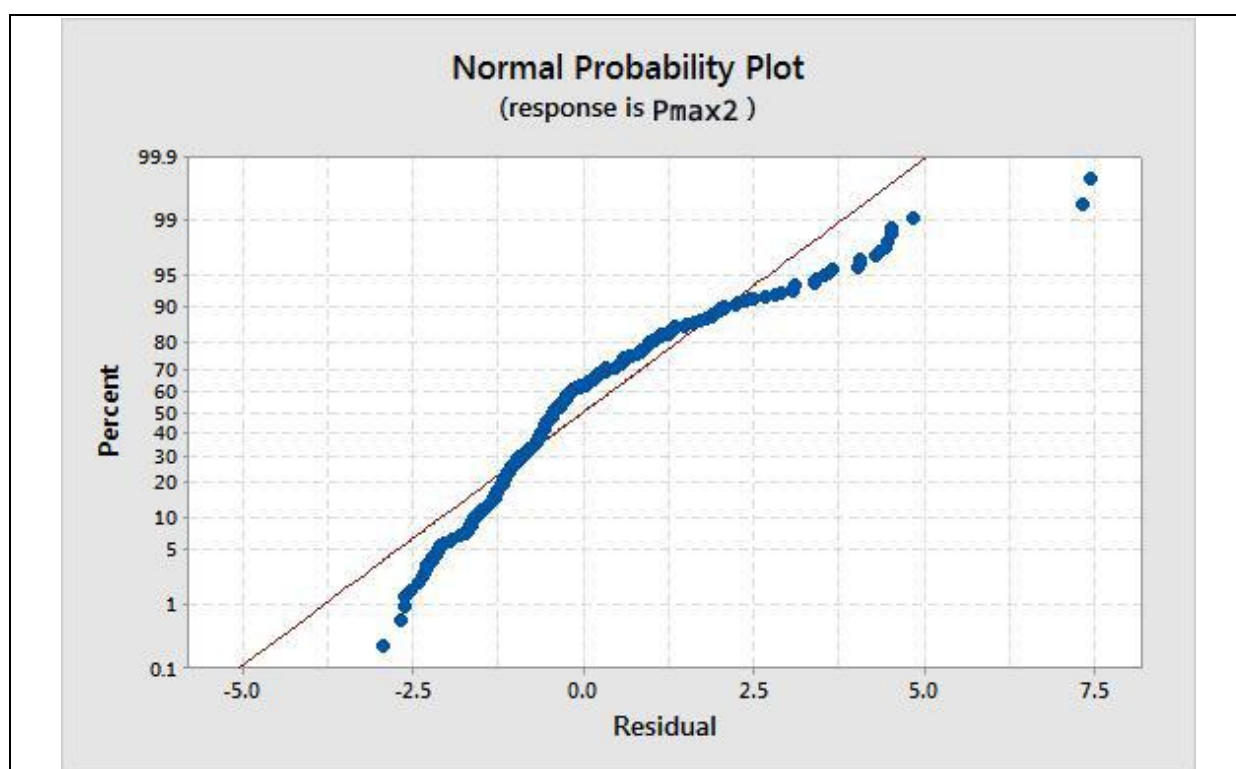
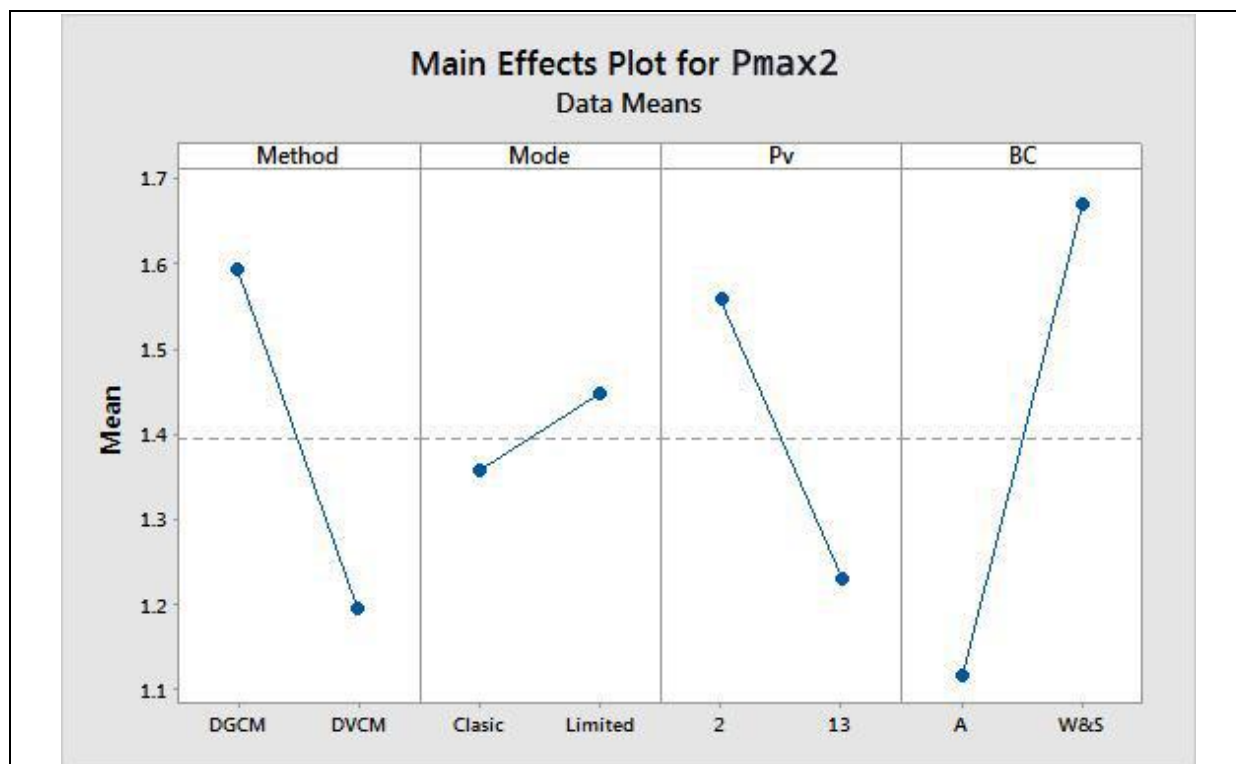
Factor Information

Factor	Type	Levels	Values
Pv	Fixed	2	2, 13
BC	Fixed	2	A, W&S
Method	Fixed	2	DGCM, DVCM
Mode	Fixed	2	Classic, Limited

Analysis of Variance

Source	DF	Adj SS	Adj MS	F-Value	P-Value
Pv	1	8.442	8.4424	3.06	0.081
BC	1	19.706	19.7060	7.13	0.008
Method	1	12.001	12.0010	4.35	0.038
Mode	1	0.596	0.5964	0.22	0.643
Pv*BC	1	0.770	0.7701	0.28	0.598
Pv*Method	1	0.335	0.3347	0.12	0.728
Pv*Mode	1	0.440	0.4397	0.16	0.690
BC*Method	1	15.878	15.8779	5.75	0.017
BC*Mode	1	1.505	1.5046	0.54	0.461
Method*Mode	1	0.344	0.3437	0.12	0.725
Error	285	787.148	2.7619		
Lack-of-Fit	5	1.321	0.2643	0.09	0.993
Pure Error	280	785.827	2.8065		
Total	295	849.324			





(b) Using unsteady friction:

### General Linear Model: Tc1 versus Method, Pv, BC, Mode

Method

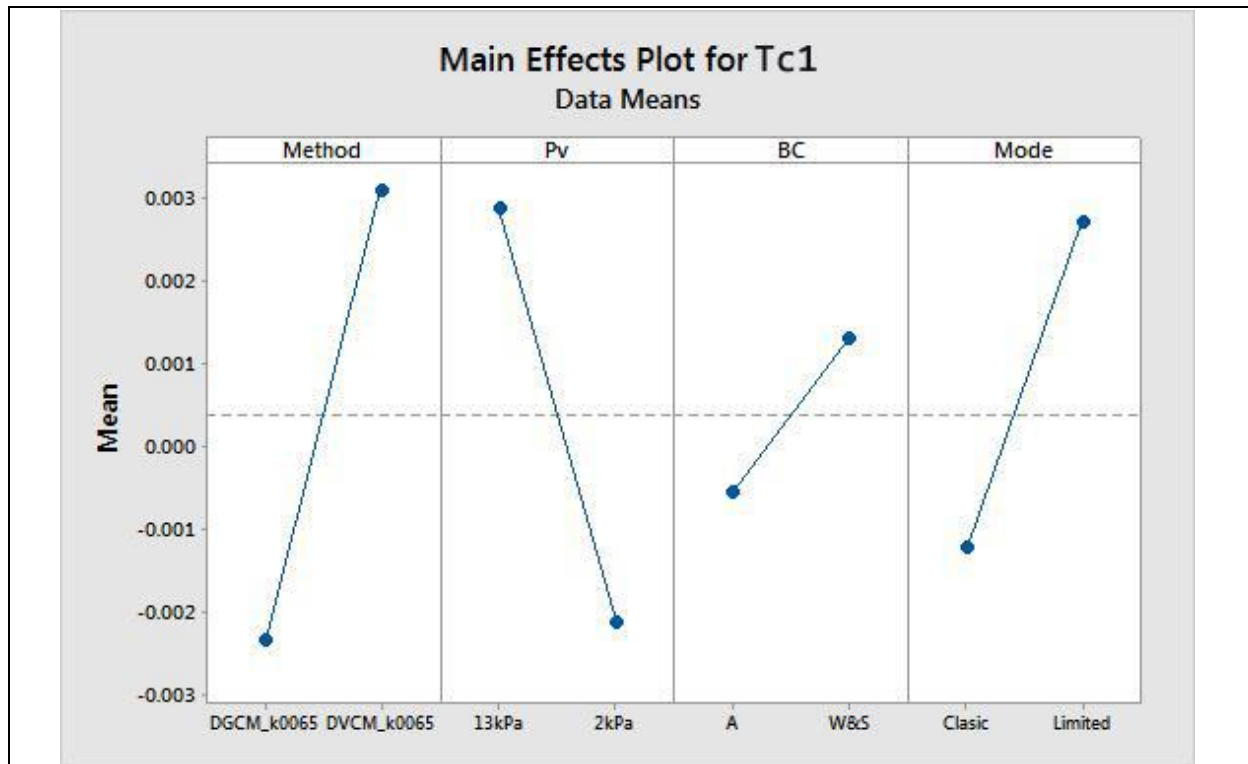
Factor coding (-1, 0, +1)

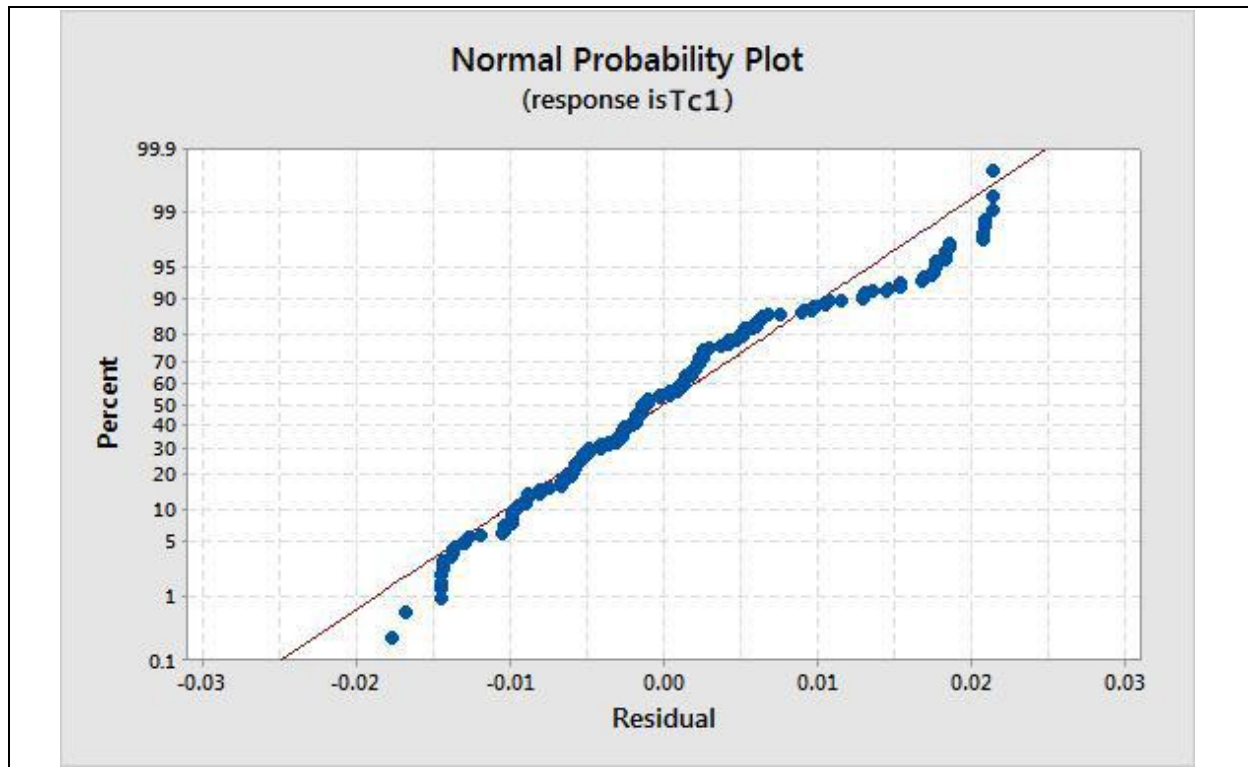
#### Factor Information

Factor	Type	Levels	Values
Method	Fixed	2	DGCM_k0065, DVCM_k0065
Pv	Fixed	2	13kPa, 2kPa
BC	Fixed	2	A, W&S
Mode	Fixed	2	Clasic, Limited

#### Analysis of Variance

Source	DF	Adj SS	Adj MS	F-Value	P-Value
Method	1	0.001850	0.001850	27.35	0.000
Pv	1	0.001504	0.001504	22.24	0.000
BC	1	0.000227	0.000227	3.35	0.068
Mode	1	0.001116	0.001116	16.51	0.000
Method*Pv	1	0.000001	0.000001	0.02	0.890
Method*BC	1	0.000216	0.000216	3.20	0.075
Method*Mode	1	0.000276	0.000276	4.08	0.044
Pv*BC	1	0.000009	0.000009	0.13	0.721
Pv*Mode	1	0.000403	0.000403	5.97	0.015
BC*Mode	1	0.000016	0.000016	0.24	0.622
Method*BC*Mode	1	0.000035	0.000035	0.52	0.473
Pv*BC*Mode	1	0.000007	0.000007	0.10	0.756
Error	283	0.019137	0.000068		
Lack-of-Fit	3	0.000008	0.000003	0.04	0.990
Pure Error	280	0.019128	0.000068		
Total	295	0.025607			





### General Linear Model: Pmax2 versus Method, Pv, BC, Mode

Method

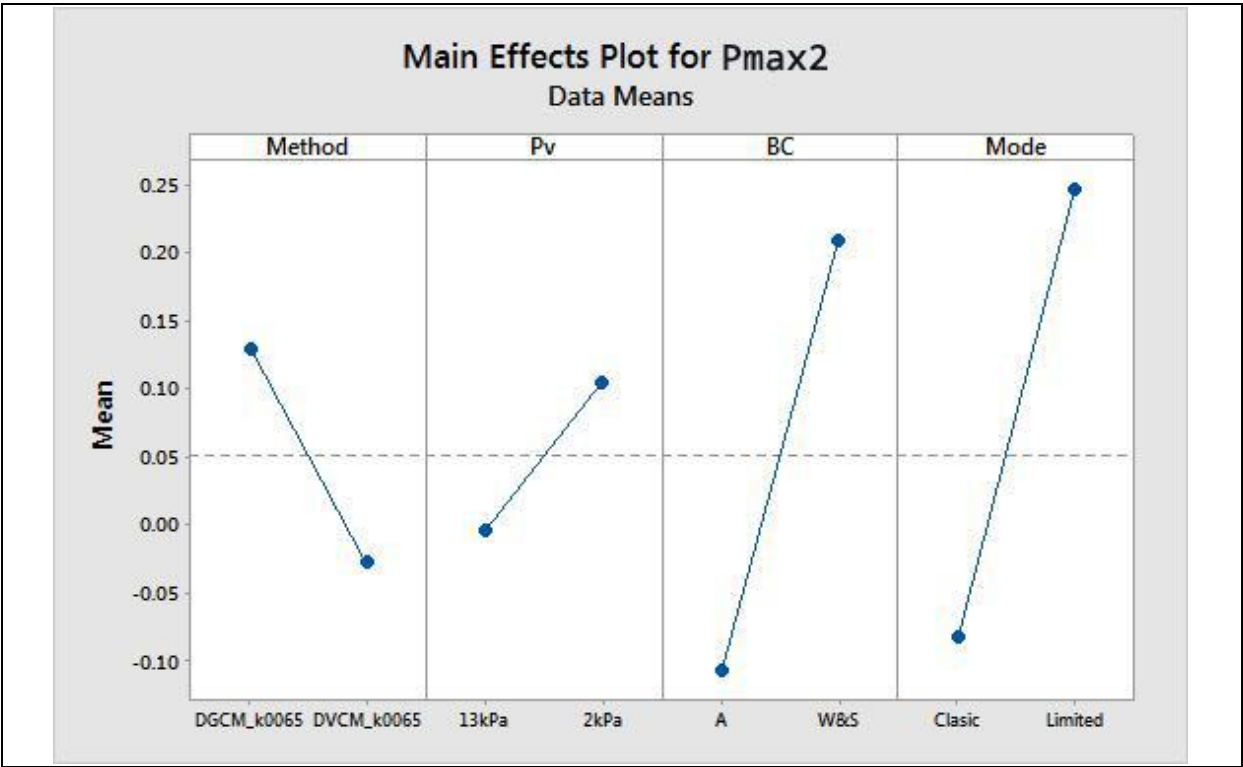
Factor coding (-1, 0, +1)

Factor Information

Factor	Type	Levels	Values
Method	Fixed	2	DGCM_k0065, DVCM_k0065
Pv	Fixed	2	13kPa, 2kPa
BC	Fixed	2	A, W&S
Mode	Fixed	2	Clasic, Limited

Analysis of Variance

Source	DF	Adj SS	Adj MS	F-Value	P-Value
Method	1	2.011	2.01055	2.74	0.099
Pv	1	0.838	0.83835	1.14	0.286
BC	1	6.345	6.34539	8.63	0.004
Mode	1	7.748	7.74834	10.54	0.001
Method*Pv	1	0.375	0.37510	0.51	0.476
Method*BC	1	0.004	0.00427	0.01	0.939
Method*Mode	1	0.264	0.26393	0.36	0.549
Pv*BC	1	0.456	0.45566	0.62	0.432
Pv*Mode	1	0.001	0.00095	0.00	0.971
BC*Mode	1	0.674	0.67381	0.92	0.339
Method*BC*Mode	1	0.054	0.05441	0.07	0.786
Pv*BC*Mode	1	0.001	0.00080	0.00	0.974
Error	283	207.992	0.73495		
Lack-of-Fit	3	0.181	0.06031	0.08	0.970
Pure Error	280	207.811	0.74218		
Total	295	227.682			



## **Appendix G.**

### **Sample of Criterial Calculation**

Run	Experiment				Calculation (DVCM-W&S-k3-13kPa)				Error			
	1st Cavity Tc1 (s)			2 <sup>nd</sup> Peak pressure Pmax2 (bar)	1st Cavity Tc1 (s)			2 <sup>nd</sup> Peak pressure Pmax2 (bar)	Absolute Error		Relative Error %	
	Start	End	Duration		Start	End	Duration		Tc1	Pmax2	Tc1	Pmax2
7	0.625	0.691406	0.066406	14.01	0.609375	0.6875	0.078125	13.19	0.0117188	-0.821	17.65	-5.86
8	0.617188	0.695313	0.078125	11.87	0.605469	0.695313	0.089844	11.68	0.0117188	-0.187	15.00	-1.58
9	0.609375	0.695313	0.085938	15.31	0.605469	0.699219	0.09375	15.51	0.0078125	0.198	9.09	1.29
10	0.613281	0.699219	0.085938	17.70	0.605469	0.699219	0.09375	17.91	0.0078125	0.212	9.09	1.20
11	0.617188	0.707031	0.089844	19.50	0.605469	0.703125	0.097656	20.53	0.0078125	1.038	8.70	5.32
12	0.609375	0.703125	0.09375	15.49	0.605469	0.703125	0.097656	16.19	0.0039063	0.701	4.17	4.53
13	0.617188	0.710938	0.09375	15.56	0.605469	0.707031	0.101563	16.12	0.0078125	0.567	8.33	3.64
14	0.617188	0.710938	0.09375	11.49	0.605469	0.707031	0.101563	12.79	0.0078125	1.295	8.33	11.26
15	0.609375	0.710938	0.101563	22.86	0.605469	0.714844	0.109375	22.84	0.0078125	-0.028	7.69	-0.12
16	0.609375	0.714844	0.105469	16.03	0.601563	0.714844	0.113281	16.09	0.0078125	0.066	7.41	0.41
17	0.609375	0.71875	0.109375	15.98	0.601563	0.714844	0.113281	16.03	0.0039063	0.044	3.57	0.28
18	0.613281	0.722656	0.109375	23.02	0.605469	0.71875	0.113281	22.14	0.0039063	-0.878	3.57	-3.82
19	0.605469	0.722656	0.117188	19.11	0.605469	0.722656	0.117188	19.24	0.0000000	0.129	0.00	0.67
20	0.609375	0.730469	0.121094	12.08	0.601563	0.726563	0.125	12.72	0.0039063	0.640	3.23	5.30
21	0.609375	0.734375	0.125	9.06	0.601563	0.730469	0.128906	9.32	0.0039063	0.261	3.13	2.88
22	0.605469	0.722656	0.117188	15.75	0.601563	0.726563	0.125	15.71	0.0078125	-0.042	6.67	-0.26
23	0.601563	0.742188	0.140625	8.82	0.601563	0.746094	0.144531	8.90	0.0039063	0.077	2.78	0.87
24	0.613281	0.742188	0.128906	15.60	0.601563	0.742188	0.140625	15.18	0.0117188	-0.420	9.09	-2.69
25	0.605469	0.738281	0.132813	18.28	0.601563	0.738281	0.136719	18.16	0.0039063	-0.111	2.94	-0.61
26	0.609375	0.753906	0.144531	11.62	0.601563	0.753906	0.152344	11.57	0.0078125	-0.051	5.41	-0.44
27	0.609375	0.773438	0.164063	8.44	0.601563	0.777344	0.175781	8.92	0.0117188	0.483	7.14	5.73
28	0.605469	0.75	0.144531	15.01	0.601563	0.765625	0.164063	14.44	0.0195313	-0.571	13.51	-3.80
29	0.609375	0.757813	0.148438	22.19	0.601563	0.761719	0.160156	20.38	0.0117188	-1.813	7.89	-8.17
30	0.609375	0.769531	0.160156	15.47	0.601563	0.78125	0.179688	16.02	0.0195313	0.550	12.20	3.55
31	0.609375	0.765625	0.15625	14.84	0.601563	0.78125	0.179688	15.97	0.0234375	1.128	15.00	7.60

32	0.605469	0.769531	0.164063	19.89	0.601563	0.773438	0.171875	18.87	0.0078125	-1.026	4.76	-5.16
33	0.609375	0.773438	0.164063	16.08	0.601563	0.785156	0.183594	16.55	0.0195313	0.465	11.90	2.89
34	0.605469	0.769531	0.164063	22.60	0.601563	0.777344	0.175781	22.37	0.0117188	-0.225	7.14	-1.00
35	0.609375	0.792969	0.183594	11.27	0.601563	0.796875	0.195313	16.52	0.0117188	5.248	6.38	46.58
36	0.609375	0.804688	0.195313	11.12	0.601563	0.800781	0.199219	12.11	0.0039063	0.994	2.00	8.94
37	0.605469	0.785156	0.179688	19.10	0.601563	0.796875	0.195313	18.98	0.0156250	-0.119	8.70	-0.62
38	0.605469	0.792969	0.1875	25.77	0.601563	0.804688	0.203125	28.66	0.0156250	2.887	8.33	11.20
39	0.605469	0.828125	0.222656	16.02	0.601563	0.820313	0.21875	16.89	-0.0039063	0.865	-1.75	5.40
40	0.613281	0.839844	0.226563	11.49	0.601563	0.832031	0.230469	11.58	0.0039063	0.095	1.72	0.83
41	0.605469	0.832031	0.226563	15.74	0.601563	0.832031	0.230469	16.37	0.0039063	0.637	1.72	4.05
42	0.609375	0.894531	0.285156	18.04	0.601563	0.898438	0.296875	18.02	0.0117188	-0.018	4.11	-0.10
43	0.613281	0.917969	0.304688	18.38	0.601563	0.914063	0.3125	19.52	0.0078125	1.134	2.56	6.17
44	0.601563	0.949219	0.347656	15.23	0.601563	0.949219	0.347656	14.22	0.0000000	-1.007	0.00	-6.62
45	0.605469	0.996094	0.390625	10.55	0.601563	1	0.398438	10.77	0.0078125	0.221	2.00	2.10
46	0.609375	0.914063	0.304688	32.36	0.601563	0.929688	0.328125	31.25	0.0234375	-1.110	7.69	-3.43
47	0.605469	0.953125	0.347656	28.79	0.601563	0.953125	0.351563	28.10	0.0039063	-0.695	1.12	-2.41
48	0.605469	0.964844	0.359375	27.09	0.601563	0.984375	0.382813	24.75	0.0234375	-2.339	6.52	-8.64
49	0.613281	1	0.386719	21.24	0.601563	1.011719	0.410156	21.17	0.0234375	-0.079	6.06	-0.37
50	0.605469	1.019531	0.414063	22.14	0.601563	1.023438	0.421875	21.12	0.0078125	-1.021	1.89	-4.61
51	0.601563	1.066406	0.464844	18.14	0.601563	1.066406	0.464844	16.61	0.0000000	-1.533	0.00	-8.45
52	0.605469	0.871094	0.265625	24.17	0.601563	0.867188	0.265625	25.69	0.0000000	1.520	0.00	6.29
53	0.605469	0.902344	0.296875	13.82	0.601563	0.894531	0.292969	14.48	-0.0039063	0.658	-1.32	4.76
54	0.609375	0.851563	0.242188	24.25	0.601563	0.855469	0.253906	22.83	0.0117188	-1.417	4.84	-5.84
55	0.605469	0.875	0.269531	16.39	0.601563	0.875	0.273438	17.02	0.0039063	0.634	1.45	3.87
56	0.605469	0.855469	0.25	28.13	0.601563	0.847656	0.246094	26.59	-0.0039063	-1.541	-1.56	-5.48
57	0.605469	0.886719	0.28125	12.29	0.601563	0.878906	0.277344	13.39	-0.0039063	1.102	-1.39	8.96
58	0.609375	0.867188	0.257813	11.60	0.601563	0.859375	0.257813	11.83	0.0000000	0.231	0.00	1.99

Run	Experiment				Calculation (DVCM-W&S-k3-13kPa)				Error			
	1st Cavity Tc1 (s)			2 <sup>nd</sup> Peak pressur e Pmax2 (bar)	1st Cavity Tc1 (s)			2 <sup>nd</sup> Peak pressure Pmax2 (bar)	Absolute Error		Relative Error %	
	Start	End	Duration		Start	End	Duration		Tc1	Pmax 2	Tc1	Pmax2
9	0.609375	0.695313	0.085938	15.31	0.605469	0.699219	0.09375	15.51	0.0078125	0.198	9.09	1.29
10	0.613281	0.699219	0.085938	17.70	0.605469	0.699219	0.09375	17.91	0.0078125	0.212	9.09	1.20
11	0.617188	0.707031	0.089844	19.50	0.605469	0.703125	0.097656	20.53	0.0078125	1.038	8.70	5.32
12	0.609375	0.703125	0.09375	15.49	0.605469	0.703125	0.097656	16.19	0.0039063	0.701	4.17	4.53
13	0.617188	0.710938	0.09375	15.56	0.605469	0.707031	0.101563	16.12	0.0078125	0.567	8.33	3.64
15	0.609375	0.710938	0.101563	22.86	0.605469	0.714844	0.109375	22.84	0.0078125	-0.028	7.69	-0.12
16	0.609375	0.714844	0.105469	16.03	0.601563	0.714844	0.113281	16.09	0.0078125	0.066	7.41	0.41
17	0.609375	0.71875	0.109375	15.98	0.601563	0.714844	0.113281	16.03	0.0039063	0.044	3.57	0.28
18	0.613281	0.722656	0.109375	23.02	0.605469	0.71875	0.113281	22.14	0.0039063	-0.878	3.57	-3.82
19	0.605469	0.722656	0.117188	19.11	0.605469	0.722656	0.117188	19.24	0.0000000	0.129	0.00	0.67
20	0.609375	0.730469	0.121094	12.08	0.601563	0.726563	0.125	12.72	0.0039063	0.640	3.23	5.30
21	0.609375	0.734375	0.125	9.06	0.601563	0.730469	0.128906	9.32	0.0039063	0.261	3.13	2.88
22	0.605469	0.722656	0.117188	15.75	0.601563	0.726563	0.125	15.71	0.0078125	-0.042	6.67	-0.26
23	0.601563	0.742188	0.140625	8.82	0.601563	0.746094	0.144531	8.90	0.0039063	0.077	2.78	0.87
24	0.613281	0.742188	0.128906	15.60	0.601563	0.742188	0.140625	15.18	0.0117188	-0.420	9.09	-2.69
25	0.605469	0.738281	0.132813	18.28	0.601563	0.738281	0.136719	18.16	0.0039063	-0.111	2.94	-0.61
26	0.609375	0.753906	0.144531	11.62	0.601563	0.753906	0.152344	11.57	0.0078125	-0.051	5.41	-0.44
27	0.609375	0.773438	0.164063	8.44	0.601563	0.777344	0.175781	8.92	0.0117188	0.483	7.14	5.73
28	0.605469	0.75	0.144531	15.01	0.601563	0.765625	0.164063	14.44	0.0195313	-0.571	13.51	-3.80
29	0.609375	0.757813	0.148438	22.19	0.601563	0.761719	0.160156	20.38	0.0117188	-1.813	7.89	-8.17
30	0.609375	0.769531	0.160156	15.47	0.601563	0.78125	0.179688	16.02	0.0195313	0.550	12.20	3.55
31	0.609375	0.765625	0.15625	14.84	0.601563	0.78125	0.179688	15.97	0.0234375	1.128	15.00	7.60
32	0.605469	0.769531	0.164063	19.89	0.601563	0.773438	0.171875	18.87	0.0078125	-1.026	4.76	-5.16
33	0.609375	0.773438	0.164063	16.08	0.601563	0.785156	0.183594	16.55	0.0195313	0.465	11.90	2.89



34	0.605469	0.769531	0.164063	22.60	0.601563	0.777344	0.175781	22.37	0.0117188	-0.225	7.14	-1.00
36	0.609375	0.804688	0.195313	11.12	0.601563	0.800781	0.199219	12.11	0.0039063	0.994	2.00	8.94
37	0.605469	0.785156	0.179688	19.10	0.601563	0.796875	0.195313	18.98	0.0156250	-0.119	8.70	-0.62
38	0.605469	0.792969	0.1875	25.77	0.601563	0.804688	0.203125	28.66	0.0156250	2.887	8.33	11.20
39	0.605469	0.828125	0.222656	16.02	0.601563	0.820313	0.21875	16.89	-0.0039063	0.865	-1.75	5.40
40	0.613281	0.839844	0.226563	11.49	0.601563	0.832031	0.230469	11.58	0.0039063	0.095	1.72	0.83
41	0.605469	0.832031	0.226563	15.74	0.601563	0.832031	0.230469	16.37	0.0039063	0.637	1.72	4.05
42	0.609375	0.894531	0.285156	18.04	0.601563	0.898438	0.296875	18.02	0.0117188	-0.018	4.11	-0.10
43	0.613281	0.917969	0.304688	18.38	0.601563	0.914063	0.3125	19.52	0.0078125	1.134	2.56	6.17
44	0.601563	0.949219	0.347656	15.23	0.601563	0.949219	0.347656	14.22	0.0000000	-1.007	0.00	-6.62
45	0.605469	0.996094	0.390625	10.55	0.601563	1	0.398438	10.77	0.0078125	0.221	2.00	2.10
46	0.609375	0.914063	0.304688	32.36	0.601563	0.929688	0.328125	31.25	0.0234375	-1.110	7.69	-3.43
47	0.605469	0.953125	0.347656	28.79	0.601563	0.953125	0.351563	28.10	0.0039063	-0.695	1.12	-2.41
48	0.605469	0.964844	0.359375	27.09	0.601563	0.984375	0.382813	24.75	0.0234375	-2.339	6.52	-8.64
49	0.613281	1	0.386719	21.24	0.601563	1.011719	0.410156	21.17	0.0234375	-0.079	6.06	-0.37
50	0.605469	1.019531	0.414063	22.14	0.601563	1.023438	0.421875	21.12	0.0078125	-1.021	1.89	-4.61
51	0.601563	1.066406	0.464844	18.14	0.601563	1.066406	0.464844	16.61	0.0000000	-1.533	0.00	-8.45
52	0.605469	0.871094	0.265625	24.17	0.601563	0.867188	0.265625	25.69	0.0000000	1.520	0.00	6.29
53	0.605469	0.902344	0.296875	13.82	0.601563	0.894531	0.292969	14.48	-0.0039063	0.658	-1.32	4.76
54	0.609375	0.851563	0.242188	24.25	0.601563	0.855469	0.253906	22.83	0.0117188	-1.417	4.84	-5.84
55	0.605469	0.875	0.269531	16.39	0.601563	0.875	0.273438	17.02	0.0039063	0.634	1.45	3.87
56	0.605469	0.855469	0.25	28.13	0.601563	0.847656	0.246094	26.59	-0.0039063	-1.541	-1.56	-5.48
57	0.605469	0.886719	0.28125	12.29	0.601563	0.878906	0.277344	13.39	-0.0039063	1.102	-1.39	8.96
58	0.609375	0.867188	0.257813	11.60	0.601563	0.859375	0.257813	11.83	0.0000000	0.231	0.00	1.99